

A LABORATORY AND NUMERICAL INVESTIGATION
OF STEADY-STATE, TWO-REGIME, RADIAL FLOW
TO A WELL FROM ROUGH, HORIZONTAL,
DEFORMABLE FRACTURES

CENTRE FOR NEWFOUNDLAND STUDIES

**TOTAL OF 10 PAGES ONLY
MAY BE XEROXED**

(Without Author's Permission)

LEE CLAFLIN ATKINSON

C. 171





National Library
of Canada

Bibliothèque nationale
du Canada

Canadian Theses Service

Services des thèses canadiennes

Ottawa, Canada
K1A 0N4

CANADIAN THESES

THÈSES CANADIENNES

NOTICE

The quality of this microfiche is heavily dependent upon the quality of the original thesis submitted for microfilming. Every effort has been made to ensure the highest quality of reproduction possible.

If pages are missing, contact the university which granted the degree.

Some pages may have indistinct print especially if the original pages were typed with a poor typewriter ribbon or if the university sent us an inferior photocopy.

Previously copyrighted materials (journal articles, published tests, etc.) are not filmed.

Reproduction in full or in part of this film is governed by the Canadian Copyright Act, R.S.C. 1970, c. C-30.

AVIS

La qualité de cette microfiche dépend grandement de la qualité de la thèse soumise au microfilmage. Nous avons tout fait pour assurer une qualité supérieure de reproduction.

S'il manque des pages, veuillez communiquer avec l'université qui a conféré le grade.

La qualité d'impression de certaines pages peut laisser à désirer, surtout si les pages originales ont été dactylographiées à l'aide d'un ruban usé ou si l'université nous a fait parvenir une photocopie de qualité inférieure.

Les documents qui font déjà l'objet d'un droit d'auteur (articles de revue, examens publiés, etc.) ne sont pas microfilmés.

La reproduction, même partielle, de ce microfilm est soumise à la Loi canadienne sur le droit d'auteur, SRC 1970, c. C-30.

**THIS DISSERTATION
HAS BEEN MICROFILMED
EXACTLY AS RECEIVED.**

**LA THÈSE A ÉTÉ
MICROFILMÉE TELLE QUE
NOUS L'AVONS REÇUE**

A LABORATORY AND NUMERICAL INVESTIGATION
OF
STEADY-STATE, TWO-REGIME, RADIAL FLOW TO A WELL
FROM
ROUGH, HORIZONTAL, DEFORMABLE FRACTURES

by

• Lee Claflin Atkinson, B.S., M.S.

A thesis submitted to the School of Graduate
Studies in partial fulfillment of the
requirements for the degree of
Doctor of Philosophy.

Department of Earth Sciences
Memorial University of Newfoundland

October 1986

Permission has been granted to the National Library of Canada to microfilm this thesis and to lend or sell copies of the film.

The author (copyright owner) has reserved other publication rights, and neither the thesis nor extensive extracts from it may be printed or otherwise reproduced without his/her written permission.

L'autorisation a été accordée à la Bibliothèque nationale du Canada de microfilmer cette thèse et de prêter ou de vendre des exemplaires du film.

L'auteur (titulaire du droit d'auteur) se réserve les autres droits de publication; ni la thèse ni de longs extraits de celle-ci ne doivent être imprimés ou autrement reproduits sans son autorisation écrite.

ISBN 0-315-36964-7

ABSTRACT

A numerical and laboratory study was undertaken to obtain a better understanding of the production-drawdown response of a well completed into an aquifer whose primary flow conduits are horizontal fractures.

In the first phase of the study, a finite-element model was developed to evaluate the effects of fracture aperture and relative roughness on the nature of flow within the fractures and the compounding effect of the fractures closing in response to drawdown-induced increases in effective stress. The flow code of the model simulates steady-state, two-regime (i.e., both laminar and turbulent) radial flow in a series of horizontal, rough fractures of fixed aperture using empirically derived flow laws from the literature. The deformation code models the rock as an elastic medium and follows a user-defined constitutive curve for the stress-deformation behavior of the fractures in order to simulate their closure under the fluid pressure distribution determined by the flow routine. A coupled solution, using fluid pressure as the linking parameter, is obtained by iterating between the two routines.

For the laboratory phase of the investigation, a concrete cylinder 1.5 m in diameter by 3.0 m high was fabricated with a single, cast-in-place horizontal fracture. More than 60 tests involving constant discharge, variable discharge, and constant injection rate were conducted on the

physical model. In addition to flow rate, the laboratory arrangement permitted the varying of boundary fluid pressures, the load applied to the top of the cylinder, and the wellbore size.

The numerical model closely simulated the results of tests when the fracture was open (i.e., with no contact area) using the true geometric characteristics of the fracture. When the fracture surfaces were in contact, however, the closest simulations were obtained using an "effective aperture" in the range of 0.3-0.8 of the best estimate of the true geometric aperture.

The results of this investigation demonstrate that non-linear flow in fractures within a few tenths of a meter of the wellbore can comprise a significant portion of the total drawdown in a well. The results also indicate that the coefficient of the well loss term in the classical step-drawdown equation is not a constant (as usually assumed) but increases as the discharge rate increases. One of the more practical findings of this study is that reaming some wellbores in fractured rock aquifers could minimize well losses and lead to improved efficiency in their performance.

Key words: aquifer evaluation aquifer testing
 dewatering drawdown
 fracture permeability groundwater flow
 groundwater movement mine drainage
 turbulent flow well hydraulics
 well testing wells

ACKNOWLEDGMENTS

I wish to express sincere appreciation to my supervisor, John Gale, for taking me in when I was orphaned as a graduate student, for providing generous financial support during the past three years, for offering many useful suggestions, particularly during the laboratory phase of the project, and for sharing with me many of his own thoughts on the nature of flow in fractured rocks. I am most fortunate to have been able to study under one of the leaders in this relatively new, but rapidly evolving field.

The laboratory model could not have been completed without the input and assistance of many people in Technical Services and in the laboratories of the Faculty of Engineering and Applied Science at Memorial University. Space limitations preclude mentioning them all. I would be remiss, however, in not mentioning three individuals who made invaluable contributions and demonstrated a keen personal interest in the project: Charlie Carter in the Welding Shop, Humphrey Dye of the Machine Shop, and Calvin Ward in the Concrete/Soils Laboratory.

Many thanks are also due to Don Cameron of the Engineering Geology Laboratory in the Department of Earth Sciences for never failing to respond to "ya gotta minute,

ACKNOWLEDGMENTS -- Continued

Jarge" and for his good natured instruction in laboratory techniques and procedures.

I extend my appreciation to the Canada Centre for Mineral and Energy Technology (CANMET) of Energy, Mines and Resources Canada; the Natural Sciences and Engineering Research Council of Canada (NSERC); and the President's NSERC Research Grant at Memorial University for funding this study through grants to John Gale. I also thank B.P. Canada, the University of Waterloo, and Memorial University for their personal financial support at various stages in my graduate studies.

Special thanks also go to Karen Shepard, Shelly Penick, Cathy Roth, and Doug Lindsay for their conscientious assistance with the word processing and technical illustration of this thesis, to Bill Brumund and Golder Associates for their support in these tasks, to Lanny Smith for the photographic reproduction, and to my father, Harry Atkinson, for help with the final editing and proofreading.

Finally, I want to extend my deepest gratitude to my parents, Harry and Peggy Atkinson; my sister and brother-in-law, Judy and Sid Baker; and some very special friends -- Lynn and Betty Brown, Michal Bukovansky, Mike Kellestine, Graeme and Renee Major, John Sharp, Donna Smith, and Joan

ACKNOWLEDGMENTS -- Continued

Stratton -- who, each in his/her own way, helped me through a most devastating personal crisis that arose toward the end of this project and who gave me the encouragement and strength to finish when quitting seemed the thing to do.

TABLE OF CONTENTS

| | <u>Page</u> |
|---|-------------|
| ABSTRACT | ii |
| ACKNOWLEDGMENTS. | -iv |
| TABLE OF CONTENTS. | vii |
| LIST OF TABLES | x |
| LIST OF FIGURES. | xi |
| NOTATION | xv |
| SELECTED TERMINOLOGY | xxi |
| 1.0 INTRODUCTION. | 1 |
| 1.1 Statement of problem | 1 |
| 1.2 Objective and scope. | 10 |
| 1.3 Previous work. | 12 |
| 1.3.1 Non-linear and two-regime flow. | 12 |
| 1.3.2 Exit loss and wellbore effects. | 16 |
| 1.3.3 Empirical determination of well loss. | 18 |
| 1.3.4 Flow in fractures | 24 |
| 1.3.4.1 General concepts | 25 |
| 1.3.4.2 Development of empirical flow laws | 28 |
| 1.3.4.3 Major laboratory investigations. | 36 |
| 1.3.4.4 Special considerations in radial, convergent flow. | 39 |
| 1.3.4.5 Fracture deformation | 43 |
| 1.3.5 Current applications in dewatering. | 45 |
| 2.0 EMPIRICAL DESCRIPTION OF TWO-REGIME, CONVERGENT, RADIAL FLOW TO A WELL FROM HORIZONTAL, DEFORMABLE FRACTURES. | 47 |
| 2.1 Formulation of analytical solution to two-regime radial flow to a well in a rigid fracture | 48 |
| 2.2 Finite element formulation of two-regime flow equation. | 58 |
| 2.2.1 Radial discretization | 58 |
| 2.2.2 Linearization of non-linear flow laws | 59 |
| 2.2.3 Galerkin formulation. | 61 |
| 2.3 Changes in fracture aperture resulting from changes in effective stress. | 64 |
| 2.4 Flow through multiple fractures. | 74 |
| 2.5 Coupled numerical solution | 75 |

TABLE OF CONTENTS -- Continued

| | <u>Page</u> |
|---|-------------|
| 3.0 NUMERICAL SIMULATION USING THE PROGRAM 'DEFLOW' | 80 |
| 3.1 Comparison of numerical solution with analytical solution. | 80 |
| 3.2 Sensitivity analysis | 82 |
| 3.3 Results with multiple fractures. | 88 |
| 3.4 Synthesized step-drawdown tests. | 90 |
| 4.0 LABORATORY TESTING OF RADIAL FLOW MODEL | 93 |
| 4.1 Description of laboratory model. | 93 |
| 4.2 Stress-deformation tests | 100 |
| 4.3 Flow tests | 102 |
| 4.3.1 Pumping tests | 104 |
| 4.3.2 Injection tests | 114 |
| 4.3.3 Step-drawdown tests | 116 |
| 5.0 COMPARISON AND INTERPRETATION OF RESULTS FROM NUMERICAL AND LABORATORY MODELS. | 121 |
| 5.1 Tests with open fractures. | 121 |
| 5.2 Tests with closed fractures. | 127 |
| 6.0 APPLICATION OF FINDINGS | 134 |
| 6.1 Re-interpretation of step-drawdown test results from fractured rock aquifers | 134 |
| 6.2 Evaluation of potential well stimulation methods. | 144 |
| 6.2.1 Increasing wellbore diameter. | 144 |
| 6.2.2 Hydraulic propping. | 148 |
| 7.0 SUMMARY | 152 |
| 7.1 Findings | 152 |
| 7.2 Recommendations for further study. | 158 |
| REFERENCES | 161 |

TABLE OF CONTENTS -- Continued

| | <u>Page</u> |
|--|-------------|
| APPENDICES | |
| A SIMILITUDE BETWEEN CIRCULAR PIPES AND FRACTURES . . . | 173 |
| B METHODS TO ESTIMATE EFFECTIVE FRACTURE APERTURE AND ROUGHNESS FROM PRESSURE PROFILES. | 178 |
| B.1 Linear Flow. | 178 |
| B.2 Fully turbulent flow | 183 |
| B.3 Dimensions and units | 187 |
| B.4 Listing of program LOUIS | 188 |
| B.5 Listing of program SATO. | 189 |
| C DESCRIPTION OF NUMERICAL MODEL. | 190 |
| C.1 Finite element discretization. | 192 |
| C.2 Description of flow code | 197 |
| C.3 Description of deformation code. | 207 |
| C.4 Determination of normal stress versus displacement relationship for a fracture | 211 |
| C.5 User's guide for DEFLOW. | 214 |
| C.5.1 Operating environment | 214 |
| C.5.2 External files. | 215 |
| C.5.3 Input files | 218 |
| C.5.4 Example of output | 221 |
| C.5.5 Additional notes on execution | 221 |
| C.6 Listing of program DEFLOW. | 236 |
| C.7 Listing of program FRACLAW | 289 |
| D SENSITIVITY ANALYSIS PLOTS. | 292 |
| E DETAILS OF DESIGN AND CONSTRUCTION OF LABORATORY MODEL. | 299 |
| E.1 Design considerations. | 299 |
| E.1.1 Size of model | 301 |
| E.1.2 Construction material for model | 304 |
| E.1.3 Surfaces of fracture. | 307 |
| E.1.4 Relative orientation of wellbore and fracture. | 309 |
| E.1.5 Flow and deformation boundary conditions. | 309 |
| E.2 Description of model as-built. | 310 |
| E.3 Product information. | 319 |

LIST OF TABLES

| | <u>Page</u> |
|---|-------------|
| 1.1 Friction factors for fracture flow and derived relationships for hydraulic conductivity | 30 |
| 1.2 Previous physical fracture flow models | 37 |
| 2.1 Critical Reynolds numbers | 54 |
| 3.1 Summary of sensitivity analysis input and results | 84 |
| 4.1 Log of laboratory tests | 105 |
| 5.1 Estimates of aperture size from Test No. 2 data | 125 |
| 5.2 Estimates of aperture size from Test No. 10 data | 132 |
| B1—Values of roughness factors for linear flow | 180 |
| B2 Values of roughness factors for fully turbulent flow | 186 |
| B3 Recommended units for calculation of aperture | 187 |
| C1 Example of input file for DEFLOW with one fracture and GRIDGEN used | 220 |
| C2 Example of input file for DEFLOW with three fractures | 223 |
| C3 Example of output file from DEFLOW | 226 |
| E1 Comparison of mechanical properties of typical rock and concrete | 306 |
| E2 Special materials used to construct physical model | 321 |

LIST OF FIGURES

| | <u>Page</u> |
|--|-------------|
| 1.1 Components of drawdown in a well | 2 |
| 1.2 Schematic diagram of two-well depressurizing system showing effects of well losses | 8 |
| 1.3 Typical production-drawdown responses of water wells in fractured rock aquifers | 21 |
| 1.4 Geometric properties of a fracture | 27 |
| 1.5 Moody-type diagram of Louis' (1969) flow test data | 31 |
| 1.6 Fracture flow law fields | 32 |
| 1.7 Schematic diagram of fracture deformation due to changes in effective stress | 44 |
| 2.1 Deformation in a discontinuous rock mass | 66 |
| 2.2 Typical normal effective stress versus displacement relationship for a fracture | 71 |
| 2.3 Structural elements and boundary conditions used in deformation code of DEFLOW | 73 |
| 2.4 Boundary conditions for flow in multiple fractures | 75 |
| 2.5 Flow chart of coupled deformation-flow solution using DEFLOW | 78 |
| 3.1 Comparison of finite element and analytical solutions for flow | 81 |
| 3.2 Increase in effective stress and fracture closure versus log radial distance | 87 |
| 3.3 Total head loss distribution in three fractures of different aperture and relative roughness | 89 |
| 3.4 Relative production from fractures of different aperture | 91 |
| 3.5 Specific drawdown versus discharge for a synthesized step-drawdown test | 92 |

LIST OF FIGURES -- Continued

| | <u>Page</u> |
|--|-------------|
| 4.1 Laboratory model as-built | 94 |
| 4.2 Schematic diagram of laboratory arrangement | 95 |
| 4.3 Plan view of location of fracture plane manometers, LVDT's, and loading centers | 96 |
| 4.4 Tracings of resin-impregnated fractures in 0.150 m diameter concrete test cylinders under different levels of stress | 98 |
| 4.5 Micro-photographs of cross-sections of cast fractures in 0.150 m diameter concrete test cylinders impregnated with resin | 99 |
| 4.6 Water jetting from fracture into wellbore | 100 |
| 4.7 Normal stress versus fracture displacement for laboratory model and concrete test cylinders | 101 |
| 4.8 Loss in pressure head versus logarithm of radial distance for open fracture under pumping conditions | 109 |
| 4.9 Loss in pressure head versus inverse radial distance for open fracture under pumping conditions | 110 |
| 4.10 Loss in pressure head versus logarithm of radial distance for closed fracture under pumping conditions | 112 |
| 4.11 Loss in pressure head versus inverse radial distance for closed fracture under pumping conditions | 113 |
| 4.12 Loss in pressure head versus logarithm of radial distance for closed fracture under injection conditions | 115 |
| 4.13 Loss in pressure head versus inverse radial distance for closed fracture under injection conditions | 116 |
| 4.14 Comparison of pressure head profiles for injection and pumping | 117 |

LIST OF FIGURES -- Continued

| | <u>Page</u> |
|--|-------------|
| 4.15 Loss in pressure head versus logarithm of radial distance of step-drawdown test of model with 0.108-m diameter wellbore | 118 |
| 4.16 Drawdown versus discharge for step-drawdown tests of laboratory model | 119 |
| 4.17 Specific drawdown versus discharge for step-drawdown tests of laboratory model | 120 |
| 5.1 Actual pressure head loss compared to pressure head loss predicted by DEFLOW for open fracture | 123 |
| 5.2 Anisotropy induced by geotextile used to cast fracture | 130 |
| 6.1 Components of specific drawdown as a function of discharge rate | 136 |
| 6.2 Production rate and drawdown as a function of wellbore size in a well intersecting a single, horizontal fracture | 146 |
| 6.3 Potential effect of fracture propping on production-drawdown response | 150 |
| A1 Geometric similitude between circular pipes and fractures | 175 |
| C1 Routines in program DEFLOW | 191 |
| C2 Finite element discretization generated by GRIDGEN for simulating laboratory model | 193 |
| C3 Finite element discretization generated by GRIDGEN for simulating hypothetical field problem with 1 fracture | 195 |
| C4 Finite element discretization (manually generated) for simulating hypothetical field problem with 3 fractures | 196 |

LIST OF FIGURES -- Continued

| | <u>Page</u> | |
|----|--|-----|
| D1 | Sensitivity of head distribution to variation in relative roughness of fracture | 293 |
| D2 | Sensitivity of head distribution to variation in fracture aperture (keeping relative roughness constant) | 294 |
| D3 | Sensitivity of head distribution to variation in fracture aperture (keeping absolute roughness constant) | 295 |
| D4 | Sensitivity of head distribution to variation in kinematic viscosity of water | 296 |
| D5 | Sensitivity of head distribution to variation in normal stiffness of fracture | 297 |
| D6 | Sensitivity of head distribution to variation in discharge rate | 298 |
| E1 | Critical radius as a function of discharge rate and fracture roughness | 305 |
| E2 | Cast-in-place components of concrete cylinder | 311 |
| E3 | Bottom half of cylinder with geotextile in place | 313 |
| E4 | Pouring top half of concrete cylinder | 314 |
| E5 | Drilling wellbore in concrete cylinder | 315 |
| E6 | Circumferential reservoir before and after outer band flanged on | 316 |
| E7 | Linear variable displacement transformers (LVDT's) for measuring concrete and fracture deformation on perimeter of model | 318 |
| E8 | LVDT system for measuring fracture deformation inside wellbore | 320 |

NOTATION

The units of measurement used in this thesis conform to the Systeme Internationale d'Unites (SI). A complete list of variables and specific units used in the computer program DEFLOW is included in the program header (see Appendix C).

| Symbol | Parameter/Quantity | M-F-L-T ¹ Dimension ² |
|------------------|--|--|
| a | coefficient of hydraulic resistance in Forchheimer equation | [T/L] |
| A | cross-sectional area of flow | [L ²] |
| A _S | area over which stiffness is applicable | [L ²] |
| b | coefficient of hydraulic resistance in Forchheimer equation | [T ² /L ²] |
| B | aquifer coefficient in Jacob, Rorabaugh, and Ramey equations | [T/L ²] |
| [B] | geometric sub-matrix of stiffness matrix | [1/L] |
| [B] ^T | transpose of [B] | [1/L] |
| c | empirical coefficient in turbulent flow laws of Louis and Lomize | [] |
| C | well coefficient in Jacob, Rorabaugh, and Ramey equations | [*] |
| C _e | exit loss coefficient | [T ² /L ⁵] |
| C _l | linear or laminar flow coefficient | [T/L ²] |
| C _L | correction factor for accelerating laminar flow | [] |
| C _n | non-linear or turbulent flow coefficient | [T ² /L ⁴] |
| C _w | wellbore flow loss coefficient | [T ² /L ⁵] |
| d | empirical coefficient in turbulent flow laws of Louis and Lomize | [] |

NOTATION -- Continued

| Symbol | Parameter/Quantity | M-F-L-T ¹ Dimension ² |
|-----------------|---|--|
| D | diameter of pipe or wellbore | [L] |
| D _C | characteristic length of closed conduit | [L] |
| D _h | hydraulic diameter | [L] |
| [D] | displacement matrix | [L] |
| e | width of slit between parallel plates | [L] |
| E _r | Young's modulus for rock | [F/L ²] |
| [E] | elasticity submatrix | [F/L ²] |
| f | roughness factor for laminar flow | [] |
| f' | roughness factor for fully turbulent flow | [] |
| f' _N | roughness factor for fully turbulent flow according to law of Nikuradse | [] |
| f' _L | roughness factor for fully turbulent flow according to Louis or Lomize | [] |
| f _w | friction factor for wellbore | [] |
| [F] | force matrix | [F] |
| g | gravitational constant | [L/T ²] |
| h | hydraulic potential or hydraulic head | [L] |
| H | total (Bernoulli) head | [L] |
| \hat{H} | approximation for H used in finite element formulation | [L] |
| H _o | total head at outer boundary | [L] |
| H _w | total head in aquifer at radius of wellbore | [L] |
| k | absolute roughness of fracture surface | [L] |

NOTATION -- Continued

| <u>Symbol</u> | <u>Parameter/Quantity</u> | <u>M-F-L-T¹ Dimension²</u> |
|------------------|---|--|
| K | hydraulic conductivity | [L/T] |
| K _n | normal fracture stiffness | [(F/L ²)/L] |
| K _s | shear fracture stiffness | [(F/L ²)/L] |
| k/D _h | relative roughness | [] |
| l | distance in direction of flow | [L] |
| L | length of wellbore from fracture inlet to pump intake | [L] |
| L() | differential operator | [] |
| m | exponent in Missbach equation | [] |
| n | exponent in Rorabaugh equation or fracture stiffness equation | [] |
| N | number of nodes in finite element formulation | [] |
| p | wetted perimeter | [L] |
| P | pressure | [F/L ²] |
| q _u | unconfined compressive strength | [F/L ²] |
| Q | volumetric discharge rate | [L ³ /T] |
| Q _c | critical discharge rate | [L ³ /T] |
| Q _w | volumetric discharge per unit width | [L ² /T] |
| r | radial coordinate or distance | [L] |
| r' | natural logarithm of r (ln r) | [] |
| r _c | critical radius | [L] |
| r _D | dimensionless radial distance | [] |

NOTATION -- Continued

| Symbol | Parameter/Quantity | M-F-L-T ¹ Dimension ² |
|-----------|--|--|
| r_o | radius of influence of well | [L] |
| r_w | radius of wellbore | [L] |
| R | total flow region | [L] |
| Re | Reynolds number | [] |
| R_h | hydraulic radius | [L] |
| R_l | relaminarization index | [] |
| R_L | linear flow sub-region | [L] |
| R_N | non-linear flow sub-region | [L] |
| R_o | overall Reynolds number | [] |
| s | total head loss or drawdown ($H_o - H_w$) | [L] |
| s_e | exit head loss | [L] |
| s_k | skin factor | [L] |
| s_l | linear aquifer head loss | [L] |
| s_n | non-linear aquifer head loss | [L] |
| s_w | wellbore head loss | [L] |
| S_1 | stiffness coefficient | [F/L ³] |
| S_2 | stiffness coefficient | [*] |
| [S] | stiffness matrix | [F/L] |
| t | thickness of aquifer | [L] |
| T | transmissivity | [L ² /T] |
| \bar{T} | average transmissivity $[(T_1 + T_2)/2]$ multiplied by 2π | [L ² /T] |

NOTATION -- Continued

| Symbol | Parameter/Quantity | M-F-L-T ¹ Dimension ² |
|-----------------|--|--|
| U | free streamline velocity | [L/T] |
| v | macroscopic fluid velocity | [L/T] |
| v _w | velocity of flow in wellbore | [L/T] |
| v | average fluid velocity in a conduit | [L/T] |
| w | dimension of fracture normal to flow and transverse to aperture | [L] |
| z | vertical coordinate or distance or elevation head | [L] |
| 2b | fracture aperture | [L] |
| 2b ₀ | initial fracture aperture | [L] |
| α | coefficient of hydraulic resistance in Darcy-type equation | [T/L] |
| β | coefficient of hydraulic resistance in Missbach equation | [*] |
| δ | displacement | [L] |
| ε | relative error for convergence | [] |
| η | kinetic energy correction factor | [] |
| θ | relaxation factor in Gauss-Siedel iteration | [] |
| λ | coefficient in Darcy-Weisbach equation (Note: λ = 4 C _f where C _f is Fanning friction factor also used in fluid mechanics and hydraulics) | [] |
| μ | Poisson's ratio | [] |
| ν | kinematic viscosity of fluid | [L ² /T] |
| ξ | head loss coefficient for exit loss or wellbore flow | [] |

NOTATION -- Continued

| Symbol | Parameter/Quantity | M-F-L-T ¹ Dimension ² |
|------------|---|--|
| ρ | mass density of fluid | [M/L ³] |
| σ_h | horizontal, lateral, or radial stress | [F/L ²] |
| σ_n | normal stress | [F/L ²] |
| σ_v | vertical or axial stress | [F/L ²] |
| ψ | empirical coefficient in laminar flow laws of Louis and Lomize | [] |
| ω | nodal basis or weighting function in finite element formulation | [] |

¹ mass-force-length-time

² [] = dimensionless, [*] = variable

SELECTED TERMINOLOGY

This study deals with a topic that is interdisciplinary, using and combining ideas developed in the fields of hydrogeology; soil science; and petroleum, geotechnical, mining, geothermal, and hydraulic engineering. Predictably, this involves terminology that varies from one discipline to another.

The following list of potentially problematic terms is not meant to provide authoritative definitions. Its only purpose is to state the meaning of the term as used in this thesis. This should prevent, not create, argument.

aquifer - any water-bearing geologic unit regardless of its yield to a well or relative hydraulic conductivity

exit loss - head loss due to flow of ground water from an aquifer into a wellbore; sometimes referred to in the literature as an entrance loss

fracture - any planar or curva-planar discontinuity in rock regardless of its origin, size, or orientation; intended as a generic term to include joints, fissures, bedding plane partings, etc.

hydraulic head - the hydraulic potential or energy per unit weight, h , comprising elevation head, z , and pressure head, $P/(\rho g)$

$$h = z + P/(\rho g)$$

linear flow - flow in which the hydraulic gradient varies in direct proportion to the velocity of the fluid to the first power; also referred to in the literature as laminar, streamline, Darcy, or Darcian flow

SELECTED TERMINOLOGY -- Continued

non-linear flow - flow in which the hydraulic gradient varies in direct proportion to the velocity of the fluid to a power greater than 1; a general term encompassing both transitional and fully developed turbulent flow; also referred to in the literature as "non-Darcy or simply turbulent flow (see also "turbulent flow" and "transitional flow")

parallel flow - flow in which the streamlines, or net direction of movement of eddies in the case of turbulent flow, are straight and parallel; not to be confused with linear flow; used to differentiate from radial flow

total head - the total (or Bernoulli) potential or energy per unit weight, H , comprising hydraulic head, h , and velocity head, $v^2/2g$

$$H = h + \frac{v^2}{2g} = z + \frac{p}{\rho g} + \frac{v^2}{2g}$$

transitional flow - flow in which the hydraulic gradient varies in direct proportion to the velocity of the fluid to a power between 1 and 2

turbulent flow - in keeping with common usage in the literature, used interchangeably with non-linear or non-Darcy flow; flow in which the hydraulic gradient varies in proportion to the fluid velocity to the 2nd power specifically will be referred to as "fully developed turbulent flow"

two-regime flow - flow which is linear in one sub-region of the flow field and non-linear in the other sub-region

1.0 INTRODUCTION

1.1 Statement of problem

In dewatering operations for mining and civil engineering projects, the objective is to depress the potentiometric surface of the ground water in a soil and/or rock mass over a specific area for one or more of the following reasons:

- 1) to drain material to be excavated,
- 2) to reduce flow of ground water into an excavation to a minimal or tolerable level, or
- 3) to reduce fluid pressures in order to improve stability (e.g., to prevent floor heave or to allow slopes to be excavated at a greater angle).

Several different dewatering techniques have been developed, the most common of which are installation of horizontal drainholes into the wall(s) of an existing excavation, driving of a drainage gallery behind a working face, or drilling pumping wells on the perimeter of the excavation. The need to dewater prior to excavation and cost considerations frequently make a series of vertical wells the most attractive system. This study specifically addresses the problem of improving the efficiency of such a dewatering system, although its findings should have applications in other areas such as ground-water resource development, geothermal energy development, and hydrocarbon extraction.

The total drawdown or head loss induced in an indi-

vidual well by pumping can have as many as four components (shown in Figure 1.1):

$$s = s_l + s_n + s_e + s_w \quad (1.1)$$

where

s = total head loss or drawdown,

s_l = linear aquifer head loss or energy lost in overcoming viscous drag as ground water moves through the aquifer under low velocity, laminar conditions,

s_n = non-linear aquifer head loss or energy lost during flow through the high velocity region in the immediate vicinity of the well,

s_e = exit head loss resulting from water moving from the aquifer into the wellbore, and

s_w = wellbore head loss resulting from flow in the wellbore to the pump intake.

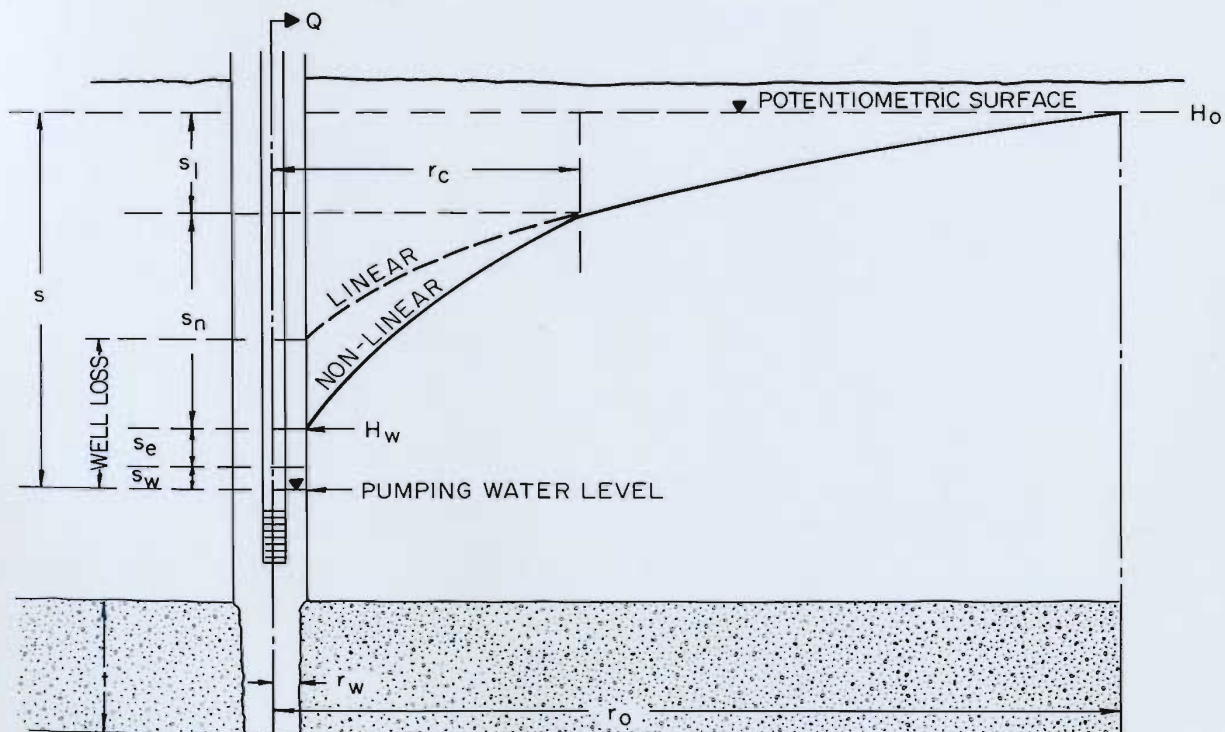


Figure 1.1 Components of drawdown in a well (after Bruin and Hudson, 1955)

The linear aquifer head loss obeys Darcy's law, which can be written for radial flow in scalar form as

$$dH/dr = \alpha v. \quad (1.2)$$

where

H = total head,

r = radial distance,

α = coefficient of hydraulic resistance, and

v = macroscopic velocity of fluid.

This indicates that the gradient of total head is directly proportional to the velocity to the first power. For reasons which will be explained in a following section, the current problem will be formulated in terms of total head instead of hydraulic head as is customarily done in most ground-water flow problems. Since

$$Q = v \cdot A = v \cdot 2\pi r \cdot t, \quad (1.3)$$

where

Q = volumetric discharge rate,

A = cross-sectional area of flow, and

t = thickness of aquifer,

Equation 1.2 can be written as

$$dH = \frac{\alpha Q}{2\pi t} \frac{dr}{r}. \quad (1.4)$$

Integrating between arbitrary radial distances r_1 and r_2 , it can be shown that for confined flow in an aquifer of constant thickness

$$H_2 - H_1 = s_1 = \frac{\alpha Q}{2\pi t} \ln \frac{r_2}{r_1} \quad (1.5)$$

The non-linear aquifer head loss can be described by similar relationships, either

$$dH/dr = \beta v^m, \quad (1.6)$$

commonly referred to as Missbach's law, or

$$dH/dr = av + bv^2, \quad (1.7)$$

known as the Forchheimer equation, where

a, b, β = coefficients of hydraulic resistance, and

m = exponent greater than 1.

If Equation 1.6 is used and if it is assumed, as it is in fully developed turbulent flow, that the value of m is 2 (Vennard and Street, 1976), Equation 1.6 can be rewritten as

$$dH = \frac{\beta Q^2}{(2\pi t)^2} \frac{dr}{r^2} \quad (1.8)$$

Integrating between arbitrary distances r_3 and r_4 ,

$$H_4 - H_3 = s_n = \frac{\beta Q^2}{(2\pi t)^2} \left[\frac{1}{r_3} - \frac{1}{r_4} \right] \quad (1.9)$$

is obtained.

By analogy to the findings of classical experimental work on flow in pipes, the last two components (Equation 1.1 on page 2) of well drawdown can both be related to the kinetic energy of the fluid in the general form

$$s_e \text{ or } s_w = \xi \frac{\bar{v}^2}{2g} \quad (1.10)$$

where

$$\begin{aligned}\xi &= \text{head loss coefficient,} \\ \bar{v} &= \text{average fluid velocity, and} \\ g &= \text{gravitational constant,}\end{aligned}$$

and, therefore, to the discharge rate squared.

Incorporating the concept of critical radius, defined as the distance from the center of the well to the point in the aquifer where the transition from linear to non-linear flow occurs (Figure 1.1), Equation 1.1 (page 2) can be expressed quantitatively as

$$s = \frac{\alpha Q}{2\pi t} \ln \frac{r_o}{r_c} + \frac{\beta Q^2}{(2\pi t)^2} \left[\frac{1}{r_w} - \frac{1}{r_c} \right] + C_e Q^2 + C_w Q^2 \quad (1.11a)$$

or

$$s = C_1 Q \ln \frac{r_o}{r_c} + C_n Q^2 \left[\frac{1}{r_w} - \frac{1}{r_c} \right] + C_e Q^2 + C_w Q^2 \quad (1.11b)$$

where

r_w = radius of wellbore,

r_o = distance from center of well to point of negligible drawdown (radius of influence),

r_c = critical radius,

C_1 = linear or laminar flow coefficient,

C_n = non-linear or turbulent flow coefficient,

C_e = exit loss coefficient, and

C_w = wellbore flow loss coefficient.

Similar equations including just the first two terms have been proposed by Rorabaugh (1953), Baker (1955), and Bruin and Hudson (1955).

The first term on the right hand side of Equations 1.11a and 1.11b, the linear component of drawdown, is the one most familiar to the majority of workers in ground water. The value of the laminar flow coefficient can be quite variable, depending on whether the aquifer is confined or unconfined, its relative isotropy and homogeneity, and whether hydrologic boundaries or leaky adjacent beds are present. Partial penetration of the pumping well and partial dewatering of the aquifer during pumping will also influence the "effective" value of this coefficient. All of these factors have been the subject of considerable research in aquifer and well hydraulics, however; and, for flow through porous media, a vast, well-known literature exists.

The wellbore loss, the exit loss, and the excess drawdown in the aquifer (relative to that which would occur if linear flow conditions prevailed throughout), due to non-linear flow create what is collectively referred to as well loss. Referring to Figure 1.1 and Equation 1.11b, it can be described by:

$$\text{well loss} = C_n Q^2 \left[\frac{1}{r_w} - \frac{1}{r_c} \right] - C_l Q \ln \frac{r_c}{r_w} + C_e Q^2 + C_w Q^2 \quad (1.12)$$

In most dewatering systems using wells, it is normally desirable to achieve the required drawdown with the minimum number of wells and sizes of pumps. Usually this also involves trying to pump each well at or near its maximum rate.

Figure 1.2 schematically indicates how well loss comprises a parasitic drawdown which hinders these objectives. The drawdown in the aquifer beyond the critical radius is, for the given set of aquifer properties, a function of discharge rate alone. Since discharge is limited by the available drawdown in the well, any well loss will result in the discharge being less than the maximum attainable. Consequently, less drawdown is propagated into the aquifer by the wells. This means that more wells at closer spacings would be required to achieve the same composite drawdown as that which would be produced by fewer wells not experiencing such losses. Another negative effect introduced into the system by well loss is that, for the given discharge rate, the pumping lift is unnecessarily high. Larger, more expensive pumps (with respect to both capital and operating costs) might be required.

These inefficiencies can have significant economic consequences. At a recent international symposium (Argall and Brawner, 1979), several papers contained the warning that in future mining operations, the effectiveness and cost of dewatering or depressurizing will likely be two of the primary factors determining the technical and economic feasibility of a mine which encounters either significant quantities of water or high pore pressures in adjacent rocks.

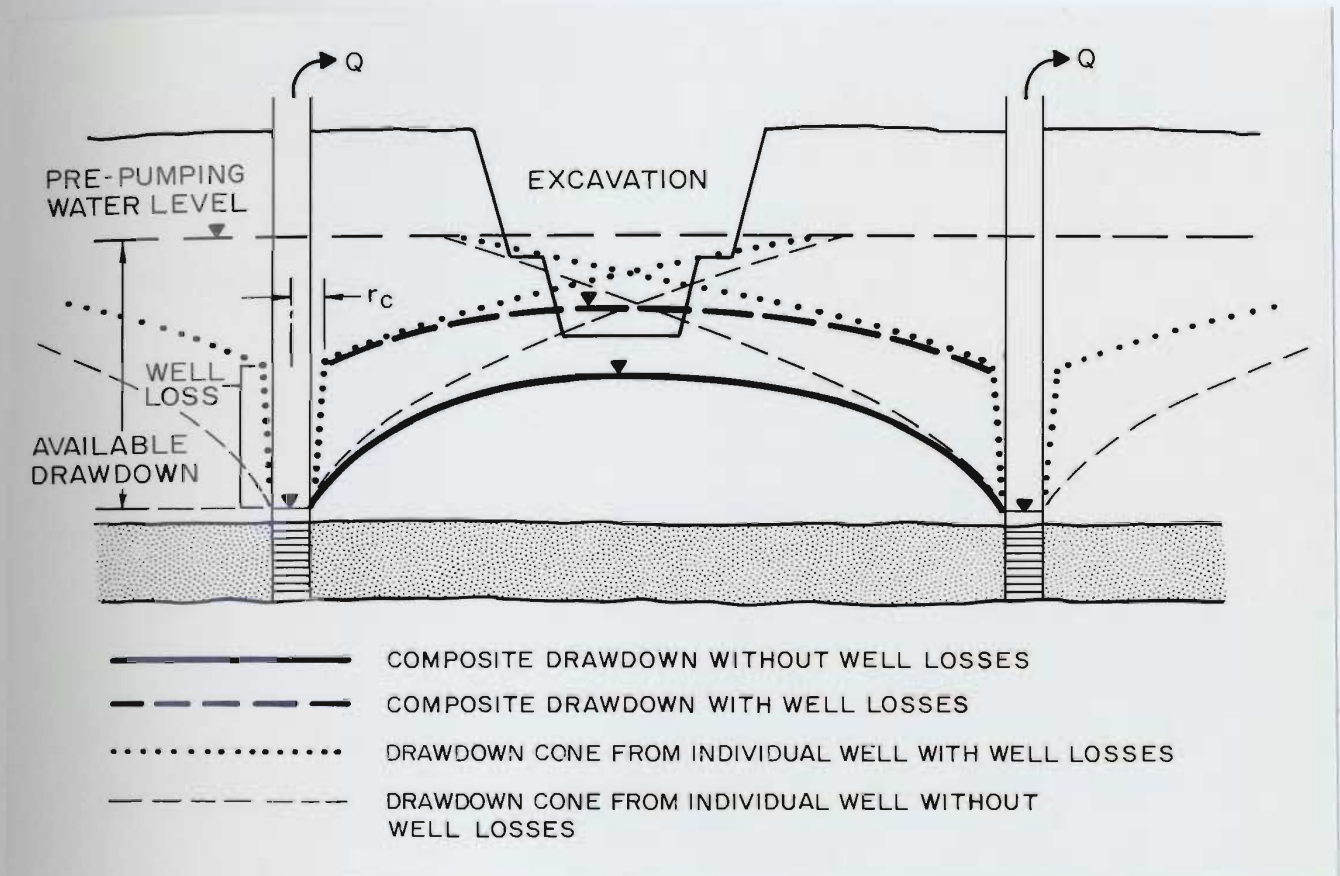


Figure 1.2 Schematic diagram of two-well depressurizing system showing effects of well losses

Despite easily recognizable problems associated with well losses, the research devoted to their understanding has been extremely limited. Sauveplane (1982) noted that the past and continuing efforts of most ground-water investigators have concentrated on evaluating only the linear aquifer response. Ramey (1982), however, sees a significant crossover in the fields of ground-water hydraulics and petroleum

engineering. Whereas the petroleum engineer has focused traditionally on the production characteristics of the well, recent interest and research have been directed toward a better understanding of the response of the entire reservoir. Conversely, the ground-water hydrologist, who historically has been more interested in aquifer hydraulics, has become increasingly aware of problems associated with the well itself.

The traditional method for evaluating well loss is by means of a multi-rate pumping or "step-drawdown" test. The results of this test are usually expressed in the form:

$$s = BQ + CQ^n \quad (1.13)$$

where

B = aquifer coefficient

C = well coefficient, and

n = exponent.

The exponent is usually considered to be 2, but its value is the subject of some controversy which is discussed in Section 1.3.3. Comparison of Equation 1.13 with Equation 1.11b (page 5) suggests they are equivalent, presuming n is 2 and that the three terms in Equation 1.11b containing Q^2 can be lumped into a single term. It has been found that Equation 1.13 with its empirically determined coefficients (and exponent, if other than 2) gives reasonable estimates of the drawdown which can be expected in a well at various pumping

rates, provided they are within the range tested. This purely empirical approach, however, provides little information on the actual nature of the well loss and no basis on which to evaluate how the wellbore and its immediate environs might be altered to improve the performance of the well.

Although well loss can occur in almost any pumping well, the problem is much more acute in aquifers whose primary source of permeability is fractures as opposed to intergranular porosity (Mackie, 1982; Uhl et al., 1976; Brereton, 1979; Kelly et al., 1980). For this reason, together with the potentially valuable application of its findings to a practical problem such as mine dewatering (which invariably involves such aquifers), this investigation focuses specifically on the problem of well losses in wells completed into fractured rock aquifers.

1.2 Objective and scope

The objective of this investigation was to develop a better understanding of the nature, causes, and magnitude of head losses that occur in the immediate vicinity of a wellbore completed into a fractured rock aquifer. Specific questions addressed were:

- 1) What are the magnitudes of well losses?
- 2) How wide is the zone around the wellbore where non-linear flow occurs?

- 3) What factors affect well loss, particularly the non-linear aquifer head loss?
- 4) Can current knowledge in fractured rock hydraulics be incorporated into a more deterministic model for the response of a well to pumping? In other words, can meaningful coefficients and boundary conditions, based on empirically derived flow laws for rough fractures, be applied to the relationship expressed by Equation 1.11b (page 5)?
- 5) What do the results from the classical step-draw-down test actually indicate?
- 6) What practical solutions are there for minimizing or eliminating well losses?

To answer these questions and to achieve the overall objective of understanding well losses on a more deterministic level, a program of investigation involving the three following primary tasks was undertaken:

- Task 1: Design, construct, and test a large scale, radial flow model with a single fracture.
- Task 2: Develop a numerical (finite element) model including both linear and non-linear fracture flow laws and the deformational response of the fracture(s) to flow-induced changes in effective stress.
- Task 3: Compare the results predicted by the numerical model to those produced by the physical model.

In the models studied, the fracture(s) were horizontal and the wellbore was vertical. The response of non-horizontal (except for the other limiting case of vertical) fractures to pumping could be highly dependent on shear displacement. Introduction of this extremely complex interaction, on which little basic research has been conducted, would overly complicate the situation and make it

very difficult to draw meaningful conclusions at this stage of understanding. Similarly, a non-orthogonal intersection between the fracture and wellbore should be the subject for another specific investigation.

It should be emphasized that focusing attention on a single fracture is not unrealistic. Several investigators (e.g., Da Cruz and De Quadros, 1984; Williamson and Woolley, 1980; and Baker, 1955) have concluded, based on the results of field data, that one fracture often totally dominates the production or injection rate of a well.

1.3 Previous work

The discussion of previous work in the primary area of ground-water flow in fractures will be preceded by a review of previous work in a few broader, but related areas of investigation.

1.3.1 Non-linear and two-regime flow

Most studies of non-linear (or non-Darcy) flow of ground water have dealt with the problem in porous media. Hannoura and Barends (1981) provide an excellent review of this work. The common approach is to describe the flow by means of a power series relationship, the most popular of

which is the Forchheimer equation (Equation 1.7 on page 4) where the coefficients a and b are considered to be constants which are characteristic of the medium (e.g., grain size, shape, uniformity) and the fluid. Their values normally are determined by fitting quadratic curves to data from permeameter tests of the particular granular material.

Stark and Volker (1967) show that theoretically a and b cannot be constant, but rather are dependent on the value of the Reynolds number. However, they conclude that, within the range of Reynolds numbers usually encountered in flow through porous media, the coefficients remain essentially invariant. Proponents of the Forchheimer equation note that the transition from laminar to fully turbulent flow is usually quite smooth in a porous medium (as opposed to the relatively abrupt change in flow through pipes) and that its use to describe conditions over a two-regime flow field (i.e., linear in one sub-region, non-linear in the other) produces results that correlate well with experimental evidence (Dudgeon, 1984).

Most relevant work investigating two-regime flow to wells has been done in Australia. The results of a very comprehensive study including numerical, laboratory, and field investigations are presented by Cox (1977), Huyakorn and Dudgeon (1976 and 1974), Dudgeon et al. (1973), Huyakorn (1973), and Dudgeon and Au Yeung (1969). In those studies,

Darcy's law is used to describe flow in the linear sub-region and the Forchheimer equation, with constant, empirically determined coefficients, is used in the entire non-linear sub-region (both transitional and fully turbulent, if that limit is reached).

Basak (1978) objects to the use of constant coefficients in the Forchheimer equation when applying it to radial flow to a well. He demonstrates that the value of b is particularly sensitive to the Reynolds number, and feels that constant values for a and b do not correctly represent conditions in a distinctly two-regime flow field.

There also appears to be some misconception, as exemplified by Phipps and Khalil (1975), regarding the equivalence of the Forchheimer equation and Equation 1.13 (page 9) with n equal to 2. It is sometimes assumed that there is a relationship based on the continuity equation between B and a and between C and b . This simple, but erroneous, mathematical manipulation totally obscures the important physically based difference between the two equations. It should be remembered that the coefficients in the Forchheimer equation are obtained from a permeameter test in which, under the given flow rate of each step, the velocity is essentially the same throughout (since the macroscopic cross-sectional area of the permeameter is constant). In other words, each data point represents conditions in a single flow regime.

(which may be either linear or non-linear). The values of the constants a and b are then derived from a "best fit" to the head loss versus velocity relationship over the entire range tested.

In a radial flow field, however, the velocity varies not only as a function of discharge rate but also of distance from the well. Therefore, if the given discharge rate exceeds the critical discharge rate (i.e., the rate above which non-linear flow begins in the vicinity of the well), the measured head loss will reflect components from two flow regimes. Intuitively (this will be developed in more detail in Chapter 2), as the flow rate increases, the critical radius also increases. Hence, as shown by once again comparing Equations 1.11a or 1.11b (page 5) and 1.13 (page 9), the coefficients B and C of Equation 1.13, which would include the radial distance terms explicit in Equations 1.11a or 1.11b, must change as the flow rate increases.

While non-linear flow in the aquifer is considered to be a relatively rare occurrence in porous media (such as in the vicinity of high yield wells in very coarse gravels), it probably is common close to the borehole in many wells in fractured rock aquifers. The related research, which is quite limited, will be discussed in Section 1.3.4.

1.3.2 Exit loss and wellbore effects

Most interest in what generally can be referred to as "exit loss" has been concerned with the effects of well screens and gravel packs which are used primarily in wells completed in unconsolidated sediments (Garg and Lal, 1971; Mogg, 1959; Peterson, 1957; Peterson et al., 1955; and Li, 1954). There is some similarity between a well producing from discrete fractures and a well in porous media which is lined with a perforated casing or with a screen of very limited entrance area. However, the findings of that research do not appear to be particularly relevant to the current study.

Wellbore diameter generally is not considered a very important parameter in the yield of a well. Assuming completely Darcian flow in the aquifer and no exit losses, it can be shown theoretically that the increase in yield resulting from doubling the wellbore size is on the order of 10 percent for a fully penetrating well in a confined aquifer. James (1970), however, states that the flow rates in many geothermal wells which he had evaluated had been found to vary in direct proportion to the borehole diameter. This suggests that the assumptions made in the preceding calculation do not hold in these cases. Norris (1976) conducted a step-drawdown test before and after a well in a dolomitic aquifer had been reamed from a diameter of 0.25 to

0.30 m. He found that this very minor change in wellbore diameter reduced the apparent well loss component by 40 to 60 percent at the higher end of the pumping rate range (12 to 82 l/s) over which he conducted the tests.

Using a plastic parallel plate model with air as the fluid for testing, Murphy and Pearce (1980) investigated the pressure losses incurred during the transition from radial convergent flow in a fracture to longitudinal flow within an orthogonal wellbore. They consider the exit loss to be complete where the longitudinal pressure gradient becomes constant within the wellbore. An empirical equation for this loss

$$s_w = 0.23 \left(\frac{D}{2b} \right)^{1.41} \left(\frac{v_w^2}{2g} \right) \quad (1.14)$$

where

D = diameter of wellbore,

$2b$ = fracture aperture, and

v_w = velocity of fluid in wellbore

can be derived from the data presented by Murphy and Pearce (1980).

The head loss due to flow in the wellbore can be estimated from the classic Darcy-Weisbach equation for flow in circular conduits. Normally it is a small and frequently disregarded source of well loss, but Stoner et al. (1979) demonstrate that design of the diameter of a deep well should consider this potential loss.

1.3.3 Empirical determination of well loss

Procedures for empirically estimating the magnitude of well loss in a pumping well have been utilized for many years in both the ground-water and petroleum industries. Ramey (1982) summarizes the somewhat parallel development in these two fields and compares and contrasts their technologies.

Jacob (1947), a ground-water hydrologist, proposed a technique by which the components of drawdown due to other than linear flow in the aquifer could be determined from results of a modified aquifer test. This is known as the step-drawdown test. The equation he proposed was

$$s = BQ + CQ^2 \quad (1.15)$$

where s , B , and C are the same as in Equation 1.13 (page 9). The recommended field procedures and method of analysis by which the coefficients B and C can be calculated are described in Jacob (1947).

Step-drawdown tests conducted by Rorabaugh (1953) produced data to which he could not make satisfactory fits using Equation 1.15. As an alternative, he proposed a more generalized form in which the exponent in the non-linear term was not restricted to the value of 2. The so-called Rorabaugh equation has already been presented as Equation 1.13. His graphic technique for determining the three

unknowns B, C, and n are described in Rorabaugh (1953). He found that the values obtained for n frequently were greater than 2, and cited examples of field data suggesting that 2.5 was a more typical value.

There is continuing debate over whose method achieves more meaningful results and whether or not Rorabaugh's method is supportable by basic hydraulic principles (Mogg, 1969). Clark (1977) and Bierschenk (1964) report satisfactory fits to their data from alluvial wells using Jacob's method. From the results of their own data and on theoretical grounds, both Brereton (1979) and Eden and Hazel (1973) conclude that the value of n does not, and should not, exceed 2. The latter investigators also propose a slightly modified, more rigorous method of graphic solution.

Rorabaugh's method of evaluation is supported by Lennox (1966) and Norris (1976). In fact, Lennox (1966) reports obtaining values of n as high as 3.5 from tests of wells completed into sedimentary rocks in Alberta. It is noteworthy that these two investigations which generated values of n greater than 2 involved wells in rock aquifers where fractures likely provided at least part of the permeability.

Mackie (1982) examined the results of more than 20 carefully controlled step-drawdown tests of wells in fractured rock aquifers and concluded that most of them could be categorized into one of three "signature responses". These responses are depicted best on a graph of

specific drawdown, s/Q , versus discharge rate (Figure 1.3). Dividing both sides of Equation 1.13 (page 9) by the discharge rate, it can be shown that

$$s/Q = B + CQ^{n-1}. \quad (1.16)$$

The straight, horizontal line (Curve 1) on Figure 1.3 represents tests during which all flow is laminar. In this case, the right hand side of Equation 1.16 becomes simply equal to B , whose value is presumed to be constant.

Curve 2 on Figure 1.3 indicates the production-drawdown response when, up to a critical discharge rate, all flow is laminar; but above that rate, head loss due to fully turbulent flow comprises an ever increasing major portion of the total drawdown. This is the response predicted by the Jacob equation (Equation 1.15, page 18) with B and C constant and n equal to 2. The total specific drawdown is composed of a constant component with value B and, beyond the critical discharge rate, Q_c , a component linearly proportional to the discharge rate. Mackie (1982) states that in many tests, only the latter portion of the curve is evident. This indicates that non-linear flow occurs even at relatively low flow rates.

The response which Mackie (1982) concludes is most common when conducting step-drawdown tests in fractured rock wells, is the concave upward curve shown by Curve 3. This curve might or might not have a short linear (either horizontal or sloping) segment at the lower production rates.

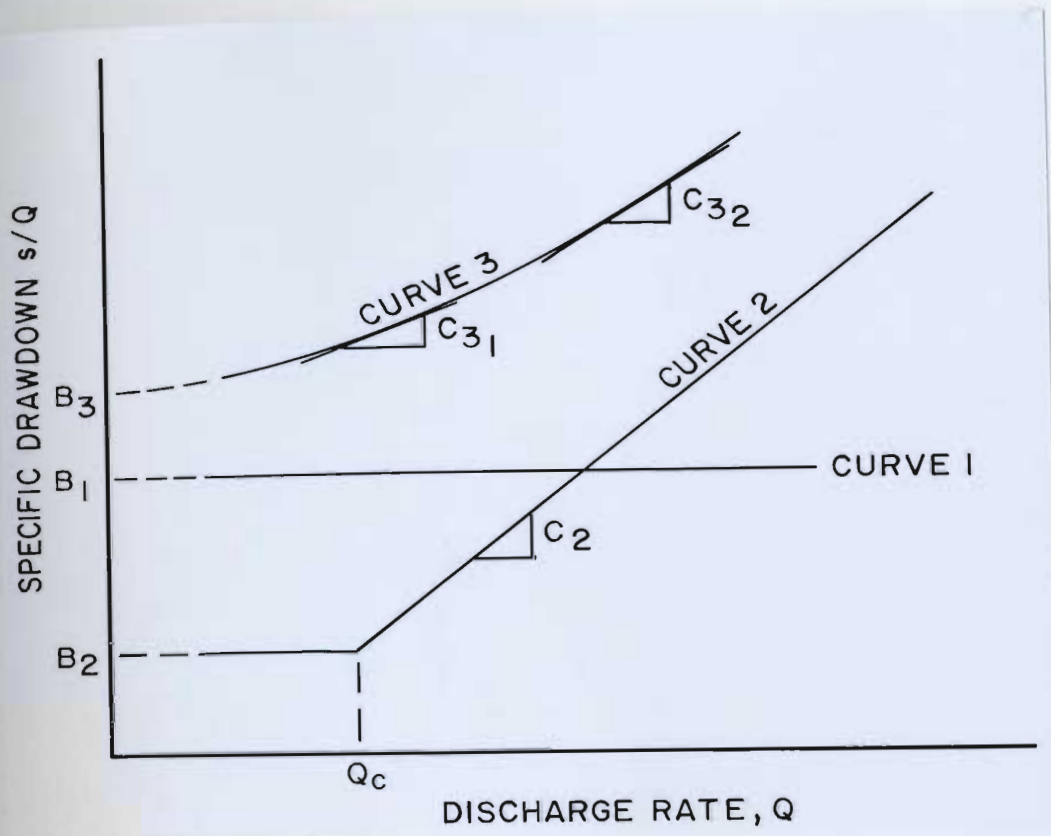


Figure 1.3 Typical production-drawdown responses of water wells in fractured rock aquifers (after Mackie, 1982)

He interprets this response as reflecting changes in the value of C due to variation in fracture geometry, roughness, and permeability.

It should be noted that Mackie (1982) considers the value of the exponent n to be 2. Therefore, he attributes any departure from a constant slope in the higher production rate part of the plot to be the result of a change in the value of the non-linear flow coefficient. Those who support Rorabaugh (1953) might argue that this response is indicative of an exponential value greater than 2. An alternative

explanation is that it represents the smooth transition from laminar to fully turbulent conditions in the non-linear sub-region near the well (Dudgeon, 1984).

A concept analogous to well loss was developed in the petroleum industry almost simultaneously by Hurst (1953) and van Everdingen (1953) to explain the frequently observed non-linearity in pressure build-up data (the equivalent of the recovery phase in ground-water testing) following flow tests in oil wells. Since the relatively low production rate of most oil wells and the viscosity of the fluid normally eliminate turbulent flow as a possible cause, the so-called "skin effect" is attributed to reduced permeability in the formation immediately adjacent to the borehole. It is thought that the greater impedance to flow is the result of drilling fluid and fine cuttings invading the formation during drilling operations. No physical dimension is ever given to this zone; in fact, it is often referred to as being of "infinitesimal" thickness.

Like well losses, the skin effect is considered to be independent of time; and the "skin factor" is considered to be constant for a given well. Many of the type curves for well test analysis which evolved during the 1960's and 1970's included this factor as a parameter (Earlougher, 1977; Raghaven, 1977; Matthews and Russell, 1967). More recently, the concept of skin effect has been expanded further to include the effects of partial penetration and

to include permeability stratification near the wellbore (Ahmed, 1982).

In field and theoretical evaluations of gas wells, it was recognized that non-Darcy flow also could have a significant effect on the performance of these wells, particularly those producing from natural or artificially induced fractures (Guppy et al., 1981; Holditch and Morse, 1976; and Wattenbarger, 1967). In order to describe the observed production-pressure loss relationships, an equation combining both skin and turbulence effects has been developed by Ramey (1982). Using ground-water notation to emphasize the similarity to Equation 1.13, it can be written as

$$s = BQ + (s_k + CQ)Q \quad (1.17)$$

where s_k is the skin factor and the other terms are the same or analogous to those previously defined. Ramey (1982) includes the graphic procedure by which the various components can be estimated.

Another expression equivalent to Equation 1.17 also is given in van Golf-Racht (1982). In his development, however, it is noteworthy that the value of C includes the term $[1/r_w - 1/r_o]$. This indicates that van Golf-Racht considers the non-linear flow coefficient to be effective over the entire flow field, as with a Forchheimer-type flow law, and not just inside the critical radius (refer to Equations 1.11a or 1.11b on page 5).

1.3.4 Flow in fractures

From ~~somewhat~~ parochial beginnings in ground-water hydrology, soils science, and chemical, hydraulic, geotechnical, geothermal, and petroleum engineering, the study of fluid flow in fractured rocks has evolved during the past 20 years into a special, yet multi-disciplinary, field of its own. Reviews of its historic development, current state of knowledge, and direction of future research and applications are presented by Wittke (1973) and Gale (1982a).

Depending on the scale of a particular problem, the developing theory in fractured rock hydrology can be used either 1) to formulate an "equivalent porous medium" (Snow, 1969) and thereby complement the continuum approach traditionally (and out of necessity) used to describe flow in granular materials, or 2) as the basis for the alternative discrete approach in which the geometric, hydraulic, and geomechanical properties of individual fractures are considered (Wilson and Witherspoon, 1970). The current problem of trying to understand the nature of head losses near the well in a fractured rock aquifer logically is more amenable to the latter approach.

1.3.4.1 General concepts

An obvious analogy to flow within a fracture is flow between two plates. For the highly idealized situation of laminar flow between smooth, parallel surfaces, an exact solution (Kovacs, 1981) of the Navier-Stokes equation yields

$$v = \frac{ge^2}{12\nu} \frac{dh}{dl} \quad (1.18)$$

where

e = width of slit between the plates,

ν = kinematic viscosity of the fluid, and

l = distance in the direction of flow.

This solution, referred to as Poiseuille's law, has been known since the 19th century. By combining it with the continuity equation, it can be shown that

$$Q_w = \frac{ge^3}{12\nu} \frac{dh}{dl} \quad (1.19)$$

where Q_w is the volumetric flow rate per unit width normal to the direction of flow (also referred to as the flux). Equation 1.19 has led to the expression "cubic law" commonly used in fractured rock hydrology.

Real fractures under field conditions would be expected to differ significantly from such an idealized model. The primary factors which control fluid movement through a real fracture are the 1) aperture and 2) relative roughness of

the fracture and 3) the Reynolds number which characterizes the flow.

There are two meanings of aperture and relative roughness which need to be considered. It should also be noted that these parameters are not always explicitly defined in the literature and that there is an inconsistency (e.g., Lomize, 1951; Parrish, 1963; Louis, 1969; Sharp, 1970) which is reconciled in Gale et al. (1985).

The geometric aperture and roughness (hereafter referred to simply as aperture and roughness), as used in this thesis, are shown in Figure 1.4. Aperture, designated $2b$, is the transverse distance between the two lines describing the "average" fracture surfaces. For a given fracture segment, the two surfaces are considered to be parallel. In his experimental work, Lomize (1951) quantified average apertures by dividing the volume of fluid extracted from his single-fracture models by the length and width of the models. Absolute roughness, k , is the amplitude of the "average" irregularity or asperity. Relative roughness is one of the most important parameters for describing flow in closed conduits. In a fracture, relative roughness is defined in this thesis as:

$$\frac{k}{D_h} = \frac{k}{2(2b)} \quad (1.20)$$

where D_h is known as the hydraulic diameter (refer to Appendix A).

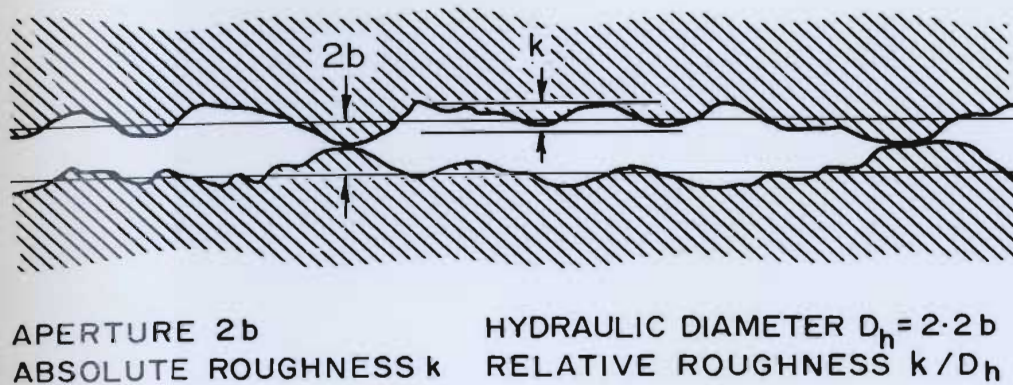


Figure 1.4 Geometric properties of a fracture

Estimates of aperture to an order of magnitude can be made by visual inspection of core, borehole images taken by camera, television, or acoustic televiewer and impression packers. Similar measurements of roughness can be obtained by means of microscopic examination of resin-impregnated samples (using methods developed by Wardlaw, 1976, for porous media) or direct profilometric techniques (Swan, 1983). More precise measurements need to be made, however, in conjunction with hydraulic measurements.

Obtaining a complete description of fracture geometry over any significant volume of rock is as impossible, of course, as describing individual pores in a granular material. Therefore, indirect techniques frequently are used. In the most common indirect method, an effective aperture is

estimated with or without consideration of roughness, from in-situ or laboratory flow test data. The calculation of effective aperture is based either on the highly simplified Poiseuille's law or on empirically derived flow laws (details are given in Appendix B). A positive aspect of this method, however, is that relatively large areas of the fracture can be "sampled".

1.3.4.2 Development of empirical flow laws

Basic laws for flow in fractures have been developed in most cases using models of artificial fractures and applying the friction factor-Reynolds number approach traditionally used to characterize flow through pipes. Appendix A includes derivations of the equivalent parameters used in this technique.

Lomize (1951) conducted parallel flow tests on smooth and roughened metal plates and corrugated plexiglas strips 0.05 m wide by 0.20 m long with measurable apertures of 0.7 to 10.2 mm and relative roughnesses of 0.027 to 0.43. He found his results were highly dependent on roughness, and distinguished between "smooth", defined as having a relative roughness less than or equal to 0.033, and "rough", having a relative roughness greater than 0.033, fractures. Lomize concluded that for his smooth fractures, the friction factors developed either theoretically from the parallel plate

model (Poiseuille's law) or on the basis of the classical experimental work on pipes by Blasius and Nikuradse adequately described the flow relationships he observed. For rough fractures, however, he proposed two new friction factors, one for laminar and one for fully developed turbulent flow, that are given in Table 1.1.

Louis (1969) conducted a similar series of tests using fractures formed between concrete slabs of various surface roughness. The apertures he simulated were in the range of 2.0 to 25.5 mm with relative roughnesses of 0.0005 to 0.36. He concurred with Lomize's (1951) findings with respect to the smooth-rough distinction and the applicability of the existing flow laws to the smooth fractures. In the case of rough fractures, however, he proposed slightly different friction factors for laminar and fully turbulent flow (refer to Table 1.1). A Moody-type diagram generated by Louis is included as Figure 1.5.

Louis (1969) also includes a roughness versus Reynolds number plot indicating flow fields in which he felt various friction factors are applicable. A version of this, as modified by Rissler (1978), is given in Figure 1.6.

One other series of basic flow tests using the friction factor-Reynolds number approach was conducted by Huitt (1956). His flow cell consisted of steel slabs 7 cm by 13.3 cm on which grains of sand were cemented and which formed

Table 1.1 Friction factors for fracture flow and derived relationships for hydraulic conductivity

| Regime | Roughness ¹ | Flow Law ² | Investigator | λ in Darcy-Weisbach Equation ⁴ | K for Parallel Flow (Darcy equation ⁵) | |
|---|------------------------|-----------------------|---|---|---|---|
| Linear (Laminar) | Smooth | 1 | theoretical parallel plate law ³ | $\frac{96}{Re}$ | $\frac{g(2b)^2}{12\nu}$ | |
| | Rough | 4 | Louis, 1969 $\psi = 8.8$ | $\frac{96}{Re} [1 + \psi(k/D_h)^{1.5}]$ | $\frac{g(2b)^2}{12\nu[1 + \psi(k/D_h)^{1.5}]}$ | |
| | | | Lomize, 1951 $\psi = 17$ | | | |
| All | | | Sato et al., 1984 | -- | $\frac{g(2b)^2}{12\nu[1+2.15(2b)^{0.206}]}$ | |
| Non-Linear | Transitional | Smooth | 2 | Blasius ³ | $0.316 \cdot Re^{-1/4}$ | $\left[\left(\frac{g}{0.079} \right)^4 \frac{2(2b)^5}{\nu(dH/dl)^3} \right]^{1/7}$ |
| | | | 3 | Nikuradse ³ $c=2, d=3.7$ | $\left[c \cdot \log \left(\frac{d}{k/D_h} \right) \right]^{-2}$ | $2c \cdot \log \left(\frac{d}{k/D_h} \right) \left[\frac{g(2b)}{dH/dl} \right]^{1/2}$ |
| | Fully Turbulent | Rough | 5 | Louis, 1969 $c=2, d=1.9$ | | |
| | | | | Lomize, 1951 $c=2.55, d=1.24$ | | |
| | | | | Huitt, 1956 | $0.305(k/D_h)^{0.472}$ | $3.62 \left(\frac{1}{k/D_h} \right)^{0.236} \left[\frac{g(2b)}{dH/dl} \right]^{1/2}$ |
| <p>Notes: 1. Smooth: $k/D_h < 0.033$; Rough: $k/D_h > 0.033$</p> <p>2. Assigned by routine FLOLAW in DEFLOW (see Appendix C)</p> <p>3. Classic work discussed in any fluid mechanics text (e.g., Vennard and Street, 1976)</p> <p>4. $\frac{dH}{dl} = \lambda \frac{1}{D} \frac{v^2}{2g}$</p> <p>5. $v = K \frac{dH}{dl}$</p> | | | | | | |

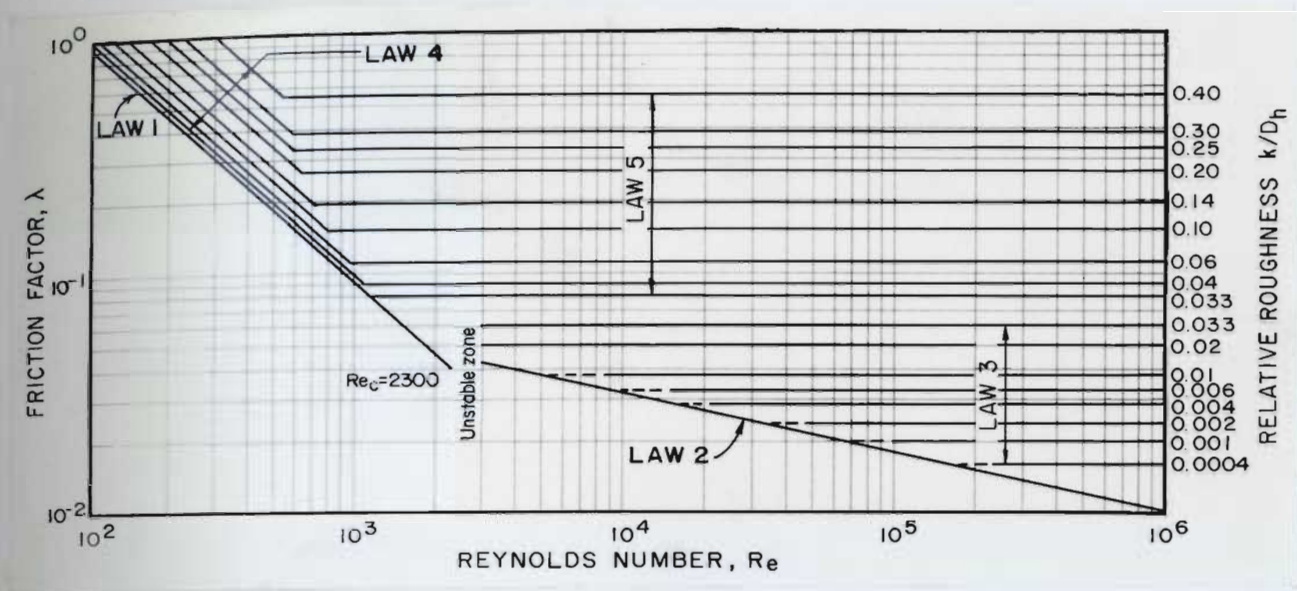


Figure 1.5 Moody-type diagram of Louis' (1969) flow test data

apertures in the range of 1.58 to 3.74 mm. Huitt concluded that in the laminar flow range, Poiseuille's law adequately described his results. For fully turbulent flow, however, he proposed the empirical friction factor shown in Table 1.1. In his study, no differentiation was made between the relative roughnesses of the fractures.

Pearce and Murphy (1979) warn against any attempts to universally apply flow laws based on the friction factor-Reynolds number approach. Implicit in this method is that hydraulic and geometric similitude exist, which is a very tenuous assumption with natural fractures. They argue that because of the large number of factors characterizing rough-

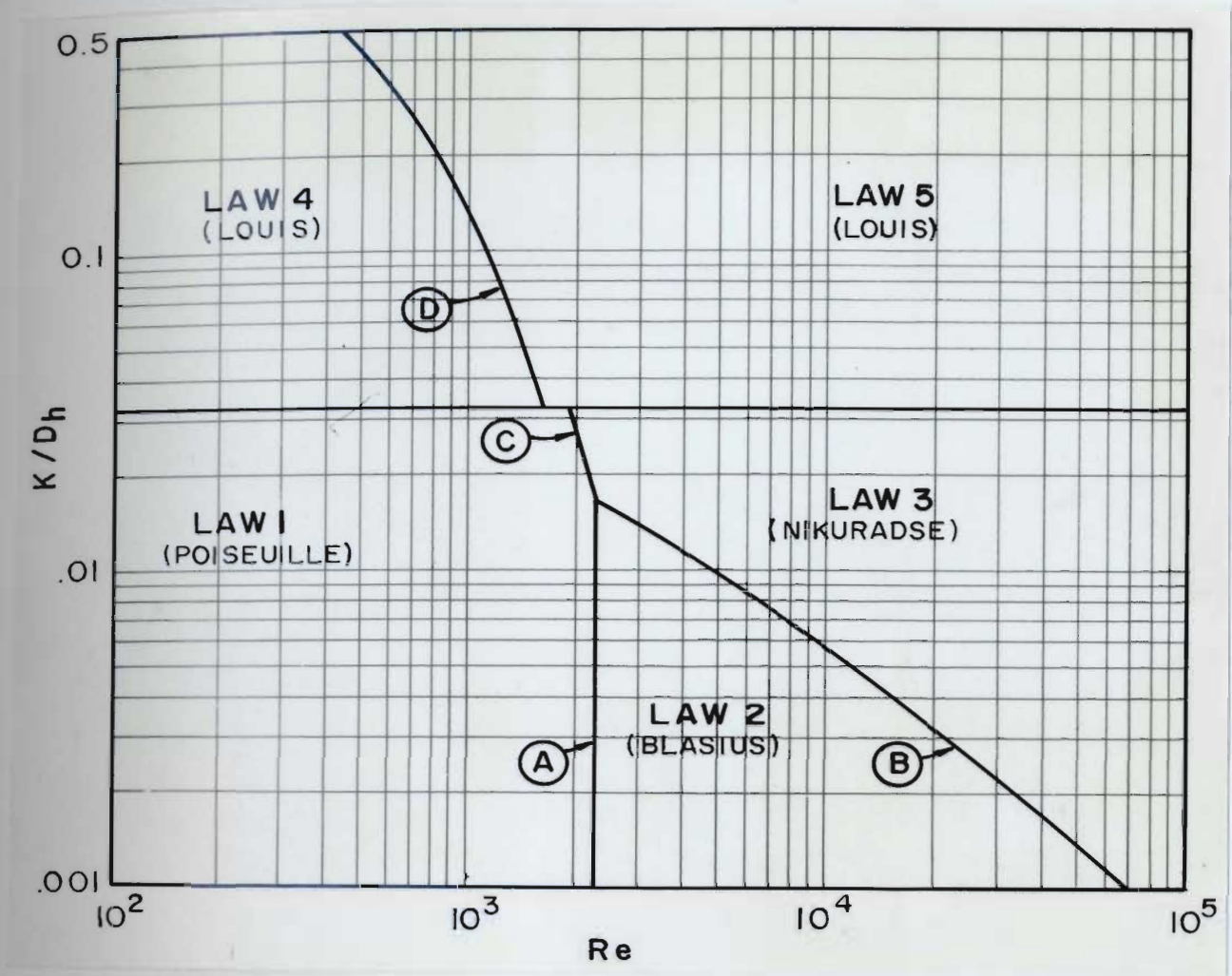


Figure 1.6 Fracture flow law fields (after Rissler, 1978). Boundaries of fields (lines labelled with letters) are described in Section 2.1 (pages 53-55).

ness (e.g., amplitude, wave length, shape, scale) a completely general correlation of friction factor with Reynolds number, similar to Nikuradse's findings for pipes with regular sand grain roughness, probably never will be developed. As evidence, they cite the variation in friction factors obtained by Lomize (1951), Huitt (1956), and Louis (1969).

Sharp and Maini (1972) suggested that the characteristic of roughness indicated by aperture distribution can have

considerable bearing on the friction factor. They state that fractures with narrow aperture distributions usually exhibit a relatively extensive laminar zone and a very abrupt transition to fully developed turbulent flow during testing. Those with a wider aperture distribution tend to show an earlier onset of non-linear, laminar flow and a relatively prolonged transition to fully developed turbulent flow. Unfortunately, Sharp and Maini (1972) do not include any actual data demonstrating these conditions.

Another factor contributing to the uncertainty of applying the friction factor-Reynolds number experimental findings to real fractures, particularly for the case of non-linear flow, is that all investigators (with the exception of Parish, 1963) have used open fractures in which a very small percentage, if any, of the fracture surfaces were in contact. By their very nature, fractures are self-propped and the apertures are the result of contact between the asperities of greatest amplitude (refer to Figure 1.4, page 27). Unlike sheet flow in the analogous parallel plate model, flow in a real fracture follows a tortuous path through a series of anastomotic channels. Maini (1971) includes photographs of flow through transparent plastic casts of real fractures which clearly demonstrate this under self-weight conditions.

An attempt to quantify the effects of contact area was made by Sundaram and Frink (1983) who made a radial flow

analog model from Teledeltos paper. Contact or no-flow areas were simulated by cutting or punching holes in the paper. They concluded that not only the percent of total area in contact, but also its specific location in the flow field, affected head losses. Iwai (1976) reached similar conclusions from tests on one of his physical models in which metal strips were inserted into the fracture in different patterns.

Tsang (1984) conducted experiments with an electrical resistor network model in an investigation of tortuosity. She calculated that when the contact area exceeded 30 percent, the effect of roughness-induced tortuosity reduces the flow rate by 3 or more orders of magnitude below that predicted by the parallel plate law. This may be an extreme case, however, because Iwai (1976) determined that even under relatively high normal loads, only about 10 percent of the surface areas of his fractures were actually in contact. His fractures were fresh, artificially induced tensile fractures and presumably mated well under load.

A totally deterministic approach to describing flow in fractures might not be necessary. In a reinterpretation of Iwai's (1976) original data, Witherspoon et al. (1980) demonstrate that an empirically determined effective aperture, which more than likely differs from the actual geometric aperture, could still be a valid concept that can be used in the discrete approach. In many respects, this

applies a continuum model where the averaging takes place over a discrete conduit rather than over the entire rock mass. It should be noted that the interpretation of Witherspoon et al. (1980) assumed laminar flow conditions only, and that they found the apparent effects of roughness to be much greater for radial flow than for parallel flow for the same rock type. A more quantitative discussion of their findings is included in Appendix B.

Sato et al. (1984) developed a laminar flow relationship by using numerical analysis to solve the Navier-Stokes equation written in terms of the stream function and incorporating the ~~vorticity equation~~. Using the results of spectral analysis of actual fracture profiles and parallel flow tests of the same fractures in order to provide representative values for the numerically derived parameters, they proposed the semi-empirical equation given in Table 1.1 (page 30). In this method, Sato et al. (1984) include the shape of the roughness (characterized by the ratio of amplitude to wavelength), which is a first step in overcoming the problems cited by Pearce and Murphy (1980). With their model, when the aperture is small, roughness causes lengthening of the streamlines (i.e., tortuosity); whereas in larger open apertures, the effects of roughness are more similar to those associated with the friction factor-Reynolds number concept in pipe flow.

A third alternative for describing fracture apertures, but one which will not be considered any further in the present study, is to use a statistically-based model. One example has been proposed by Neuzil and Tracy (1981) in which apertures vary by some given statistical distribution, but only in the direction orthogonal to flow. This appears to be a rather unrealistic concept in that variation of aperture in a real fracture would obviously also take place in the direction of flow.

1.3.4.3 Major laboratory investigations

In addition to the previously described laboratory work which has resulted in development of basic fracture flow laws, there have been several other related laboratory investigations. They are summarized chronologically in Table 1.2, and a few of the more relevant ones will be described briefly.

Baker (1955) was the first to address the specific problem of two-regime, convergent, radial flow to a well from a fracture. He created a fracture by pouring a 3-m diameter cylinder of concrete onto a concrete floor and subsequently separating the two surfaces. Tests were conducted under either completely laminar or completely turbulent flow conditions with apertures ranging from 1.3 to 10.2 mm. Baker

Table 1.2 Previous physical fracture flow models

| Researcher(s) | Materials | Type of Flow ¹ | | | | Deformation ² | | Researcher(s) | Materials | Type of Flow ¹ | | | | Deformation ² | |
|---------------|--|---------------------------|---|---|----|--------------------------|----|-------------------------|--------------------------------------|---------------------------|-----|---|----|--------------------------|-----|
| | | P | R | L | NL | HS | HD | | | P | R | L | NL | HS | HD |
| Lomize, 1951 | sand-coated metal and plastic with different shapes. | x | | x | x | no | no | Rayneau, 1972 | pie-shaped metal plates | c | x | x | | yes | no |
| Baker, 1955 | concrete with cast fracture | | c | x | x | no | no | Iwai, 1976 | rock with artificial fractures | x | d | x | | yes | no |
| Huitt, 1956 | sand-coated metal | x | | x | x | no | no | Gale, 1977 | rock with artificial fractures | x | c,d | x | | yes | yes |
| Parrish, 1963 | sand-coated glass | x | | x | x | no | no | Rissler, 1978 | striated plastic | | d | x | x | no | no |
| Louis, 1969 | concrete with cast fractures | x | | x | x | no | no | Murphy, 1979 | plastic | | c | x | x | no | no |
| Sharp, 1970 | rock with natural fractures | x | | x | x | yes | no | Thorpe et al., 1980 | rock with multiple natural fractures | | d | x | | yes | yes |
| Maini, 1971 | rock with natural fractures and plastic casts | x | c | x | x | no | no | Schrauf and Evans, 1983 | rock with natural fractures | x | d | x | x | yes | no |
| Jouanna, 1972 | rock with natural fractures | x | | x | | yes | no | Sato et al., 1984 | rock with natural fractures | x | | x | | no | no |
| | | | | | | | | THIS STUDY | concrete with cast fracture | | c,d | x | x | yes | yes |

¹ Flow geometry: P = parallel, R = radial (c = convergent, d = divergent)
Flow regime: L = linear, NL = non-linear

² Indicates if fracture(s) deformed during testing, and if so, whether the measured deformations were merely the hydrostatic (HS) response to changes in effective stress created by changing the applied boundary load or included measurements of the deformations resulting from a hydrodynamic (HD) response to changes in effective stress induced by flow.

did not attempt to quantify roughness; and the flow coefficients he derived were entirely empirical. An important finding of this early study was that the production-drawdown response of a well producing from a fracture was very sensitive to aperture size and, to a lesser degree, wellbore size.

The work of Rayneau (1972) was quite innovative in that he not only incorporated the recently developed flow laws of Louis (1969) into a numerical model for two-regime radial flow, but he also was one of the first researchers to include the relationship between fracture deformation and changes in permeability in both his numerical and laboratory models. Rayneau conducted his two-regime, convergent, radial flow experiments with a 0.8 m radius, pie-shaped (33 degree wedge) parallel plate model made of aluminum.

Gale (1975) tested an approximately 1-m diameter cylinder of rock in which two artificial fractures were made, one by tensile failure and the other by wire saw. The cylinder was placed in a large triaxial cell in which an axial load was applied and kept constant during radial (both convergent and divergent) flow tests in which flow was assumed to be laminar. By careful measurement of displacements in both the rock and fractures, Gale was able to demonstrate that fractures deform in response to changes in effective stress resulting from either fluid injection or fluid withdrawal.

Further discussion of this problem is presented in Section 1.3.4.5.

Rissler (1978) applied the empirical flow laws of Louis (1969) to create a numerical model for two-regime, divergent radial flow that could be used to improve the interpretation of the traditional Lugeon (also known as packer or injection) test. In the laboratory phase of his study, he performed flow tests in a 2 m diameter parallel plate model made of lucite. A servo-controlled hydraulic piston connected to an external steel frame was used to maintain a constant aperture. He concluded that Louis' (1969) flow laws quite satisfactorily predicted the critical head (the injection pressure at which turbulent flow first occurs) measured in his tests. It should be noted, however, that the artificial fracture in Rissler's (1978) model was of the "open" type.

1.3.4.4 Special considerations in radial, convergent flow

Radial flow to a well through a fracture introduces two factors which are not usually taken into consideration in most ground-water flow problems: 1) the velocity head or kinetic energy of the fluid can become sufficiently large that it can no longer be disregarded, and 2) the acceleration of the fluid can affect its resistance to flow.

Citing potential theory, Louis and Maini (1970) emphasize the fact that the "driving" force for flow of ground water is the difference in total head. The total (or Bernoulli) head, H , is

$$H = \frac{P}{\rho g} + z + \frac{v^2}{2g} = h + \frac{v^2}{2g} \quad (1.21)$$

where

P = fluid pressure,

ρ = density of fluid,

h = hydraulic head, and

z = elevation head.

Therefore, the difference in total head between any two points along a streamline under steady state conditions is

$$H_2 - H_1 = h_2 + \frac{\eta v_2^2}{2g} - h_1 - \frac{\eta v_1^2}{2g} \quad (1.22)$$

or

$$H_2 - H_1 = (h_2 - h_1) - \eta (v_1^2 - v_2^2)/2g \quad (1.23)$$

where η is the kinetic energy correction factor. According to Louis and Maini (1970), η is equal to 1.2 for laminar flow and 1.0 for turbulent flow. The different values for η reflect the difference in the shape of the velocity profile in a closed conduit under laminar and turbulent flow conditions.

The right-hand side of Equation 1.23 should be used in the left-hand side of Equations 1.5 (page 4) and 1.9 (page 4) when fluid velocity is large. For radial flow under laminar conditions, it can be shown, using points r_1 and r_2 for generality, that

$$(h_2 - h_1) - \frac{1.2(v_1^2 - v_2^2)}{2g} = \frac{\alpha Q}{2\pi t} \ln \frac{r_2}{r_1} \quad (1.24)$$

or

$$h_2 - h_1 = \frac{\alpha Q}{2\pi t} \ln \frac{r_2}{r_1} + \frac{0.6}{g} (v_1^2 - v_2^2). \quad (1.25)$$

Using Equations 1.9 and 1.23, it can be shown similarly that for radial, fully turbulent flow

$$(h_2 - h_1) - \frac{(v_1^2 - v_2^2)}{2g} = \frac{\beta Q^2}{(2\pi t)^2} \left[\frac{1}{r_1} - \frac{1}{r_2} \right] \quad (1.26)$$

or

$$h_2 - h_1 = \frac{\beta Q^2}{(2\pi t)^2} \left[\frac{1}{r_1} - \frac{1}{r_2} \right] + \frac{1}{2g} (v_1^2 - v_2^2). \quad (1.27)$$

According to Murphy (1979), the parabolic velocity profile for a fluid moving under laminar conditions between two plates, which is predicted theoretically by the Navier-Stokes equation, elongates when it is accelerated. This distortion causes greater resistance to flow, which means that the friction factor based on Poiseuille's law (Table 1.1, page 30) underestimates the true head loss. For the

case of radially accelerating laminar flow in a fracture, Murphy proposes, instead of η equals 1.2, the empirical kinetic energy correction factor $\hat{\eta}$

$$C_L = \sqrt{1 + \left(\frac{0.36}{r_D}\right)^2} \quad (1.28)$$

where r_D is a dimensionless radial distance given by

$$r_D = \frac{2r}{(2b)\sqrt{Ro}} \quad (1.29)$$

and Ro is the "overall Reynolds number" defined as

$$Ro = \frac{Q}{2\pi v(2b)} \quad (1.30)$$

Acceleration also has been found to have a stabilizing effect on turbulent flow in closed conduits. By causing the viscous or laminar sub-layer to thicken, acceleration can actually initiate a reverse-transition, or "relaminarization", in which the friction factor decreases below that predicted on the basis of Reynolds number and roughness. An example of one of the relaminarization indices, R_1 , cited by Murphy (1979) from the literature is

$$R_1 = \frac{v}{U^2} \frac{dU}{dr} = 3.5 \times 10^{-6} \quad (1.31)$$

where U is the velocity of flow in the turbulent core. Index values above this limit indicate that complete relaminarization (i.e., the friction factor is that predicted for laminar flow) has taken place.

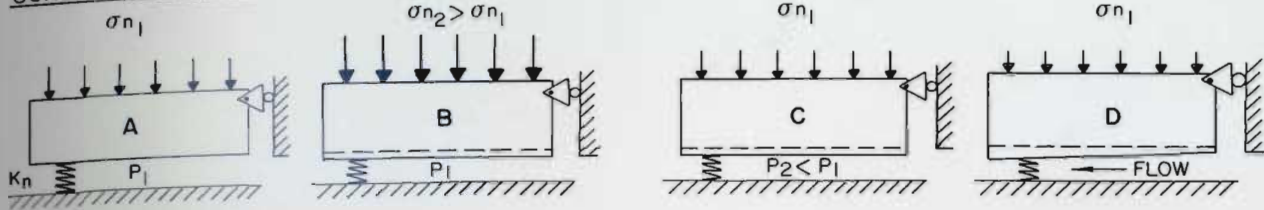
1.3.4.5 Fracture deformation

Gale (1975) demonstrates with the results of field, laboratory and numerical investigations that real fractures deform in response to changes in effective stress resulting from either increased applied stress or changes in fluid pressure induced by injection or withdrawal. This concept, using the example of fracture closing, is shown schematically in Figure 1.7. Other field tests showing the effect of increasing load on flow are described by Carlsson and Olson (1983) and Jouanna (1972).

Since volumetric flow rate may be a function of fracture aperture to the third power (refer to Equation 1.19, page 25), a small change in aperture can result in a substantial change in discharge. For the case of two-regime, convergent radial flow in a fracture with uniform aperture, however, it is important to note that the greatest changes in effective stress occur over a relatively small area.

Bandis et al. (1983) have investigated the deformation of several different rock types under both normal and shear stresses. They concluded that fracture stiffness (i.e., the resistance to deformation) was a function of initial contact area, roughness, strength of the asperities, deformation history, and the properties of any infilling material. They present several constitutive curves for normal stress versus

SCHEMATIC MODELS



STRESS DIAGRAMS

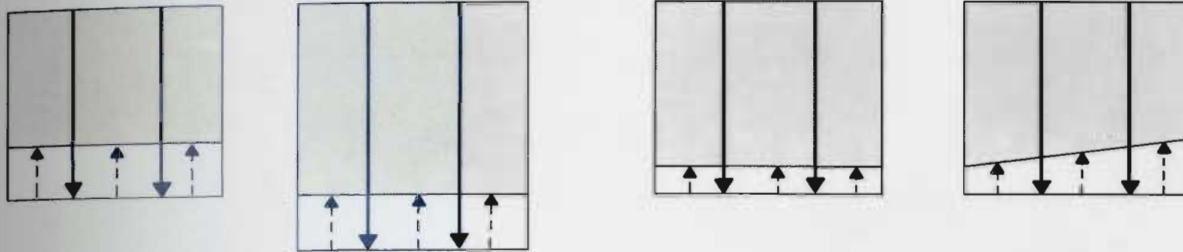


Figure 1.7 Schematic diagram of fracture deformation due to changes in effective stress. Case A: Reference condition with applied normal stress σ_{n1} (represented by heavy arrows in lower diagram), hydrostatic fluid pressure P_1 (represented by dashed arrows), and normal fracture stiffness K_n . Resulting effective stress is represented by shaded area in lower diagram. Case B: Deformation resulting from increase in applied normal stress. Since fluid pressure remains same, effective stress also increases. Case C: Deformation resulting from uniform decrease in hydrostatic fluid pressure resulting in increase in effective stress. Case D: Deformation resulting from increase in effective stress caused by flow-induced decrease in fluid pressure.

closure which show that, although the specific response can be quite variable, the general relationship is highly non-linear. Bandis et al. (1983) suggest that the best fits to their laboratory data are provided by hyperbolic functions.

Tsang and Witherspoon (1981) claim to have developed a numerical model which, with input of data for normal stress versus deformation for both the rock and fractures and an

estimate of the initial fracture contact area, can deduce the height of the tallest asperities, generate roughness profiles, and thereby predict flow rate as a function of stress. In a follow-up study (Tsang and Witherspoon, 1983), they indicate with another numerical model that it is the large scale roughness (i.e., the undulations) that control both the mechanical and hydraulic behavior of a fracture. They warn that tests on samples smaller than the typical undulation wavelength may not represent the fracture roughness properly and could yield misleading results. The results of neither of these studies have been verified, however, by laboratory or field data.

1.3.5 Current applications in dewatering

In most of the literature which could be found on dewatering operations using wells (Williams et al., 1986; Juvkam-Wold, 1980; Carpenter and Young, 1980; Vogwill, 1976; Stubbins and Munro, 1965) and on numerical models which are used to plan and design such dewatering models (Schmidt, 1985; McClure et al., 1985; Bair, 1980; Hargis, 1980), there appears to be a total disregard for the performance and efficiency of the wells.

Greenslade and Condrat (1979) provide the only specific acknowledgment of the significance of well losses in a

dewatering operation. In their design of a shaft depressurizing system for which they had no data other than the aquifer characteristics, it was arbitrarily assumed that 30 percent of the total available drawdown in each well would be consumed by well losses. Although this in itself is a noteworthy and commendable step, it clearly demonstrates the need for a more rational approach to the problem.

In a study of the technical feasibility and cost effectiveness of dewatering underground coal mines, Wahler and Associates (1979) report that transmissivities calculated from data on pumping wells completed into fractured rock aquifers are usually an order of magnitude less than those based on observation well data. No explanation was given in their report for this discrepancy; and although there are other possible causes (e.g., partial penetration of the pumping wells), there is a strong suggestion that well losses could have been an important component of the total drawdown in those wells.

2.0 EMPIRICAL DESCRIPTION OF TWO-REGIME, CONVERGENT, RADIAL FLOW TO A WELL FROM HORIZONTAL, DEFORMABLE FRACTURES

In this chapter, an empirical description of two-regime, convergent radial flow to a well from horizontal deformable fractures is developed. The term empirical is appropriate in that, although every attempt is made to include basic physical relationships (the deterministic approach) for both flow and deformation, the fracture flow laws themselves and the range (defined by roughness and Reynolds number) over which they are applicable and the deformational response of fractures to changes in stress are completely empirical.

Following the mathematical convention used in the statement of the problem (Section 1.1), the flow equation for a single, rigid fracture first is developed in a form that can be solved analytically for second type boundary conditions at the well (i.e., when the discharge rate is known). Then it is reformulated for solution by the finite element method. The numerical technique is more generalized in that it permits a first type boundary condition (i.e., head) to be specified at the well and is much more amenable to coupling with the other numerical code describing the deformational response of the fracture to pumping. The boundary conditions necessary for applying the method to more than one horizontal fracture are shown, and finally the

technique of coupled solution using pressure head as the linking term is described.

The assumptions used in the following mathematical development are:

- 1) The flow is steady state (a rather comprehensive assumption which includes fixed values for r_o and H_w and which allows wellbore storage to be ignored).
- 2) The matrix is impermeable (i.e., all head losses occur within the fracture). The additional complexity introduced by use of a dual porosity model is not justifiable for the current problem.
- 3) The hydraulic conductivity is radially isotropic.
- 4) The absolute roughness is uniform over the entire fracture surface.
- 5) There is no fracture infilling.
- 6) The fracture(s) is/are horizontal and the wellbore is vertical.
- 7) No dewatering of the fracture(s) occurs (i.e., the fracture(s) remains fully saturated and the pumping level in the well is always above the uppermost fracture).
- 8) The system is isothermal.
- 9) The rock is homogeneous and elastic.
- 10) Although the flow laws and their fields of applicability determined empirically by Louis (1969) are far from universal, they are the best currently available and are incorporated into the numerical model.

2.1 Formulation of analytical solution to two-regime radial flow to a well in a rigid fracture

As described in Section 1.3.4.2, Louis' (1969) fracture flow laws were developed using the friction factor-Reynolds

number approach which involves the Darcy-Weisbach equation (see Appendix A for derivation of the various parameters)

$$\frac{dH}{dr} = \lambda \frac{1}{D_h} \frac{v^2}{2g} = \lambda \frac{1}{2(2b)} \frac{v^2}{2g} \quad (2.1)$$

To demonstrate how values for hydraulic conductivity can be obtained from the friction factors, the simplest case of Poiseuille's law (Law 1 in Table 1.1 on page 30), where

$$\lambda = \frac{96}{Re} \quad (2.2)$$

will be used. Substituting Equation 2.2 and the definition of Reynolds number,

$$Re = \frac{vD_h}{\nu} = \frac{v \cdot 2(2b)}{\nu} \quad (2.3)$$

into Equation 2.1 and solving for v , it can be shown that

$$v = \frac{g(2b)^2}{12\nu} \frac{dH}{dr} \quad (2.4)$$

This is simply another version of Darcy's law (Equation 1.2, page 3) where K , the hydraulic conductivity or inverse of hydraulic resistance, is equal to

$$K = \frac{1}{\alpha} = \frac{g(2b)^2}{12\nu} \quad (2.5)$$

Equation 2.4 is equivalent to Equation 1.18 (page 25), which should be expected since the preceding was an "inverse derivation". The friction factor $96/Re$ used above was determined from the theoretical solution to the Navier-Stokes equation for flow between parallel plates. The procedure nevertheless indicates how hydraulic conductivity values can

be derived from the other linear friction factors given in Table 1.1 (except for the law of Sato et al., 1984, which was not derived solely by the friction factor technique).

Introducing the concept of transmissivity, T , defined as the product of hydraulic conductivity and thickness, and recognizing that the analogous "aquifer thickness" for a single fracture between an impermeable matrix is its aperture so that

$$T = K \cdot t = K(2b) , \quad (2.6)$$

Equation 1.5 (page 3) can be rewritten as,

$$H_2 - H_1 = \frac{Q}{2\pi T} \ln \frac{r_2}{r_1} . \quad (2.7)$$

This form of the equation is usually referred to in the ground-water literature as the Theim equation. Finally, by combining Equations 2.5 through 2.7, the relationship between head loss and flow rate for radial flow between smooth parallel plates is given by

$$H_2 - H_1 = \frac{6Q\nu}{\pi g(2b)^3} \ln \frac{r_2}{r_1} . \quad (2.8)$$

For linear flow in rough ($k/D_h > 0.033$) fractures, it can be shown similarly using Louis' (1969) law (Law 4, Table 1.1 on page 30) that

$$H_2 - H_1 = \frac{6Q\nu \{1 + 8.8 [k / (2 \cdot 2b)]^{1.5}\}}{\pi g(2b)^3} \ln \frac{r_2}{r_1} . \quad (2.9)$$

Both Equations 2.8 and 2.9 are forms of the cubic law (Equation 1.19 on page 25).

In the case of non-linear flow, Equation 2.1 (page 49) can be combined with Equation 1.6 (page 4) to show that

$$\frac{dH}{dr} = \beta v^2 = \lambda \frac{1}{2(2b)} \frac{v^2}{2g} \quad (2.10)$$

or

$$\beta = \frac{\lambda}{4(2b)g} \quad (2.11)$$

Substituting this value into Equation 1.9 (page 4), again recognizing that $t = 2b$,

$$H_4 - H_3 = \frac{\lambda Q^2}{16\pi^2 g (2b)^3} \left[\frac{1}{r_3} - \frac{1}{r_4} \right] \quad (2.12)$$

is obtained. Note that for non-linear flow, the analogous cubic law is between drawdown and the square of the discharge rate. Using for an example, Louis' (1969) law for rough, fully turbulent flow (Law 5 in Table 1.1, page 30), Equation 2.12 becomes

$$H_4 - H_3 = \frac{Q^2}{64\pi^2 g (2b)^3 [\log\{1.9/[k/(2 \cdot 2b)]\}]^2} \left[\frac{1}{r_3} - \frac{1}{r_4} \right] \quad (2.13)$$

The exit loss can be approximated from the empirical relationship derived from data given in Murphy and Pearce (1980), previously presented in Section 1.3.2. Applying the continuity equation to the wellbore,

$$s_e = 0.23 \left(\frac{2r_w}{2b} \right)^{1.41} \frac{Q^2}{2g\pi^2 r_w^4} \quad (2.14)$$

Finally, head loss due to flow in the wellbore can be estimated from the Darcy-Weisbach equation for flow in a pipe,

$$s_w = f_w \frac{L}{D} \frac{v^2}{2g} \quad (2.15)$$

or

$$s_w = f_w \frac{LQ^2}{4\pi^2 g r_w^5} \quad (2.16)$$

where

L = length of wellbore from fracture inlet to pump intake, and

f_w = friction factor for the wellbore.

Murphy and Pearce (1980) included with their exit loss all head losses up to the point in the wellbore where the pressure head gradient becomes constant. They experimentally found this to be a distance of approximately 5 wellbore diameters. Therefore, correcting the length over which additional flow losses in the wellbore occur, Equation 2.16 can be re-written as

$$s_w = f_w \frac{(L - 10r_w)Q^2}{4\pi^2 g r_w^5} \quad (2.17)$$

Representative values for f_w can be obtained from any published version of the Moody diagram (e.g., refer to Figure 9.5 in Vennard and Street, 1976).

The total drawdown in a vertical well pumping at a discharge rate Q from a single, rigid, rough ($k/D_h > 0.033$), horizontal fracture can be estimated by the summation of Equations 2.9, 2.13, 2.14, and 2.17. Recalling the concept of critical radius (Section 1.1), this becomes

$$\begin{aligned}
 s = & \frac{6Q\nu\{1+8.8[k/(2\cdot 2b)]^{1.5}\}}{\pi g(2b)^3} \ln \frac{r_o}{r_c} \\
 & + \frac{Q^2}{64\pi^2 g(2b)^3 [\log\{1.9/[k/(2\cdot 2b)]\}]^2} \left[\frac{1}{r_w} - \frac{1}{r_c} \right] \\
 & + 0.23 \left(\frac{2r_w}{2b} \right)^{1.41} \frac{Q^2}{2g\pi^2 r_w^4} + f_w \frac{(L-10r_w)Q^2}{4\pi^2 g r_w^5}, \quad (2.18)
 \end{aligned}$$

a semi-deterministic version of Equations 1.11a or 1.11b (page 5). Equation 2.18 can also be written in the form

$$\begin{aligned}
 s = & \left[\frac{6\nu\{1+8.8[k/(2\cdot 2b)]^{1.5}\}}{\pi g(2b)^3} \ln \frac{r_o}{r_c} \right] Q \\
 & + \left[\frac{1}{64\pi^2 g(2b)^3 [\log\{1.9/[k/(2\cdot 2b)]\}]^2} \left(\frac{1}{r_w} - \frac{1}{r_c} \right) \right. \\
 & \left. + 0.23 \left(\frac{2r_w}{2b} \right)^{1.41} \frac{1}{2g\pi^2 r_w^4} + f_w \frac{(L-10r_w)}{4\pi^2 g r_w^5} \right] Q^2 \quad (2.19)
 \end{aligned}$$

for more direct comparison with Equations 1.13 (page 9) and 1.15 (page 18).

Probably the most important factor in Equation 2.19, yet the one with the most uncertainty (Sharp and Maini,

1972; Pearce and Murphy, 1979; Kovacs, 1981) is the critical radius which is dependent on the critical Reynolds number. Louis (1969) found that up to a relative roughness of 0.0168, the critical Reynolds number, Re_c , the Reynolds number at which flow in a fracture becomes non-linear, is essentially constant and equal to approximately 2300. The boundary between smooth, transitional and smooth, fully turbulent flow was found to be a function of roughness, as were the boundaries between flow regimes when roughness is greater than 0.0168. By solving the various friction factor relationships simultaneously, Rissler (1978) derived equations for the boundaries of Louis' flow fields. These are summarized in Table 2.1 and are shown graphically in Figure 1.6 (page 32).

Table 2.1 Critical Reynolds numbers

| Applicable Range of Rela- tive Roughness | Re_c | Line on Figure 1.6 |
|--|---|-----------------------|
| < 0.0168 | 2300 | A |
| < 0.0168 | $2.552 \left(\log \frac{3.7}{k/D_h} \right)^8$ | B |
| $0.0168 \leq \frac{k}{D_h} \leq 0.033$ | $\left[142000 \left(\log \frac{3.7}{k/D_h} \right)^2 \right]^{0.568}$ | C |
| > 0.033 | $\left[142000 \left(\log \frac{1.9}{k/D_h} \right)^2 \right]^{0.568}$ | D |

From the basic definitions of Reynolds number,

$$Re = \frac{vD_h}{\nu} = \frac{QD_h}{A\nu} = \frac{Q(2 \cdot 2b)}{2\pi r(2b)\nu} \quad (2.20)$$

an estimate of critical radius can be derived using

$$r_c = \frac{Q}{\pi\nu Re_c} \quad (2.21)$$

This indicates that except for very smooth fractures ($k/D_h < 0.0168$), critical radius is a function of kinematic viscosity, discharge, and, as shown in Table 2.1, roughness. Equation 2.21 has led some investigators (e.g., Baker, 1955) to remark that critical radius is independent of the size of the fracture aperture. This is not entirely true, since relative roughness is a function of the aperture and any significant changes in aperture during pumping could alter the critical radius.

Incorporating the appropriate value for critical radius from Equation 2.21 and Table 2.1, Equation 2.19 can be written in the final form

$$s = \left\{ \frac{6Q\nu \{1 + 8.8[k/(2 \cdot 2b)]^{1.5}\}}{\pi g(2b)^3} \right\} \\ + \left\{ \ln \frac{r_o \nu \pi}{Q} \left(142000 [\log \{1.9/[k/(2 \cdot 2b)]\}]^2 \right)^{0.568} \right\} \\ + \left\{ \frac{Q^2}{64\pi^2 g(2b)^3 [\log \{1.9/[k/2 \cdot 2b)]\}]^2} \right\} \\ \left\{ \frac{1}{r_w} - \frac{\nu \pi \left(142000 [\log \{1.9/[k/(2 \cdot 2b)]\}]^2 \right)^{0.568}}{Q} \right\}$$

$$+ 0.23 \left(\frac{2r_w}{2b} \right)^{1.41} \frac{Q^2}{2g\pi^2 r_w^4} + f_w \frac{(L-10r_w)Q^2}{4\pi^2 g r_w^5} \quad (2.22)$$

Equation 2.22 is an empirical version of Equation 1.11a or 1.11b (page 5) for relative roughness greater than 0.033.

A concept that is related to critical radius and that is particularly useful in describing the results of step-drawdown tests (see Section 1.3.3 and Figure 1.3, page 21) is that of critical discharge, Q_c . By rearranging Equation 2.21 and inserting the wellbore radius, it can be shown that

$$Q_c = \pi r_w v Re_c \quad (2.23)$$

Thus, critical discharge is the discharge rate at which non-linear flow in the fracture just begins at the wellbore boundary.

A solution to the problem of two-regime, radial flow to a well from a rigid, horizontal fracture can be approximated using Equation 2.22 when Q , r_w and temperature (since viscosity is temperature dependent) are known and reasonable estimates for r_o , $2b$, and k can be made. If s is also known, combinations of the values for $2b$ and k can be estimated by the trial and error method. Appendix B describes graphical techniques by which the latter parameters can be estimated.

Although rather straightforward in its development and simple to use, the analytical solution using discharge for

the boundary condition at the well has limited application. First, and more or less from an academic standpoint, it cannot be used when head is specified at the well. Secondly, and of more practical significance, this limitation means that it is not adaptable to the problem of flow from more than one fracture. Initial estimates of discharge rates Q_i from individual fractures in a well intersecting multiple fractures could be made from

$$Q_i = \sum_{j=1}^n Q_j \left(\frac{(2b_i)^3}{\sum_{j=1}^n (2b_j)^3} \right) \quad (2.24)$$

and then inserted into Equation 2.22. The procedure would require trial and error iteration until the proportions of the total discharge rate (assumed to be known) and individual drawdowns converged to a compatible solution. This would become quite complex and time consuming when several fractures are involved.

A third problem is that the transmissivities can change within a given flow regime, not just at the critical radius, since the aperture (and, hence, relative roughness) can vary and the friction factor is affected by acceleration (Murphy, 1979). This problem can be overcome by discretizing the flow field into smaller segments. Once that is done, however, it is just as easy to use the more versatile numerical model that is developed in the following section.

2.2 Finite element formulation of two-regime flow equation

Solution by numerical methods provides a flexible alternative, and it was decided to model flow using one-dimensional (radial isotropy assumed), linear finite elements. In applying this technique to two-regime radial flow, however, two inherent problems are encountered: 1) using discretization schemes commonly used in ground-water problems, the linear basis functions (described below) poorly represent flow conditions near a well where the change in head is linear with respect to the natural logarithm of changes in radial distance, and 2) non-linear flow laws must be considered. The procedures by which these potential problems were resolved are described in the next two sections.

2.2.1 Radial discretization

Different solutions to the first problem have been proposed, usually involving either numerical integration or creation of relatively complicated grids (e.g., see Reilly, 1984; Tharp, 1982; Pinder and Gray, 1977; or Huyakorn, 1973). For this investigation, a much simpler discretization scheme was used. The flow nodes were assigned at

logarithmically increasing radial distances away from the wellbore so that the Theim equation (Equation 2.7, page 50) can be transformed into

$$Q = 2\pi T \frac{\Delta H}{\Delta \ln r} = 2\pi T \frac{dH}{dr'} \quad (2.25)$$

where r' is the natural logarithm of r . Applying the concept of continuity to Equation 2.25, the differential equation

$$\frac{dQ}{dr'} = 2\pi T \frac{d^2 H}{dr'^2} = 0 \quad (2.26)$$

is obtained which can be applied directly in the Galerkin formulation (Section 2.2.3). As long as the convention is consistently adhered to throughout the formulation and careful attention is given to dimensions, there do not appear to be any problems associated with this discretization.

2.2.2 Linearization of non-linear flow laws

In Section 2.1 it was shown that the friction factors developed by various investigators for linear flow could be incorporated into values of hydraulic conductivity and then transmissivity for use in the analytical solution. The same values for the linear flow laws again will be applicable in the finite element solution, but it will be necessary to "linearize" the non-linear flow laws in order to use them in Equation 2.25. By substituting Darcy's law for the v^2 term

in the Darcy-Weisbach equation (Equation 2.1, page 49), it can be shown that

$$\frac{dH}{dr} = \lambda \frac{1}{D_h} \frac{v^2}{2g} = \frac{\lambda}{2gD_h} K^2 \left(\frac{dH}{dr} \right)^2 \quad (2.27)$$

or

$$K = \left[\frac{2gD_h}{\lambda (dH/dr)} \right]^{1/2} \quad (2.28)$$

Using the example of Louis' (1969) Law 5 (Table 1.1, page 30), Equation 2.28 becomes

$$K = \left[\frac{4g(2b)}{(dH/dr)} \right]^{1/2} 2 \cdot \log \left(\frac{1.9}{k/D_h} \right) \quad (2.29)$$

or

$$K = 4 \cdot \log \left(\frac{1.9}{k/D_h} \right) \left[\frac{g(2b)}{(dH/dr)} \right]^{1/2} \quad (2.30)$$

Similar "linearized" expressions for hydraulic conductivity according to the laws of Blasius and Nikuradse for use in Equation 2.25 are given in Table 1.1. It should be noted that the gradient terms which they contain are with respect to r and not r' .

As indicated by Equations 2.28 and 2.30, the resulting expression for hydraulic conductivity to be used in the finite element solution includes a term for total head, the unknown for which the solution is sought. Therefore, an iterative technique must be employed in which after each iteration, the transmissivity term is updated based on the

latest value of total head. This procedure is described in more detail in Appendix C. A similar method also was used by Cox (1977) and Huyakorn and Dudgeon (1976) for solving the quadratic Forchheimer equation.

2.2.3 Galerkin formulation

The theory of the Galerkin solution and its specific application to problems of ground-water flow are explained by Frind and Pinder (1970). Very briefly, in this method the solution to a set of partial differential equations describing flow in a discretized region is sought by minimizing the errors resulting from approximate solutions to each equation. For the present case, this can be expressed by

$$\int_R L(H)\omega_i dr' = 0 \quad i = 1, N \quad (2.31)$$

where

$L(H)$ = is a differential operator on H ,

ω_i = nodal basis or weighting function,

i = node number, and

N = total number of nodes.

The total flow region, R , is comprised of a linear, R_L , and a non-linear R_N , subregion such that

$$R = R_L + R_N \quad (2.32)$$

Using the differential equation describing steady state flow derived in Equation 2.26 for the differential operator such that

$$L(H) = 2\pi T \frac{d^2 H}{dr'^2}, \quad (2.33)$$

Equation 2.31 can be re-written as

$$\int_{R_L} \bar{T} \left[\frac{d^2 H}{dr'^2} \right] \omega_i dr' + \int_{R_N} \bar{T} \left[\frac{d^2 H}{dr'^2} \right] \omega_i dr' = 0. \quad (2.34)$$

The term \bar{T} is the average transmissivity of the two nodes comprising each element; and, in order to eliminate repetition of the constant geometric factor in the following development, it will also include the 2π term. Thus,

$$\bar{T} = 2\pi \left[\frac{(T_i + T_{i+1})}{2} \right]. \quad (2.35)$$

Upon integration by parts to avoid second order derivatives, Equation 2.34 becomes

$$- \left[\int_{R_L} \bar{T} \frac{dH}{dr'} \frac{d\omega_i}{dr'} + \int_{R_N} \bar{T} \frac{dH}{dr'} \frac{d\omega_i}{dr'} \right] dr' + \left[\bar{T} \omega_i \frac{dH}{dr'} \right]_{r'_w}^{r'_o} = 0 \quad (2.36)$$

where the last term is the so-called natural boundary condition which comes directly out of the finite element formulation. Substituting the approximation expression

$$H \cong \sum_{j=1}^N \hat{H}_j \omega_j(r'), \quad (2.37)$$

where \hat{H}_j is the approximate value for total head at each node, and by multiplying through by -1 , Equation 2.36 becomes

$$\left[\int_{R_L} \bar{T} \frac{d\omega_i}{dr'} \frac{d}{dr'} \left(\sum_{j=1}^N \hat{H}_j \omega_j \right) + \int_{R_N} \bar{T} \frac{d\omega_i}{dr'} \frac{d}{dr'} \left(\sum_{j=1}^N \hat{H}_j \omega_j \right) \right] dr - \left[T\omega_i \frac{dH}{dr'} \right]_{r'_w}^{r'_o} = 0 \quad (2.38)$$

and by taking $\sum_{j=1}^N \hat{H}_j$ outside the integrals

$$\sum_{j=1}^N H_j \left\{ \sum_e \left(\left[\int_{R_L} \bar{T} \frac{d\omega_i}{dr'} \frac{d\omega_j}{dr'} + \int_{R_N} \bar{T} \frac{d\omega_i}{dr'} \frac{d\omega_j}{dr'} \right] dr' \right) \right\} - \left[T\omega_i \frac{dH}{dr'} \right]_{r'_w}^{r'_o} = 0 \quad (2.39)$$

where \sum_e indicates summation over all the elements. If, as will be shown in Appendix C, the natural boundary term can be replaced by the volumetric flux vector, Equation 2.39 can be expressed in matrix form as

$$[T]\{H\} - \{Q\} = 0 \quad (2.40)$$

or

$$[T]\{H\} = \{Q\} \quad (2.41)$$

where the matrices/vectors and their dimensions are

$[T]$ = transmissivity $[N \times N]$,

$\{H\}$ = total head $[N \times 1]$, and

$\{Q\}$ = volumetric flux $[N \times 1]$, which is null except for the first term.

Solution of matrix Equation 2.41 yields the values of total head at each nodal point. By subtracting the elevation and velocity heads at each node (refer to Equations 1.21 through 1.28, pages 40 to 42), values of pressure head are obtained. The exit loss and wellbore flow loss are calculated externally to the finite element solution by the same two expressions used in the analytical solution (Equation 2.22).

The basis functions, selection of transmissivity values in the two regime flow field, calculation of velocity, assembly (and, if necessary, the partitioning) of the matrices, and the iterative solution scheme (necessitated by the non-linear transmissivity terms) are all described in Appendix C.

2.3 Changes in fracture aperture resulting from changes in effective stress

In the preceding formulations, it has been assumed that the fracture is rigid, that is, the aperture remains constant. As described in Section 1.3.4.5, however, part of the "propping force" in a fluid-filled fracture is the fluid pressure. Therefore, when fluid pressure changes as the result of flow and effective stress change, displacements in

the fracture can occur. Depending on the relative orientation between the fracture and the directions of principal stress, the displacements can be normal and/or shear. In the current problem, however, shear displacements were found to be negligible and attention will be focused on normal, vertical displacements.

The response of a fracture to changes in stress that was shown schematically in Figure 1.7 (page 44) included only deformation of the fracture. The actual response of a fractured rock mass, however, is more complex and involves both the rock matrix and the fractures. Figure 2.1 depicts a cylinder of rock with a single, greatly exaggerated horizontal fracture. In diagram A, the system is at equilibrium subject to an axial stress σ_{v1} and fluid pressure P_1 . If the fluid pressure is decreased ($P_2 < P_1$), the resulting deformation in the discontinuous rock mass will consist of three components (diagrams B and C in Figure 2.1): relaxation in both the top and the bottom cylinders of the rock and deformation or crushing of the fracture, asperities due to increased effective stress.

Although there are some similarities between the model of interest and a thick-walled cylinder, the analytical solutions applicable to the latter are not able to take into account the discontinuity of the fracture. Therefore, only a numerical solution to the problem will be considered.

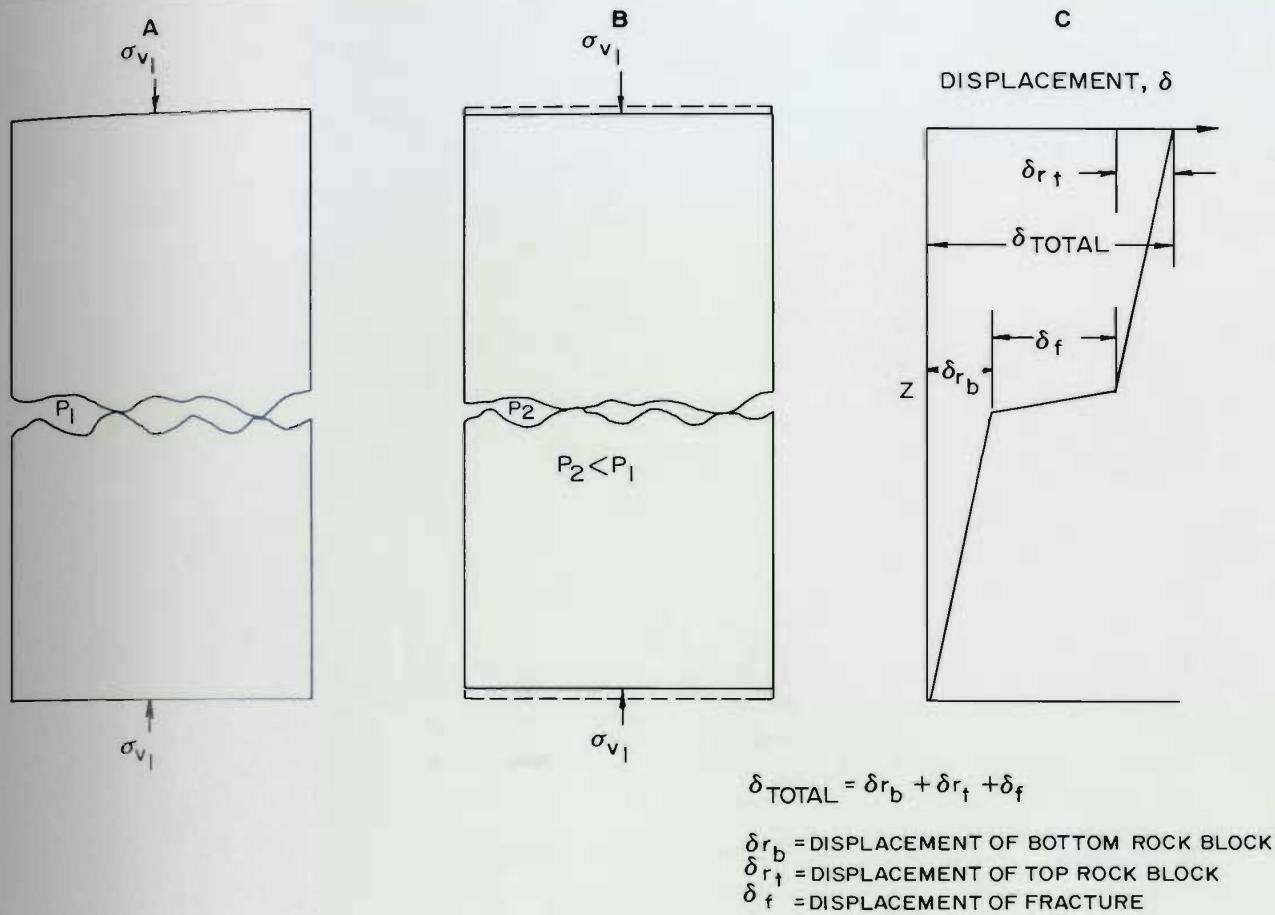


Figure 2.1 Deformation in a discontinuous rock mass. A) Block of rock with a single, fluid-filled (pressure P_1) fracture and subject to vertical stress σ_{v1} . B) Deformation in system caused by decrease in fluid pressure. C) Schematic diagram showing relative components of rock displacement ("relaxation") and fracture displacement (closure). Note that the reference point for displacement is the center of the fracture.

In the numerical model, the rock is assumed to be a linearly elastic material whose deformational characteristics can be described by a constant Young's modulus and Poisson's ratio.

Axisymmetric elements formed by rotation of 2-dimensional triangles (with nodes, i , j , and k) around the axis of the wellbore are used to simulate the rock matrix. Only a brief description of the formulation will be given here; a more complete discussion of axisymmetric stress analysis is given by Zienkiewicz (1971).

The so-called stiffness matrix for an individual element is given by

$$[S]_e = 2\pi \int [B]^T [E] [B] \cdot r \cdot dr \cdot dz \quad (2.42)$$

The matrix $[B]_i$ and its transpose $[B]_i^T$ for each nodal point are the equivalent of the basis functions in the flow equation (Section 2.2.3 and Appendix C) and include the geometric properties of the element given by

$$[B]_i = \frac{1}{2\Delta} \begin{bmatrix} 0 & c_i \\ b_i & 0 \\ \frac{a_i}{r} + b_i + \frac{c_i z}{r} & 0 \\ c_i & b_i \end{bmatrix} \quad (2.43)$$

where (r, z) is the coordinate of the node and a_i , b_i , and c_i are obtained by cyclic permutation of the coordinates of the three nodes comprising the triangular element such that

$$\begin{aligned} a_i &= r_j z_k - r_k z_j \\ b_i &= z_j - z_k \end{aligned} \quad (2.44)$$

$$c_i = r_k - r_j$$

and 2Δ , twice the area of the triangle, is given by

$$2\Delta = \begin{bmatrix} 1 & r_i & z_i \\ 1 & r_j & z_j \\ 1 & r_k & z_k \end{bmatrix} \quad (2.45)$$

The mechanical properties of the rock (Young's modulus, E_r , and Poisson's ratio, μ) are contained in the axisymmetric elasticity matrix $[E]$

$$[E] = \frac{E_r(1-\mu)}{(1+\mu)(1-2\mu)} \begin{bmatrix} 1 & \frac{\mu}{1-\mu} & \frac{\mu}{1-\mu} & 0 \\ \frac{\mu}{1-\mu} & 1 & \frac{\mu}{1-\mu} & 0 \\ \frac{\mu}{1-\mu} & \frac{\mu}{1-\mu} & 1 & 0 \\ 0 & 0 & 0 & \frac{1-2\mu}{2(1-\mu)} \end{bmatrix} \quad (2.46)$$

Equation 2.42 either can be evaluated approximately for a centroidal point (\bar{r}, \bar{z}) or by exact integration. The routine used in DEFLOW, the program developed in this study, is based on a code by Gale (1975) which uses exact integration. Examination of the dimensions of the various matrices comprising Equation 2.42 indicates that $[S]_i$ has the dimensions

$$\begin{aligned} [S]_i &= [2 \times 4][4 \times 4] [4 \times 2] \\ &= [2 \times 4] [4 \times 2] \\ &= [2 \times 2] \end{aligned} \quad (2.47)$$

for each node so that for a 3-node triangular element, the element stiffness matrix has the dimensions $[6 \times 6]$.

The fractures are modeled by a line of 2-node (i and j) elements, each pair corresponding to a flow node. Under static conditions, it can be shown that for the fracture element undergoing both normal or vertical (z) and shear or radial (r) displacement

$$A_S \begin{bmatrix} K_n & -K_n \\ -K_n & K_n \end{bmatrix} \begin{Bmatrix} D_{z_i} \\ D_{z_j} \end{Bmatrix} = \begin{Bmatrix} F_{z_i} \\ F_{z_j} \end{Bmatrix} \quad (2.48)$$

and

$$A_S \begin{bmatrix} K_s & -K_s \\ -K_s & K_s \end{bmatrix} \begin{Bmatrix} D_{r_i} \\ D_{r_j} \end{Bmatrix} = \begin{Bmatrix} F_{r_i} \\ F_{r_j} \end{Bmatrix} \quad (2.49)$$

where

K_n = normal stiffness,

K_s = shear stiffness,

A_S = area over which stiffness is applicable,

D = displacement, and

F = force.

In DEFLOW, the applicable area is calculated from the midpoint between adjacent nodal pairs.

Whereas the stiffness of the rock elements is constant since the Young's modulus and Poisson's ratio are considered to be constant within the range of stresses to be modeled, stiffness of the fracture(s) is stress-dependent and is generally quite non-linear. Figure 2.2 is an example of a

typical plot of normal displacement versus normal effective stress for a fracture. By definition, stiffness is the tangent to the curve. Various investigators have used different mathematical expressions to describe the non-linear relationship shown in Figure 2.2 (Bandis et al., 1983). In this study, actual laboratory data are analyzed by non-linear regression to obtain an expression in the form:

$$\sigma_n = S_1 \delta + S_2 \delta^n \quad (2.50)$$

where

σ_n = normal stress,

S_1, S_2 = stiffness coefficients,

δ = normal displacement, and

n = an exponent > 1 .

The derivation of the normal equations used in the regression analysis and a listing of the computer program used to determine the values for S_1 , S_2 , and n are included in Appendix C.

The stiffness matrices for the 2-node fracture elements and the 3-node triangular rock elements are assembled into a single global stiffness matrix, and the resulting stiffness equation for the entire discontinuous rock mass can be written as:

$$[S]\{D\} - \{F\} = 0 \quad (2.51)$$

or

$$[S]\{D\} = \{F\} \quad (2.52)$$

where the matrices/vectors and their dimensions are

$[S]$ = stiffness $[2N \times 2N]$,

$\{D\}$ = displacement $[2N \times 1]$, and

$\{F\}$ = force $[2N \times 1]$.

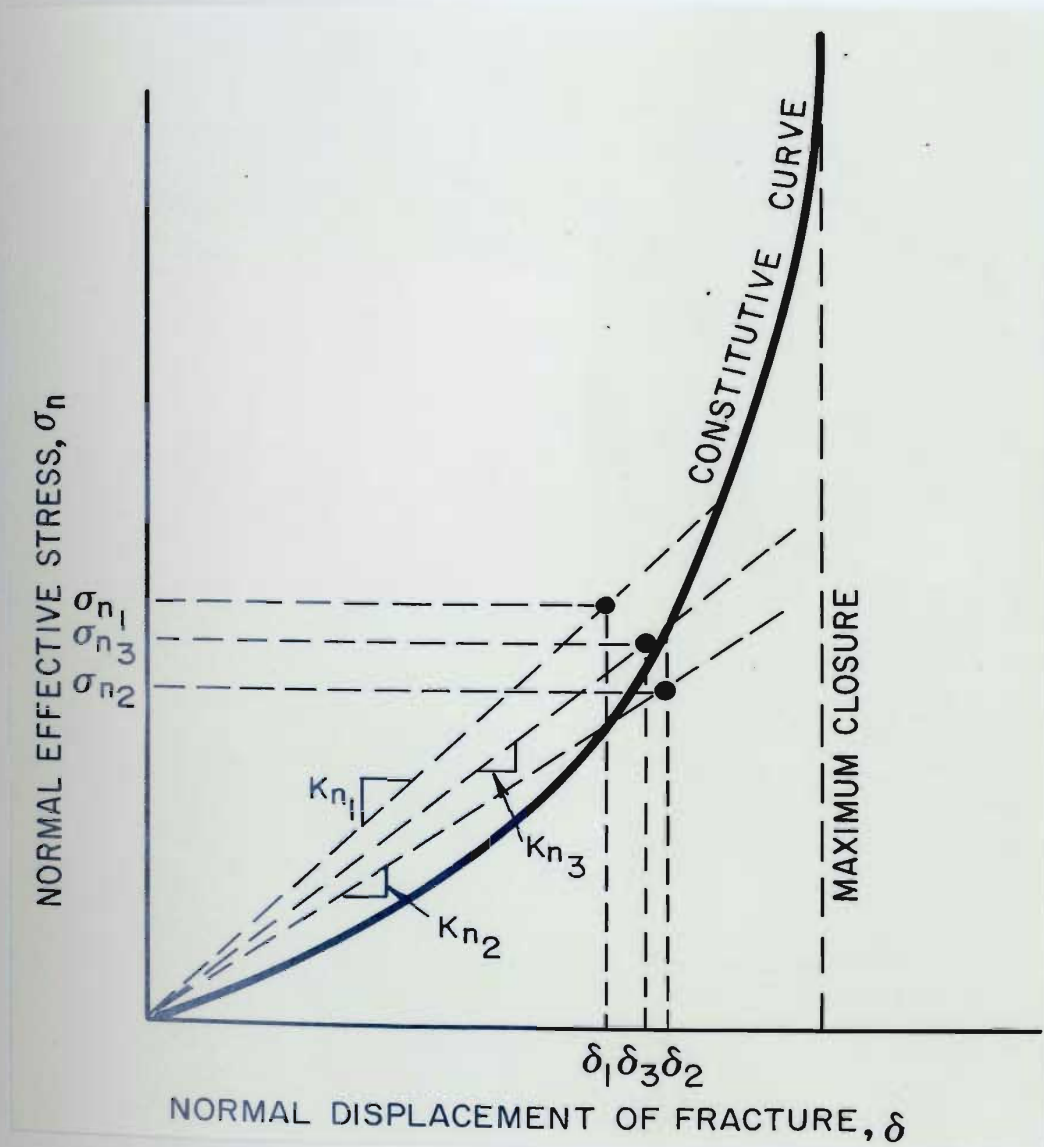
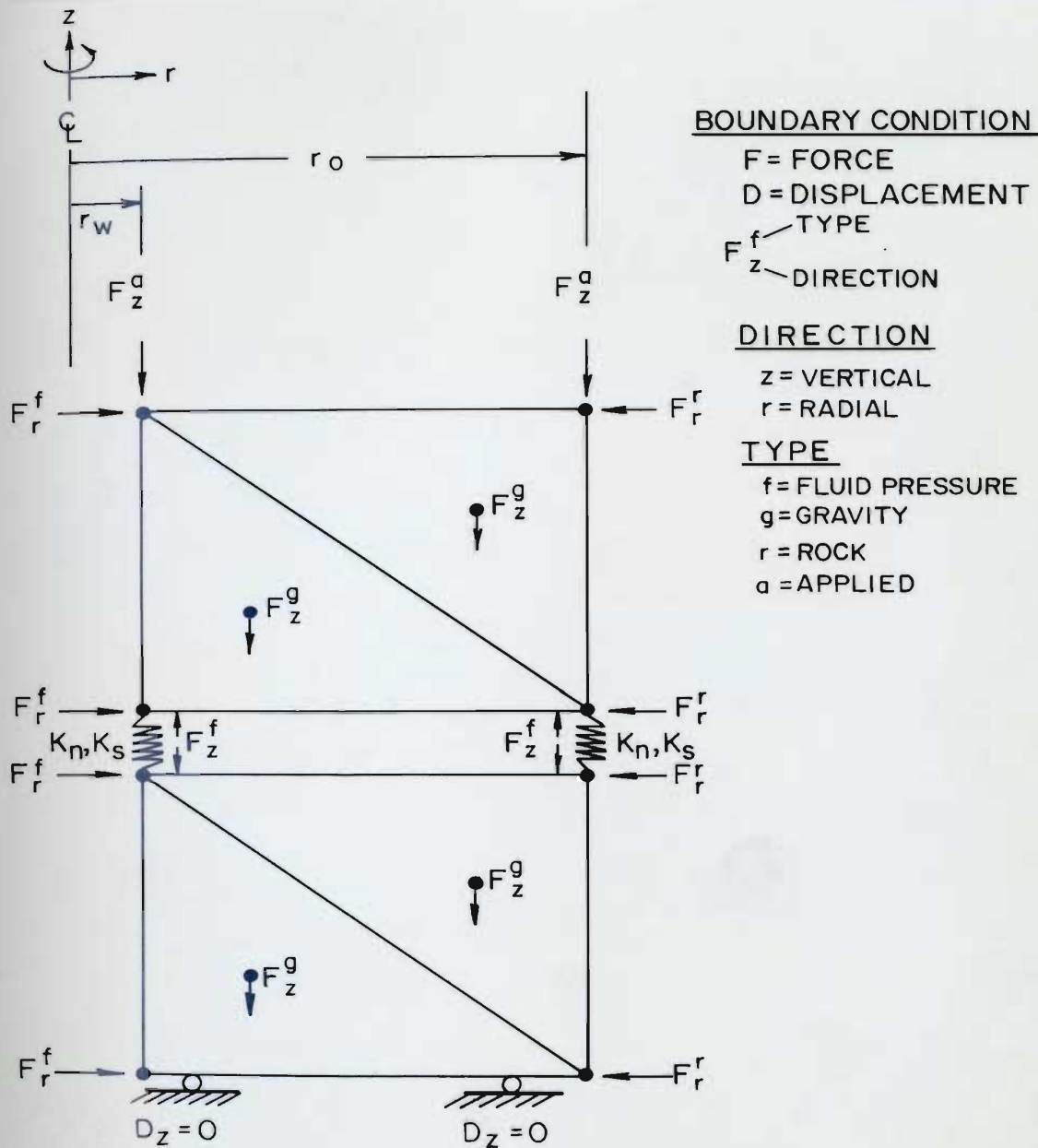


Figure 2.2 Typical normal effective stress versus displacement relationship for a fracture

Note that the dimensions of the matrices are twice the number of nodes since there are two components (radial and vertical) of displacement and force for every node.

The force vector includes all of the external boundary forces as well as the internal body or gravity forces which must be calculated for each of the rock elements. The external boundary forces, which actually act over an entire surface, must be assigned to end nodal points; the appropriate point loads are calculated from equilibrium considerations. The gravity forces are defined at the centroids of the axisymmetrical elements, but again under consideration of static equilibrium, are proportionately assigned to the three nodes comprising the element. A complete set of boundary conditions for a schematic 4-element case is shown on Figure 2.3. The actual discretization used for the deformation code is described in Appendix C.

Solution of Equation 2.52 gives the vertical and radial components of displacement of all nodes in the system. Because of the non-linear stiffness of the fracture node, the solution must be achieved iteratively. As the fracture closes, it becomes stiffer and the new stiffness affects the response of the entire system. A method of successive approximations based on the secant method (Figure 2.2) is used (see Appendix C).



| ROCK PROPERTIES | FRACTURE PROPERTIES | FLUID PROPERTIES |
|-----------------|---------------------|------------------|
| E_r | K_n | ρ |
| μ | K_s | v |
| ρ_r | | |

Figure 2.3 Structural elements and boundary conditions used in deformation code of DEFLOW

The only displacements of real interest to this study are those of the fracture nodes. By determining the relative vertical displacements (the shear or horizontal displacements are not significant to this problem) between the two nodes comprising each fracture node pair and subtracting that displacement from the initial aperture of the fracture, a new fracture aperture can be estimated for each flow node.

2.4 Flow through multiple fractures

The computer program DEFLOW has been written so that up to three fractures can be included in the analysis. The only limitation to expanding the code to consider even more fractures is the effort required for generating the finite element grid.

Whereas the case of one-fracture can be solved with either first or second type boundary conditions at the well, the case of multiple fractures can only be executed under first type boundary conditions. The total head in the wellbore at the lowermost fracture is specified. Beginning with that fracture, the head distribution in the fracture is calculated. Then the exit loss and wellbore flow loss are calculated and the net total head is assigned as the wellbore boundary head for the next fracture up. This is shown schematically in Figure 2.4

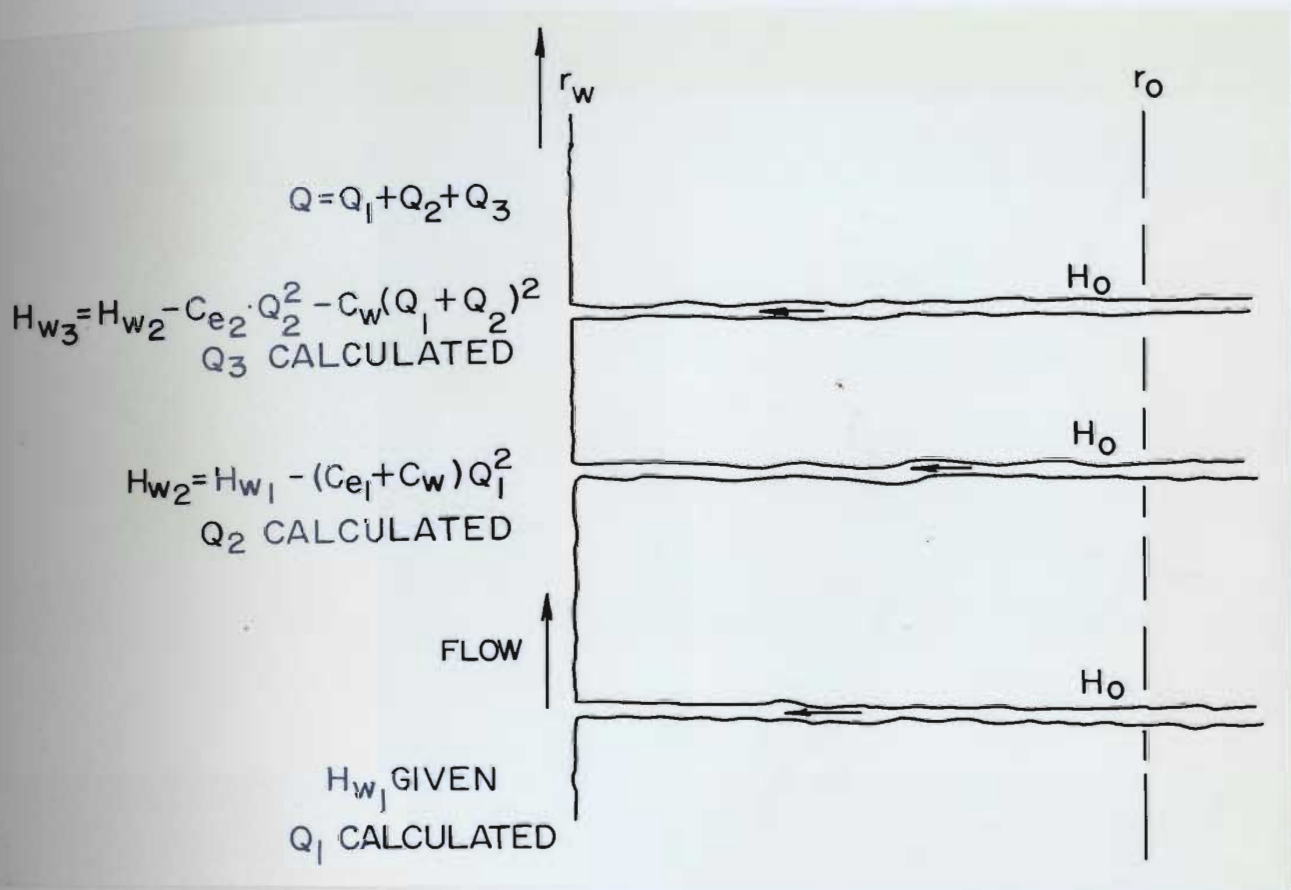


Figure 2.4 Boundary conditions for flow in multiple fractures

2.5 Coupled numerical solution

A coupled numerical solution to the problem of two-regime radial flow to a well through horizontal, deformable fractures is obtained using the program DEFLOW which was specifically written for this study. The iterative solution scheme which it follows is outlined in the flow chart given in Figure 2.5. Pressure head, which is common to both the flow (as output) and deformation (as a boundary condition) routines, is used as the linking term. A more detailed

description of the program and its various codes; a brief user's guide, and a complete listing are included in Appendix C.

As indicated in Figure 2.5, there are three modes in which DEFLOW can be run. They are initiated by the character variable commands "GOFLOW", "GODRILL", and "GOBOTH". In the first mode, the fractures are assumed to be rigid, and only the flow codes are activated. With "GODRILL", the system is considered to be under hydrostatic conditions, and the deformation codes alone are used to calculate the displacements resulting from stress concentrations due to drilling of the vertical wellbore.

The complete, coupled solution is initiated by the control word "GOBOTH", and proceeds as follows:

- 1) Initial conditions are specified. These include applied boundary loads, internal body or gravity loads, fixed displacements, and the properties and dimensions of the fluid, fracture(s), and rock layers.
- 2) Displacements due to initial loads (either gravity or applied) are considered to be pre-existing. Therefore, it is necessary first to determine the "background" displacements so that they can be subtracted from the total displacements resulting from disturbances to the system in the subsequent calculations.
- 3) Although the effects have been found to be negligible, for the sake of completeness, the displacements due to drilling of the well are calculated and are used to modify the initial fracture apertures.

- 4) The total head distribution in each fracture is calculated for the given fracture apertures and fluid boundary conditions. Because of non-linear flow laws, this must be done iteratively. From the total heads, pressure heads are then calculated.
- 5) The resulting fluid pressure distribution determines the new loads at the fracture nodes, and the displacements are re-calculated for the new set of boundary conditions. In the deformation code, any significant changes in the fracture aperture will result in changes in its stiffness. This in turn will alter the displacements. Therefore, the deformation code also must be solved iteratively ensuring that the constitutive relationship of the fracture(s) is maintained at all times. Once convergence has been met (a convergence criterion of 1 or 2 percent is generally used), the relative displacements of the fracture nodes are calculated and the apertures modified accordingly.
- 6) Using the new fracture apertures, the total head and the pressure head distribution are recalculated and the pressure heads are compared to the previous set of values. If the values are within a user-designated tolerance, the program is terminated. If not, the deformation routine is re-run under the new fluid pressure boundary conditions. The flow-deformation iteration is continued until convergence is achieved. Again, a user-defined convergence criterion (usually 1 or 2 percent) is used.

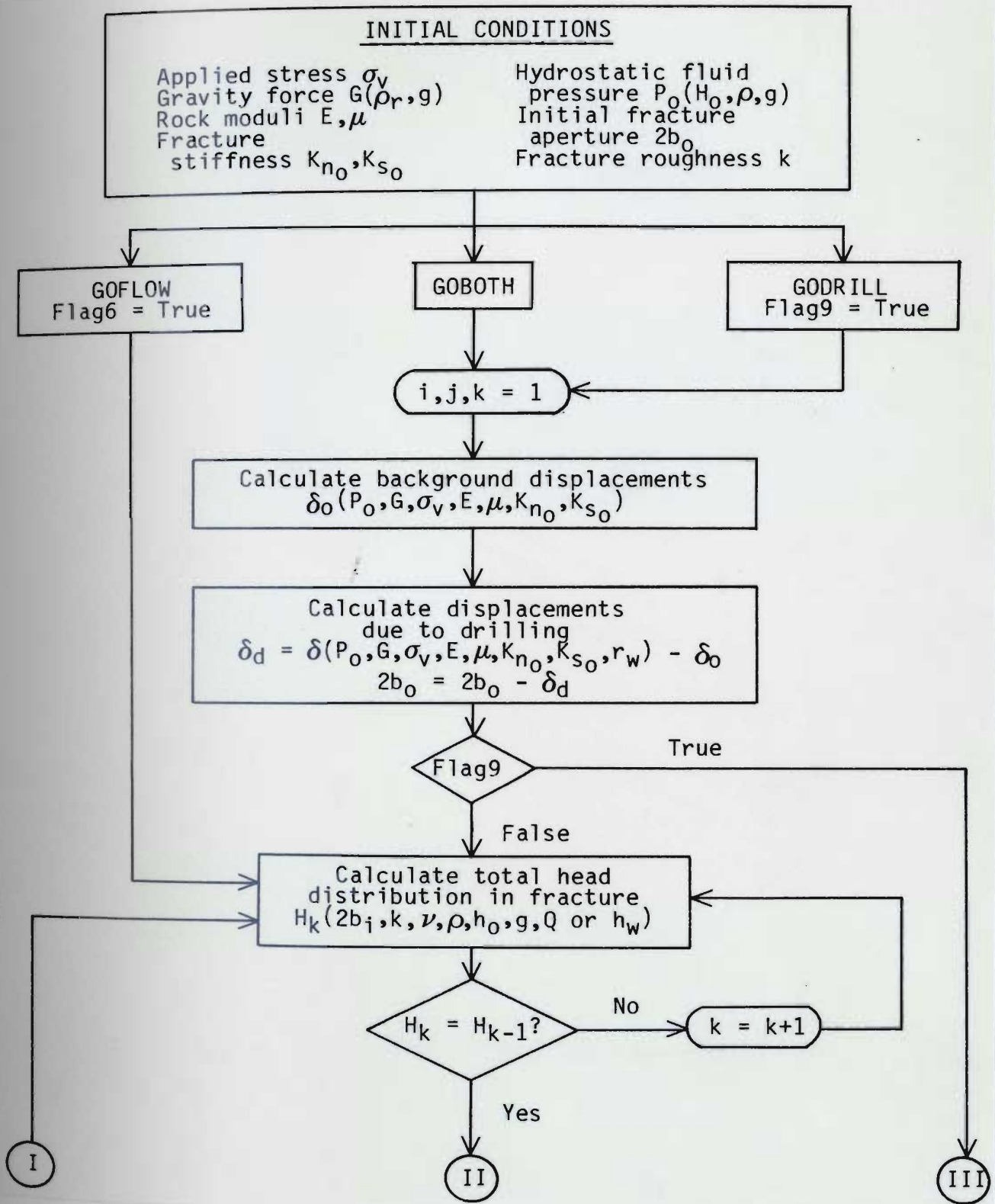


Figure 2.5 Flow chart of coupled deformation-flow solution using DEFLOW

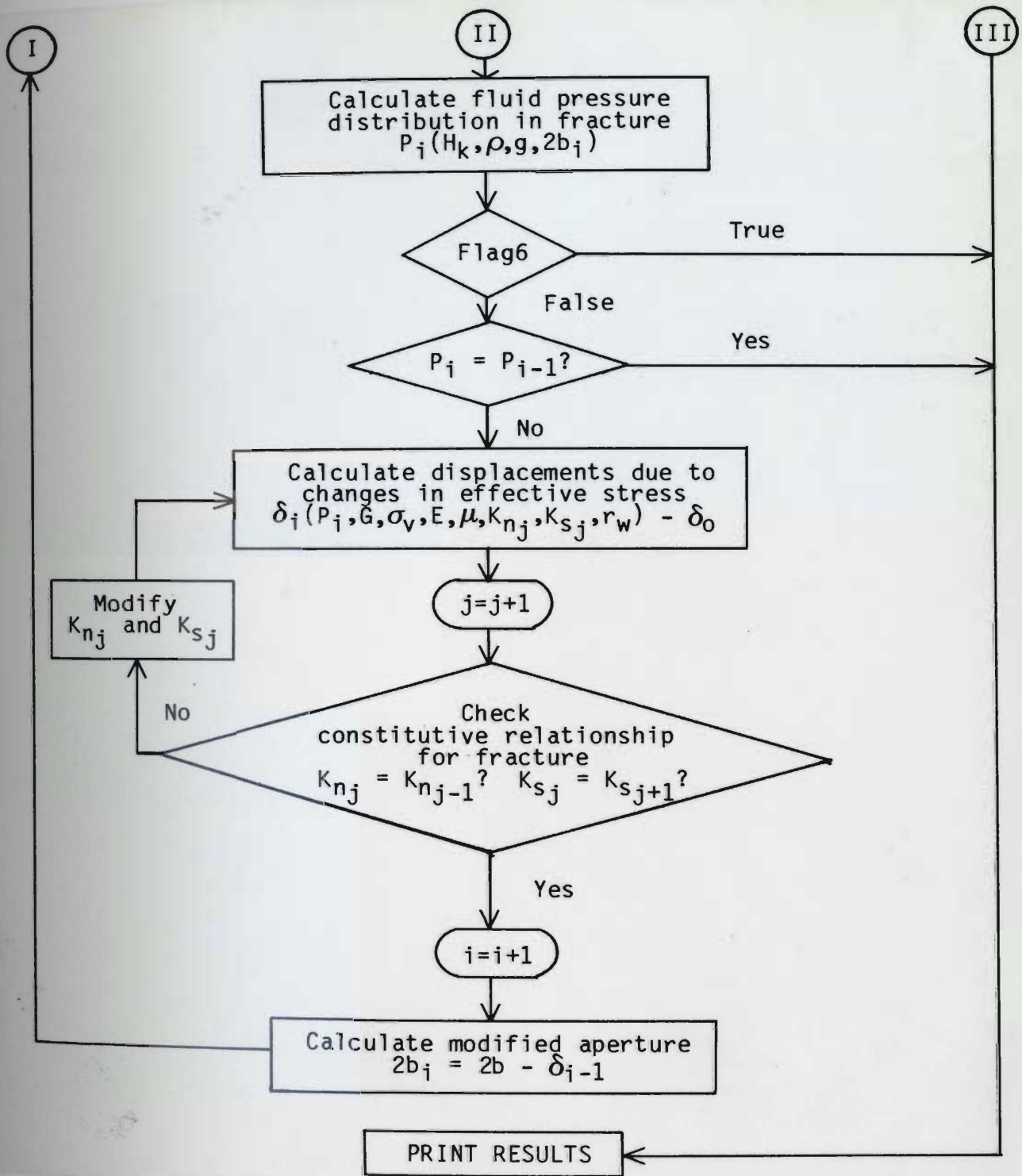


Figure 2.5 (Continued) Flow chart of coupled deformation-flow solution using DEFLOW

3.0 NUMERICAL SIMULATION USING THE PROGRAM 'DEFLOW'

Using DEFLOW, a series of numerical simulations were conducted in order to 1) compare the results from the numerical model with those from an analytical solution for the case of a rigid fracture and, in the coupled mode, 2) perform sensitivity analysis to demonstrate which fracture flow parameters have the greatest influence on the production-drawdown response of a well, 3) extend the numerical findings for flow in a single horizontal fracture to multiple horizontal fractures, and 4) attempt to synthesize the results of a step-drawdown test of a well intersecting horizontal fractures.

3.1 Comparison of numerical solution with analytical solution

The drawdown distribution in a horizontal fracture predicted both by DEFLOW (for both first and second type boundary conditions at the well) and by an analytical solution incorporating Equation 2.22 (page 56) are compared graphically in Figure 3.1. As can be seen in this total head loss versus the logarithm of radial distance plot, the solutions are virtually indistinguishable from the outer boundary to the critical radius (indicated by the break in slope). Radially inward from that point, in the non-linear flow

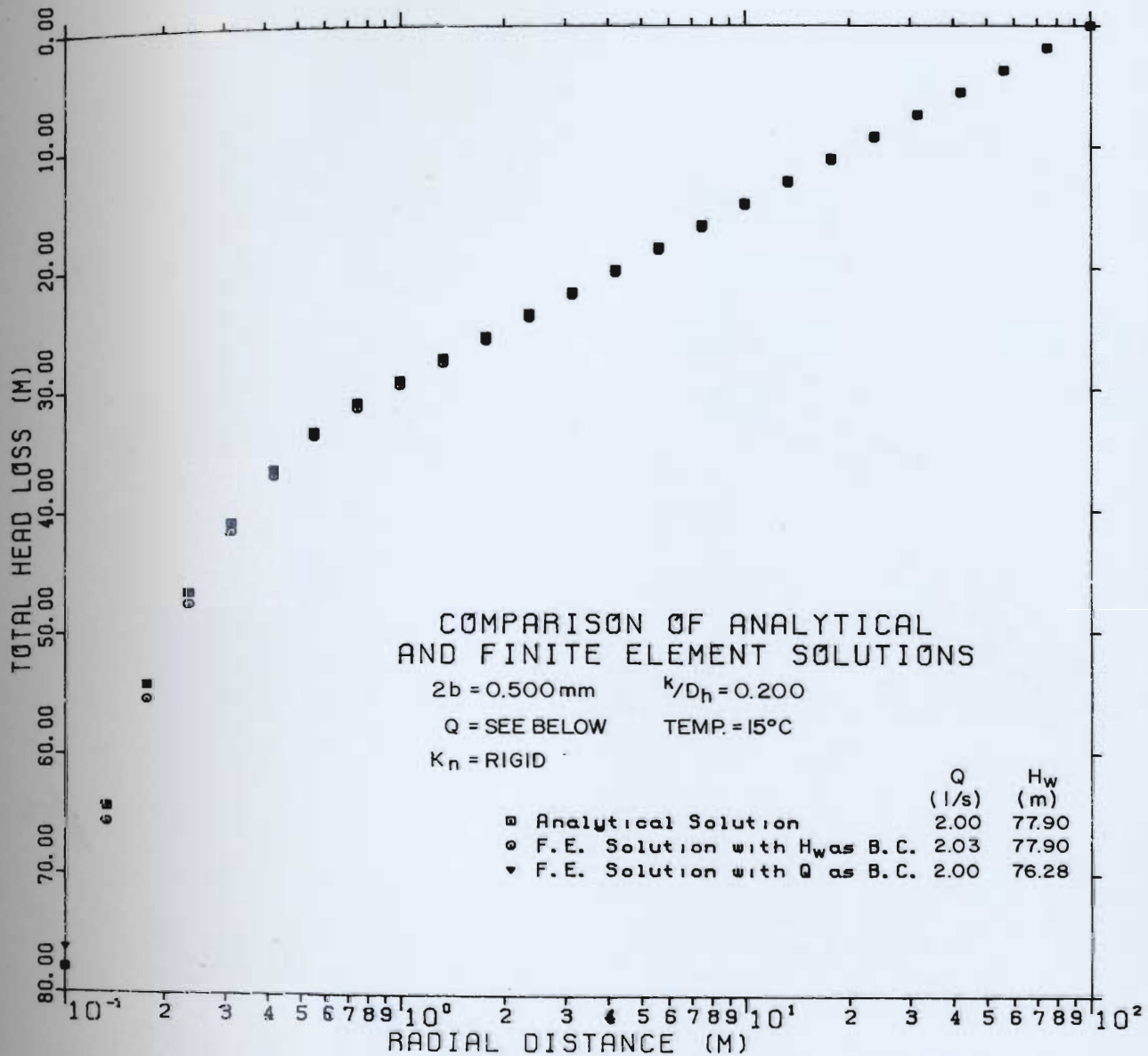


Figure 3.1 Comparison of finite element and analytical solutions for flow

region, there is some divergence. Under a first type boundary condition (using the same head in the well as calculated by the analytical solution), the discharge calculated by DEFLOW for this example was 1.5 percent greater than that from the analytical model. The heads in the wellbore

differed by 2.2 percent when a second type boundary condition (the same discharge rate as used in the analytical solution) was used in the numerical model.

The goodness of fit between the analytical and numerical solutions is a function of the number of flow nodes used in the numerical model. The accuracy shown in Figure 3.1 using only 25 nodes, however, was considered to be acceptable; and for most problems using this numerical model, there appears to be no need to use more nodes. In fact, similar accuracy was obtained in attempting to simulate the laboratory model (Section 5.0) using only 15 flow nodes.

The numerical simulations made for comparison with the analytical solution were for flow only, and DEFLOW was run just in the GOFLOW mode (see Appendix C). No closed form analytical solutions are known to exist for determining axisymmetric deformation under the relatively complex boundary conditions of this problem, so a similar comparison with the results from the deformation code (and, hence, with the numerical model in the coupled mode) could not be made.

3.2 Sensitivity analysis

A sensitivity analysis was conducted to quantitatively assess the absolute and relative influence of the various fracture flow parameters on the drawdown (total head loss)

response of a well intersecting a single horizontal fracture. Although the analysis was done using the numerical model, reference to Equation 2.22 (page 56) helps to visualize the role of the various parameters in the first three components of total drawdown (the wellbore losses were neglected in this analysis).

The reference case for the analysis had the following physical dimensions and boundary conditions:

$$\begin{aligned}
 r_w &= 0.1 \text{ m,} \\
 r_o &= 100.0 \text{ m,} \\
 H_o &= 100.0 \text{ m,} \\
 \text{temp.} &= 15^\circ\text{C,} \\
 Q &= 1.0 \times 10^{-3} \text{ m}^3/\text{s,} \\
 2b &= 0.500 \text{ mm,} \\
 k/B_h &= 0.200, \\
 f_w &= 0.07, \text{ and} \\
 K_n &= \text{totally rigid.}
 \end{aligned}$$

The changes made to the primary parameters are shown in Table 3.1. The primary parameters are aperture, roughness, and viscosity (temperature is used as the variable); but variation in discharge rate, which is actually a boundary condition, has been included in the analysis to indicate its major influence on the critical radius (Equation 2.21 on page 55). The resultant drawdowns, which are plotted in Figures D1-D6 (Appendix D), are also included in Table 3.1.

The sensitivity ratio is defined by

$$\text{sensitivity ratio} = \frac{\frac{s_{\max} - s_{\min}}{s_{\min}}}{\frac{x_{\max} - x_{\min}}{x_{\min}}} \quad (3.1)$$

Table 3.1 Summary of sensitivity analysis input and results

| Parameter | Units | Input Values | Resultant Drawdowns | Sensitivity Ratio |
|-----------------------------|--------------------------------|--------------|---------------------|-------------------|
| k/D_h | [] | 0.1-0.4 | 17.5-52.1 | 0.66 |
| 2b (k/D_h same) | mm | 0.3-0.7 | 8.8-125.9 | 10.2 |
| 2b (k same) | mm | 0.3-0.7 | 7.2-199.1 | 20.5 |
| Temperature | $^{\circ}\text{C}$ | 5-20 | 24.6-32.6 | 0.11 |
| σ_v ("stiffness") | MPa | 1.0-2.0 | 76.4-91.4 | 0.20 |
| Q | $10^{-3} \text{ m}^3/\text{s}$ | 0.5-2.0 | 11.2-76.4 | 1.90 |

where x is the parameter or dependent variable which influences the drawdown, s . This ratio is not an absolute indicator of sensitivity because most of the variables are in non-linear functions. Therefore, the sensitivity ratio for each parameter will depend on the range of the dependent variable used. However, it is believed that the range of input values is representative of field conditions that could be encountered so that the resulting sensitivity ratios are an indication of relative sensitivity.

Most of this analysis and its results are straightforward. However, differentiation needs to be made between the changes in aperture with and without change in the rela-

tive roughness. (in the latter, the absolute roughness must be changed to keep the relative roughness the same as aperture changes). For the case of the absolute roughness being kept constant, the sensitivity ratio is actually a compounded value reflecting changes of two parameters, aperture and relative roughness.

The sensitivity ratio calculated nominally for change in "stiffness" and the assumptions made in this specific part of the analysis also require additional explanation. In order to get a significant response in aperture deformation, two boundary conditions had to be adjusted: 1) the discharge rate had to be increased to $2.0 \times 10^{-3} \text{ m}^3/\text{s}$ in order to generate a greater change in effective stress; and 2) initially the fracture had to be made very "soft" by using a relatively low applied top load to static hydraulic head ratio in the range of 1.1 to 2.2. The latter factor corresponds hydrogeologically to highly artesian flowing conditions. Under a normal geostatic gradient of 0.027 MPa/m (Goodman, 1980), this represents a fracture at a depth of 42 to 79 meters (including the thickness of the top rock layer used in the numerical model) containing water with a static hydraulic head of 100 meters, an anomalous condition at best.

A relatively moderate fracture stiffness also had to be assigned in this part of the analysis to get any significant

fracture deformation. For this purpose, the stiffness of the fracture in the laboratory model, defined by the constitutive relationship $\sigma_n = 6.33 \times 10^{-3} \delta + 2.50 \delta^{3.82}$, was used. The differences in drawdown under these conditions are shown in Figure D5 in Appendix D. Since the results showed less sensitivity to the fracture stiffness used, that parameter (or relationship) was kept constant; and the analysis was performed by modifying the initial fracture stiffness (i.e., by changing the top applied boundary load, σ_z).

The increase in effective stress and resulting deformation in the fracture as calculated by DEFLOW for the case with $\sigma_z = 1.0$ MPa is shown in Figure 3.2. For a total fracture displacement or closure of about 30 μm (approximately 25 μm in the upper surface and 5 μm in the lower) at the wellbore boundary and the displacement distribution shown in Figure 3.2, the resulting drawdown was approximately 15.0 m more than under completely rigid conditions (see Figure D5).

It should be noted that the structural elements and boundary conditions used in the analysis of sensitivity to stiffness are highly idealized. The fracture displacement calculated by DEFLOW is due solely to elastic deformation in the horizontal fracture and in the rock, assuming a continuum from the wellbore to the outer boundary, a distance,

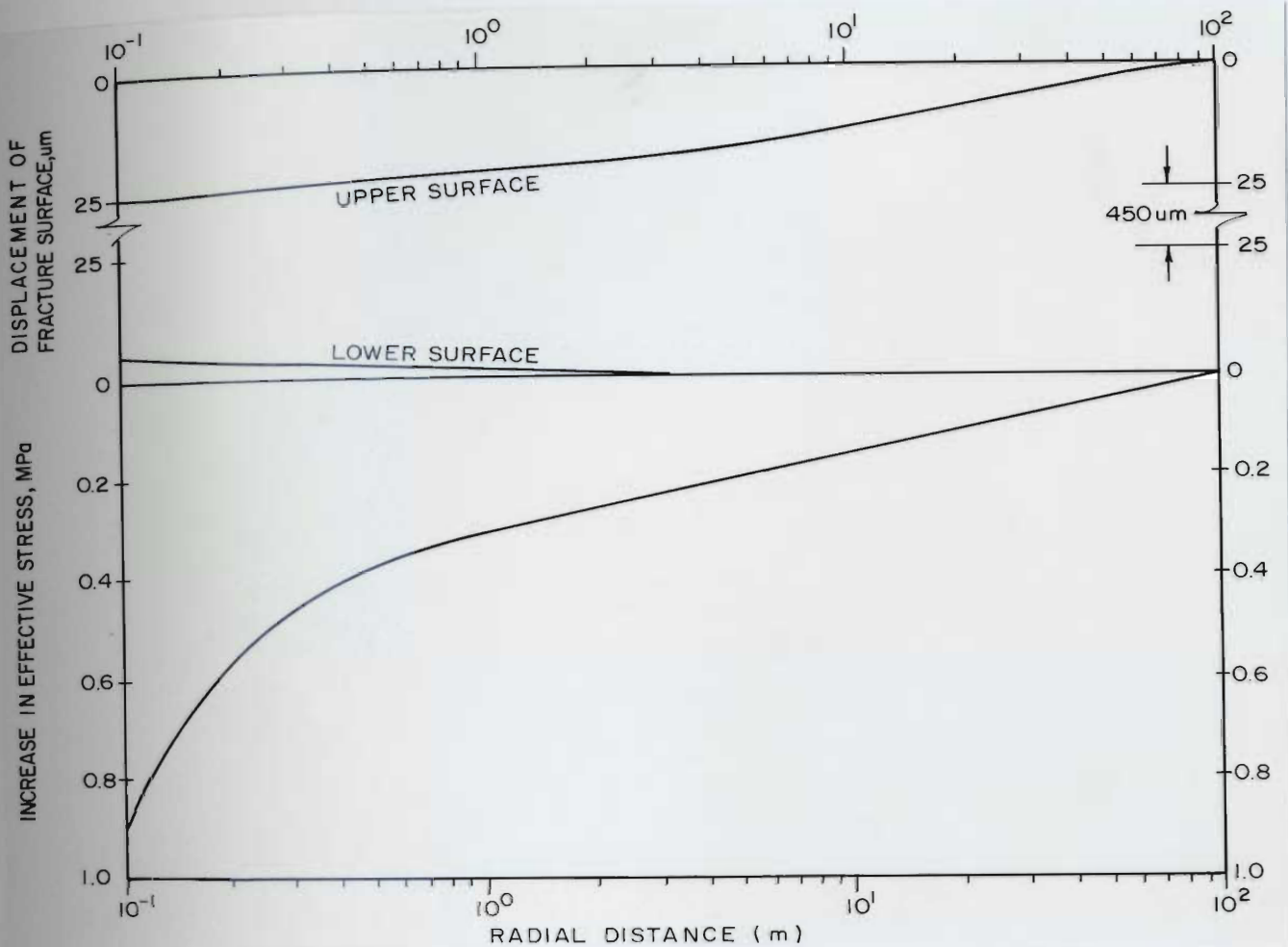


Figure 3.2 Increase in effective stress and fracture closure versus log radial distance

for the case analyzed, of 99.9 m. It is highly unlikely in the field that such an expanse of intact rock would exist without some high angle discontinuities. These discontinuities could permit vertical displacements of smaller blocks of rock near the wellbore. Simulation of such displacements, however, is not within the capability of DEFLOW.

3.3 Results with multiple fractures

DEFLOW was also used to analyze the production-drawdown response in a well tapping multiple horizontal fractures. Although the numerical model is capable of handling any number of fractures (the size of the computer used being the only limiting factor), setting up the finite element grids for multiple fracture cases is time consuming (see Section C.1 in Appendix C). Only multiple fracture problems with three fractures were simulated, but the general findings should be able to be extrapolated to more fractures. As explained in Section 2.4 (page 74), only first type boundary conditions can be used at the wellbore in the case of multiple fractures.

Figure 3.3 shows the total head loss versus log radial distance for three fractures with apertures ranging from 0.4 to 0.6 mm and having different relative roughnesses. As in the plots shown in Appendix D, the distance-drawdown format is used because it clearly indicates the critical radius and emphasizes the short radial distance over which the greatest head losses occur, especially where non-linear flow occurs. The simulation shown in Figure 3.3 was conducted, as noted, with a rigid fracture. A simulation using the same fractures, but allowing fracture deformation (with $\sigma_v = 2.0$ MPA and using the fracture stiffness described in Section 3.2)

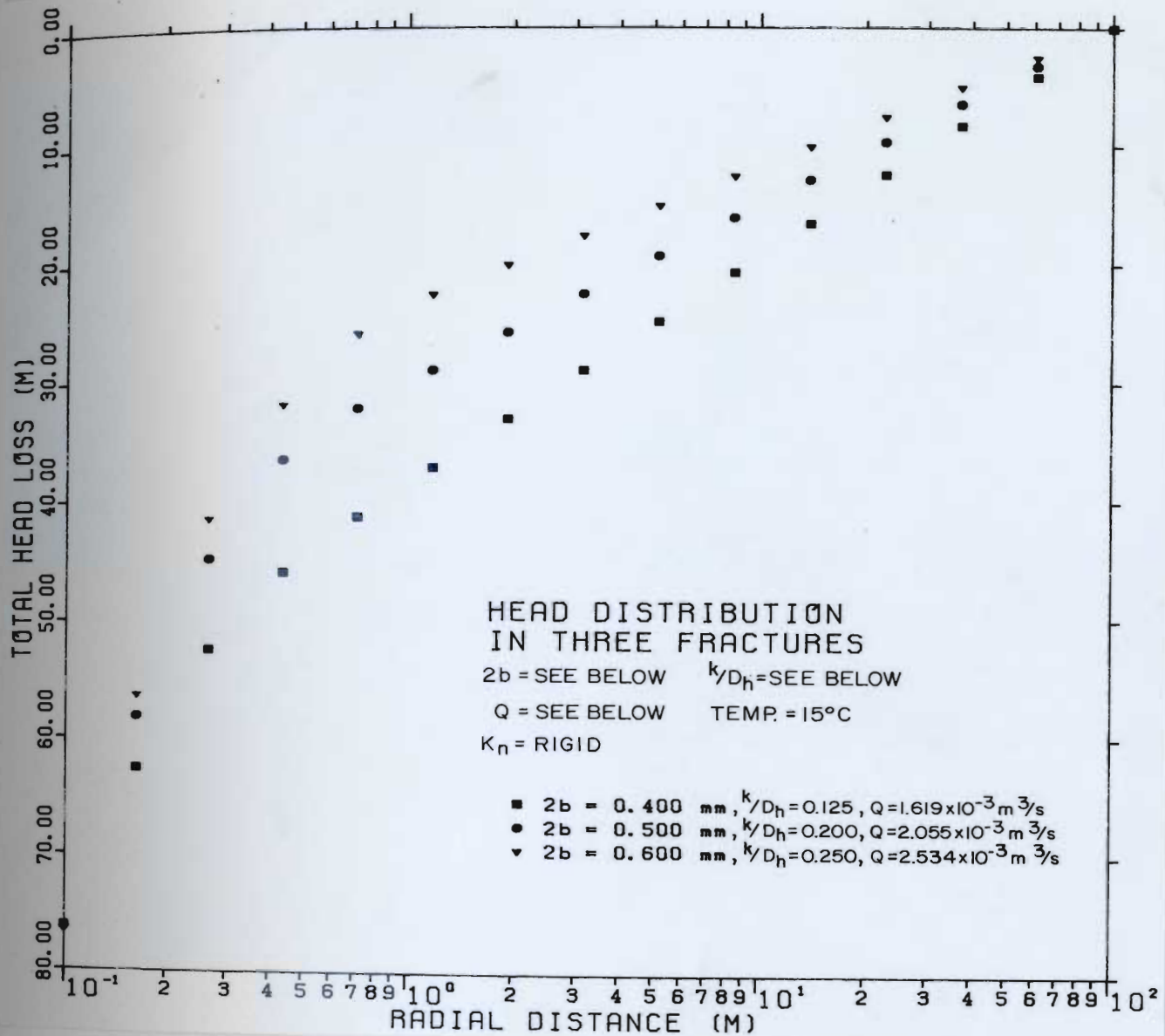


Figure 3.3 Total head loss distribution in three fractures of different aperture and relative roughness

resulted in a cumulative discharge 3.9% less than that for the rigid fractures.

A noteworthy observation made during the simulations of flow through multiple fractures is the significant departure

of relative discharge from those predicted by the so-called cubic law (Equation 1.19 on page 25) that can occur. This law indicates that discharge is a function of the aperture cubed and, therefore, that the relative discharge to a well from fractures of different aperture should follow that ratio. As shown in Figure 3.4, the relative discharge from a fracture with a larger aperture (assuming relative roughness is the same) can be less than that predicted by the cubic law. This is because with two-regime flow a greater portion of the head loss in the larger fracture occurs in the non-linear flow region (see Figure 3.3). Thus, for a given drawdown, the relative discharge from the larger fracture is less than that predicted by the cubic law which assumes completely laminar flow.

3.4 Synthesized step-drawdown tests.

A step-drawdown test of a well tapping a single deformable, horizontal fracture was synthesized using DEFLOW by calculating the drawdown at pumping rates of 0.1 to 2.0 l/s in increments of 0.1 l/s for the following physical dimensions and boundary conditions:

$$\begin{array}{ll}
 r_w = 0.1 \text{ m} & 2b = 0.500 \text{ mm} \\
 r_o = 100.0 \text{ m} & k/D_h = 0.200 \\
 H_o = 100.0 \text{ m} & f_w = 0.07 \\
 \sigma_v = 2.5 \text{ MPa} & \text{temp.} = 15^\circ\text{C} \\
 \sigma_n = 6.33 \times 10^{-3} \delta + 2.50 \delta^{3.82} &
 \end{array}$$

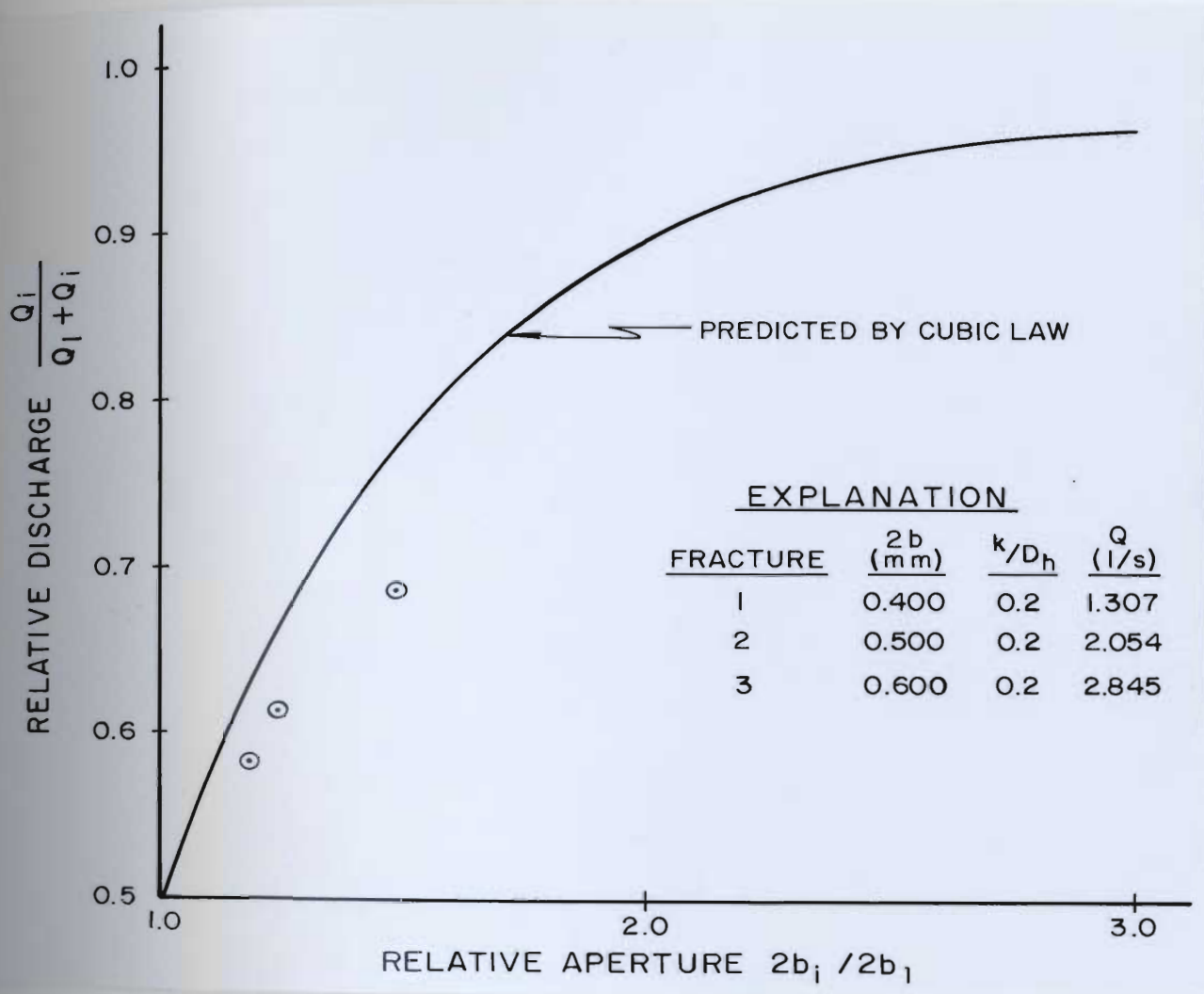


Figure 3.4 Relative production from fractures of different aperture

The results of the simulation are plotted as specific draw-down versus discharge rate in Figure 3.5. It is immediately obvious that these data produce the "curve 3" shape described by Mackie (1982) and discussed in Section 1.3.3 (pages 19-22). It should also be noted that the best fit to these data by FASTEP, a computer solution by Labadie and

Helweg (1975) which uses non-linear regression, was found to be $s_w = 19.7 Q + 7.67 Q^{2.45}$.

A second simulated step-drawdown test with inflow from three fractures was performed. Its results yielded a curve very similar to that of Figure 3.5 and a drawdown equation of $s_w = 5.75 Q + 0.64 Q^{2.34}$. The significance of the shape of these plots and of the values of the exponent in the second term being greater than 2 will be discussed in Section 6.1.

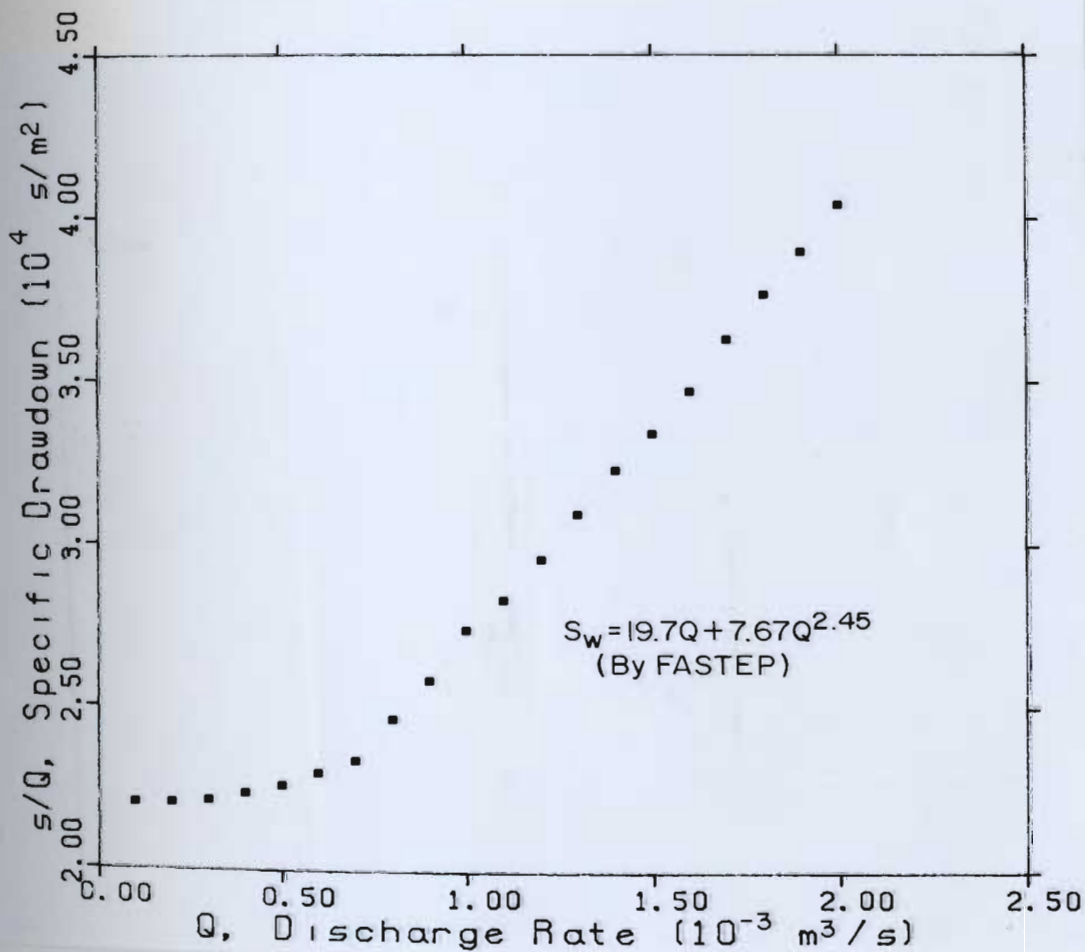


Figure 3.5 Specific drawdown versus discharge for a synthesized step-drawdown test

4.0 LABORATORY TESTING OF RADIAL FLOW MODEL

The second major component of this study (the first being the development of the numerical model) was the design, construction, and testing of a large scale laboratory model. The following section is a brief description of the model. Details of its design and construction are given in Appendix E, and it is suggested that the reader review this appendix before proceeding.

4.1 Description of laboratory model

A 1.50 m diameter by 3.02 m high concrete cylinder with a cast-in-place joint and with a diamond-cored hole along its axis was used to simulate a wellbore intersecting a single horizontal fracture. A photograph of the model as-built is shown in Figure 4.1, and a schematic diagram illustrating its primary components is presented as Figure 4.2.

A closed plumbing system, in which the water was cooled to offset heat generated by the pump, recirculated water between the well collar and a circumferential reservoir which straddled the fracture. For "pumping" tests, water was introduced under regulated pressure to the circumferential reservoir (this arrangement is depicted in Figure 4.2). To simulate "injection" tests, the flow lines were reversed



Figure 4.1 Laboratory model as-built

so that the pressurized water was introduced at the well collar. In either case, flow rates were measured using an electronic paddlewheel flowmeter. Pressure heads were measured in the reservoir, in the wellbore, and in several manometers in the fracture by two transducers connected to the manometers via a multiplexing valve arrangement. A series of linear variable displacement transformers (LVDT's) were used to measure displacements of the fracture and deformation in the concrete. The locations of both the fracture manometers and LVDT's are shown in plan view in Figure 4.3.

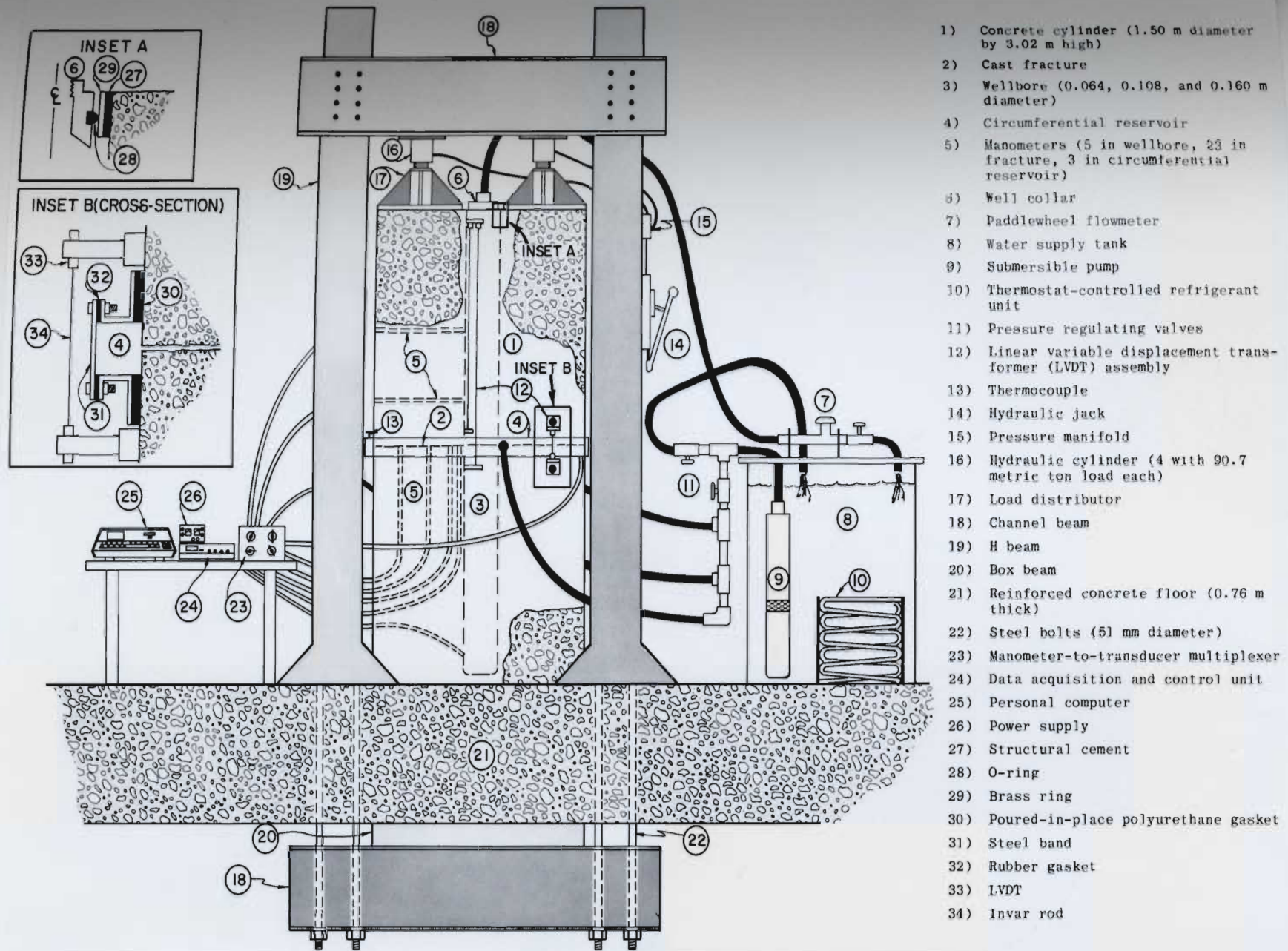


Figure 4.2 Schematic diagram of laboratory arrangement

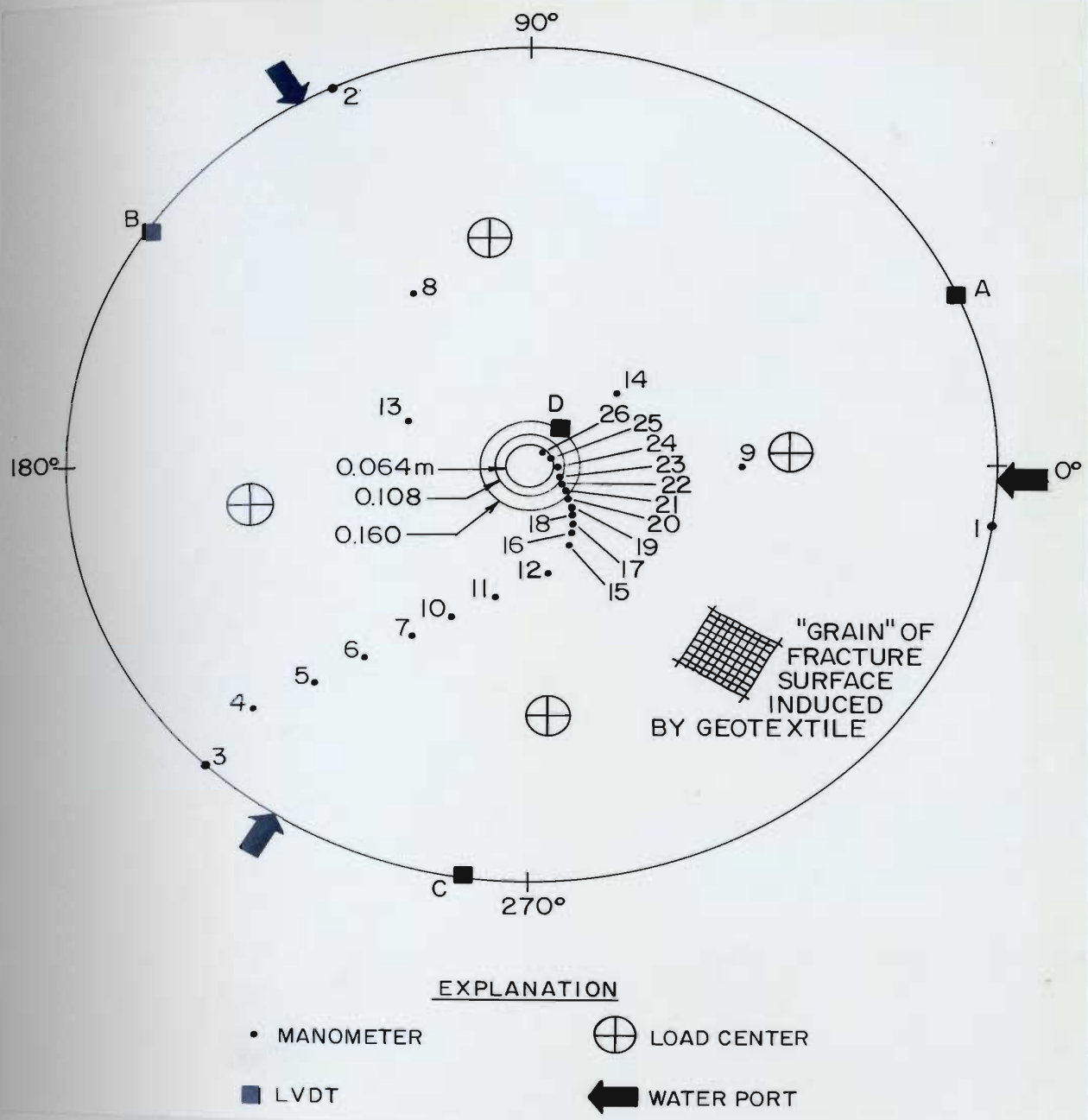


Figure 4.3 Plan view of location of fracture plane manometers, LVDT's, and loading centers

Axial loads, both to prevent hydrostatic pressure from lifting the top cylindrical block and to simulate geostatic pressure at depth, were applied by means of four hydraulic

jacks connected to specially fabricated, gusseted jack stands. In order to prevent possible damage to the floor of the laboratory, the existing loading frame had to be modified so that the concrete cylinder and floor were sandwiched together between the top cross-member and a similar steel set installed in a gallery beneath the laboratory.

Axial load, pressure head, fracture and concrete deformations, and water temperature (a thermocouple was installed in the circumferential reservoir) data were read and stored using an HP-85 micro-computer and data acquisition unit. A software package was written to control and monitor the tests, convert the voltage outputs to engineering units, and record the data onto tape cassettes. These data were subsequently transferred to the mainframe VAX computer at Memorial University for the purposes of plotting and analysis.

The key to the realism of this laboratory model is the degree to which the cast joint in the concrete cylinder simulates a natural fracture. The various theoretical and practical considerations which were incorporated into design and construction of the artificial fracture are discussed in Appendix E. As shown in Figures 4.4 and 4.5, the texture of the woven geotextile used to cast the joint imparted a "pea-pod" configuration to its surfaces. Under load, these surfaces form a series of interconnected tubes instead of a

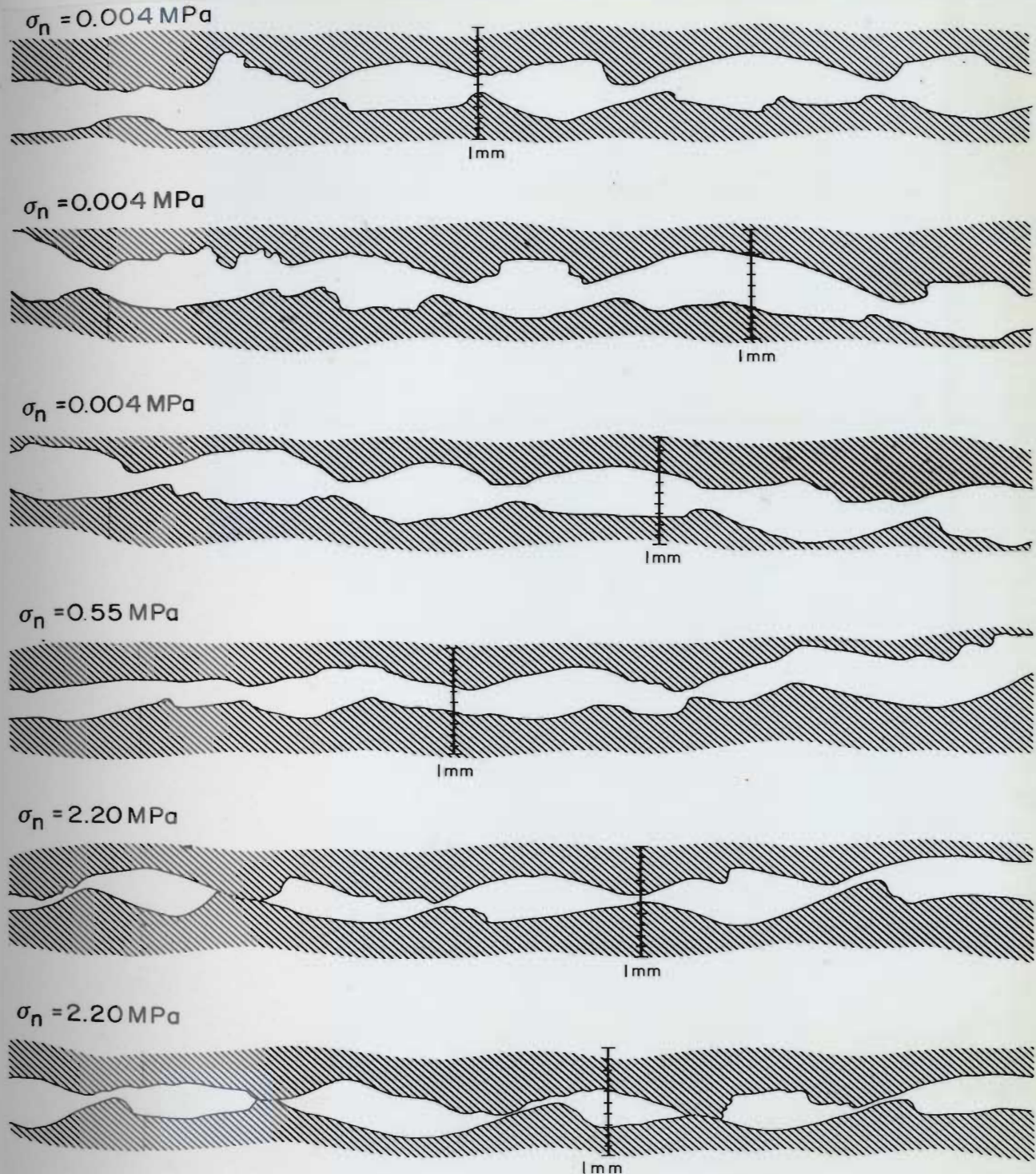


Figure 4.4 Tracings of resin-impregnated fractures in 0.150 m diameter concrete test cylinders under different levels of stress

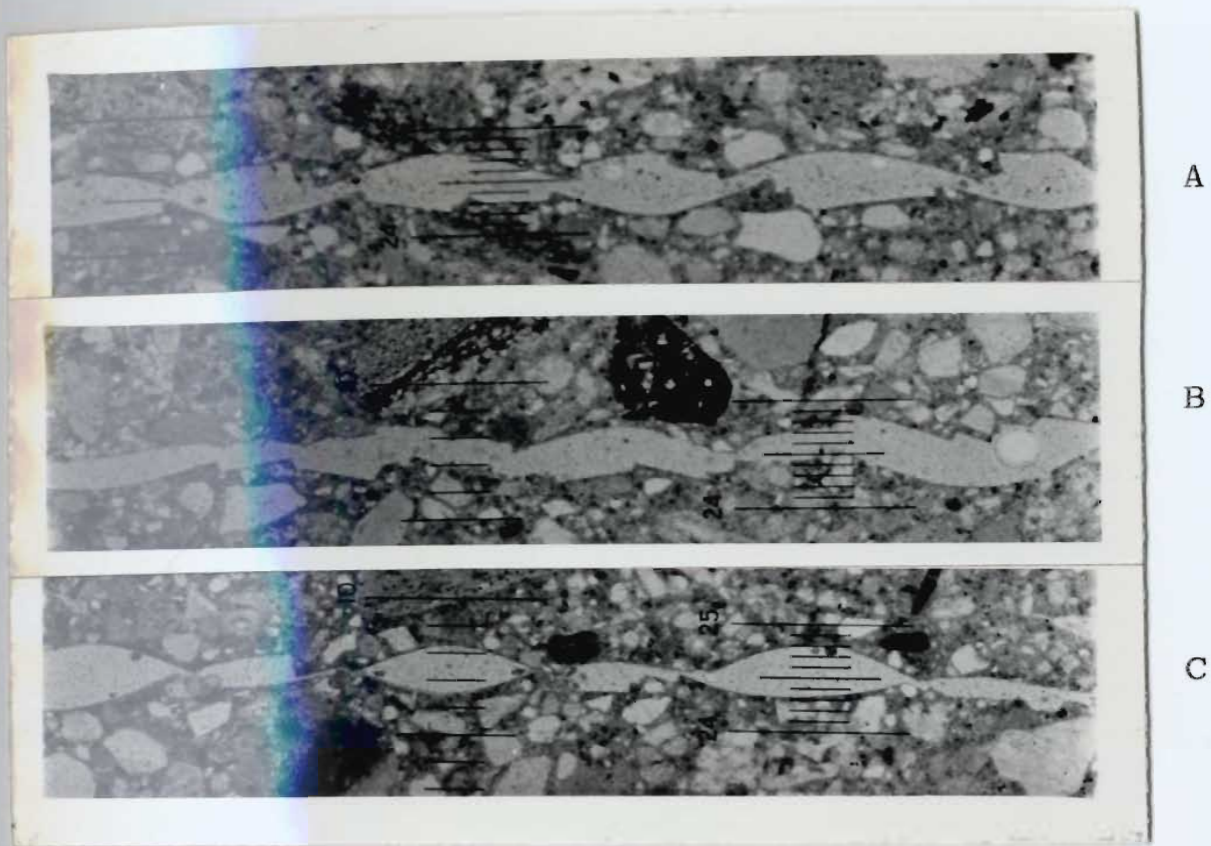


Figure 4.5 Micro-photographs of cross-sections of cast fractures in 0.150 m diameter concrete test cylinders impregnated with resin. A) $\sigma_n = 0.004$ MPa; section oriented parallel to geotextile "grain", B) $\sigma_n = 0.55$ Mpa; section oriented 35 degrees from geotextile "grain" (see Figure 4.3), C) $\sigma_n = 2.2$ Mpa; section oriented parallel to geotextile "grain".

planar or "parallel plate" void. The result is clearly illustrated by the jet-like, instead of sheet-like, flow into the wellbore that was observable during one of the wellbore reaming operations (Figure 4.6). The nature of these flow channels and their influence on the findings of the experimental work will be discussed in Section 5.2.

4.2 Stress-deformation tests

A series of stress-displacement tests of both standard concrete test cylinders with cast fractures (using the same geotextile and concrete mixes as in the large model) and the large laboratory model was conducted in order to determine the Young's modulus and Poisson's ratio for the concrete and the normal stiffness of the fracture. The results of the fracture stiffness tests, after hysteresis was overcome, are shown graphically in Figure 4.7. The most obvious feature of these data is the significant difference in normal stiffness, defined as the change in unit normal stress per change

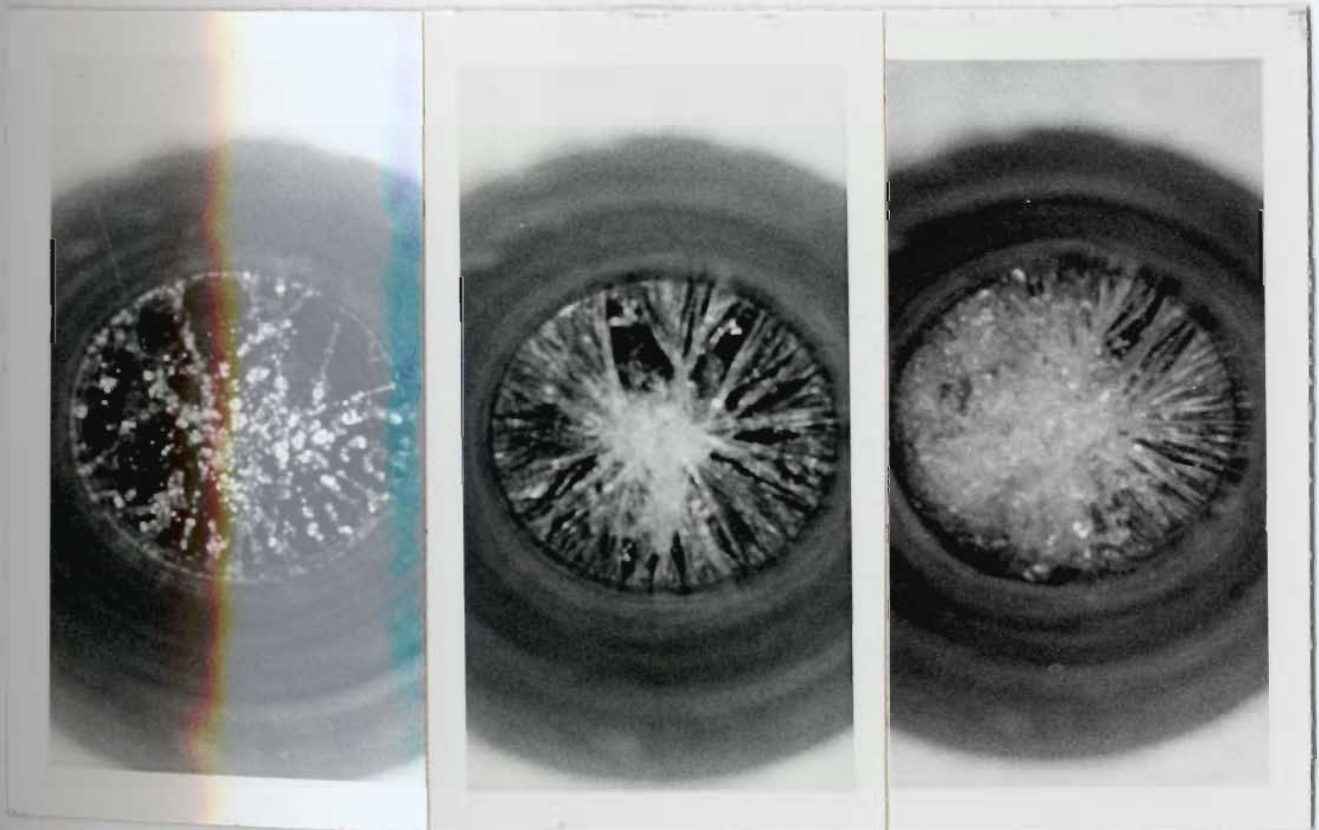


Figure 4.6 Water jetting from fracture into wellbore

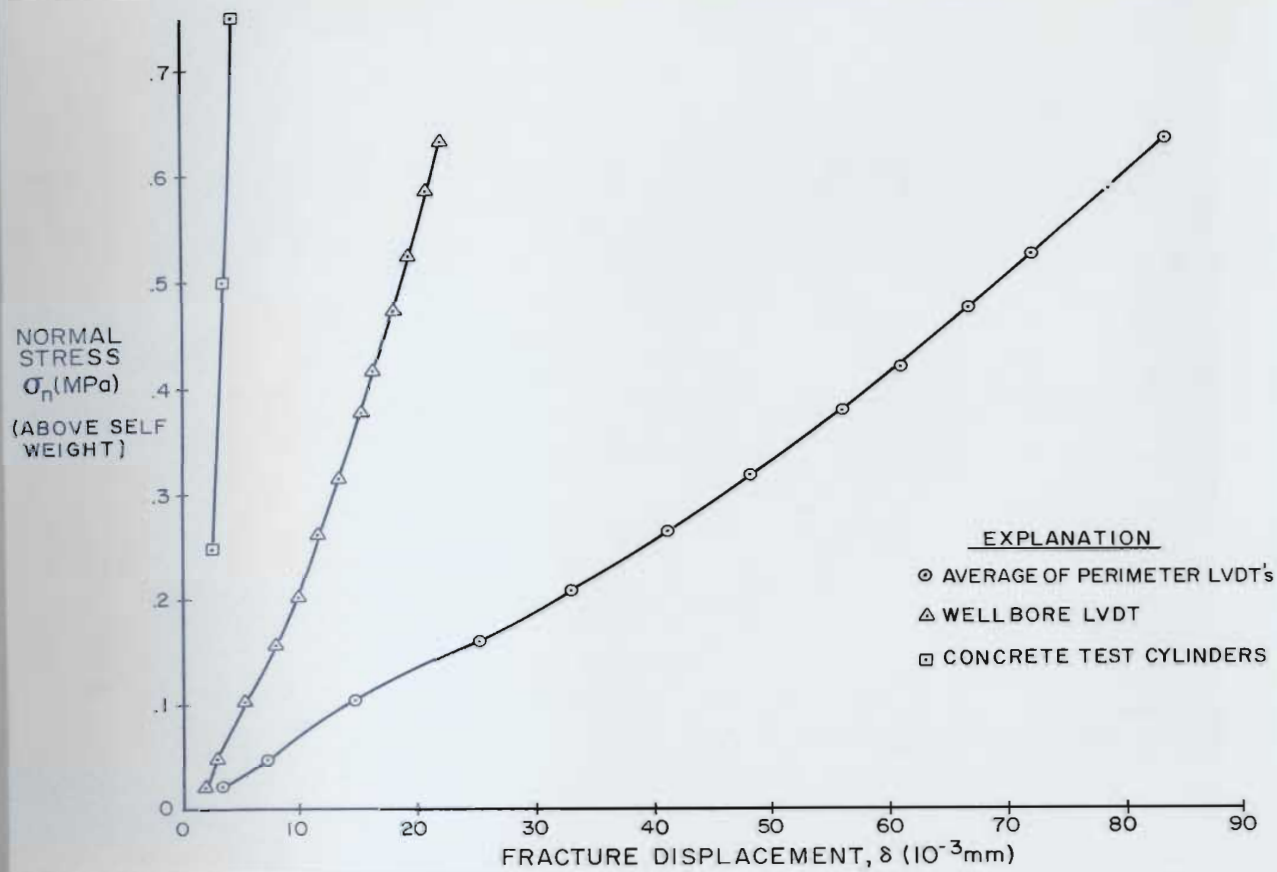


Figure 4.7 Normal stress versus fracture displacement for laboratory model and concrete test cylinders

in unit normal displacement, between the laboratory model and the test cylinders. It is believed, similarly to the conclusion reached by Witherspoon (1981), that this difference is attributable to scale. In the small cylinders, the stress is more likely to be uniformly distributed over the entire surface because of contact between asperities which comprise first-order roughness (Figures 4.4 and 4.5). With the large model, it is possible that stress is concentrated in some localized areas as the result of undulations in the

fracture surface (a large-scale roughness that was purposely troweled into the top surface of the lower cylinder during its construction) and that other areas continue to deform after these contact areas transfer most of the load. The borehole LVDT, which for logistical reasons was installed only after the wellbore had been enlarged to a diameter of 0.16 m, indicates an intermediate stiffness. These results are anomalous but could indicate the borehole LVDT is located at or near a major contact zone.

With the displacement data from the three perimetric LVDT's on the large cylinder and using the non-linear regression analysis that is described in Section C.4 of Appendix C, a deformational constitutive relationship of $\sigma_n = 6.33 \times 10^{-3} \delta + 2.50 \delta^{3.82}$ was derived for the fracture of the model.

4.3 Flow tests

Sixty-eight radial fracture flow tests including pumping tests, injection tests, and step-drawdown tests were conducted with the laboratory model under various hydraulic and mechanical boundary conditions. All the tests were conducted under steady-state conditions. In the pumping tests, water under a controlled pressure was pumped into the circumferential reservoir, flowed radially convergently to

the wellbore, and was extracted at the well collar at a constant, regulated rate. For injection tests, the flow lines were reversed so that pressurized water was introduced at a constant rate at the well collar, flowed radially divergently to the circumferential reservoir, and back to the tank. The step-drawdown tests were simply modified pumping tests in which the pumping rate was increased in steps rather than being kept constant.

Each of the flow tests was performed in the following three stages:

Stage 1 A top boundary stress, σ_v , was applied using the hydraulic jacks. Water in the borehole and fracture was maintained at atmospheric pressure (actually the pressure head in the fracture was equal to the height of the wellbore, 1.51 m, above the fracture but this was referenced as $H_0 = 0$). Initial LVDT readings were taken, and displacements of the fracture during Stage 2 were referenced to this position.

Stage 2 The hydrostatic pressure of the system, H_0 , was increased to some specified value by regulating the amount of direct return from the pump to the tank, but without allowing any flow through the fracture. This decreased the effective stress on the fracture, σ_{eff} . The resulting normal displacement of the fracture was then recorded.

Stage 3 The discharge valve was opened to a specified discharge rate, Q , and pressure heads were measured in the various manometers. Three complete sets of pressure head readings were taken and average values were recorded in order to minimize the effects of any transients that could be generated by small surges in the submersible pump.

Normal displacements in the fracture were again measured, this time being referenced to the position of the fracture in Stage 2.

A log of all tests including boundary conditions and results is presented in Table 4.1. Examples of typical test results will be shown and discussed in the following sections, and the method by which the fracture apertures were estimated is described in detail in Appendix B.

4.3.1 Pumping tests

Forty-five pumping tests were performed under different combinations of effective stress and flow rate and with three wellbore radii of 0.032, 0.054, and 0.080 m. Plots of hydraulic head loss versus the logarithm of radial distance and versus the inverse of radial distance were produced for all of the tests. Although the total drawdown and gradients differed significantly depending on the boundary conditions used in the tests, all of the log radial distance plots could be categorized into one of two shapes, either a curve with an ever-increasing slope toward the well or one with two inflection points.

The first type of curve, exemplified by the results from Test No. 2 shown in Figure 4.8, was the typical response when the fracture was "open"; that is, when the effective stress was negative and hydraulic pressure

Table 4.1 Log of laboratory tests

| r_w (m) | Test No. | Boundary Conditions | | | | Temp (°C) | Q^3 (l/s) | Calculated Fracture Aperture ⁴ | | | Measured Normal Displacement of Fracture ⁵ | | | |
|--------------|-------------|---------------------|--------------|-------------------------|----------------|--------------|----------------|---|--------------|---------------|--|-----------|-----------|-----------|
| | | σ_v (MPa) | H_0 (m) | σ_{off} (MPa) | h_w^2 (m) | | | Linear | | Non-Linear | A (mm) | B (mm) | C (mm) | D (mm) |
| | | | | | | | | Louis (mm) | Sato (mm) | Louis (mm) | | | | |
| 0.032 | 1 | 0.048 | 13.35 | -0.046 | 12.92 | 23.6 | 0.453 | 1.409-1.471 | 1.608 | 1.027-1.191 | 1.325 | 1.258 | 1.580 | NM |
| 0.032 | 2 | 0.048 | 13.68 | -0.049 | 10.42 | 25.6 | 1.528 | 1.326-1.391 | 1.733 | 1.111-1.284 | 1.290 | 1.227 | 1.630 | NM |
| 0.032 | 3 | 0.050 | 13.93 | -0.049 | 9.48 | 26.7 | 1.886 | 1.457-1.518 | 1.664 | 1.113-1.308 | 1.355 | 1.285 | 1.696 | NM |
| 0.032 | 4 | 0.200 | 28.34 | -0.040 | 26.21 | 28.9 | 1.265 | 1.433-1.495 | 1.636 | 1.114-1.287 | 1.299 | 1.347 | 1.622 | NM |
| 0.032 | 5 | 0.205 | 28.44 | -0.036 | 23.16 | 29.7 | 1.833 | 1.421-1.483 | 1.668 | 1.044-1.209 | 1.211 | 1.260 | 1.511 | NM |
| 0.032 | 6 | 0.238 | 13.85 | 0.140 | 11.64 | 23.6 | 0.010 | 0.346-0.407 | 0.320 | ND | 0.012 | 0.004 | 0.003 | NM |
| 0.032 | 7 | 0.244 | 13.78 | 0.146 | 5.47 | 26.4 | 0.026 | 0.328-0.388 | 0.300 | ND | 0.013 | 0.001 | 0.003 | NM |
| 0.032 | 8 | 0.245 | 14.25 | 0.143 | 0.76 | 28.4 | 0.037 | 0.340-0.401 | 0.313 | ND | 0.014 | 0.002 | 0.000 | NM |
| 0.032 | 9 | 0.242 | 28.22 | 0.003 | 21.80 | 29.5 | 0.031 | 0.342-0.403 | 0.336 | ND | 0.087 | 0.010 | 0.099 | NM |
| 0.032 | 10 | 0.251 | 28.58 | 0.009 | 12.42 | 28.9 | 0.047 | 0.380-0.443 | 0.316 | ND | 0.062 | 0.020 | 0.095 | NM |
| 0.032 | 11 | 0.248 | 28.54 | 0.006 | 3.07 | 25.9 | 0.061 | 0.298-0.355 | 0.364 | ND | 0.048 | 0.021 | 0.071 | NM |
| 0.032 | 12A | 0.481 | 42.73 | 0.100 | 39.63 | 26.0 | 0.011 | ND | ND | ND | 0.052 | 0.006 | 0.060 | NM |
| 0.032 | 12B | 0.478 | 42.53 | 0.099 | 31.63 | 27.0 | 0.029 | 0.395-0.458 | 0.398 | ND | 0.054 | 0.009 | 0.055 | NM |
| 0.032 | 12C | 0.478 | 42.63 | 0.099 | 25.43 | 28.2 | 0.039 | ND | ND | ND | 0.062 | 0.017 | 0.067 | NM |
| 0.032 | 12D | 0.478 | 42.81 | 0.097 | 18.35 | 28.2 | 0.049 | 0.304-0.362 | 0.292 | ND | 0.068 | 0.023 | 0.077 | NM |
| 0.032 | 13A | 0.477 | 42.88 | 0.095 | 8.76 | 28.4 | 0.060 | 0.339-0.399 | 0.332 | ND | ND | ND | ND | NM |
| 0.032 | 13B | 0.477 | 42.71 | 0.097 | 3.06 | 28.8 | 0.066 | 0.316-0.375 | 0.305 | ND | ND | ND | ND | NM |

Table 4.1 (Continued) Log of laboratory tests

| r_w (m) | Test No. | Boundary Conditions | | | | Temp (°C) | Q^3 (1/s) | Calculated Fracture Aperture ⁴ | | | Measured Normal Displacement of Fracture ⁵ | | | |
|--------------|-------------|---------------------|--------------|---------------------------|----------------|--------------|----------------|---|-------|---------------------|--|--------|-------|----|
| | | σ_v (MPa) | H_o (m) | σ_{eff}^1 (MPa) | h_w^2 (m) | | | Linear Louis | Sato | Non-Linear Louis | A | B | C | D |
| 0.054 | 14 | 0.053 | 11.84 | -0.028 | 11.73 | 21.7 | 0.100 | ND | ND | ND | 1.334 | 0.982 | 1.351 | NM |
| 0.054 | 15 | 0.051 | 11.45 | -0.024 | 8.61 | 24.1 | 1.524 | 1.189-1.254 | 1.369 | 0.960-1.116 | 1.223 | 0.956 | 1.194 | NM |
| 0.054 | 16 | 0.055 | 12.13 | -0.027 | 8.66 | 25.4 | 1.856 | 1.206-1.270 | 1.333 | 1.008-1.169 | 1.313 | 0.987 | 1.293 | NM |
| 0.054 | 17 | 0.098 | 12.60 | 0.012 | 9.84 | 25.4 | 0.019 | 0.315-0.373 | 0.304 | ND | 0.181 | 0.055 | 0.084 | NM |
| 0.054 | 18 | 0.100 | 13.16 | 0.008 | 5.04 | 26.5 | 0.050 | 0.356-0.417 | 0.352 | ND | 0.181 | 0.045 | 0.100 | NM |
| 0.054 | 19 | 0.101 | 12.94 | 0.010 | 3.99 | 24.7 | 0.041 | 0.314-0.373 | 0.303 | ND | 0.136 | 0.044 | 0.074 | NM |
| 0.054 | 20 | 0.231 | 12.91 | 0.012 | 3.84 | 24.9 | 0.022 | 0.291-0.348 | 0.277 | ND | 0.020 | 0.005 | 0.002 | NM |
| 0.054 | 21 | 0.477 | 12.75 | 0.389 | 3.44 | 25.4 | 0.019 | 0.255-0.312 | 0.235 | ND | 0.006 | 0.003 | 0.005 | NM |
| 0.054 | 22 | 0.200 | 26.23 | -0.019 | 24.10 | 29.0 | 1.233 | 1.062-1.128 | 1.191 | 0.919-1.070 | 1.323 | 0.929 | 1.158 | NM |
| 0.054 | 23 | 0.201 | 26.42 | -0.020 | 21.75 | 29.4 | 1.802 | 1.027-1.093 | 1.149 | 0.895-1.043 | 1.374 | 0.910 | 1.082 | NM |
| 0.054 | 24 | 0.239 | 27.63 | 0.006 | 20.21 | 27.3 | 0.176 | 0.412-0.476 | 0.418 | 0.216-0.275 | 0.334 | 0.065 | 0.220 | NM |
| 0.054 | 25 | 0.241 | 28.43 | 0.000 | 12.64 | 28.3 | 0.374 | 0.445-0.510 | 0.457 | 0.263-0.328 | 0.402 | 0.061 | 0.292 | NM |
| 0.054 | 26 | 0.233 | 27.10 | 0.005 | 3.84 | 30.3 | 0.112 | 0.401-0.465 | 0.406 | ND | 0.211 | -0.049 | 0.135 | NM |
| 0.054 | 27 | 0.462 | 27.17 | 0.233 | 23.06 | 23.3 | 0.009 | 0.243-0.296 | 0.225 | ND | 0.022 | 0.009 | 0.001 | NM |
| 0.054 | 28 | 0.461 | 27.22 | 0.232 | 12.73 | 24.9 | 0.028 | 0.295-0.352 | 0.281 | ND | 0.028 | 0.013 | 0.001 | NM |
| 0.054 | 29 | 0.462 | 27.38 | 0.231 | 3.72 | 25.8 | 0.041 | ND | ND | ND | 0.029 | 0.015 | 0.008 | NM |

Table 4.1 (Continued) Log of laboratory tests

| r_w (m) | Test No. | Boundary Conditions | | | | Temp (°C) | Q^3 (1/s) | Calculated Fracture Aperture ⁴ | | | Measured Normal Displacement of Fracture ⁵ | | | |
|--------------|-------------|---------------------|--------------|---------------------------|----------------|--------------|----------------|---|--------------|-----------------------------|--|-----------|-----------|-----------|
| | | σ_v (MPa) | H_o (m) | σ_{eff}^1 (MPa) | h_w^2 (m) | | | Linear Louis (mm) | Sato (mm) | Non-Linear Louis (mm) | A (mm) | B (mm) | C (mm) | D (mm) |
| 0.054 | 30A | 0.462 | 38.66 | 0.121 | 34.89 | 23.8 | 0.008 | ND | ND | ND | 0.046 | 0.021 | 0.049 | NM |
| 0.054 | 30B | 0.462 | 38.90 | 0.119 | 28.27 | 24.5 | 0.021 | ND | ND | ND | 0.049 | 0.022 | 0.049 | NM |
| 0.054 | 30C | 0.462 | 38.63 | 0.121 | 24.95 | 25.0 | 0.025 | ND | ND | ND | 0.050 | 0.023 | 0.049 | NM |
| 0.054 | 30D | 0.462 | 38.36 | 0.124 | 20.80 | 25.6 | 0.030 | ND | ND | ND | 0.053 | 0.027 | 0.050 | NM |
| 0.054 | 30E | 0.463 | 38.38 | 0.125 | 11.17 | 26.2 | 0.040 | ND | ND | ND | 0.060 | 0.031 | 0.059 | NM |
| 0.054 | 30F | 0.464 | 37.44 | 0.135 | 3.50 | 27.0 | 0.047 | ND | ND | ND | 0.062 | 0.036 | 0.061 | NM |
| 0.080 | 31 | 0.056 | 13.08 | -0.035 | 11.94 | 25.0 | 1.178 | 1.145-1.210 | 1.291 | 0.923-1.074 | 1.090 | 1.006 | 1.268 | 1.072 |
| 0.080 | 32 | 0.053 | 12.96 | -0.037 | 11.98 | 21.0 | 1.092 | 1.308-1.571 | 1.485 | 0.902-1.051 | 1.160 | 1.065 | 1.316 | 1.138 |
| 0.080 | 33A | 0.058 | 13.21 | -0.034 | 12.15 | 23.0 | 1.163 | 1.348-1.411 | 1.539 | 0.936-1.089 | 1.100 | 1.034 | 1.241 | 1.073 |
| 0.080 | 33B | 0.058 | 13.18 | -0.034 | 10.92 | 23.0 | 1.691 | 1.108-1.173 | 1.246 | 0.923-1.074 | 1.094 | 1.026 | 1.243 | 1.080 |
| 0.080 | 33C | 0.058 | 13.22 | -0.034 | 10.64 | 23.0 | 1.819 | 1.214-1.279 | 1.374 | 0.927-1.079 | 1.099 | 1.033 | 1.249 | 1.076 |
| 0.080 | 34A | 0.095 | 13.10 | 0.004 | 7.88 | 24.0 | 0.005 | 0.257-0.311 | 0.237 | ND | 0.037 | 0.018 | 0.057 | 0.017 |
| 0.080 | 34B | 0.096 | 13.13 | 0.005 | 3.49 | 24.0 | 0.009 | 0.265-0.319 | 0.246 | ND | 0.035 | 0.016 | 0.056 | 0.014 |
| 0.080 | 35 | 0.096 | 12.98 | 0.006 | 1.20 | 24.0 | 0.011 | 0.262-0.317 | 0.243 | ND | 0.039 | 0.013 | 0.062 | 0.014 |
| 0.080 | 36 | 0.230 | 13.56 | 0.134 | 1.33 | 24.0 | 0.008 | 0.238-0.291 | 0.216 | ND | 0.009 | 0.021 | 0.015 | 0.004 |
| 0.080 | 37 | 0.475 | 13.53 | 0.135 | 1.39 | 24.0 | 0.007 | 0.260-0.314 | 0.241 | ND | 0.003 | 0.012 | 0.008 | 0.003 |
| 0.080 | 38 | 0.204 | 27.79 | -0.031 | 26.56 | 25.0 | 1.329 | 1.205-1.270 | 1.363 | 0.969-1.125 | 1.222 | 1.112 | 1.229 | 1.135 |
| 0.080 | 39 | 0.194 | 26.52 | -0.028 | 24.40 | 24.0 | 1.767 | 1.167-1.231 | 1.316 | 0.810-0.948 | 1.150 | 1.138 | 1.219 | 1.118 |
| 0.080 | 40A | 0.238 | 27.20 | 0.009 | 19.31 | 25.0 | 0.019 | 0.364-0.426 | 0.362 | ND | 0.058 | 0.100 | 0.065 | 0.033 |
| 0.080 | 40B | 0.238 | 27.27 | 0.008 | 17.16 | 25.0 | 0.022 | 0.332-0.392 | 0.324 | ND | 0.056 | 0.098 | 0.068 | 0.035 |
| 0.080 | 40C | 0.238 | 27.28 | 0.008 | 3.92 | 25.0 | 0.024 | 0.273-0.328 | 0.256 | ND | 0.040 | 0.085 | 0.065 | 0.016 |

Table 4.1 (Continued) Log of laboratory tests

| r_w (m) | Test No. | Boundary Conditions | | | | Temp (°C) | Q^3 (l/s) | Calculated Fracture Aperture ⁴ | | | Measured Normal Displacement of Fracture ⁵ | | | |
|--------------|-------------|---------------------|--------------|---------------------------|----------------|--------------|----------------|---|--------------|-----------------------------|--|-----------|-----------|-----------|
| | | σ_v (MPa) | H_o (m) | σ_{eff}^1 (MPa) | h_w^2 (m) | | | Linear Louls (mm) | Sato (mm) | Non-Linear Louls (mm) | A (mm) | B (mm) | C (mm) | D (mm) |
| 0.080 | 41A | 0.462 | 27.30 | 0.232 | 19.92 | 25.0 | 0.044 | ND | ND | ND | 0.005 | 0.033 | 0.016 | 0.008 |
| 0.080 | 41B | 0.463 | 27.20 | 0.234 | 14.22 | 25.0 | 0.006 | 0.216-0.266 | 0.191 | ND | 0.007 | 0.034 | 0.017 | 0.007 |
| 0.080 | 41C | 0.464 | 27.80 | 0.229 | 3.82 | 25.5 | 0.014 | 0.251-0.304 | 0.230 | ND | 0.007 | 0.035 | 0.014 | 0.004 |
| 0.080 | 42A | 0.473 | 40.45 | 0.114 | 36.33 | 22.8 | 0.004 | ND | ND | ND | 0.015 | 0.078 | 0.037 | 0.012 |
| 0.080 | 42B | 0.474 | 40.22 | 0.118 | 27.08 | 23.0 | 0.010 | 0.282-0.339 | 0.267 | ND | 0.018 | 0.081 | 0.039 | 0.009 |
| 0.080 | 42C | 0.474 | 41.12 | 0.109 | 20.69 | 23.0 | 0.013 | 0.278-0.334 | 0.262 | ND | 0.020 | 0.089 | 0.042 | 0.007 |
| 0.080 | 42D | 0.505 | 46.13 | 0.091 | 18.05 | 24.0 | 0.015 | 0.258-0.312 | 0.238 | ND | 0.023 | 0.091 | 0.045 | 0.004 |
| 0.080 | 42E | 0.517 | 40.78 | 0.155 | 7.81 | 24.0 | 0.016 | 0.275-0.331 | 0.258 | ND | 0.020 | 0.070 | 0.036 | 0.003 |
| 0.080 | 42F | 0.517 | 40.38 | 0.159 | 4.95 | 24.0 | 0.017 | 0.265-0.320 | 0.247 | ND | 0.022 | 0.072 | 0.037 | 0.001 |
| 0.080 | 43A | 0.085 | 12.92 | -0.004 | 13.09 | 25.5 | -1.306 | ND | ND | ND | 1.619 | 1.370 | 1.965 | 1.592 |
| 0.080 | 43B | 0.085 | 12.78 | -0.003 | 13.23 | 25.5 | -1.815 | ND | ND | ND | 1.606 | 1.357 | 1.960 | 1.581 |
| 0.080 | 44A | 0.091 | 2.26 | 0.106 | 12.94 | 25.0 | -0.030 | 0.287-0.343 | 0.272 | ND | 0.421 | 0.151 | 0.568 | 0.356 |
| 0.080 | 44C | 0.091 | 0.47 | 0.123 | 12.95 | 24.7 | -0.031 | 0.283-0.349 | 0.267 | ND | 0.412 | 0.151 | 0.568 | 0.356 |
| 0.080 | 45A | 0.222 | 8.35 | 0.177 | 27.75 | 24.0 | -0.017 | 0.220-0.270 | 0.195 | ND | 0.512 | 0.242 | 0.608 | 0.413 |
| 0.080 | 45B | 0.219 | 0.49 | 0.251 | 27.82 | 24.0 | -0.018 | 0.225-0.275 | 0.201 | ND | 0.512 | 0.242 | 0.608 | 0.413 |

¹ $\sigma_{eff} = \sigma_v + \sigma_g - H_o \rho g$ where σ_g is from gravity load (weight) of top cylinder.

² Velocity head could not be measured directly, so only hydraulic head given. ³ Negative sign indicates injection.

⁴ Calculated by graphical techniques described in Appendix B. Aperture range for calculations according to flow laws of Louls (1969) corresponds to range of absolute roughness of 0.100 to 0.240 mm estimated from microphotographs of resin-impregnated fractures. ND = not determinable.

⁵ See Figure 4.3 for locations of LVDT's at which displacements measured. Displacements are relative to position of fracture under hydrostatic conditions with $H_o = 0$. NM = not measured (device for measuring deformation of fracture in wellbore was not installed until wellbore reamed to $r_w = 0.080$).

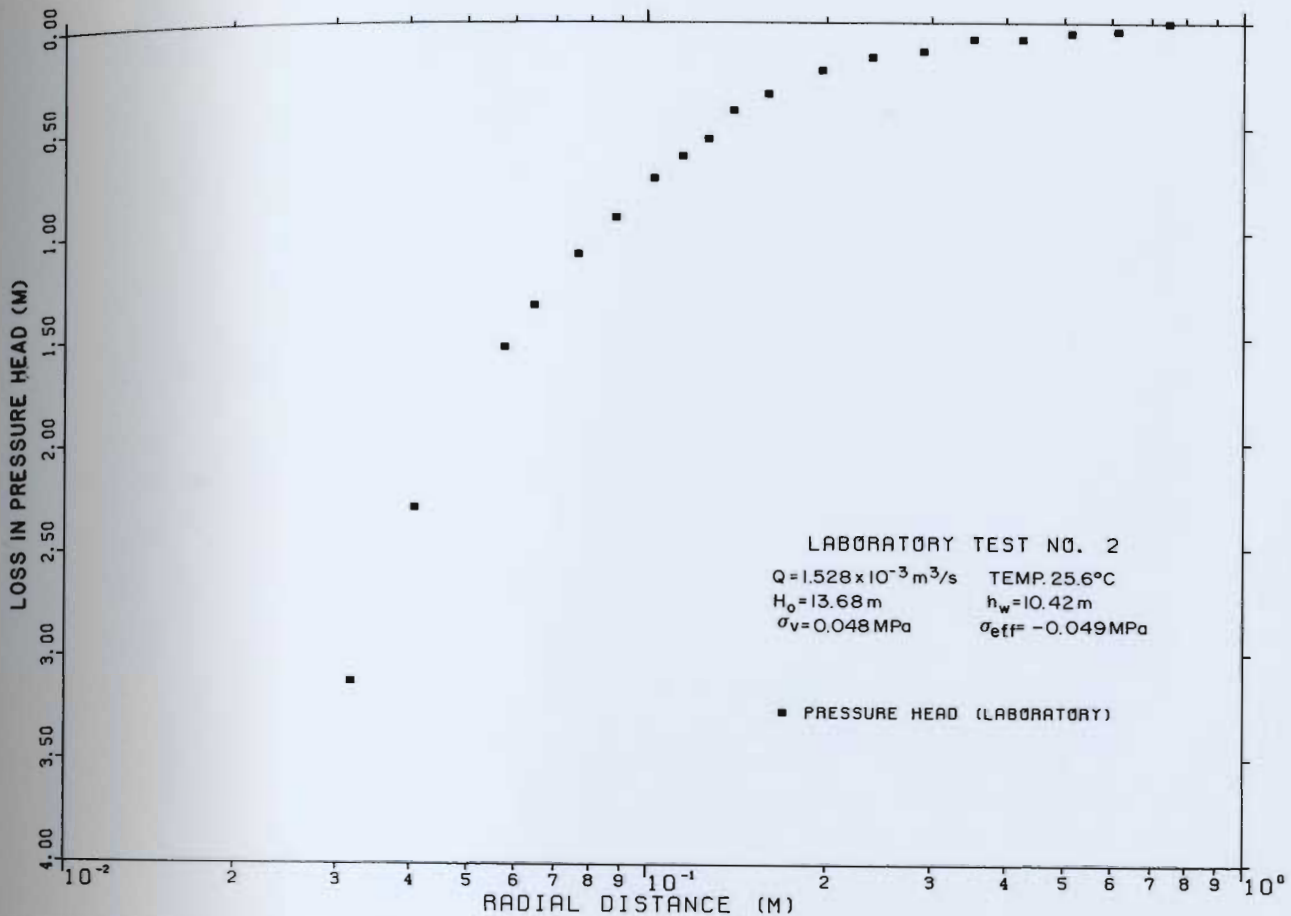


Figure 4.8 Loss in pressure head versus logarithm of radial distance for open fracture under pumping conditions

actually propped open the fracture. As explained in Appendix B, such a plot of head loss versus the logarithm of radial distance can be used for two purposes: 1) to identify the critical radius, and 2) to estimate the size of the effective aperture of the fracture. In Figure 4.8, the critical radius, indicated by the point at which the plot ceases to be linear (in the radially inward direction), appears to be approximately 0.3 m.

Figure 4.9 represents the same head loss data from Test No. 2, but plotted against the inverse of radial distance. As explained in Section B.2 of Appendix B, data from a fully turbulent flow region would fall on a straight line on such a plot. Data from Test 2 beyond about 4 1/m (corresponding to a radial distance of 0.25 m) clearly do that.

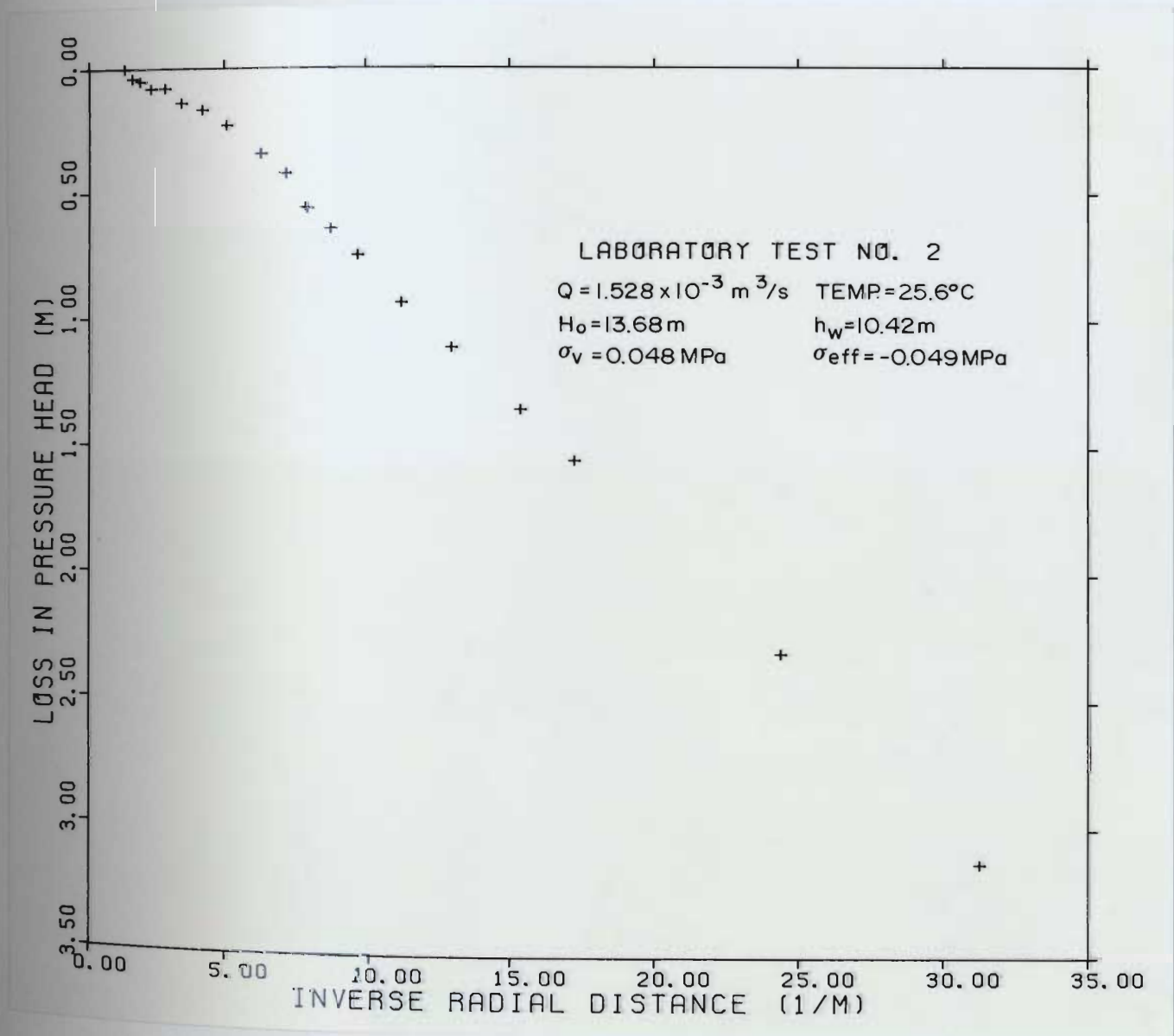


Figure 4.9 Loss in pressure head versus inverse radial distance for open fracture under pumping conditions

Table 4.1 includes estimates of effective aperture size for the "open" tests (Tests 1-5, 14-16, 22-26, 31-33C, 38, and 39) calculated with data from both the linear and non-linear flow regions. Note that in almost all these cases, the apertures calculated from linear flow data using the relationship of Sato et al. (see Appendix B) were the largest, followed by those estimated from Louis' law for rough, linear flow, and finally by aperture estimates based on Louis' law for rough, non-linear flow. These estimates had a rather consistent relative ratio of about 1.4:1.2:1 for all of the tests. The absolute value of the aperture estimates will be discussed in Section 5.1.

The second main group of pumping tests was composed of the "closed" tests in which the fracture was under a net externally applied axial load. All of these tests (Tests 6-11, 17-21, 24-29, 34A-37, and 40A-41C) produced curves with double inflections on both the logarithm of radial distance and inverse radial distance plots. None of these data exhibit either a well defined linear region or evidence of fully turbulent flow. Typical examples of plots derived from the "closed" tests are given in Figures 4.10 and 4.11.

As with the pumping tests with an "open" fracture, estimates of fracture aperture size were made using the more radially distant data from the logarithm of radial distance plots and the flow laws of Sato et al. and Louis. However,

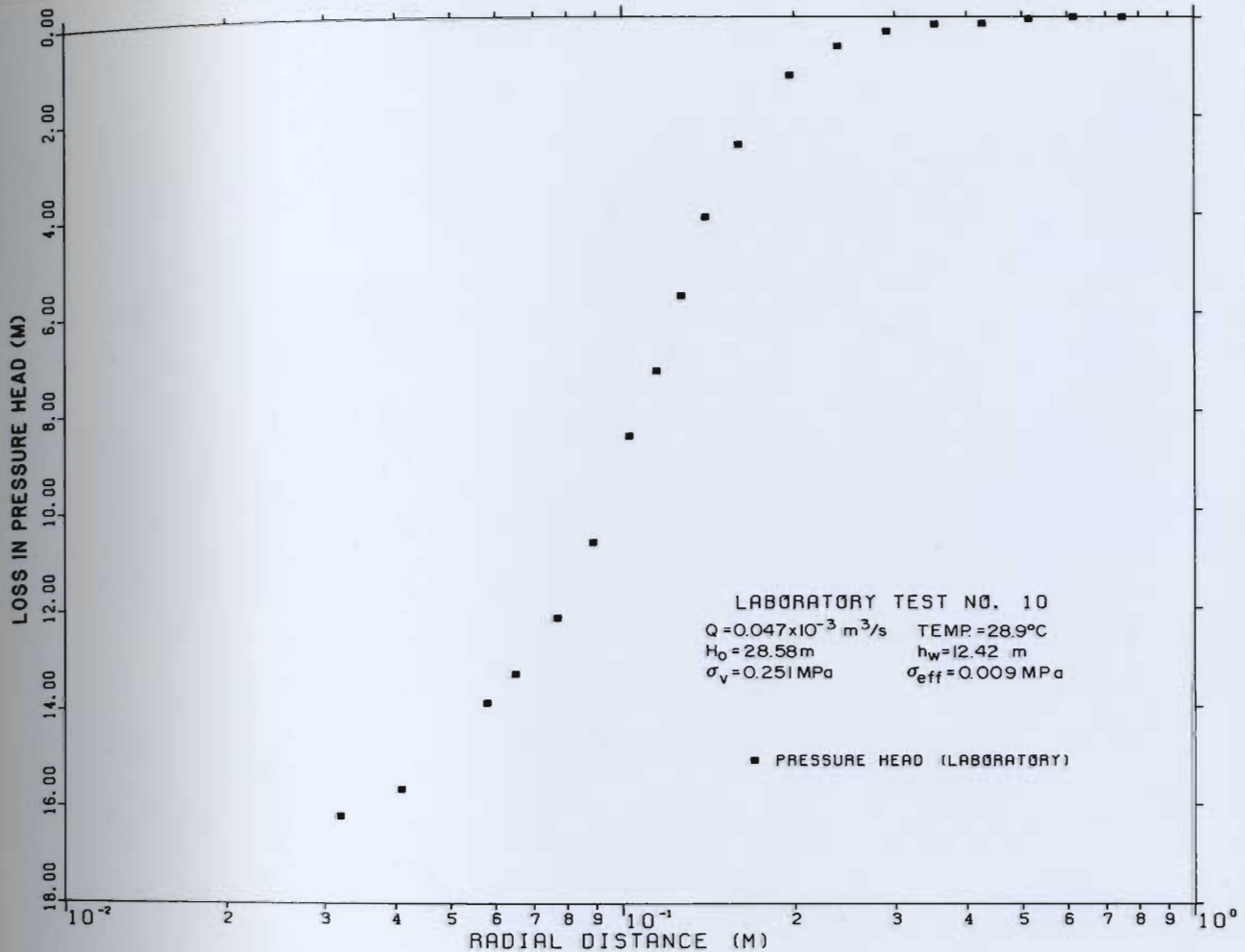


Figure 4.10 Loss in pressure head versus logarithm of radial distance for closed fracture under pumping conditions

no equivalent calculations could be made using the inverse radial distance plots of data from these tests. Interestingly, under "closed" conditions, the apertures calculated from the flow law of Sato et al. were smaller by a factor of approximately 0.9 to 0.95 than those calculated according to Louis' law for linear flow in rough fractures.

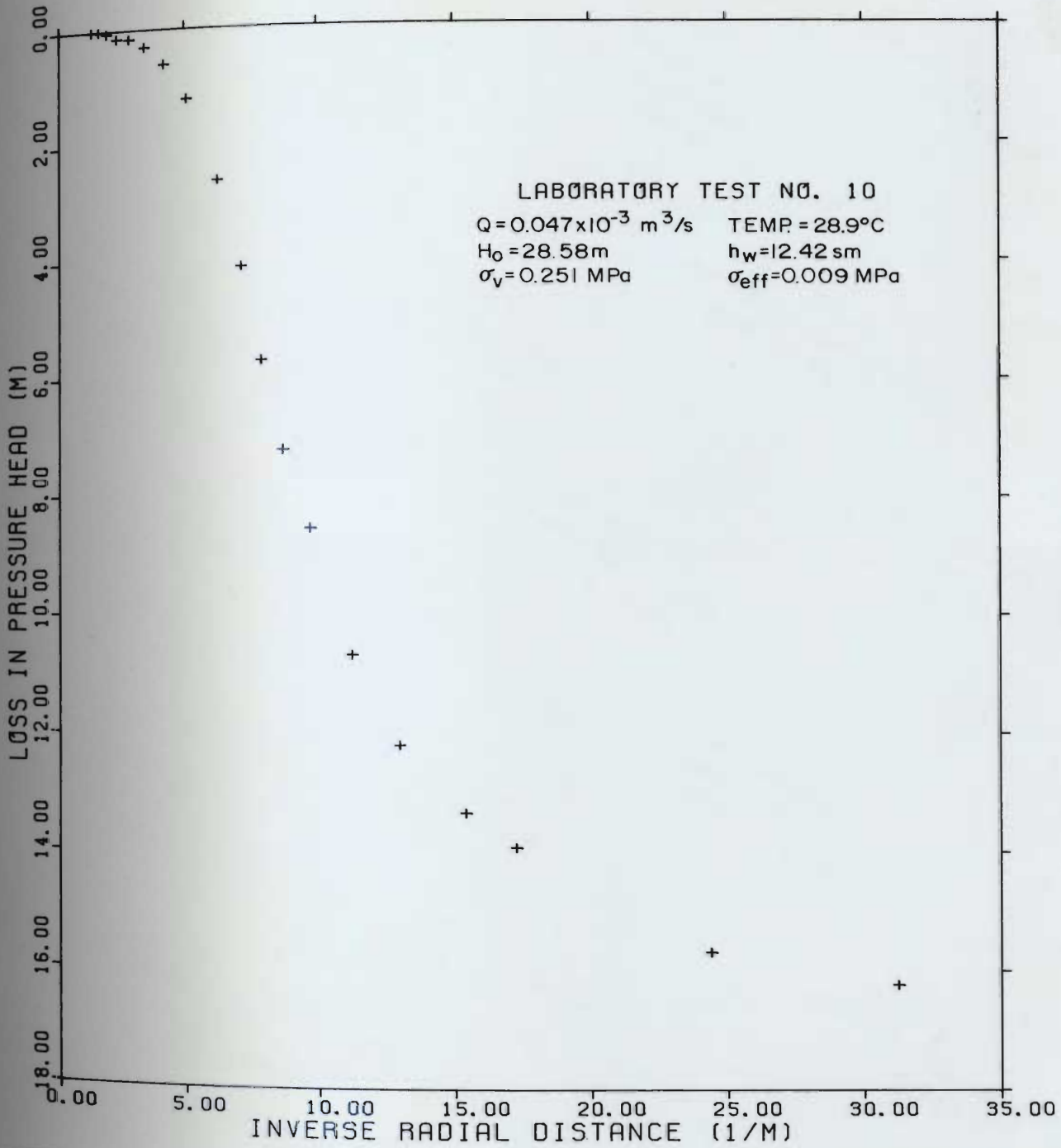


Figure 4.11 Loss in pressure head versus inverse radial distance for closed fracture under pumping conditions

4.3.2 Injection tests

A limited number of injection tests were conducted with the laboratory model after the wellbore had been reamed to a diameter of 0.160 m. The results of Test 44C, which was conducted with the fracture in a "closed" condition, are shown in Figures 4.12 and 4.13. In both figures, only the beginning of an inflection in the curve near the wellbore is apparent, typical of the pumping tests under "closed" conditions. Note, however, that several of the near-well manometers whose data more clearly defined this inflection in the earlier tests with a smaller diameter wellbore (refer back to Figure 4.10 on page 112) had been removed during reaming of the wellbore.

Estimates of fracture aperture sizes from the injection test data were again made using the techniques outlined in Appendix B. Although the inverse radial distance plot shown in Figure 4.13 suggests the existence of a fully-turbulent flow region, the computer program LOUIS (see Section B.4 in Appendix B), based on the the non-linear flow law of Louis, would not converge to a solution.

One of the more striking, yet completely predictable, results of the injection tests was their reciprocal response to that of the pumping tests. Figure 4.14 is a combined plot of data from Test 35, a "closed" pumping test; and from injection Test 44C, two tests which, for other than flow

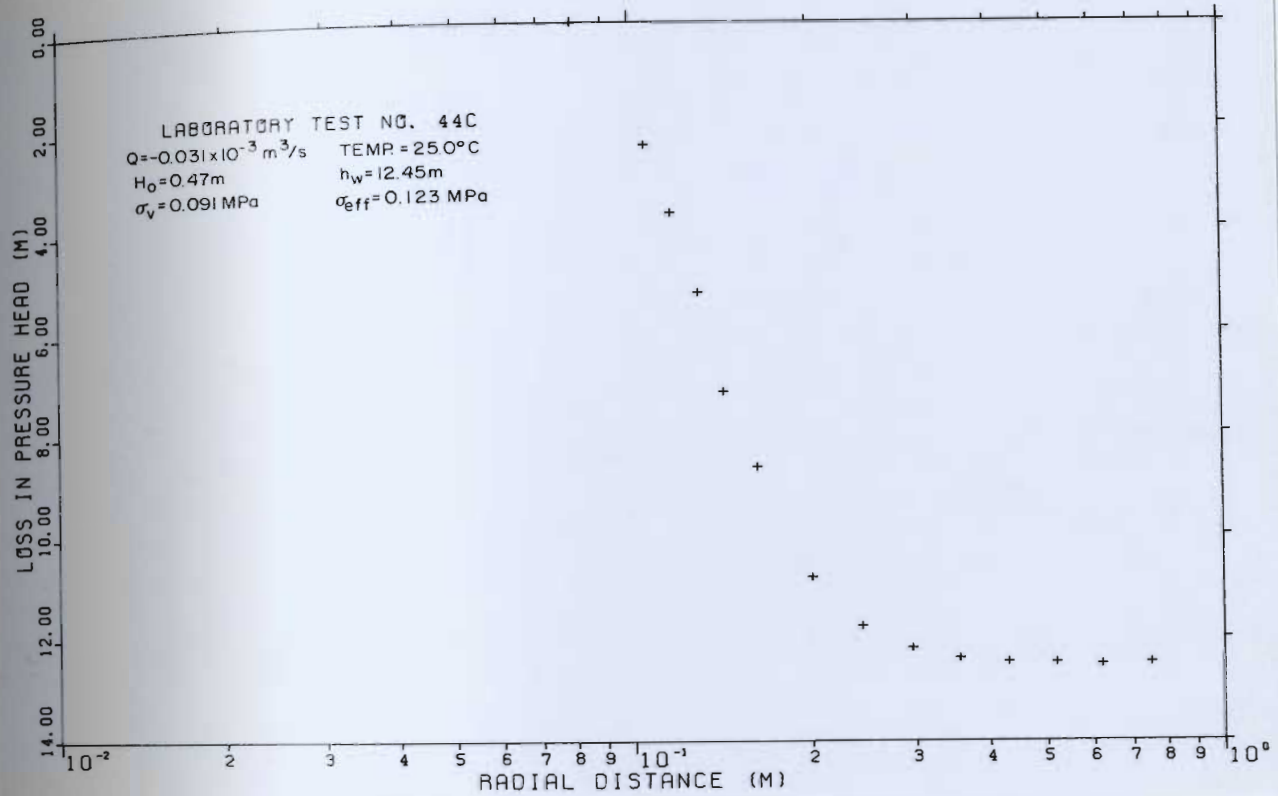


Figure 4.12 Loss in pressure head versus logarithm of radial distance for closed fracture under injection conditions

direction, were run under very similar boundary conditions. To facilitate comparison, the head loss data for the latter have been inverted. Although the pressure head profiles are very similar, it is noteworthy that the injection rate was nearly three times the pumping rate.

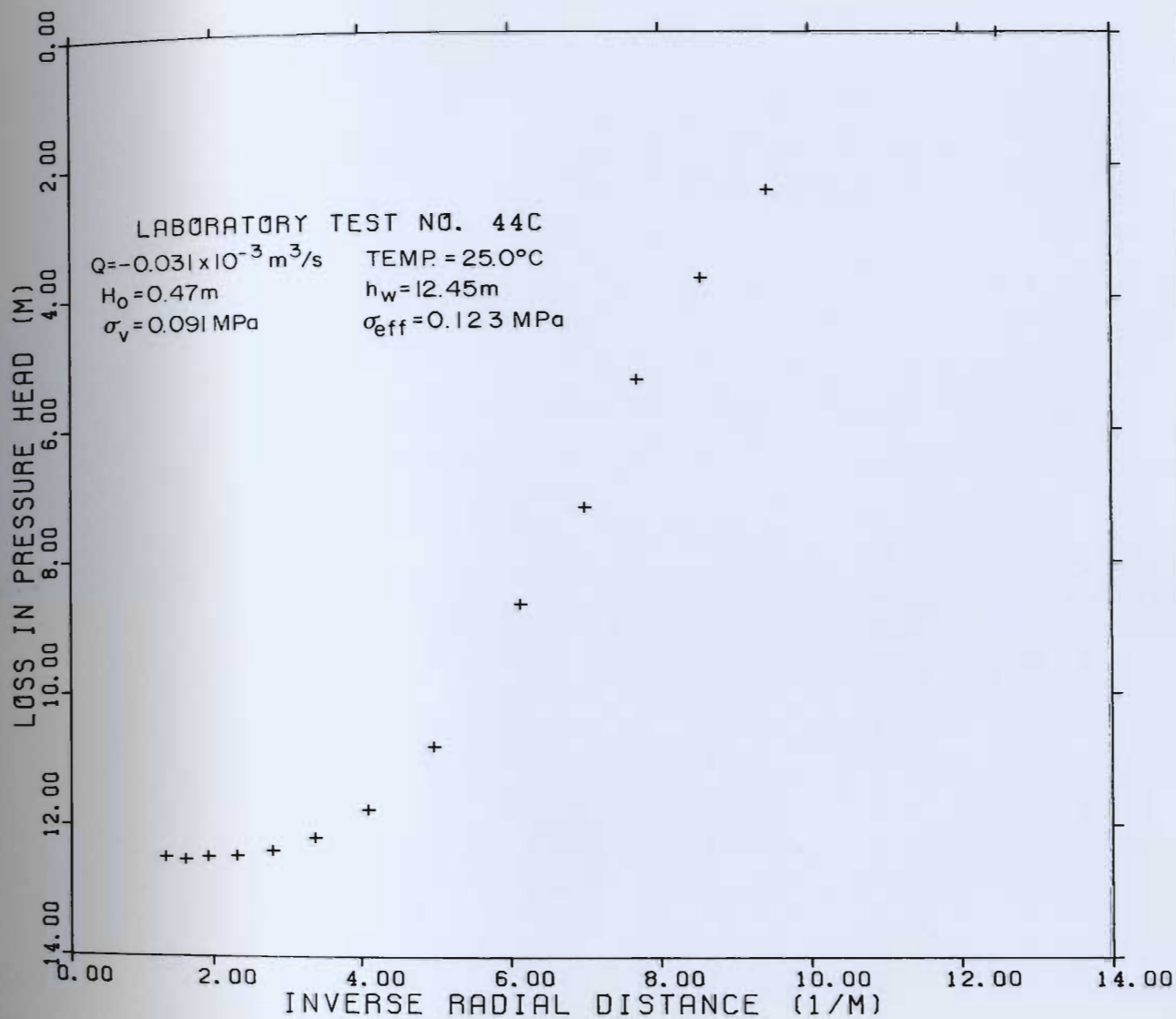


Figure 4.13 Loss in pressure head versus inverse radial distance for closed fracture under injection conditions

4.3.3 Step-drawdown tests

A step-drawdown test in which the top boundary load and outer boundary pressure head were kept constant but in which six different pumping rates were used was conducted with the

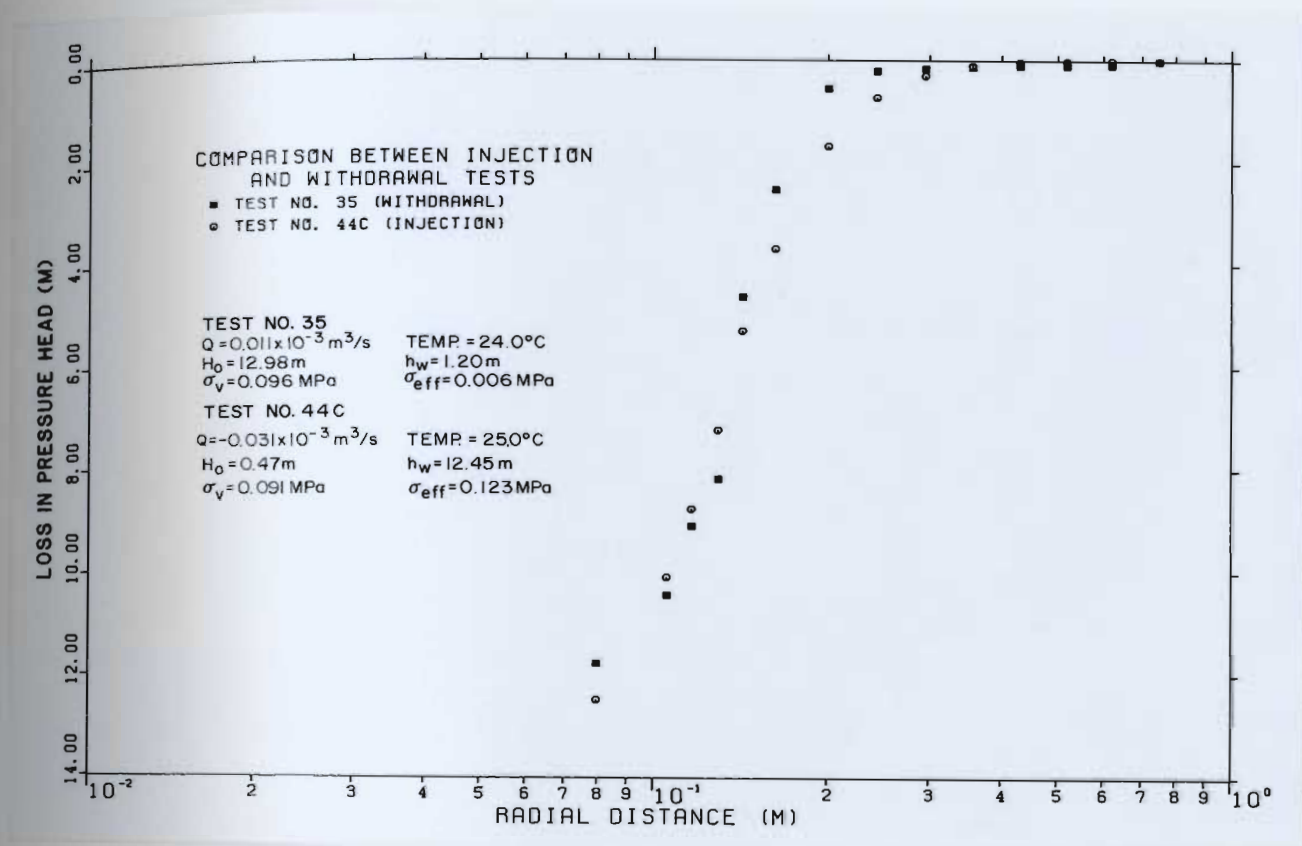


Figure 4.14 Comparison of pressure head profiles for injection and pumping

laboratory model for each of the wellbore sizes. In all of these tests, the fracture was in a "closed" condition. With the fracture "open", significantly variable discharge rates could not be produced with the existing pumping system.

Figure 4.15 is a composite pressure head loss versus the logarithm of radial distance plot for the six steps of the test when the model had a 0.108-m diameter wellbore. All six pressure head loss profiles exhibit the double inflection shape characteristic of the "closed" fracture tests.

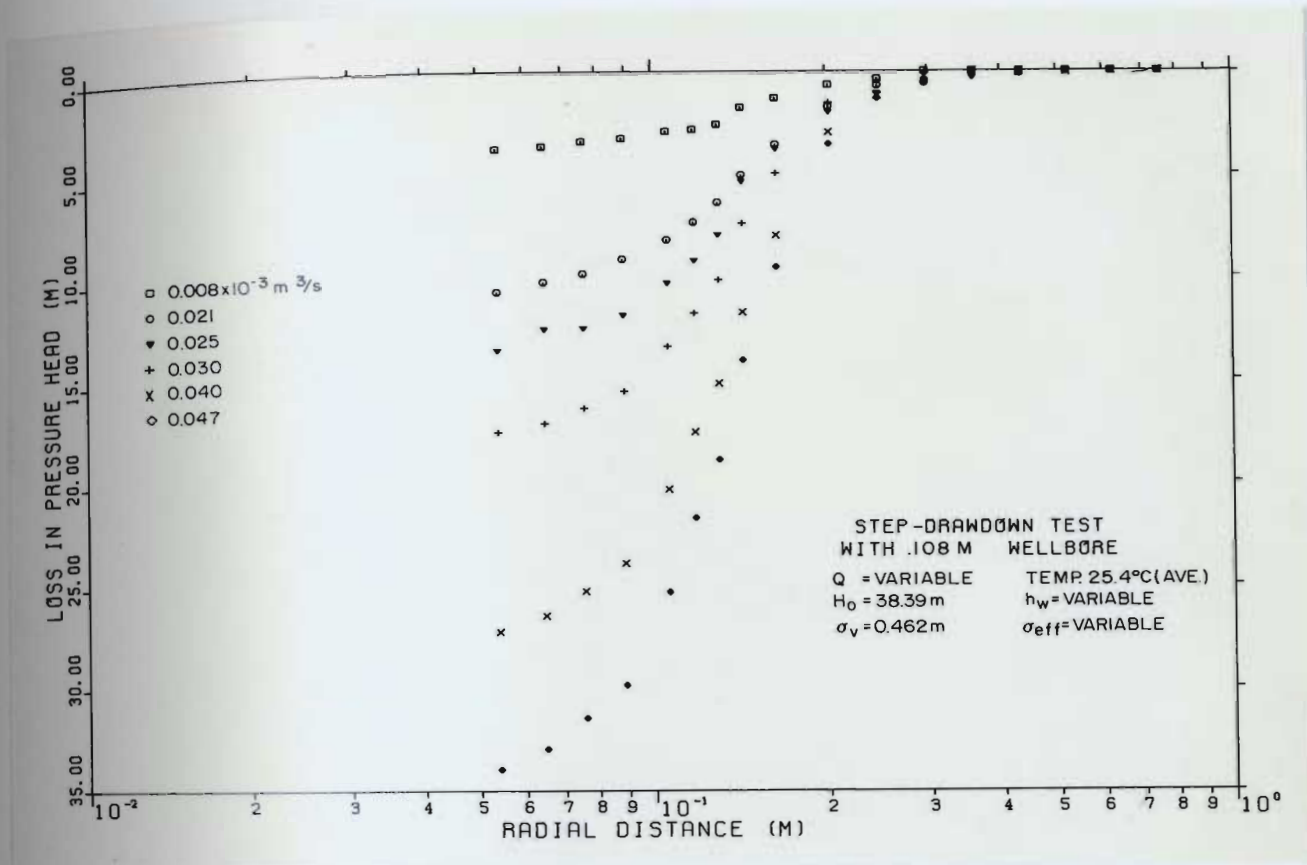


Figure 4.15 Loss in pressure head versus logarithm of radial distance for step-drawdown test of model with 0.108-m diameter wellbore

Figure 4.16 is a plot of drawdown versus discharge for all three step-drawdown tests. Contrary to what had been expected, these data indicate that the discharge for a given drawdown apparently decreased with an increase in wellbore size. Upon closer examination of the data, however, it appears, that despite every effort to keep all parameters but the size of the wellbore constant, the fracture aperture was not the same in each set of tests. Fracture apertures

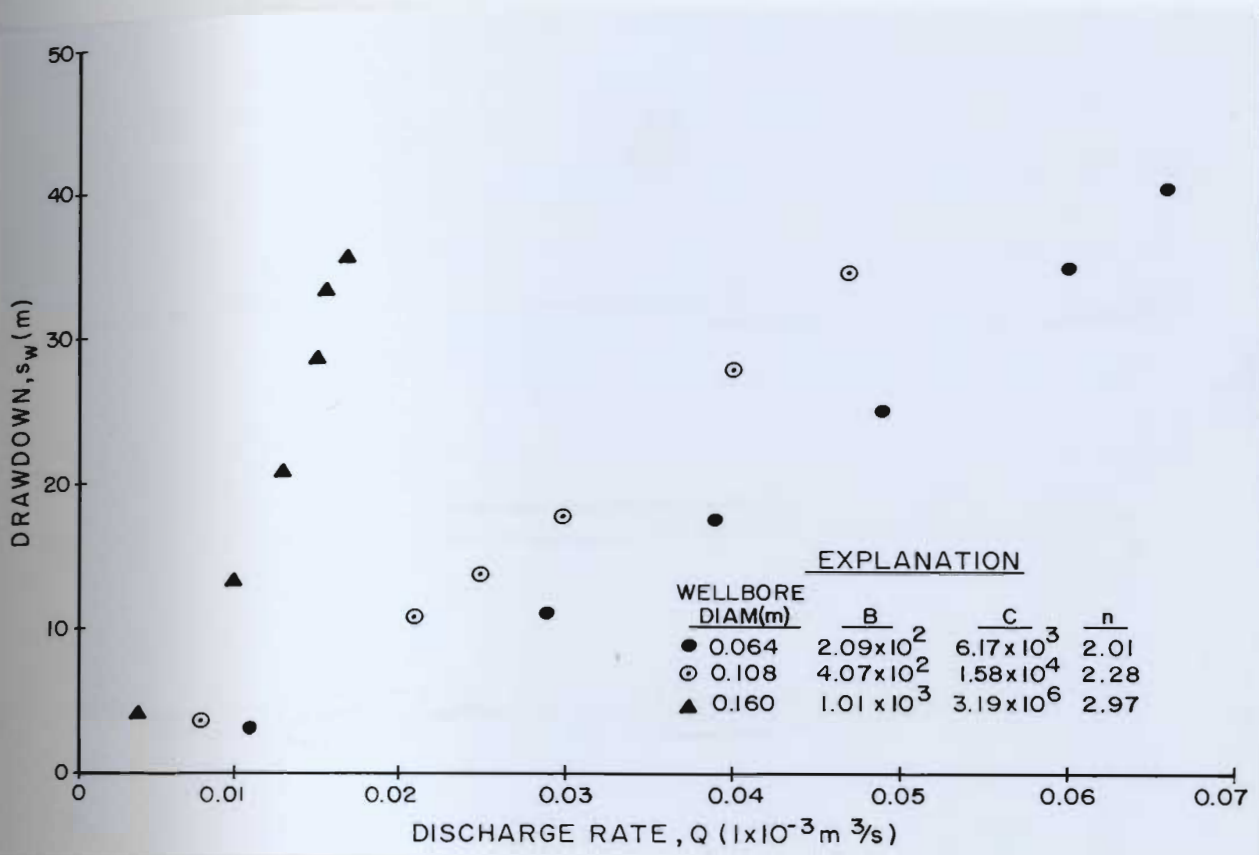


Figure 4.16 Drawdown versus discharge for step drawdown tests of laboratory model

could not be calculated from test results with the 0.108-m wellbore, but estimates of effective aperture for the tests with the 0.064-m and 0.160-m diameter wellbore were 350 to 370 μm and 250 to 300 μm , respectively. The differences in discharge most likely are reflecting the difference in this key parameter. This precluded an empirical evaluation of the effect of wellbore size on the production-drawdown response of a well that will be discussed theoretically in Section 6.2.1.

Specific drawdown versus discharge for the step-drawdown tests is plotted in Figure 4.17. All three sets of data follow either the "curve 2" or "curve 3" response described by Mackie (1982) and discussed in Section 1.3.3 (pages 19 to 22). It should also be noted (as shown in Figure 4.16) that the value of the exponent in the second term of the discharge-drawdown equation (Equation 1.13, page 9) was determined by non-linear regression to be greater than 2 using the computer program FASTEP (Labadie and Helweg, 1975). These results will be interpreted in Sections 5.3 and 6.1.

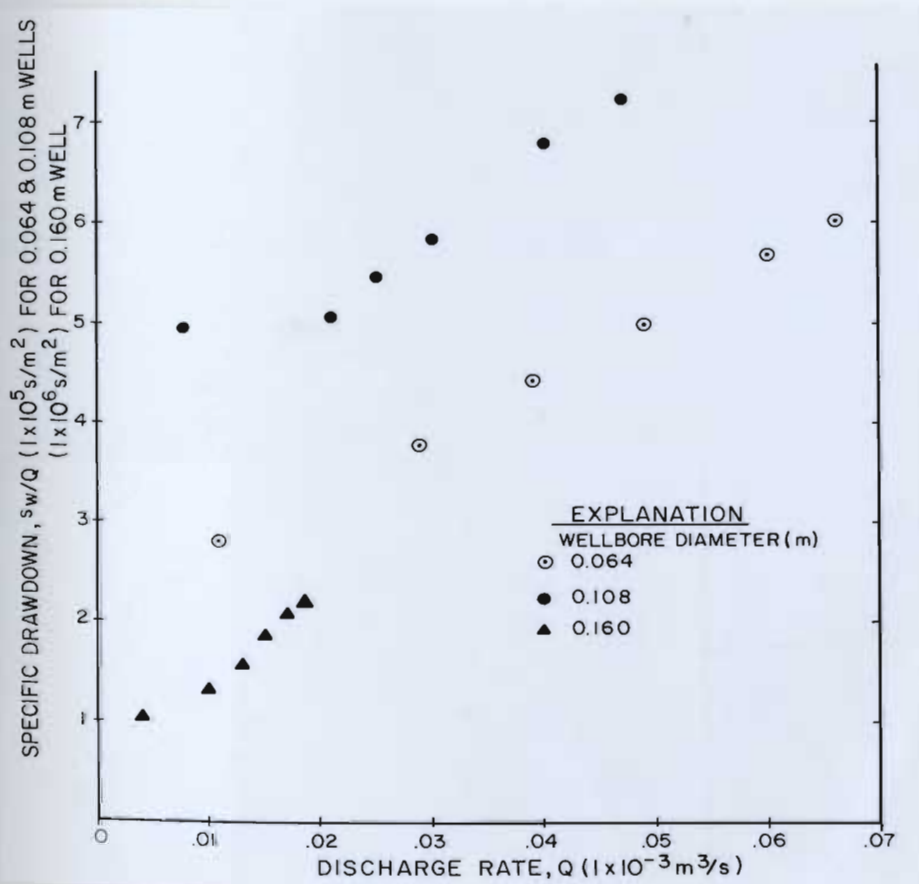


Figure 4.17 Specific drawdown versus discharge for step-drawdown tests of laboratory model

5.0 COMPARISON AND INTERPRETATION OF RESULTS FROM NUMERICAL AND LABORATORY MODELS

Of major interest in this study was how well the mathematical description of two-regime, convergent, radial flow to a well from a horizontal, deformable fracture that was described in Chapter 2.0 could match the empirical data obtained from tests of the large scale laboratory model. The comparison between the results of the numerical and physical models would indicate just how deterministic the numerical model developed in the study was in describing the production drawdown response of wells in fractured rock aquifers.

As described in Section 4.3.1 (page 104), all of the pumping tests of the laboratory model could be put into one of two categories, those in which the fracture was in an "open" position and those in which the fracture was "closed." For reasons which will become apparent in the following sections, the attempts to simulate these tests with the numerical model DEFLOW had to follow this same differentiation.

5.1 Tests with open fractures

The tests with the fracture in an "open" position (i.e., under a negative effective stress such that the fracture was hydraulically propped open and no surface

roughness asperities were in contact) all demonstrated a similar trend in pressure head distribution. Test No. 2, whose results are plotted in Figure 4.8 (page 109), is typical of these tests and will be analyzed in detail.

The "curve fitting" using DEFLOW was initiated by assigning the boundary conditions used in the laboratory test (a second type boundary condition was assigned at the well) and by using as a first guess for aperture size the value that had been estimated from the linear part of the logarithm of radial distance versus pressure head plot (Figure 4.9) by a method described in Section B.1 of Appendix B. Then, by trial and error, the values of aperture for each flow node in the numerical model were modified until the best fit (by visual inspection) was obtained. For Test No. 2, this involved decreasing the aperture radially inward. The laboratory data for normal displacement of the fracture (see Table 4.1, page 105) had indicated a differential "tilt" of almost 0.4 mm, most likely due to a slightly asymmetric positioning of the hydraulic jacks. Using a simple 3-point solution, the differences in aperture at each manometer location due to this tilting were estimated.

The best fit, shown in Figure 5.1, was obtained using apertures of 1.38 to 1.50 mm under the assumption that the absolute roughness of the fracture was 0.24 mm as observed in the photographs of resin-impregnated fractures (Figures

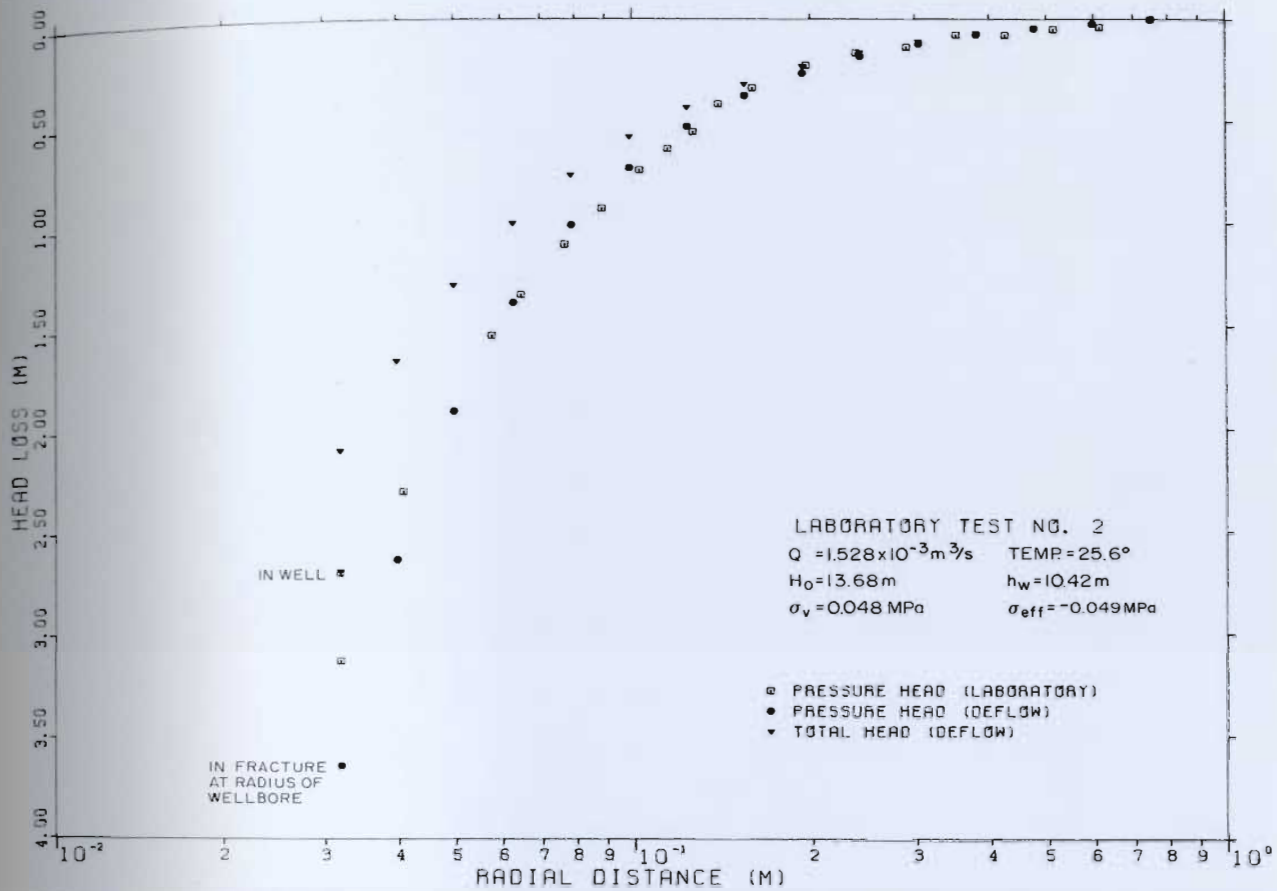


Figure 5.1 Actual pressure head loss compared to pressure head loss predicted by DEFLOW for open fracture

4.4 and 4.5, pages 98 and 99). As seen in Figure 5.1, the fit is very good from the outer boundary inward to a radial distance of approximately 0.05 m. Radially inward from that point, the actual and predicted pressure head loss curves diverge, with DEFLOW predicting approximately 11 percent more loss at the radius of the well. DEFLOW, which incorporates an empirical expression for exit loss (Equation 2.14, page 51), predicted that the head loss due to flow exiting from the fracture into the wellbore would be

approximately 0.59 m or about 38-percent of the velocity head (the difference between the total head and pressure head curves shown in Figure 5.1). The laboratory model data, however, suggest that very little, if any, of the velocity head was recoverable in the wellbore. This means that the exit loss coefficient in an expression such as Equation 1.10 (page 4) is essentially 1.0, more similar to the case for flow exiting from a relatively small pipe into a large reservoir than to the situation observed in laboratory experiments with an open fracture with parallel surfaces and mathematically described by Murphy and Pearce (1980).

Table 5.1 summarizes various estimates of the fracture aperture size that existed under the boundary conditions of Test No. 2. It includes 1) estimates by trial and error using DEFLOW, 2) the results of calculations of effective aperture by graphical analysis of the individual flow regions as described in Appendix B, and 3) an estimate of the geometric aperture based on direct measurement of microphotographs of resin-impregnated fractures in 0.150 m diameter concrete test cylinders and, 4) LVDT data from the test. The latter two were combined to determine

$$2b = 2b_o + \delta_h \quad (5.1)$$

where

$2b$ = aperture in hydraulically propped position,

$2b_o$ = aperture under self weight (from Figure 4.4, page 98) and

Table 5.1 Estimates of aperture size from Test No. 2 data

| Method | Aperture (mm) | Relative Roughness ¹ |
|---|------------------|------------------------------------|
| Resin casts ² and LVDT data ³ | 1.83-2.00 | 0.06 |
| Trial and error with DEFLOW | 1.38-1.55 | 0.08-0.09 |
| Data from linear region of plot (Louis) ⁴ | 1.39 | 0.09 |
| Data from linear region of plot (Sato et al.) ⁴ | 1.73 | 0.05 |
| Data from non-linear region of plot (Louis) ⁶ | 1.28 | 0.09 |

¹ Assuming $k = 0.240$ mm (see Figure 4.4, page 98).

² From tracings of slides of resin-impregnated fractures in 0.150 m diameter concrete test cylinders under self-weight (see Figure 4.4).

³ Measured normal displacement of fracture due to hydraulic propping (see Table 4.1, page 105).

⁴ See head loss versus logarithm of radial distance plot in Figure 4.8 (page 109). Method of calculation is described in Section B.1 of Appendix B.

⁵ See head loss versus inverse of radial distance plot in Figure 4.9 (page 110). Method of calculation is described in Section B.2 of Appendix B.

⁶ Roughness not a parameter in flow law of Sato et al.

δ_h = displacement (measured by LVDT's) as result of negative effective stress.

Based on the profiles shown in Figure 4.4 (page 98), the artificial fracture of the laboratory model had an aperture under self weight (corresponding to a normal stress of approximately 0.04 MPa) on the order of 0.45 mm and an absolute roughness of about 0.24 mm.

Although the estimate of aperture of 1.83 to 2.00 mm provided by the resin casts and LVDT data cannot be considered to be an absolutely correct reference, it is interesting to note that the apertures used by DEFLOW to produce the pressure head profile in Figure 5.1 are 0.45 mm less than the former, the same value as the estimate for $2b_0$. In other words, the effective apertures based on the flow laws of Louis (which are incorporated into DEFLOW) which gave the best fit to the laboratory results do not include the aperture of the unproped fracture. It should also be noted that the aperture sizes estimated according to the flow law of Sato et al., which are larger than those calculated using the flow laws of Louis, provide the closest approximation to the best estimate of the geometric aperture of the fracture. The results of Test No. 2 (also refer back to Figures 4.8 and 4.9 on pages 109 and 110) appear to clearly demonstrate two-regime flow. DEFLOW calculated the critical radius to be approximately 0.46 m. Although the limited number of data points shown on Figure 5.1 make it difficult to determine precisely, the departure from linearity on the laboratory data plot appears to occur at 0.3 m.

By extrapolating the gradient within the laminar flow region to the wellbore radius (0.032 m), it is possible to obtain an estimate of the drawdown that would have occurred had laminar conditions prevailed to that point. This drawdown, 0.36 m, subtracted from the total drawdown of 3.26 m

indicates that an additional 2.90 m of pressure head was lost to fully turbulent flow. Using for the definition of well efficiency

$$\text{well efficiency} = \frac{\text{drawdown under completely laminar conditions}}{\text{actual drawdown}} \quad (5.2)$$

the well simulated by the laboratory model in this test exhibited an efficiency of only 11 percent. If, to simulate a more realistic distance for the outer boundary (i.e., the radius of influence), the slope in the laminar flow region (0.248 m per log cycle) was extrapolated outward 2.5 log cycles to a radial distance of approximately 320 m, the resulting well efficiency would be only 25 percent.

5.2 Tests with closed fractures

A similar attempt was made using DEFLOW to match the pressure head data for the tests of the laboratory model under so-called "closed" conditions. A typical example of the results from a test under these conditions is the doubly inflected curve shown in Figure 4.10 (page 112) for Test No. 10. Attempting both first and second type boundary conditions at the well corresponding to the observed drawdown and discharge, respectively, a solution could not be obtained that produced compatibility between the discharge, drawdown, and increased steepening of the head loss versus

logarithm of radial distance plot. Even more problematic was the near-well inflection in the curve.

Three possible causes were considered for the second inflection in the plot: 1) relaminarization, a phenomenon in accelerating, turbulent flow which was described in Section 1.3.4.4 (page 42), 2) an increase in the size of the fracture aperture near the wellbore, or 3) anisotropy in the fracture. Relaminarization was immediately eliminated from further consideration for two reasons. First, using Equation 2.23 (page 56), the critical discharge rate assuming the relative roughness was in the range of 0.2 to 0.3, was determined to be 5.4 to $6.8 \times 10^{-5} \text{ m}^3/\text{s}$. That is greater than the discharge rate of the test ($4.7 \times 10^{-5} \text{ m}^3/\text{s}$). Concluding the entire flow region was laminar, this precludes relaminarization and, equally important, it requires an explanation other than the onset of turbulent flow for the first inflection in the curve. A second, confirmatory reason for disregarding relaminarization is that the near-well inflection was also seen (although it is not as well defined because of the elimination by reaming of several of the close-in manometers) in plots for the injection tests where the inflection, if any, due to transition from turbulent to laminar flow would be in the other direction.

The possibility that both inflections were due to changes in aperture, first a gradual decrease and then a gradual increase, seemed unlikely. Consequently, it was

concluded that flow in this closed test was completely laminar and that both inflections were due to anisotropy. Several possible causes were considered, but the texture of the geotextile used to cast the fracture provided the most credible explanation. As shown in Figures 5.2A and 5.2B, the geotextile consists of a woven polypropylene fabric. The resulting cast (Figure 5.2C) of the opposite concrete surfaces produces a "pea pod" cross-section under load (Figure 5.2D). Figure 5.2E shows in two dimensions that this creates an orthogonal system of flow channels in which impedance to flow would be at a minimum in the two orthogonal directions parallel to the flow channels and at a maximum at an intermediate or 45° orientation. Mathematically, this can be described by a double ellipse or "rosette" (Figure 5.2F).

The configuration of the fracture plane manometers (see Figure 4.3, page 96) complicates the analysis of this situation. The manometers had been laid out in a spiral, under the assumption that the transmissivity of the fracture would be isotropic, to minimize the effects of any turbulence that might be generated by the manometer openings in the fracture surface. That problem would have been cumulative if all of the manometers had been on a common ray. With the fracture exhibiting strong anisotropy, the solution to one problem created another.

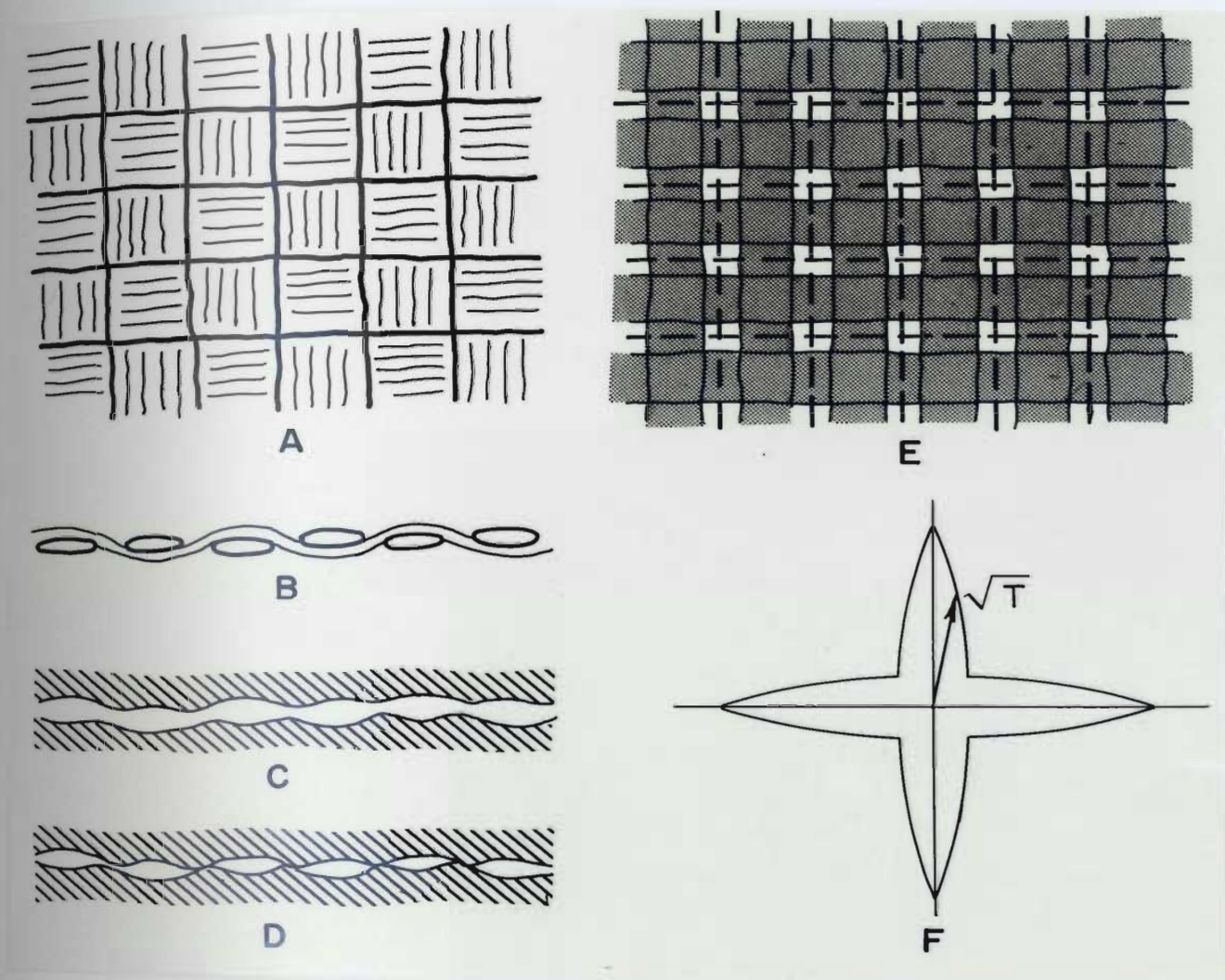


Figure 5.2 Anisotropy induced by geotextile used to cast fracture. Woven MIRAFI geotextile in A) plan view and B) cross-section. C) Void in cement after geotextile removed. D) Same void under load. Note resemblance to Figures 4.4 and 4.5 (pages 98 and 99). E) Resulting orthogonal flow channels (shown by stippled pattern) in fracture plane under load. F) Resulting transmissivity "rosette."

An attempt was made to characterize the anisotropy of the fracture using the steady-state method described in van

Golf-Racht (1982, pages 434-445). Data from several combinations of manometers, including the two sets of three manometers each (manometers 7-8-9 and 12-13-14 on Figure 4.3, page 96) which had been incorporated into the network specifically for this purpose, would not yield a solution. This is because the nature of the anisotropy (refer back to Figure 5.2F) cannot be described by the single, two-dimensional ellipse implicit in the van Golf-Racht solution. In fact, no analytical methods are known to exist that would quantitatively define the anisotropy exhibited by the fracture of the laboratory model. Even if the anisotropy could have been described, however, it would not have been possible to incorporate it directly into the one-dimensional, radial flow code of DEFLOW.

Estimates of the effective aperture of the "closed" fracture were made using the same techniques for the laminar flow region as for the "open" fracture. The results are given in Table 5.2. Data from the outermost or first slope of the curve yielded an estimate of 0.38 to 0.44 mm according to the flow law of Louis and 0.32 mm according to the flow law of Sato et al. As can be seen in Figure 4.3 (page 96) radial flow lines past these manometers would be parallel to one of the "flow tube" directions. Radial flow past manometers number 7 through about number 20 would have to follow a much more tortuous path around the asperities in

Table 5.2 Estimates of aperture size from Test No: 10 data

| Method | Aperture (mm) | Relative Roughness ¹ |
|---|------------------|------------------------------------|
| Resin casts ² and LVDT data ³ | 0.51-0.52 | 0.24 |
| Data from first ⁴ slope (Louis) ⁵ | 0.38-0.44 | 0.13-0.27 |
| Data from first ⁴ slope (Sato et al.) ⁵ | 0.32 | __6 |
| Data from second ⁴ slope (Louis) ⁵ | 0.11-0.13 | 0.5 ⁷ |
| Data from second ⁴ slope (Sato et al.) ⁵ | 0.10 | __6 |

¹ Assuming $k = 0.240$ mm (see Figure 4.4, page 98).

² From tracings of slides of resin-impregnated fractures in 0.150 m diameter concrete test cylinders under self-weight (see Figure 4.4).

³ Measured normal displacement of fracture due to hydraulic propping (see Table 4.1, page 105).

⁴ See Figure 4.10 (page 112).

⁵ Method of calculation, described in Section B.1 of Appendix B.

⁶ Roughness not a parameter in flow law of Sato et al.

⁷ For $k = 0.24$ mm, relative roughness would be greater than 0.5. Following convention of this study, value was set to upper limit of 0.5.

contact (Figure 5.2E). Data from these manometers comprise the steepest part of the curve in Figure 4.10 (page 112) and yield estimates of fracture apertures ranging from 0.10 to 0.13 mm. Flow past the next group of closer-in manometers parallels the orthogonal set of flow tubes; and, if there

were more radially inward data, it is likely the curve after the inflection would parallel the first segment.

The two slopes (which reflect the transmissivity of the fracture) of the curves differ by a factor of approximately 36. Consequently, according to the cubic law, the effective apertures should differ by a factor of about 3.3. As indicated in Table 5.2, the calculated effective apertures are in all cases less than the best estimate for the geometric aperture of the fracture under closed conditions.

6.0 APPLICATION OF FINDINGS

The findings from this study, which will be summarized in Section 7.0, provide a more deterministic basis than was previously available for evaluating the hydraulic response of a vertical well to pumping from a horizontal fracture. Two of the more important applications of these findings are in the proper interpretation of step-drawdown tests of wells in fractured rock and in assessing the potential effects of certain well stimulation procedures. To the present, investigations in both of these areas have been based almost purely on empirical observations.

6.1 Re-interpretation of step-drawdown test results from fractured rock aquifers

The results of the step-drawdown tests synthesized by the numerical model DEFLOW and the actual variable rate pumping tests conducted on the large scale laboratory model were described in Sections 3.4 (pages 90-92) and 4.3.3 (pages 116-120), respectively. The findings of previous investigations using step-drawdown tests and the controversy regarding the more correct form of the polynomial discharge-drawdown equation (either Equation 1.13, page 9 or Equation 1.15, page 18) were discussed in Chapter 1.0. This section will resolve some of this controversy and demonstrate two of

the more important practical observations that can be made using step-drawdown test data. Although the numerical model has been used more extensively in this study, the following explanation is more straightforward and easier to relate to graphically with the use of the analytical solution for two-regime, convergent radial flow to a well from a single horizontal fracture given by Equation 2.18 (page 53). If both sides of Equation 2.18 are divided by Q in order to put it in terms of specific drawdown, s/Q ,

$$\begin{aligned} \frac{s}{Q} = & \frac{6\nu \{1 + 8.8[k/(2 \cdot 2b)]^{1.5}\}}{\pi g(2b)^3} \ln \frac{r_o}{r_c} \\ & + \frac{Q}{64\pi^2 g(2b)^3 [\log\{1.9/[k/(2 \cdot 2b)]\}]^2} \left[\frac{1}{r_w} - \frac{1}{r_c} \right] \\ & + 0.23 \left(\frac{2r_w}{2b} \right)^{1.41} \frac{Q}{2g\pi^2 r_w^4} + f_w \frac{(L - 10r_w)Q}{4\pi^2 g r_w^5} \end{aligned} \quad (6.1)$$

is obtained. The four components of specific discharge described by this equation are plotted in Figure 6.1 for the hypothetical situation of a single, horizontal fracture with the following properties and boundary conditions:

$$\begin{array}{ll} r_o = 100 \text{ m} & \text{temp.} = 20^\circ\text{C} \\ r_w = 0.152 \text{ m} & f_w = 0.05 \\ 2b = 0.500 \text{ mm} & L = 10 \text{ m} \\ k/D_h = 0.100 & \end{array}$$

It is immediately apparent in Figure 6.1 that the exit and wellbore losses for this example are negligible (they

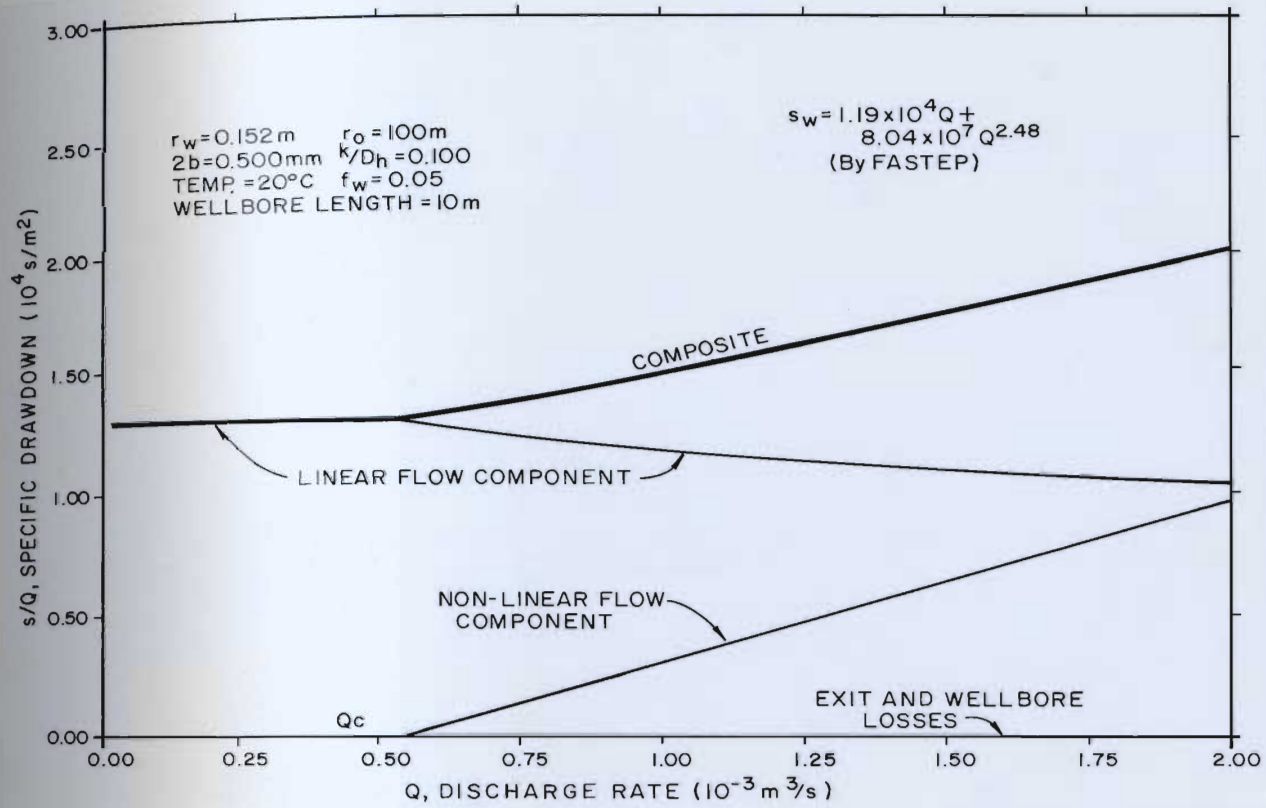


Figure 6.1 Components of specific drawdown as a function of discharge rate

are so small that their combined value cannot be differentiated from the baseline), so attention can be focused on the first two components of drawdown described by Equation 6.1. As shown in the figure and by referring back to Equation 6.1, at discharge rates less than the theoretical critical discharge rate, Q_c (see Equation 2.23 on page 56), the critical radius, r_c , is less than or equal to the radius of the wellbore, r_w . Therefore, for practical purposes, r_c is set equal to r_w and only the linear flow component exists. The first term in the equation, therefore, is a constant,

dependent only on the flow system boundaries (i.e., $\ln r_o/r_w$), the fracture (roughness and aperture), and the fluid (viscosity) properties. At discharge rates greater than the critical discharge rate, the critical radius is greater than the radius of the wellbore and non-linear flow arises. If the discharge rate continues to increase, the linear flow component of specific drawdown decreases non-linearly as a function of $\ln r_o/r_c$ while the non-linear component increases as the function

$$\left(\frac{s}{Q}\right)_n = f\left(Q\left[\frac{1}{r_w} - \frac{1}{r_c}\right]\right) \quad (6.2)$$

As described by Equation 2.21 (page 55) and Table 2.1 (page 54), the critical radius is a function of the discharge rate, fracture roughness, and the fluid viscosity. Substituting Equation 2.21 into Equation 6.2

$$\left(\frac{s}{Q}\right)_n = f\left(Q\left[\frac{1}{r_w} - \frac{\pi\nu Re_c}{Q}\right]\right) \quad (6.3)$$

or

$$\left(\frac{s}{Q}\right)_n = f\left(Q/r_w - \pi\nu Re_c\right) \quad (6.4)$$

is obtained. For the case of a rigid fracture in which the critical Reynolds number, Re_c , stays constant, Equation 6.4 plots as a straight line as shown in Figure 6.1. If the fracture is deformable and closure occurs, the relationships given in Table 2.1 indicate that Re_c decreases so that the total value represented by Equation 6.4 would increase. This would result in a slightly upward curvature to the non-linear flow component.

The composite of all four components, shown by the heavy line in Figure 6.1, is a curve which is a horizontal line up to the critical discharge value and which becomes concave upward beyond that point. Note that this is the "curve 3" response cited by Mackie (1982) as being typical for step-drawdown tests of wells in fractured rock (refer back to pages 19-22). It is also noteworthy that the best fit to the composite curve of Figure 6.1 by non-linear regression using the program FASTEP (Labadie and Helweg, 1975) is $s_w = 1.19 \times 10^4 Q + 8.04 \times 10^7 Q^{2.48}$.

An explanation can now be developed for obtaining best fits to the polynomial discharge-drawdown equation with step-drawdown test data using a value for the exponent greater than two as reported by Rorabaugh (1953) and Lennox (1966). In all the existing methods of step-drawdown test analysis, it is assumed that the value of C, the coefficient of the second term in the polynomial equation, is constant. However, by comparing Equation 1.16 (page 20) under the assumption that n is equal to 2 (as it has been shown to be theoretically correct) to Equation 6.1 and substituting in the expression given in Equation 6.3,

$$C = \frac{1}{64\pi^2 g(2b)^3 [\log \{1.9/[k/(2 \cdot 2b)]\}]^2} \left[\frac{1}{r_w} - \frac{Re_c}{Q} \right] \quad (6.5)$$

is obtained. It is obvious from Equation 6.5 that C, which also is the slope of the composite specific drawdown curve

beyond where it is horizontal, is not a constant but rather a function of Q . This same conclusion, though less quantitatively, was previously drawn by Mackie (1983) and Basak (1978). The correct expression for the production-drawdown response of a well under fully turbulent, two-regime flow conditions is, therefore,

$$s_w = BQ + C(Q)Q^2 \quad (6.6)$$

Although Equation 6.6 is the theoretically correct statement for the production-drawdown relationship, the need to determine a discharge dependent value for $C(Q)$ makes it unwieldy. This study has found that the polynomial expression

$$s_w = BQ + CQ^n \quad (6.7)$$

which assumes C is a constant but allows the value of n to "float" in the solution achieves better fits to the data than Equation 1.15 (page 18), the Jacob equation which assumes C is constant and n is equal to 2. Similarly to the previous observations by Rorabaugh (1953), this study found that values of n in the range of 2.3 to 2.7 usually gave the best fits to the data.

It is concluded that solution by Equation 6.7, though a mathematical manipulation, yields a result that should be acceptable for most practical purposes. Although extrapolation of test results beyond the actual range of the discharge rates of the specific step-drawdown test is risky,

it has also been found that Equation 6.7 tends to yield more reliable extrapolated values than Equation 1.15.

Two other observations, and ones of even greater practical significance, can be made with step-drawdown test data. The first, which is qualitative, can be used to determine whether the primary source of water to the well is a horizontal or a vertical fracture. This provides an alternative to the determination based on a constant discharge test developed by Gringarten (1982). The second observation can be used to estimate the effective aperture of a horizontal fracture.

If turbulent flow in a horizontal fracture is the reason for the "well losses," it has been shown that the specific drawdown versus discharge rate curve resulting from a step-drawdown test should be concave upward in its higher discharge segment. As previously described, this is the "curve 3" response cited by Mackie (1982). If, however, the main sources of "well losses" are exit losses (including losses in screens or perforated casings) and wellbore losses, the resulting curve should be comprised of a horizontal initial segment and a latter segment of constant slope. That is because the exit and wellbore losses are functions of Q^2 (see Equation 6.1) and, therefore, their components of specific drawdown would be lines of constant slope. In the absence of a non-linear flow regime in the horizontal fracture, there would be no decrease in the

linear flow component of specific drawdown as a function of $\ln r_o/r_c$; and, without this decrease, there would be no concavity to the composite curve. The composite curve would, therefore, be like the "curve 2" of Mackie (1982) shown in Figure 1.3 (page 21).

Another cause of the "curve 2" type response is turbulent flow in a vertical fracture. In the case of a wellbore intersecting a vertical fracture, flow in the fracture near the well is parallel instead of radially convergent. Although the concepts of critical Reynolds number

$$Re_c = \frac{vD_h}{\nu} = \frac{QD_h}{Av} = \frac{Q(2 \cdot 2b)}{2b \cdot w \cdot \nu} = \frac{2Q}{w \cdot \nu} \quad (6.8)$$

where w is the vertical dimension of the fracture, and critical discharge rate

$$Q_c = \frac{Re_c \cdot w \cdot \nu}{2} \quad (6.9)$$

are applicable, there is no equivalent to the critical radius of convergent radial flow. Therefore, flow is either completely laminar or completely turbulent within the entire extent of the vertical fracture whether the discharge rate is less than or greater than the critical discharge rate. As in the case of radial flow, the component of specific drawdown due to turbulent flow would be directly proportional to Q (this can be derived from Missbach's law, Equation 1.6 on page 4, assuming m equals 2) and, hence, would be a

straight line of constant slope on a plot of specific drawdown versus discharge. Without the associated logarithmic (i.e., $\ln r_o/r_c$) decline in the laminar flow component, however, the composite curve would simply be a straight line of constant slope beyond the critical discharge point. It is believed that turbulent flow in vertical or nearly vertical fractures is more likely the cause of the "curve 2" responses observed by Mackie (1982) than either exit or wellbore losses.

If a "curve 3" response is derived from a step-drawdown test of a well completed into fractured rock, there is a strong indication that turbulent flow is occurring in one or more horizontal fractures. By comparing Equation 6.1 (page 135) with Equation 6.7 (page 139), it can be shown that, at discharge rates less than the critical discharge rate,

$$\frac{s}{Q} = B = \frac{6\nu \{1 + 8.8[k/(2 \cdot 2b)]^{1.5}\}}{\pi g(2b)^3} \ln \frac{r_o}{r_w} \quad (6.10)$$

Therefore, similarly to the derivation of Equation B2 (page 179) in Appendix B and using the value of B (the value of the horizontal segment) from the specific drawdown versus discharge plot, an estimate of the fracture aperture can be made from

$$2b = \left(\frac{6\nu \{1 + 8.8[k/(2 \cdot 2b)]^{1.5}\}}{\pi gB} \ln \frac{r_o}{r_w} \right)^{1/3} \quad (6.11)$$

or

$$2b = f \left(\frac{6\nu \ln(r_o/r_w)}{\pi g B} \right)^{1/3} \quad (6.12)$$

where f is an unknown roughness factor. As shown in Table B1 (page 180), the value of this factor can range from 1.085 for a relative roughness of 0.100 (using the relationship derived by Louis, 1969) to 1.602 for a relative roughness of 0.500. In addition to this unknown, the value of the radius of influence, r_o , can only be estimated. However, the solution is not very sensitive to this value (e.g., the calculated values of $2b$ for r_o equal to 1000 m and r_o equal to 100 m differ by only approximately 10 percent). It should be noted that this method for estimating the fracture aperture from a multi-rate pumping test is very similar to that developed by Rissler (1978) for estimating the aperture from an injection test using the concept of "critical head."

Once an estimate of the effective aperture is available, predictions can then be made of how certain changes in the wellbore environment might improve the efficiency of the well. The following section will evaluate the potential effects of two methods of eliminating or at least minimizing the effects of non-linear flow losses in wells intersecting horizontal fractures.

6.2 Evaluation of potential well stimulation methods

Two relatively inexpensive methods that have been observed empirically to improve the drawdown-production response of wells in fractured rocks have been 1) by simply increasing the wellbore size (Norris, 1976; Caswell, 1985a, b) and 2) by propping existing fractures (Williamson and Woolley, 1980). It should be noted that hydrofracturing, which is considerably more expensive and requires specialized equipment and materials, usually results in the creation of vertical fractures. For these reasons, it will not be included in the following discussion. The intent of the following sections is to attempt to quantify the results of stimulation that might be achievable under realistic field conditions.

6.2.1 Increasing wellbore diameter

As early as three decades ago, Baker (1955) suggested that the most obvious way to increase the yield of a well producing from horizontal fractures was to enlarge its diameter. He produced a graph indicating that relative increases of about 30 percent might be experienced by enlarging the radius of the wellbore from 0.076 m (a standard size in the petroleum industry) to 0.114 m in a well intersecting a horizontal fracture with an aperture of 1.016 mm (considered by

Baker, 1955, to be representative). Following that pioneering work, DEFLOW (using the flow code only) has been used to attempt to predict both the increase in production (using a first type boundary condition of $H_0 = 5.00$ m at the well) and the decrease in drawdown (using a second type boundary condition of $Q = 1.2 \times 10^{-3}$ m³/s) for various wellbore sizes and the following assumed parameters:

$$\begin{array}{ll} 2b = 0.500 \text{ mm} & r_0 = 100 \text{ m} \\ k = 0.200 \text{ mm} & H_w = 100.0 \text{ m} \\ \text{temp.} = 15 \text{ C} & \end{array}$$

The results are plotted in Figure 6.2. Also included in this plot for reference is a production curve based on the Theim equation (Equation 2.7, page 50) that indicates the increase in production that would be expected under purely laminar flow conditions. For that case, the production increase is related only to the change in the $\ln r_0/r_w$ function. Figure 6.2 shows a significant difference between that curve and the one predicted by DEFLOW for the given case in which two regime flow occurs. The relatively large change in the latter is the result, despite the increase in the critical radius as a direct function of the discharge rate (see Equation 2.21, page 55), of the decrease in the radial distance, $r_c - r_w$, of the non-linear flow regime. Since less hydraulic head is consumed by non-linear flow, a greater yield can be achieved with the given available drawdown. It should be noted that the relative increase predicted by this curve for

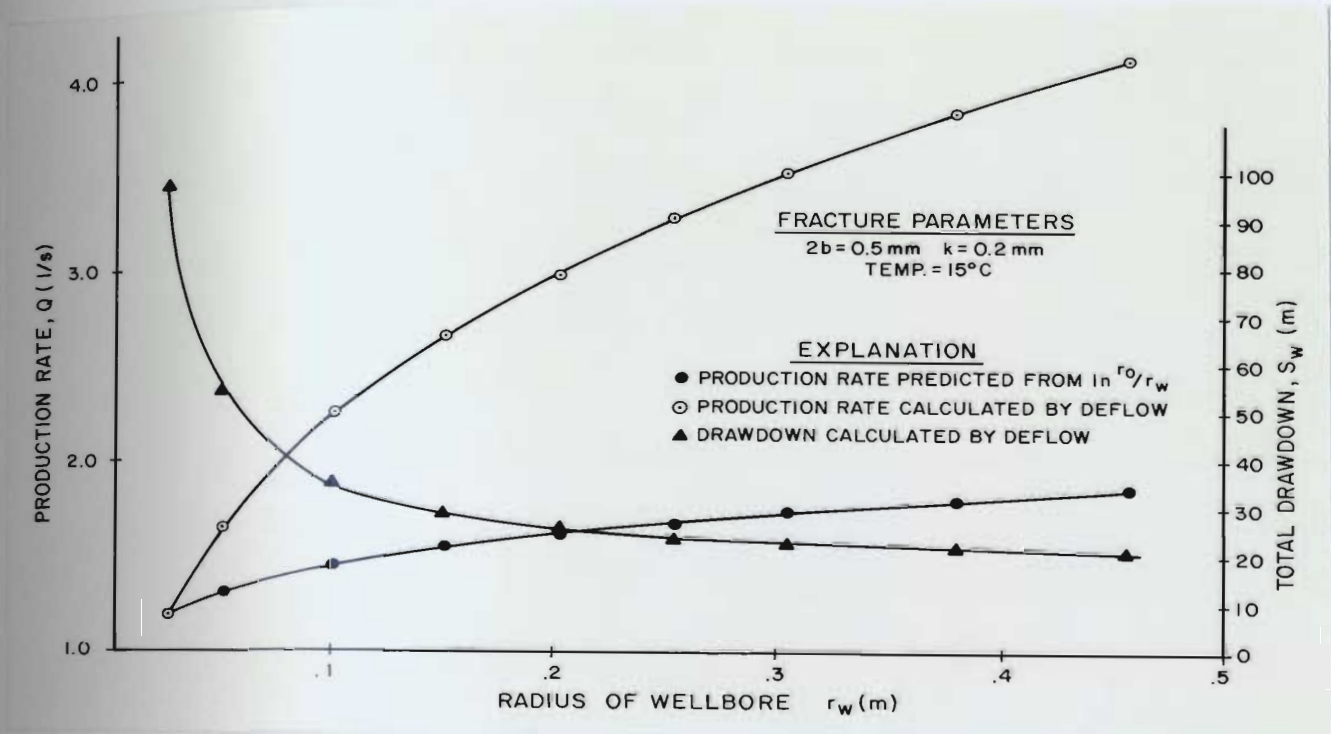


Figure 6.2 Production rate and drawdown as a function of wellbore size in a well intersecting a single, horizontal fracture

the same wellbore enlargement that was used by Baker (1955) in the previously cited example is about 37 percent. This same curve suggests increases on the order of 33 percent by enlarging the wellbore from a radius of 0.102 to 0.203 m. These sizes are in the range of typical dewatering wells.

The drawdown curve in Figure 6.2 shows a very significant change with size initially, but the relative change decreases quickly past a radius of about 0.1 m. Beyond that radial distance, the change in the $(1/r_w - 1/r_c)$ term (refer back to Equation 6.1 on page 135) becomes very small. It

should be noted that the critical radius calculated for this example from Equation 2.21 (page 55) and from the values in Table 2.1 (page 54) is 0.407 m.

These theoretical predictions based on the empirical numerical model could not be tested by the laboratory model even though that was one of the primary reasons for reaming the wellbore of the concrete cylinder. It appears (refer back to Section 4.3.3 on page 116) that changes in the fracture aperture occurred between the tests with the different size wellbores. It is not known whether this was due to differences in loading (the loading frame had to be completely disassembled to ream the wellbore and then re-assembled to resume testing) or the result of a thin "mortar rind" (a normal development during the curing of concrete) that appeared to have formed on the fracture surface. In either case, this precluded an empirical observation of the effects of wellbore size alone on the production-drawdown response of a well.

The preceding analysis suggests that enlarging the wellbore diameter could be a simple, yet effective means of increasing the production of a well obtaining water from a horizontal fracture and provides theoretical support to the field observations of Norris (1976) and Caswell (1984a,b). Since it would be necessary only to enlarge the interval(s) containing the intersection of the fracture(s) with the

wellbore, it could be more cost-effective to conduct selective reaming instead of drilling larger diameter wellbores over their entire extent. Based on the results of logs (e.g., geologic, geophysical, acoustic televiewer, television), pumping tests using a downhole flowmeter or double packers, or injection tests, the individual water-bearing zones could be identified. Although there are no known cases of such reaming in hard rock, there is no reason that the under-reaming methods currently used for casing through overburden or for completing large diameter wells in unconsolidated materials could not be adapted for this purpose (Lanser, 1985).

6.2.2 Hydraulic propping

Another method which has been used to stimulate wellbores in fractured rock is hydraulic propping (Williamson and Woolley, 1980). Hydraulic propping differs from hydraulic fracturing in that in the former, existing fractures are widened by injection of fluid under excess pressure (relative to normal formation pressure) with or without propping agents (e.g., sand, plastic beads). The results of attempts to stimulate water wells by this technique have been quite variable (Williamson, 1982).

Using the coupled deformation-flow solution, DEFLOW was used in both the injection and pumping mode to simulate a

multi-cycle hydraulic propping operation. The following properties and boundary conditions were used:

| | |
|--|--|
| $r_w = 0.100 \text{ m}$ | $k = 0.200 \text{ mm}$ |
| $r_o = 100.0 \text{ m}$ | temp. = 15°C |
| $H_o = 80 \text{ m}$ | $\sigma_n = 2.5 \text{ MPa}$ |
| $H_w = 250 \text{ m}$ (injection) | $\gamma_r = 2.75 \times 10^3 \text{ kg/m}^3$ |
| $H_w = 5 \text{ m}$ (pumping) | $E_r = 30 \text{ GPa}$ |
| $2b_o = 0.500 \text{ mm}$ | $\mu = 0.25$ |
| $\sigma_n = 6.33 \times 10^{-3} \delta + 2.50 \delta^{3.82}$ | |

It was also assumed in this simulation that 1) the fracture was laterally continuous to r_o , 2) no shear or tangential displacements could occur, and 3) all displacement in the fracture was "absorbed" between cycles by the adjacent rock. This final assumption means that the fracture would remain at its new aperture and that no residual stresses would remain after each injection cycle. Without this assumption, only the first cycle would be theoretically possible since, during injection, the hydraulically induced stresses are in equilibrium with the stresses resulting from applied loads, gravity loads, and the elastic strain of the rock matrix.

The results, shown in Figure 6.3, indicate that a 12 percent increase in discharge rate (using the same boundary conditions for pumping as for the initial, pre-propping condition) is achieved as the result of opening the fracture in the immediate vicinity of the wellbore on the order of 20 μm . The two subsequent cycles of injection show subsequent relative increases of about 8 percent each for a total net increase (relative to the initial discharge rate) of about 30 percent.

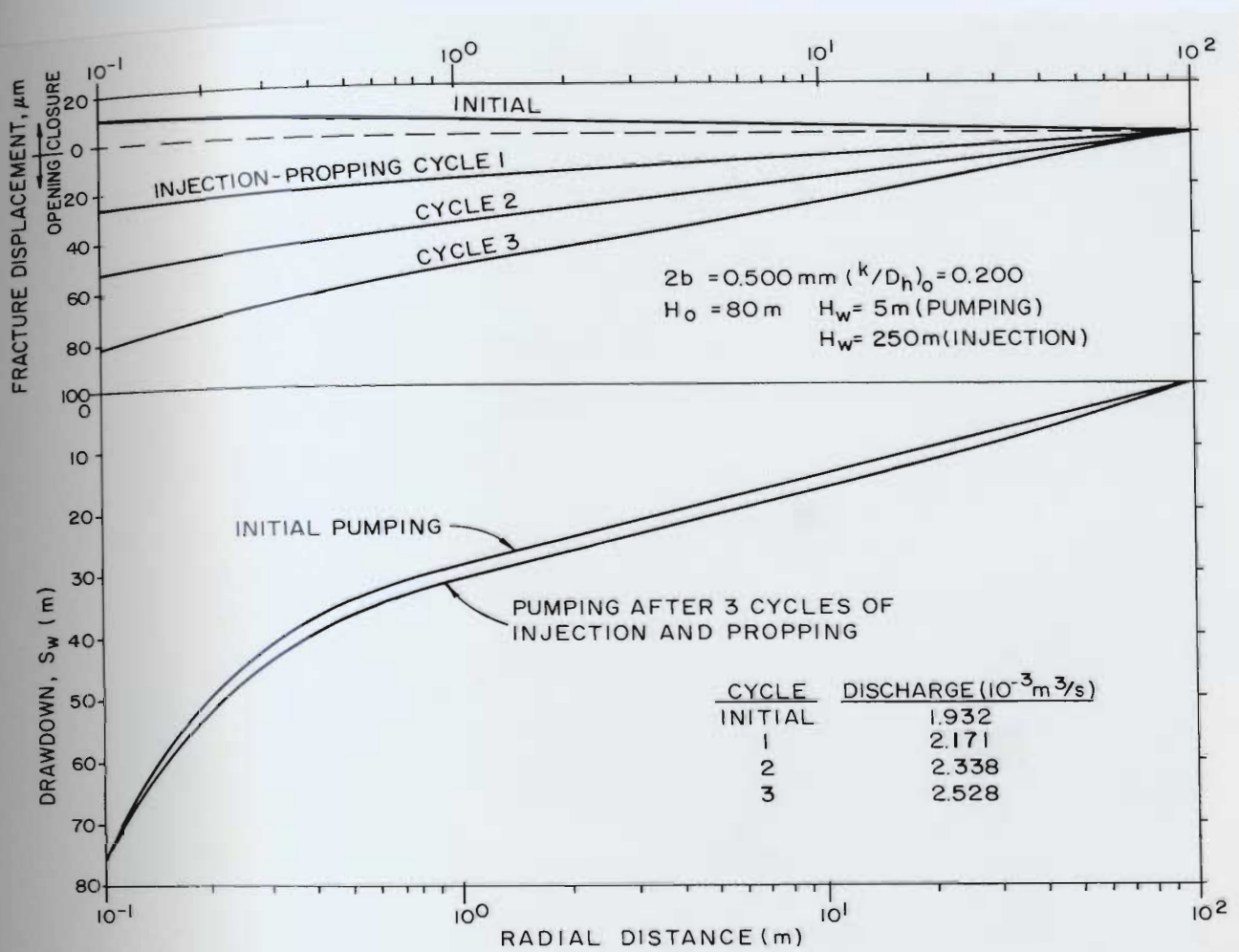


Figure 6.3 Potential effect of fracture propping in production-drawdown response

The assumptions used in this simulation are not very realistic, but they tend to offset one another. It is unlikely that residual stresses would not exist during subsequent cycles, so the effectiveness of multiple cycles is probably exaggerated. However, it is also unlikely that there would be no other fractures, either vertical ones which would allow tangential displacement or adjacent horizontal ones whose closure would permit a greater amount of

propping in the fracture of interest than would result from the elastic deformation of the rock matrix alone. The analysis does indicate, however, that even a very small (i.e., on the order of few tens of microns) propping can result in significant production increases.

One observation worth noting because of its practical significance is the temperature of the water that would be injected during propping. The colder the water the more viscous it is; and the excess injection pressure would be more concentrated near the wellbore where it can achieve the best results. Chemical viscosity enhancers are frequently used in the petroleum industry during hydrofracturing operations, but some of the chemicals used are toxic and their use in water wells would be highly questionable. Also, while the preceding analysis using DEFLOW assumed isothermal conditions, cold water would result in some contraction of the rock matrix which could induce further opening of the fracture.

7.0 SUMMARY

7.1 Findings

This section summarizes, in relatively concise point form, the more significant findings of this study in the area of theoretical and applied fractured rock hydraulics. All of the initial objectives of the study as outlined in Section 1.2 (pages 10 and 11) are addressed.

- 1) The aperture of the fracture is the single most important parameter in fracture flow. In terms of relative sensitivity, the effect on head loss of changes in aperture is 30 times greater than for changes in roughness, 100 times greater than for changes in fracture stiffness, and 190 times greater than for changes in fluid viscosity.
- 2) The effect of flow-induced decreases in fluid pressure increasing the effective stress and resulting in fracture deformation (closure) is less important in radial flow, particularly in the case of two-regime flow, than in parallel flow. This is because the greatest changes in stress act only over relatively small areas near the boundary of the wellbore.

- 3) Flow of water through fractures, as suggested by Witherspoon et al. (1980) and Maini (1971), is usually through an intricate assemblage of interconnected tubes of varying cross-section separated by asperities, some of which are in contact, rather than through a curvilinear channel. This was most visually demonstrated by the laboratory model built for this study (see Figure 4.6 on page 100). Using existing flow laws, however, the net flow geometry can be attributed to an equivalent effective aperture between two rough, parallel surfaces.
- 4) Although the true geometric properties (the aperture under similar stress levels and the roughness) of the model were not measured, estimates of these parameters were made from microphotographs of resin-impregnated fractures in similarly cast 0.150 m diameter concrete test cylinders. Using the flow laws of Louis (1969) and Sato et al. (1984), calculated effective apertures were on the order of 0.7 to 0.8 of the best estimates of true geometric apertures (1.8-2.0 mm) for pumping tests with an open fracture. When the fracture was closed by applying a net axial load, considerable anisotropy developed due to the texture of the artificial fracture surface. Estimates of effective aperture under these conditions ranged from 0.8 of the best estimate of geometric aperture in the direction

parallel to the "grain" of the roughness to 0.2 in the orthogonal direction.

Three possible reasons for the effective apertures being smaller than the true geometric apertures are:

- a) tortuosity causing the actual flow paths to be greater, resulting in the gradients being over-estimated,
 - b) the geometric equivalence between a smaller parallel plate aperture with no contact area and a real fracture with a considerable portion of its cross-sectional area being contacts between asperities, and
 - c) the constant acceleration/deceleration of the water through a flow path of different cross-sectional area causes more head loss than is predicted by the parallel plate model with constant fluid velocity.
- 6) As shown in Table 4.1 (pages 105-108), the calculated effective apertures usually remained within 5 to 8 percent when the flow boundary conditions in the large scale laboratory model were changed.
- 7) In the case of two-regime flow in open fractures, the same effective aperture could be used to describe head distributions in both flow regions.
- 8) The relative discharge to a well from fractures with different apertures under two-regime flow conditions is

not accurately predicted by the classical cubic law. A greater portion of the total head loss in the larger fracture occurs in the non-linear flow region. Therefore, for a given drawdown, its relative discharge is on the order of 10 percent less than that predicted by the cubic law which assumes laminar flow only.

- 9) The general graphical "signature", typical of step-drawdown test results of wells completed into fractured rock aquifers, was reproducible with the mathematical description of two-regime, convergent, radial flow to a well from horizontal, deformable fractures developed in this study. This indicates that the mathematical model (either the analytical or numerical version) is reasonably deterministic and should be useful in evaluating step-drawdown tests and potential well stimulation procedures.
- 10) Head losses due to non-linear flow can constitute as much as 80 percent of the total head losses in a well pumping under two-regime conditions from a horizontal fracture.
- 11) The laboratory results suggest that in the case of high velocity radial flow, most of the kinetic energy of the fluid is lost when the water jets into the wellbore.

In other words, the exit loss is essentially the entire $v^2/2g$ component of head instead of the smaller value predicted by the findings of Murphy and Pearce (1980).

12) For discharge flow rates on the order of 1 to 2 l/s, the critical radius based on the work of Rissler (1978) should have been in the range of 0.35 to 1.07 m. The apparent critical radii in the laboratory tests, however, were less (usually on the order of two-thirds) than the predicted values.

13) Tests of the laboratory model with an open fracture clearly demonstrated two-regime flow. The fully turbulent, non-linear flow component was evident on head versus the inverse of radial distance plots. Non-linear flow could not be initiated with the fracture in the closed position.

14) The most correct version of the polynomial expression for the production-drawdown response of a well pumping from a horizontal fracture is

$$s = BQ + C(Q)Q^2$$

where $C(Q)$ implies a coefficient dependent on the discharge rate. The variability of this term, however, limits its usefulness in the application to step-drawdown test analysis. It was found that the relationship first suggested by Rorabaugh (1951)

$$s = BQ + CQ^n$$

where n is an exponent greater than 2 (frequently in the range of 2.3 to 2.6) provides an adequate interpretation of step-drawdown test results for most practical purposes.

- 15) The shape of the specific drawdown versus discharge plot of data from a multi-rate pumping test of a well in fractured rock can indicate whether the primary water-producing fracture(s) is(are) horizontal or vertical. A curve which is curvilinear and concave upward beyond the critical discharge is strong evidence of non-linear flow in a horizontal fracture.
- 16) If the step-drawdown test is properly conducted so that a well defined linear flow segment is apparent, an estimate of the effective aperture of the fracture can be made using existing flow laws and assumed values for roughness and the radius of influence.
- 17) Simple reaming of wells obtaining water from relatively high yield horizontal fractures could be a cost-effective method of increasing their specific capacity. The numerical model predicts that increases in specific capacity on the order of 33 percent could be achieved by reaming from a radius of 0.102 m to 0.203 m (typical standard wellbore sizes). Since only the diameter of the wellbore at the intersection with the fracture is

important, select under-reaming at specific depths should be considered.

- 18) Hydraulic propping of existing fractures could be another method of stimulating well production. The numerical model suggests that increases on the order of 30 percent could be achieved by propping a fracture with an original uniform aperture of 0.500 mm by only 0.025 mm in the immediate vicinity of the wellbore. It should be noted that relatively improbable boundary conditions were imposed, however, in this numerical simulation; and that the quasi-three-dimensional, axisymmetric deformation code of DEFLOW is not well suited for synthesizing the mechanical response to hydraulic propping.

7.2 Recommendations for further study

It is believed that this study has contributed to the state of knowledge in fractured rock hydraulics from both a theoretical and a practical standpoint. It would be desirable, however, for it to have directly or indirectly identified areas for further research and to have provided encouragement for such study. A few areas for future consideration recommended by this investigator are:

Theoretical -

- 1) Additional generic research to develop laws for fluid flow in fractures, particularly for "closed" fractures in which a considerable portion of the fracture surfaces are in contact, should be conducted. Alternative methods to the classical friction factor versus Reynolds number approach such as that used by Sato et al. (1984) should be pursued.
- 2) The flow code of DEFLOW, the numerical model developed in this study, should be expanded to two dimensions so that it can include the effects of anisotropy.
- 3) A two-dimensional flow code should be coupled with a fully three-dimensional deformation code (as opposed to the quasi-three-dimensional, axisymmetric code used in this study). The resulting model would be able to simulate tangential displacements along vertical discontinuities in addition to the normal fracture displacement and rock matrix deformation modeled by DEFLOW. It is believed that such a model, which would show greater response to flow-induced closure and hydraulic propping, would be considerably more realistic.

Practical -

- 4) More field investigations similar to those conducted by Norris (1976), Williamson and Woolley (1980), and Caswell (1985a,b) should be conducted. However, such

future investigations should attempt to be both more quantitative and more deterministic by using the findings of Rissler (1978) and this study.

- 5) The polynomial expression describing the production drawdown response of a well should be incorporated into numerical models for dewatering and water supply well field design in order to quantify fully the cumulative effects of well losses. The model should be capable of predicting the technical and economic benefits of well stimulation procedures in order to assess the potential cost-effectiveness of such an operation.
- 6) The procedure of selective under-reaming should be investigated to determine whether or not it would be a technically feasible, cost-effective method of improving the production-drawdown response of wells in fractured rock.

REFERENCES

- Ahmed, U., 1982, Combined effects of wellbore damage, partial penetration and permeability stratification on well performance: Petroleum Society of CIM, Preprint Paper 82-33-01, 8 pp.
- Argall, G.O., Jr., and Brawner, C.O., editors, 1979, Mine drainage: Proceedings of 1st International Mine Drainage Symposium, Denver, Miller Freeman Publications, 848 pp.
- Bair, E.S., 1980, Estimating dewatering rates and designing deep-well dewatering systems for open-pit mines by use of numerical simulation: Soc. Mining Engrs. of AIME, Preprint 80-355, 16 pp.
- Baker, W.J., 1955, Flow in fissured formations in Proceedings of 4th World Petroleum Congress, Rome, Sec II/E, Paper 7, pp. 379-393.
- Bandis, S.C., Lumsden, A.C., and Barton, N.R., 1983, Fundamentals of rock joint deformation: Intern. Journ. Rock Mech. Min. Sci. & Geomech. Abstrs., vol. 20, no. 6, pp. 249-268.
- Barker, J.A., 1981, A formula for estimating fissure transmissivities from steady-state injection test data: Journal of Hydrology, vol. 52, no. 3/4, pp. 337-346.
- Basak, P., 1978, Analytical solutions for two-regime well flow problems: Journal of Hydrology, vol. 38, pp. 147-159.
- Bierschenk, W.H., 1964, Determining well efficiency by multiple step-drawdown tests: International Assoc. of Scientific Hydrology, Publication No. 64, pp. 493-507.
- Booton, M., 1984, Associate Professor, Faculty of Engineering and Applied Science, Memorial University, personal communication.
- Brereton, N.R., 1979, Step-drawdown pumping tests for the determination of aquifer and borehole characteristics: Water Research Centre (England), Technical Report TR103, 26 pp.
- Bruin, J., and Hudson, H.E., Jr., 1955, Selected methods for pumping test analysis: Illinois State Water Survey, Report of Investigation 25, pp. 29-37.

REFERENCES -- Continued

- Canadian Portland Cement Association, 1981, Design and control of concrete structures: Engineering Bulletin EB101.03T, 131 pp.
- Carlsson, A., and Olsson, T., 1983, Stress and water flow relation in fractured rock: Bulletin International Association of Engineering Geology, no. 26-27, pp. 371-375.
- Carpenter, T.L., and Young, R., 1980, Deep-well dewatering at Gibraltar Mines: CIM Bulletin, vol. 73, no. 816, pp. 63-68.
- Caswell, B., 1985a, Better yields from large diameter wells in crystalline rock: Water Well Journal, vol. 39, no. 4, pp. 34-36.
- _____, 1985b, Drilling a high yielding industrial well in granite: Water Well Journal, vol. 39, no. 1, pp. 40-41.
- Clark, L., 1977, Analysis and planning of step drawdown tests: Quart. Journ. Engr. Geol., vol. 10, pp. 125-143 (related discussion in Quart. Journ. Engr. Geol., vol. 12, p. 134).
- Coates, D.F., 1970, Rock mechanics principles: Mines Branch Monograph 874, Canadian Department of Energy, Mines and Resources, Ottawa.
- Cox, R.J., 1977, A study of near well groundwater flow and the implications in well design: New South Wales Univ. Water Research Laboratory Report No. 148, 187 pp.
- Da Cruz, P.T., and De Quadros, E.F., 1984, Analysis of water losses in basaltic rock units in Proceedings of 5th Congress of International Society for Rock Mechanics, Melbourne, pp. B119-B123.
- Doe, T., and Remer, J., 1980, Analysis of constant-head well tests in nonporous fractured rock in Proceedings of 3rd Invitational Well-Testing Symposium, Lawrence Berkeley Laboratory Report LBL-12076, pp. 84-89.
- Dudgeon, C.R., 1984, Director, Water Research Laboratory, University of New South Wales, personal communication while Visiting Professor at Memorial University.

REFERENCES -- Continued

- Dudgeon, C.R., Huyakorn, P.S., and Swan, W.H.C., 1973, Hydraulics of flow near wells in unconsolidated sediments: University of New South Wales Water Resources Laboratory Report No. 126, vol. 2, Field Studies, 98 pp.
- Dudgeon, C.R., and Au Yeung, C.N.; 1969, Non-Darcy flow in the vicinity of wells in Proceedings of Groundwater Symposium, University of New South Wales, Paper No. 2, pp. 13-27.
- Earlougher, R.C., 1977, Advances in well test analysis: Monograph Series, Vol. 5., Society of Petroleum Engineers of AIME, 264 pp.
- Eden, R.N., and Hazel, C.R., 1973, Computer and graphical analysis of variable discharge pumping tests of wells: Civil Engineering Transactions, Institute of Engineers (Australia), vol. CE 15, nos. 1-2, pp. 5-10.
- Francis, R.M., 1981, Hydrogeological properties of a fractured porous aquifer, Winter River Basin, Prince Edward Island: M.Sc. thesis, University of Waterloo, 154 pp.
- Frind, E.O., and Pinder, G.F., 1970, Galerkin solution of the inverse problem for aquifer transmissivity: Water Resources Research, vol. 9, pp. 1397-1410.
- Gale, J.E., Rouleau, A., and Atkinson, L.C., 1985, Hydraulic properties of fractures in Hydrogeology of Rocks of Low Permeability, Memoires of International Association of Hydrogeologist, Vol. XVII, Part 1, pp. 1-16.
- Gale, J.E., 1982a, Assessing the permeability characteristics of fractures in Recent Trends in Hydrogeology, Geol. Soc. America, Special Paper No. 189, pp. 163-181.
- _____, 1982b, The effects of fracture type (induced versus natural) on the stress-fracture closure-fracture permeability relationships in Issues in Rock Mechanics, Proceedings of the 23rd Symposium on Rock Mechanics, Berkeley, p. 290-298.
- _____, 1982c, Changes in fracture permeability as a function of sample size, fracture type, and stress history: Office of Nuclear Waste Isolation, Report No. ONWI/81/E515-04400-23, 80 pp.

REFERENCES -- Continued

- _____, 1982d, Fundamental hydraulic characteristics of fractures from field and laboratory investigators in Papers of the Groundwater in Fractured Rock Conference, Canberra, pp. 79-94.
- _____, 1977, A numerical, field, and laboratory study of flow in rocks with deformable fractures: Scientific Series No. 72, Inland Waters Directorate, Environment Canada, 145 pp. (published version of 1975 Ph.D. thesis, University of California, Berkeley).
- _____, 1975, Unpublished computer code: Department of Civil Engineering, University of California, Berkeley.
- Garg, S.P., and Lal, J., 1971, Rational design of well screens: Journ. Irrig. and Drain. Div., Proc. of ASCE, vol. 97, no. IRI, pp. 131-147.
- Goodman, R.E., 1980, Introduction to rock mechanics: John Wiley and Sons, 478 p.
- _____, 1976, Mechanical properties of discontinuities in Methods of Geological Engineering, West Publishing Company, Ch. 5, p. 158-208.
- Greenslade, W.M., and Condrat, G.W., 1979, Depressurization of a multi-layered artesian system for water and grout control during deep mine-shaft development: Journal of Hydrology, vol. 43, pp. 517-536.
- Gringarten, A.C., 1982, Flow-Test evaluation of fractured reservoirs in Recent Trends in Hydrogeology, Geological Society of America Special Paper 189, pp. 237-263.
- Guppy, K.H., Cinco-Ley, H., and Ramey, H.J., Jr., 1981, Effect of non-Darcy flow on the constant-pressure production of fractured wells: Journ. Soc. Petrol. Engr., vol. 21, no. 3, pp. 390-400.
- Hannoura, A.A., and Barends, F.B.J., 1981, Non-Darcy flow: a state of the art in Transport in Porous Media, Proc. of Euromech 143, Delft, pp. 37-51.
- Hargis, D.R., 1980, Application of a digital computer model to mine dewatering design: Preprint 80-354, SME-AIME Fall Mtg., Minneapolis, 11 pp.

REFERENCES -- Continued

- Holditch, S.A., and Morse, R.A., 1976, The effects of non-Darcy flow in the behavior of hydraulically fractured gas wells: Journ. Petrol. Tech., pp. 1169-1179.
- Hornbeck, R.W., 1975, Numerical Methods: Quantum Publishers, New York, 310 p.
- Huitt, J.L., 1956, Fluid flow in simulated fractures: Amer. Inst. of Chem. Engineers Journal, vol. 2, no. 2, pp. 259-263.
- Hurst, W., 1953, Establishment of the skin effect and its impediment to flow in a wellbore: Petroleum Engineering vol. 25, p. B-6.
- Huyakorn, P.S., and Dudgeon, C.R., 1976, Investigation of two-regime well flow: Journ. Hydraulics Div., Proc. of ASCE, vol. 102, no. HY9, pp. 1149-1165.
- _____, 1974, Finite element programs for analyzing flow towards wells, University of New South Wales, Water Resources Laboratory Report No. 135, 316 pp.
- Huyakorn, P.S., 1973, Finite element solution of two-regime flow towards wells, University of New South Wales, Water Resources Laboratory Report No. 137, 191 pp.
- Iwai, K., 1976, Fundamental studies of fluid flow through a single fracture: Ph.D. thesis, University of California, Berkeley, 208 pp.
- Jacob, C.E., 1947, Drawdown test to determine effective radius of artesian well: Transactions of ASCE, vol. 112, no. 2321, pp. 1047-1070.
- James, R., 1970, Factors controlling borehole performance: Geothermics, vol. 2, part 2, pp. 1502-1515.
- Jouanna, P. 1972, Effet des sollicitations mecaniques sur les ecoulement dans certains milieux fissures (Effect of mechanical loads on flow in particular fractured media), Docteur Es-Sciences Physiques these, L'Universite Paul Sabatier de Toulouse, France, 262 pp. (in French).
- Juykam-Wold, H.C., 1980, Dewatering of Ambrosia Lake mines: Soc. Mining Engrs. of AIME, Preprint 80-84, 10 pp.

REFERENCES -- Continued

- Kelley, J.E., Anderson, K.E., and Burnham, W.L., 1980, The cheat sheet: a new tool for the field evaluation of wells by step-testing: *Ground Water*, vol. 18, no. 3, pp. 294-298.
- Kovacs, G., 1981, Hydraulic conductivity and intrinsic permeability of fissured rocks in *Seepage Hydraulics*, Elsevier Scientific Publishing Company, Section 3.4, pp. 396-472.
- Labadie, J.W., and Helweg, O.J., 1975, Step-drawdown test analysis by computer: *Ground Water*, vol. 13, no. 5, pp. 438-450.
- Lanser, G., 1985, Regional Engineer, Layne-Western Company, Denver, Colorado, personal communication.
- Lennox, D.H., 1966, Analysis and application of step-drawdown tests: *Journ. Hydraulics Div., Proc. of ASCE*, vol. 92, no. HY6, pp. 25-48.
- Li, W.H., 1954, Interaction between well and aquifer: *Proceedings of ASCE*, vol. 80, Separate No. 578, 14 pp.
- Lomize, G.M., 1951, Water flow in jointed rock: Gosenergoizdat (in Russian; translation on Ch. 7, Flow of water in fractures of variable cross section and curvilinear outline, pp. 84-92, obtained through Lawrence Berkeley Laboratory).
- Louis, C., and Maini, T., 1970, Determination of in situ hydraulic properties in jointed rock in *Proceedings of 2nd Cong. Int. Soc. Rock Mechanics, Belgrade*, vol. 1, pp. 235-245.
- Louis, C., 1969, A study of groundwater flow in jointed rock and its influence on the stability of rock masses: *Rock Mechanics Research Report No. 10.*, Imperial College, London, 90 pp.
- McClure, C.R., Farrell, C.R., and Segol, G., 1985, Numerical analysis and implementation of a permanent dewatering system: *Bulletin Assoc. of Engineering Geologists*, vol. 22, no. 3, pp. 241-257.
- Mackie, C.D., 1983, Determination of non-linear formation losses in pumping wells in *Proceedings of International Conference on Groundwater and Man, Sydney*, pp. 199-210.

REFERENCES -- Continued

- _____, 1982, Multi-rate testing in fractured formations in Papers of the Groundwater in Fractured Rock Conference, Canberra, pp. 139-150.
- Maini, Y.N.T., Noorishad, J., and Sharp, J.C., 1972, Theoretical and field considerations on the determination of in situ hydraulic parameters in fractured rock in Symposium on Percolation through Fissured Rock, Stuttgart, pp. T1-E1 to T1-E8.
- Maini, Y.N.T., 1971, In situ hydraulic parameters in jointed rock - their measurement and interpretation: PhD thesis, Imperial College, London, 312 pp.
- Matthews, C.S., and Russell, D.G., 1967, Pressure buildup and flow tests in wells: Monograph Series, Vol. 1, Society of Petroleum Engineers of AIME, 167 pp.
- Mogg, J.L., 1969, Step drawdown test needs critical review: Ground Water, vol. 7, no. 1, pp. 28-34.
- _____, 1959, Effect of aquifer turbulence on well drawdown: Journ. Hydraulics Div., Proc. of ASCE, vol. 85, no. HY11, pp. 99-112.
- Murphy, H. and Pearce R., 1980, Pressure losses at the transition from radial flow within fractures to longitudinal flow within production wells: Los Alamos Scientific Laboratory, Report LA-8197-MS, 22 pp.
- Murphy, H.D., 1979, Flow near the outlet of a geothermal energy reservoir: Los Alamos Scientific Laboratory, Thesis LA-7906-T, 262 pp.
- Neuzil, C.E., and Tracy, J.V., 1981, Flow through fractures: Water Resources Research, vol. 17, no. 1, pp. 191-199.
- Noorishad, J., Witherspoon, P.A., and Brekke, T.L., 1971, A method for coupled stress and flow analysis of fractured rock masses: Department of Civil Engineering, University of California, Publication No. 71-6, 128 pp.
- Norris, S.E., 1976, Change in drawdown caused by enlarging a well in a dolomite aquifer: Ground Water, vol. 14, no. 4, pp. 191-193.

REFERENCES -- Continued

- Parrish, D.R., 1963, Fluid flow in rough fractures: Preprint SPE 5631, SPE Production Research Symposium, Norman, Oklahoma, 9 pp.
- Pearce, R., and Murphy, H., 1979, Roughness effects on flow in hydraulic fractures - survey of the literature: Unpublished report, Los Alamos Scientific Laboratory, 32 pp.
- Peterson, D.F., Jr., 1957, Hydraulics of wells: Transactions of ASCE, vol. 122, pp. 502-517.
- Peterson, J.S., Rohwer, C., and Albertson, M.L., 1955, Effect of well screens on flow into wells: Transactions of ASCE, vol. 120, no. 2755, pp. 563-607.
- Phipps, S.C., and Khalil, J.N., 1975, A method for determining the exponent value in a Forchheimer-type flow equation: Journal of Petroleum Technology, pp. 883-884.
- Pinder, G.F., and Gray, W.F., 1977, Finite element simulation in surface and subsurface hydrology: Academic Press, New York, 295 pp.
- Raghaven, R., 1977, Pressure behavior of wells intercepting fractures in Proceedings of 1st Invitational Well-Testing Symposium, Lawrence Berkeley Laboratory Report LBL-7027, pp. 117-160.
- Ramey, H.J., Jr., 1982, Well-loss function and the skin effect: a review in Recent Trends in Hydrology, Geol. Soc. America, Special Paper No. 189, pp. 265-271.
- Rayneau, C., 1972, Contribution a l'etude des ecoulements autour d'un forage en milieu fissure (Contribution to the study of flow around a borehole in a fractured medium); Docteur-Ingenieur these, Universite des Sciences et Techniques du Languedoc, Academie de Montpellier, France, 75 pp. (in French).
- Read, R.E., 1982, Estimation of drilling depth in fractured rock in Papers of the Groundwater in Fractured Rock Conference, Canberra, pp. 191-197.

REFERENCES -- Continued

- Reddish, D.J., and Smith, S.F., 1982, Underground measurement of fracture permeability of coal within a shaft pillar: International Journal of Mine Water, no. 3, pp. 13-22.
- Reilly, T.E., 1984, A Galerkin finite-element flow model to predict the transient response of a radially symmetric aquifer: U.S. Geological Survey Water-Supply Paper 2198, 33 pp.
- Rissler, P., 1978, Determination of the water permeability of jointed rock: vol. 5, Publications of the Institute for Foundation Engineering, Soil Mechanics, Rock Mechanics, and Water Ways Construction, RWTH Aachen (West Germany), 150 pp. (published version of Ph.D. thesis, Technische Hochschule Aachen).
- Rorabaugh, M.I., 1953, Graphical and theoretical analysis of step-drawdown test of artesian wells: Proceedings of ASCE, vol. 79, Separate No. 362, 23 pp.
- Sato, K., Watanabe, K., and Kotajimi, N., 1984, Fundamental study of flow resistance in rock fissures: Soils and Foundations, vol. 24, no. 1, pp. 1-8.
- Sauveplane, C., 1982, Skin-effect and well losses evaluation: a critical review of concepts and methods in Proceedings of 2nd National Hydrogeological Conference, Winnipeg, pp. 100-107.
- Schmidt, R.D., 1985, Fracture zone dewatering to control ground water inflow in underground coal mines: U.S. Bureau of Mines Report of Investigations RI8981, 84 pp.
- Schrauf, T.W., and Evans, D.D., 1983, Laboratory studies of gas flow through a single natural fracture (abstract): EOS, vol. 64, no. 45, p. 704.
- Sharp, J.C., and Maini, Y.N.T., 1972, Fundamental considerations on the hydraulic characteristics of joints in rocks in Symposium on Percolation through Fissured Rock, Stuttgart, pp. T1-F1 to T1-F15.
- Sharp, J.C., 1970, Fluid flow through fissured media: Ph.D. thesis, Imperial College, London, 181 pp.

REFERENCES -- Continued

- Snow, D.T., 1969, Anisotropic permeability of fractured media: Water Resources Research, vol. 5, no. 6; pp. 1273-1289.
- Stark, K.P., and Volker, R.E., 1969, Non-linear flow through porous media - some theoretical aspects: Research Bulletin No. 1, Dept. of Civil Engineering, James Cook University, Queensland.
- Stewart, G.W., 1978, Hydraulic fracturing of drilled water wells in crystalline rocks of New Hampshire: New Hampshire Dept. of Resources and Economic Development, 161 pp.
- Stoner, R.F., Milne, D.M., and Lund, P.J., 1979, Economic design of wells: Quart. Journ. Engr. Geol., vol. 12, pp. 63-78.
- Stubbins, J.B., and Munro, P., 1965, Open pit mine dewatering - Knob Lake: CIM Bulletin, vol. 58, no. 640, pp. 814-822.
- Sundaram, P.N., and Frink, D., 1983, Electrical analogy of hydraulic flow through rock fractures: Geotechnical Testing Journal, vol. 6, no. 1, pp. 3-9.
- Swan, G., 1983, Determination of stiffness and other joint properties from roughness measurements: Rock Mechanics and Rock Engineering, vol. 16, no. 1, pp. 19-38.
- Tharp, T.M., 1982, An enriched finite element for simulation of groundwater flow to a well or drain: Journal of Hydrology, vol. 55, pp. 237-245.
- Thorpe, R., Watkins, D.J., Ralph, W.E., Hsu, R., and Flexser, S., 1980, Strength and permeability tests on ultra-large Stripa granite core: Lawrence Berkeley Laboratory, Report LBL-11203, 48 pp.
- Tsang, Y.W., 1984, The effect of tortuosity on fluid flow through a single fracture: Water Resources Research, vol. 20, no. 9, pp. 1209-1215.
- Tsang, Y.W., and Witherspoon, P.A., 1983, The dependence of fracture mechanical and fluid flow properties on fracture roughness and sample size: Journal of Geophysical Research, vol. 88, no. B3, pp. 2359-2366.

REFERENCES -- Continued

- _____, 1981, Hydromechanical behavior of a deformable rock fracture subject to normal stress: Journal of Geophysical Research, vol. 86, no. B10, pp. 9287-9298.
- Uhl, V.W., Jr., Joshi, V.G., Alpheus, A., and Sharma, G.K., 1976, The application of step-drawdown pumping tests to water wells in consolidated rock aquifers: Indian Geohydrology, vol. 11, nos. 3-4, pp. 124-149.
- van Everdingen, A.F., 1953, The skin effect and its influences on the productive capacity of a well: Transactions (Petroleum) of AIME, vol. 198, pp. 171-176.
- van Golf-Racht, T.D., 1982, Fundamentals of fractured reservoir engineering: Elsevier Scientific Publishing Co., ch. 6, pp. 299-351.
- Vennard, J.K., and Street, R.L., 1976, Elementary fluid mechanics: John Wiley & Sons, 740 pp.
- Vogwill, R.I.J., 1976, Some practical aspects of open-pit mine dewatering at Pine Point: CIM Bulletin, vol. 69, no. 769, pp. 76-88.
- Wahler, W.A., and Associates, 1979, Dewatering active underground coal mines - technical aspects and cost effectiveness: U.S. Environmental Protection Agency, Report EPA-600/7-79-124, 123 pp.
- Wardlaw, C.N., 1976, Pore geometry of carbonate rocks as revealed by pore casts and capillary pressure: Bulletin of American Association of Petroleum Geologists, Vol. 60, pp. 245-257.
- Watkins, D.J., 1981, Acquisition and preparation of specimens of rock for large-scale testing: Geophysical Research Letters, vol. 8, no. 7, pp. 679-682.
- Wattenbarger, R.A., 1967, Effects of turbulence, wellbore damage, wellbore storage, and vertical fractures on gas well testing: PhD thesis, Stanford University.
- Whincup, P., and Domahidy, G., 1982a, The Agnew nickel project - groundwater supply in Papers of the Groundwater in Fractured Rock Conference, Canberra, pp. 251-260.

REFERENCES -- Continued

- _____, 1982b, the Agnew nickel project - No. 1 mine dewatering in Papers of the Groundwater in Fractured Rock Conference, Canberra, pp. 261-272.
- Williams, R.E., Winter, G.V., Bloomsburg, G.L., and Ralston, D.R., 1986, Mine hydrology: Society of Mining Engineers, 169 pp.
- Williamson, W.H., and Woolley, D.R., 1980, Hydraulic fracturing to improve the yield of bores in fractured rock: Australian Water Resources Council, Tech. Paper No. 55, 73 pp.
- Wilson, C.R., and Witherspoon, P.A., 1970, An investigation of laminar flow in fractured porous rocks: Dept. Civil Engr., Publ. No. 70-6, Univ. of California, Berkeley, 178 pp.
- Witherspoon, P.A., 1981, Effect of size on fluid movement in rock fractures: Geophysical Research Letters, vol. 8, no. 7, pp. 659-661.
- Witherspoon, P.A., Wang, J.S.Y., Iwai, K., and Gale, J.E., 1980, Validity of cubic law for fluid flow in a deformable rock fracture: Water Resources Research, vol. 16, no. 6, pp. 1016-1024.
- Wittke, W., 1973, General report on the symposium "Percolation through fissured Rock", Bulletin of the International Association of Engineering Geology, no. 7, pp. 3-28.
- Woolley, D.R., 1982, Depth-yield relationships of bores in fractured rocks in New South Wales in Papers of the Groundwater in Fractured Rock Conference, Canberra, pp. 283-292.
- Zienkiewicz, O.C., 1971, The finite element method in engineering science: McGraw-Hill, 521 pp.

APPENDIX A
SIMILITUDE BETWEEN CIRCULAR PIPES AND FRACTURES

Flow in closed conduits is usually characterized by the relative ratio of inertial (driving) to viscous (resisting) forces. This ratio is expressed by the Reynolds number, Re,

$$Re = \bar{v}D_c/\nu \quad (A1)$$

where

\bar{v} = the average fluid velocity,

D_c = a "characteristic length" of the conduit, and

ν = the kinematic viscosity of the fluid.

For flow in a circular pipe, the characteristic length is its diameter, D, so that

$$Re \text{ (pipe)} = \bar{v}D/\nu. \quad (A2)$$

The principles developed for flow in pipes can be related to flow in other non-circular conduits through the concept of hydraulic radius, R_h ,

$$R_h = A/p \quad (A3)$$

where

A = cross-sectional area of flow, and

p = wetted perimeter (i.e., the length of the boundary between the fluid and the wall of the conduit).

For a pipe of radius r , it can be shown (Figure A1) that

$$R_h \text{ (pipe)} = \frac{A}{p} = \frac{\pi r^2}{2\pi r} = \frac{r}{2} = \frac{D}{4} = \frac{D_h \text{ (pipe)}}{4} \quad (\text{A4})$$

In other words, the hydraulic diameter, D_h , of a pipe is four times its hydraulic radius (not simply two times as in the relationship between geometric radius and diameter). Substituting this value into Equation A2,

$$Re \text{ (pipe)} = \bar{v} \cdot 4R_h / \nu \quad (\text{A5})$$

is obtained. For a fracture, idealized as a rectangular conduit (Figure A1) of infinite lateral dimension (so that drag along lateral boundaries can be ignored), the hydraulic radius is equal to

$$R_h \text{ (fracture)} = \frac{A}{p} = \frac{w(2b)}{2w} = \frac{2b}{2} \quad (\text{A6})$$

where

w = arbitrary length normal to the direction of flow and transverse to the aperture, and

$2b$ = fracture aperture.

Therefore, the analogous hydraulic diameter of the fracture becomes

$$D_h \text{ (fracture)} = 4R_h = 4(2b)/2 = 2(2b) \quad (\text{A7})$$

Substituting Equation A7 into Equation A5,

$$Re \text{ (fracture)} = \frac{\bar{v}4R_h}{\nu} = \frac{\bar{v}D_h}{\nu} = \frac{\bar{v}2(2b)}{\nu} \quad (\text{A8})$$

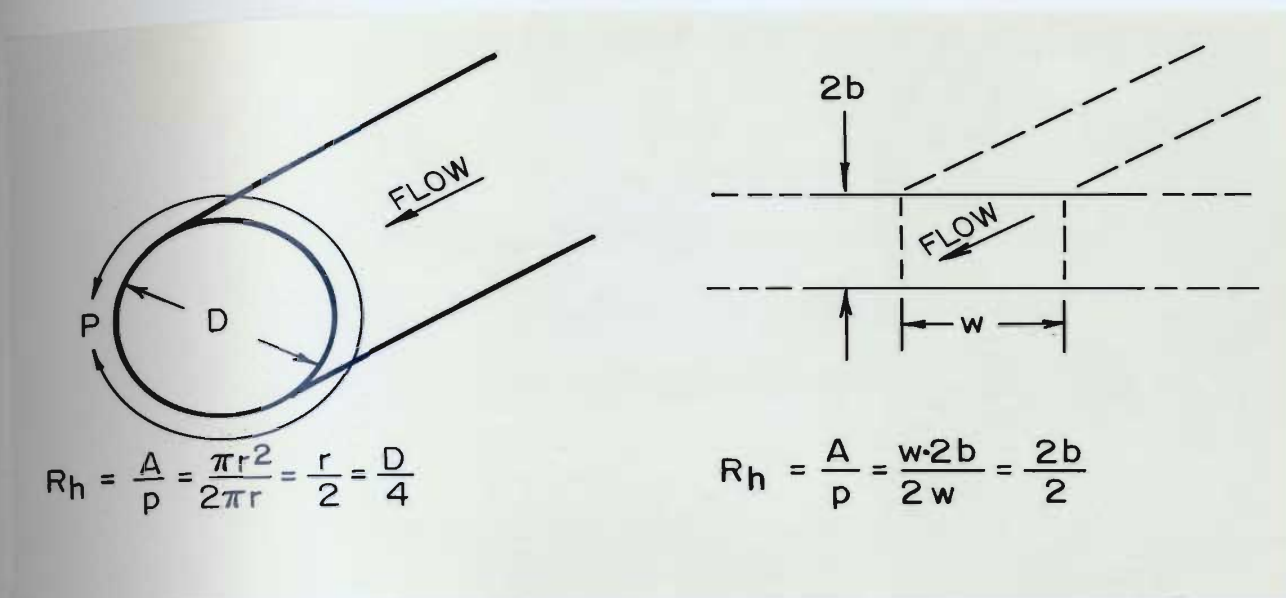


Figure A1 Geometric similitude between circular pipes and fractures

The same concept also is used to extend the Darcy-Weisbach relationship derived from experimental work on pipes to non-circular conduits. This relationship for pipes is written as

$$\frac{dH}{dl} = \lambda \frac{1}{D} \frac{\bar{v}^2}{2g} \quad (\text{A9})$$

where

H = total head,

l = length in direction of flow,

λ = friction factor, and

g = gravitational constant.

As in the main text of the thesis, the flow-related equations will be written in terms of total head instead of

hydraulic head. Generalizing Equation A9 in terms of the hydraulic radius,

$$\frac{dH}{dl} = \lambda \frac{1}{4R_h} \frac{\bar{v}^2}{2g} = \lambda \frac{1}{D_h} \frac{\bar{v}^2}{2g} \quad (\text{A10})$$

is obtained, so that for a fracture

$$\frac{dH}{dl} = \lambda \frac{1}{2(2b)} \frac{\bar{v}^2}{2g} \quad (\text{A11})$$

A Moody diagram is a logarithmic plot of friction factor versus Reynold's number with relative roughness as the parameter. For pipes, relative roughness is defined as:

$$k/D = k/D_h \quad (\text{A12})$$

where k is the "equivalent sand grain roughness". For a fracture, this term becomes

$$\frac{k}{D_h} = \frac{k}{2(2b)} \quad (\text{A13})$$

and is the analogous parameter in a Moody-type diagram for fractures.

It is very important to mention that the above definitions and derivations are not universal throughout the literature. The reader needs to give careful attention to notation used by a particular investigator or author. For example, Lomize (1951) uses $k/2b$ as the relative roughness parameter in his plots, and his empirical equations had to be converted in order to make direct comparison to those of Louis (1969) who uses the above convention. Many people in

fluid mechanics and hydraulics (e.g., Huitt, 1956) use the Fanning friction factor instead of the Darcy-Weisbach friction factor that is adhered to in this thesis. As indicated in the "Notation" section, the Darcy-Weisbach friction factor, λ , is equal to four times the Fanning friction factor.

APPENDIX B

METHODS TO ESTIMATE EFFECTIVE FRACTURE APERTURE
AND ROUGHNESS FROM PRESSURE PROFILES

One of the most important features of a plot of hydraulic gradient using data from a fracture flow test is that it can be used to estimate effective fracture aperture and roughness. The method used depends on whether the data points in the calculation are from the laminar or fully turbulent region of flow.

B.1 Linear flow

Any measuring points which are within the linear flow region should fall on an approximately straight line on a ΔH versus $\log r$ graph. In Equation 2.7 (page 50), it was shown that

$$H_2 - H_1 = \frac{Q}{2\pi K(2b)} \ln \frac{r_2}{r_1} = \frac{Q}{2\pi T} \ln \frac{r_2}{r_1} \quad (B1)$$

where

H = total potential or head,

Q = volumetric discharge rate,

K = hydraulic conductivity,

T = transmissivity, and

r = radial distance.

By substituting the value of K for laminar flow according to either Lomize (1951) or Louis (1969) from Table 1.1 (page 30) and re-arranging, it can be shown that

$$2b = \left(\frac{6Qv \ln(r_2/r_1) \{1 + \psi [k / (2 \cdot 2b)]^{1.5}\}}{\pi g (H_2 - H_1)} \right)^{1/3} \quad (B2)$$

where

v = kinematic viscosity,

ψ = empirical coefficient

($\psi = 8.8$ after Louis, 1969,

$\psi = 17$ after Lomize, 1961),

$2b$ = fracture aperture,

k = absolute roughness, and

g = gravitational constant:

By factoring out the "non-Poiseuille" term, this can be written as

$$2b = f \left(\frac{6Qv \ln(r_2/r_1)}{\pi g (H_2 - H_1)} \right)^{1/3} \quad (B3)$$

The variable f in Equation B3 can have two slightly different, but importantly different, interpretations. Both Louis (1969) and Lomize (1951) used the traditional friction factor-Reynolds number method of analysis. By conducting their tests on fractures of measurable aperture and absolute roughness, they were able to include an empirical factor (explicitly shown in Equation B2) which incorporated these parameters to describe the deviation from results predicted theoretically by Poiseuille's law. The factor f in Equa-

tion B3 is simply that factor taken outside the cubic root operand in order to simplify a quantitative understanding of its effect on the ideal parallel plate relationship. Table B1 indicates the value of this factor for a representative number of roughness values.

Table B1 Values of roughness factors for linear flow

| $k/(2 \cdot 2b)$ | f after Louis, 1969 | f after Lomize, 1951 |
|------------------|------------------------|-------------------------|
| .033 | 1.017 | 1.033 |
| .050 | 1.032 | 1.060 |
| .100 | 1.085 | 1.154 |
| .200 | 1.214 | 1.361 |
| .300 | 1.347 | 1.560 |
| .400 | 1.478 | 1.744 |
| .500 | 1.602 | 1.914 |

Rissler (1978) states that if injection tests are conducted such that the critical head (i.e., the injection head at which turbulent flow commences in the fracture just at the radius of the wellbore) can be determined precisely, the aperture can be estimated to within 8 percent by completely neglecting the effects of roughness. Table B1 suggests that the error would be more on the order of 50 to 80 percent. It should be stated, however, that in either case, a questionable amount of accuracy is being put on values based on empirically derived flow laws.

Witherspoon et al. (1980), on the other hand, analyzed results from tests in which they could not directly measure the geometric properties of the fracture. Re-evaluating Iwai's (1976) original data, they first demonstrated the validity of the cubic exponent in a generalized head loss versus flow rate relationship. It should be noted that they were testing relatively small fractures under axial loads that intuitively would have had a significant portion of their total area in contact. Then, by assuming the validity of the cubic law, they used multiple regression to determine an "effective aperture" (assuming smooth parallel walls) and a "fracture surface characteristic factor" that gave the best fit to their data. Values of f derived by this technique ranged from 1.04 to 1.65, obviously within the range based on the more deterministic approach of Louis and Lomize. No mention was made by Witherspoon et al. (1980), however, of what physical relationship their f values had to the actual geometric characteristics of the fracture.

Using the flow law derived by Sato et al. (1984), an alternative expression for estimating fracture aperture under laminar flow conditions can also be derived:

$$2b = \left(\frac{6Qv \ln(r_2/r_1) [1 + 2.15(2b)^{0.206}]}{\pi g (H_2 - H_1)} \right)^{1/3} \quad (B4)$$

Equation B3 with f usually assumed to be equal to 1 (i.e., using Poiseuille's law) is used the most frequently

for interpreting laboratory and field tests in fractured rock. In laboratory tests, usually only two pressures are known: H_o at the outer boundary, r_o , and H_w at the radius of the wellbore, r_w . In field applications, which rarely involve data from observation wells, it is normally necessary to assume a value for r_o . Because of the logarithmic relationship, however, the solution is not very sensitive to this parameter, and a "reasonable" value of 100 m is often used.

As demonstrated by numerous investigators (e.g., Maini, 1970; Rissler, 1978) it is extremely important, both when conducting pressure tests and in their interpretation, to ensure that the pressure values used for estimating aperture are taken under laminar flow conditions. By inadvertently including non-linear head loss in the calculation, the aperture will be significantly underestimated. Compounding this error could be an underestimation from neglecting the effects of roughness.

In each of the above equations for laminar flow through a fracture, the right hand side contains the unknown. Therefore, solution for the aperture value must be done iteratively. An initial estimate of the aperture has to be made, and the expression is solved for an updated estimate of $2b$. This is continued until convergence is achieved, usually after 3 to 5 iterations.

Programs were written in HP BASIC (for use on the HP 85 micro-computer) to perform the iterative calculations needed to solve Equations B2 and B4. Listings of the programs, LOUIS and SATO, are given at the end of this appendix.

B.2 Fully turbulent flow

A similar graphical and algebraic technique can be used if any head measuring points are within the fully turbulent flow regime. Starting with the Darcy equation (Equation 1.2, page 3)

$$\frac{dH}{dr} = \alpha v = \frac{1}{K} v^2, \quad (B5)$$

where

α = coefficient of hydraulic resistance,

K = hydraulic conductivity, and

v = macroscopic velocity of fluid,

squaring both sides of the equation, and separating the $(dH/dr)^2$ term,

$$\frac{dH}{dr} = \frac{1}{K^2 (dH/dr)^2} v^2 \quad (B6)$$

is obtained. Equation B6 is the same as Equation 1.6 (page 4) assuming the value of the exponent m in the latter is 2.

Substituting a value for K from Table 1.1 (page 30) according to either Louis (1969), Lomize (1951), or Nikuradse, it can be shown that

$$\beta = \frac{1}{K^2 (dH/dr)} \quad (B7)$$

or

$$\beta = \frac{1}{4c^2 g(2b) [\log \{d/[k/(2 \cdot 2b)]\}]^2 \frac{dH}{dr}} \quad (B8)$$

where

β = coefficient of hydraulic resistance, and
c, d = empirical coefficients.

By substituting β and 2b (for the aquifer thickness) into Equation 1.9 (page 4),

$$H_2 - H_1 = \frac{\beta Q^2}{[2\pi(2b)]^2} \left[\frac{1}{r_1} - \frac{1}{r_2} \right] \quad (B9)$$

and by re-arranging, 2b can be determined from

$$2b = \left(\frac{Q^2 (r_2 - r_1)}{16c^2 \pi^2 g r_1 r_2 (H_2 - H_1) [\log \{d/[k/(2 \cdot 2b)]\}]^2} \right)^{1/3} \quad (B10)$$

where c and d are defined in Table 1.1 (page 30).

Analogous to the procedure used for laminar flow, the terms containing the roughness-related parameters c and d can be factored out of Equation B10 such that

$$2b = f' \left(\frac{Q^2(r_2 - r_1)}{16\pi^2 g r_1 r_2 (H_2 - H_1)} \right)^{1/3} \quad (\text{B11})$$

where f' is the roughness factor for fully turbulent flow. In the case of linear flow, the effects of roughness are referred to completely smooth (i.e., $[k/(2 \cdot 2b)] = 0$) conditions for which f (see Equations B2 and B3) reduces simply to 1. For fully turbulent flow, however, the friction factor is dependent on relative roughness in all parts of the flow field (Figure 1.5, page 31). Therefore, the relative effects of roughness on flow in rough fractures (i.e., $[k/(2 \cdot 2b)] > 0.033$) must be referenced to the friction factor for flow according to the law of Nikuradse as given by

$$f'_N = \frac{1}{\left(4[\log\{3.7[k/(2 \cdot 2b)]\}]^2 \right)^{1/3}} \quad (\text{B12})$$

The value of f' for relative roughnesses greater than 0.033, thus, is given by

$$f' = \frac{f'_L}{f'_N} \quad (\text{B13})$$

where f'_L , the roughness factor for fully turbulent flow according to Louis (1969) or Lomize (1951), is given by

$$f'_L = \frac{1}{\left(c^2 [\log\{d/[k(2 \cdot 2b)]\}]^2 \right)^{1/3}} \quad (\text{B14})$$

Using the values of c and d from Table 1.1 (page 30), the following table of values of f' can be generated.

Table B2 Values of roughness factors for fully turbulent flow

| $k/(2 \cdot 2b)$ | f' N | f' after Louis, 1969 | f' after Lomize, 1951 |
|------------------|-----------|---------------------------|----------------------------|
| .033 | .390 | 1.108 | 1.015 |
| .050 | .415 | 1.119 | 1.034 |
| .100 | .467 | 1.145 | 1.081 |
| .200 | .538 | 1.189 | 1.163 |
| .300 | .594 | 1.229 | 1.245 |
| .400 | .645 | 1.267 | 1.334 |
| .500 | .692 | 1.309 | 1.439 |

It is evident from Equation B9 that use of this equation implies a linear relationship between ΔH and the inverse of radial distance. Therefore, to determine if any of the measuring points are in fact in the fully turbulent flow field and suitable for analysis by this technique, the data must first be plotted on an arithmetic plot of ΔH versus $1/r$. Only points which fall on a reasonably straight line should be used for the calculation. Since $2b$ also appears on the right hand side of Equation B10, the solution, as with linear flow, must be obtained iteratively. The program LOUIS, whose listing is included at the end of this appendix, also includes the iterative solution for Equation B10.

B.3 Dimensions and units

The user of this appendix is cautioned to check the units of his/her input before making any calculations. Any set of dimensionally consistent units is permissible, but the units in Table B3 are recommended to eliminate the necessity for additional conversion factors in the equations. Although not specifically stated by Sato et al. (1984), dimensional analysis of Equation B4 indicates that the coefficient 2.15 must have the dimensions $[L^{-0.206}]$.

Table B3 Recommended units for calculation of aperture

| <u>Parameter</u> | <u>Dimension</u> | <u>SI Unit</u> |
|------------------|------------------|----------------|
| Q | $[L^3/T]$ | m^3/s |
| r_1, r_2 | $[L]$ | m |
| H_1, H_2 | $[L]$ | m |
| k | $[L]$ | m |
| 2b | $[L]$ | m |
| g | $[L/T^2]$ | m/s^2 |
| v | $[L^2/T]$ | m^2/s |

B.4 Listing of program LOUIS

```

10 REM Program to estimate 2b
20 REM using Louis formulae
30 OPTION BASE 1
40 DIM V(11)
50 FOR I=1 TO 11
60 READ V(I)
70 NEXT I
80 DATA .9799,.9569,.9348,.9136
      .893,.8733,.8543,.8358,.818
      1,.801,.7845
90 DISP "Q", @ INPUT Q
100 Q=Q/1000
110 DISP "R2"; @ INPUT R2
120 DISP "R1"; @ INPUT R1
130 DISP "H2"; @ INPUT H2
140 DISP "H1"; @ INPUT H1
150 DISP "LAM OR TURB"
160 INPUT L$
170 IF L$="L" THEN 370
180 K=.1
190 N=1
200 DISP "INITIAL GUESS FOR 2b"
210 INPUT B
220 IF K<B THEN 240
230 K=B
240 B=Q^2*(R2-R1)/(6194*(R1*R2)*
      (H2-H1)*LGT(1.9/(K/(2*B)))^2
      )
250 B=B^(1/3)*1000
260 DISP USING 270 ; K
270 IMAGE "K = " D.DDD
280 DISP USING 290 ; B
290 IMAGE "B = " D.DDD
300 DISP "ANOTHER ITERATION?"
310 INPUT Y$
320 IF Y$="Y" THEN 220
330 ON N GOTO 340,640
340 N=2
350 K=.24
360 GOTO 200
370 DISP "TEMP";@ INPUT T
380 GOSUB 560
390 K=.1
400 N=1
410 DISP "INITIAL GUESS OF 2b"
420 INPUT B
430 F=1+8.8*(K/(2*B))^1.5
440 B=Q*.19475*F*LOG(R2/R1)*V1/(
      H2-H1)
450 B=B (1/3)*1000
460 DISP
470 DISP using 480 ; B
480 IMAGE DD.DDD
490 DISP "ANOTHER ITERATION"
500 INPUT Y$
510 IF Y$="Y" THEN 430
520 ON N GOTO 530,640
530 N=2
540 K=.24
550 GOTO 410
560 REM Subroutine to assign
570 REM value of viscosity
580 REM for given temperature
590 T=T-20
600 X=IP(T)
610 Y=FP(T)
620 V1=(V(X)-Y*(V(X)-V(X+1)))*.0
      00001
630 RETURN
640 END

```

B.5 Listing of program SATO

```

10 REM Program to estimate 2b
20 REM using Sato formula
30 OPTION BASE 1
40 DIM V(11)
50 FOR I=1 TO 11
60 READ V(I)
70 NEXT I
80 DATA .9799,.9569,.9348,.9136
      ,.893,.8733,.8543,.8343,.818
      1,.801,.7845
90 DISP "Q", @ INPUT Q
100 DISP "R2", @ INPUT R2
110 DISP "R1", @ INPUT R1
120 DISP "H2", @ INPUT H2
130 DISP "H1", @ INPUT H1
140 DISP "TEMP", @ INPUT T
150 GOSUB 300
160 DISP "INITIAL GUESS OF 2b"
170 INPUT B
180 B=Q/1000*.19475*LOG(R2/R1)*V
      1*(1+2.15*(B/1000)^.206)/(H2
      -H1)
190 B=B^.333333333333*1000
200 DISP
210 DISP USING 220 ; B
220 IMAGE DD.DDD
230 DISP "ANOTHER ITERATION"
240 INPUT Y$
250 IF Y$="Y" THEN 180
260 GOTO 350
270 REM Subroutine to assign
280 REM value of viscosity
290 REM for given temperature
300 T=T-20
310 X=IP(T)
320 Y=FP(T)
330 V1=(V(X)-Y*(V(X))-V(X+1))*0.
      00001
340 RETURN
350 END

```

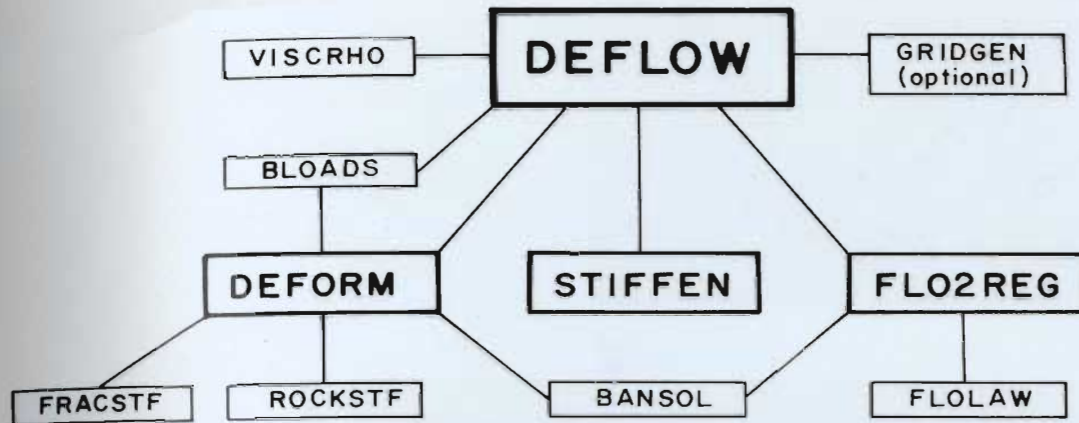
APPENDIX C
DESCRIPTION OF NUMERICAL MODEL

A numerical model using the finite element method was developed for this study to simulate the deformation-flow relationship in a number of deformable, horizontal fractures in the vicinity of a pumping well. The program, called DEFLOW, consists of two principal codes:

- 1) an original flow code which calculates the distribution of total head and pressure head in the fracture(s) under the assumption that their apertures, initially specified and subsequently modified by the deformation code, are fixed at a given node, and
- 2) a deformation code based in part on earlier work by Noorishad et al. (1971) and Gale (1975) that, using the fluid pressures determined by the flow code for boundary conditions, calculates the changes in aperture due to changes in effective stress.

The two codes are linked through the pressure head term and must be solved interactively. A flow chart describing the coupled, iterative method of solution is shown in Figure 2.5 (pages 78 and 79).

The routines comprising DEFLOW are summarized in Figure C1, and a few of the more important operations will be described in more detail below. A brief user's guide is also included, followed by a complete listing of the program.



| <u>Routine</u> | <u>Function(s)</u> |
|----------------|---|
| BANSOL | Solves both flow and stiffness matrix equations (which have banded, symmetric coefficient matrices) by Gaussian elimination and backward substitution. |
| BLOADS | Calculates point loads on fracture node pairs and wellbore nodes due to fluid pressures. |
| DEFLOW | Program driver. Does all reading of input and all printing of output. |
| DEFORM | Calculates radial and vertical displacements of all nodes under given boundary and gravity forces. |
| FLOLAW | Assigns hydraulic conductivity (derived from flow laws of Louis, 1969) to each flow node according to relative roughness and Reynolds number. |
| FLO2REG | Calculates radial distance-total head distribution in rigid fracture under linear and non-linear flow conditions. |
| FRACSTF | Calculates normal and shear stiffness of fracture node pairs. |
| GRIDGEN | Optional routine when only 1 fracture. Generates finite element grid complete with nodal coordinates, fracture/flow node pairs, element incidences, and boundary condition codes. |
| ROCKSTF | Calculates stiffness and gravity forces of axis-symmetric rock elements (after Gale, 1975). |
| STIFFEN | Assigns new stiffnesses to fracture node pairs as fracture undergoes displacement. |
| VISCHRO | Assigns values of kinematic viscosity and density of water for given temperature. |

Figure C1 Routines in program DEFLOW

C.1 Finite element discretization

As described in Section 2.2.1 (page 58) and in the following section, a simple, yet most effective way of discretizing the flow nodes is to assign them logarithmically increasing radial distances from the wellbore radius, r_w , to the outer boundary r_o . Then, in order to incorporate maximum sensitivity to changes in effective stress and as an essential part of the linking concept, it is important to have a direct 1-to-1 correspondence between the flow nodes and fracture node pairs of the deformation code.

For the case with one fracture, DEFLOW has a built-in grid generator, subroutine GRIDGEN, which assigns nodal coordinates, fracture/flow node pairs, element incidences, and boundary condition codes under the above considerations. An example of a mesh created by GRIDGEN, the one used to simulate the laboratory model, is shown in Figure C2. Because axisymmetric elements are used and radial isotropy is assumed, only one half of the cross-section needs to be defined.

Figure C2(A) shows the laboratory model and the location of nodes used in the numerical model at true scale. This discretization avoids extreme aspect ratios (the ratio of length to width) in the structural elements without

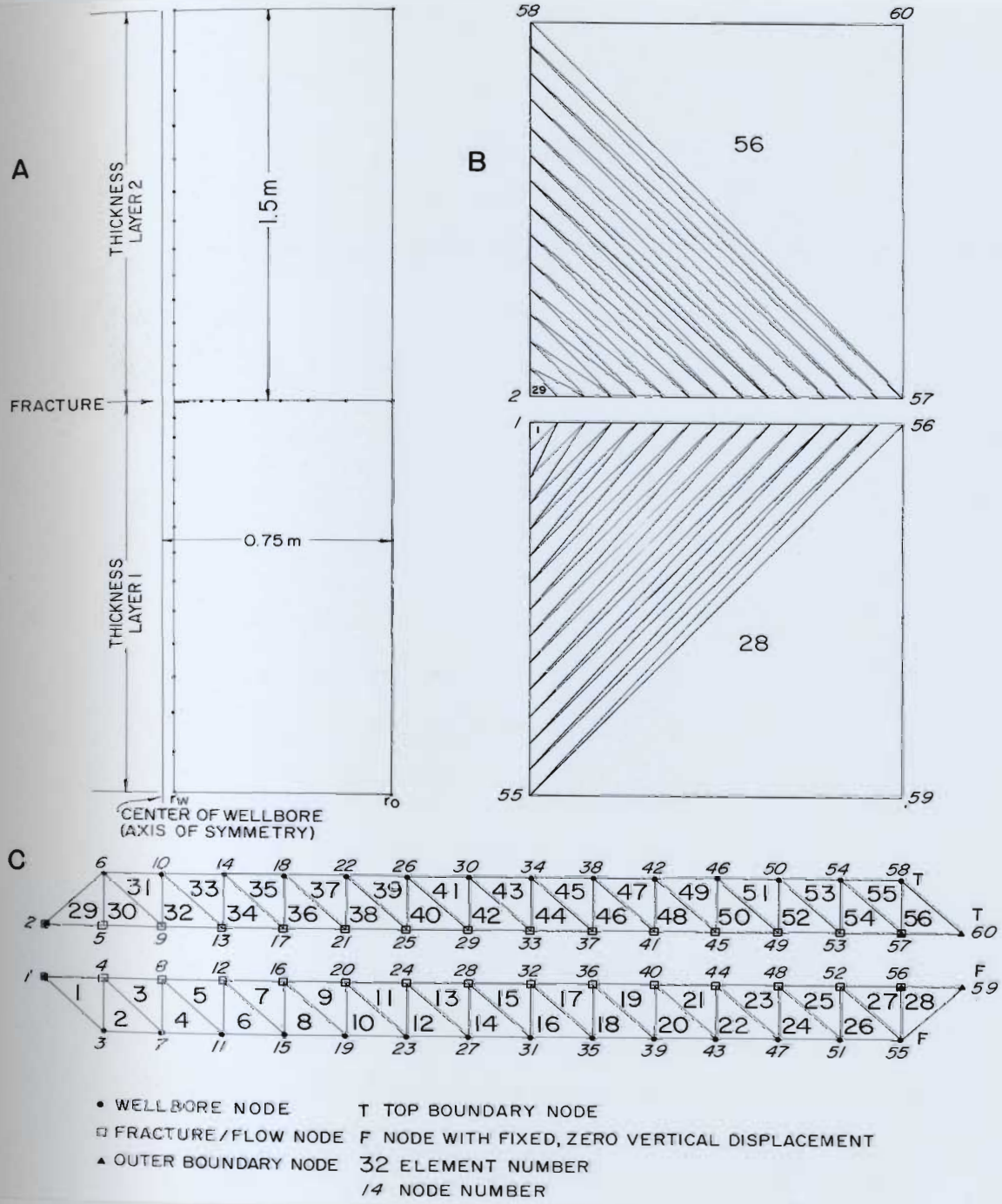


Figure C2

Finite element discretization generated by GRID-GEN for simulating laboratory model. A) Cross-section (one half only), to scale, showing nodal points. B) "Log-log" diagram indicating even logarithmic spacing of fracture/flow nodes and boundaries of triangular axisymmetric elements. C) Schematic diagram or "map" of grid indicating numbering scheme for nodes and elements and boundary conditions at various nodes.

needing to change scale frequently in the node generating code. In Figure C2(B), the same nodal arrangement is depicted on a "log-log" scale, and the diagram also includes the outlines of the triangular axisymmetric elements. Finally, Figure C2(C) provides a schematic "map" of the finite element grid showing the numbering scheme for the nodes and elements (selected in order to minimize the bandwidth of the stiffness matrix) and the boundary conditions at the various nodes.

The discretization assigned by GRIDGEN is based on the relative thickness of the rock layers compared to the radial distance to the outer boundary, r_0 . An example of another grid where r_0 is much greater than the thickness of either the top or bottom rock unit (typical of a field situation) is shown in Figure C3. Note that beyond a radial distance greater than the thickness of the rock layer, the pattern changes from that of Figure C2. The 3-triangle groupings (elements b-c-d and j-k-l) are examples of the "tri-clusters" referred to in subroutine GRIDGEN.

Figure C4 shows the discretization used for a problem with 3 fractures. Although this grid was hand-generated, it follows the same general scheme used by GRIDGEN.

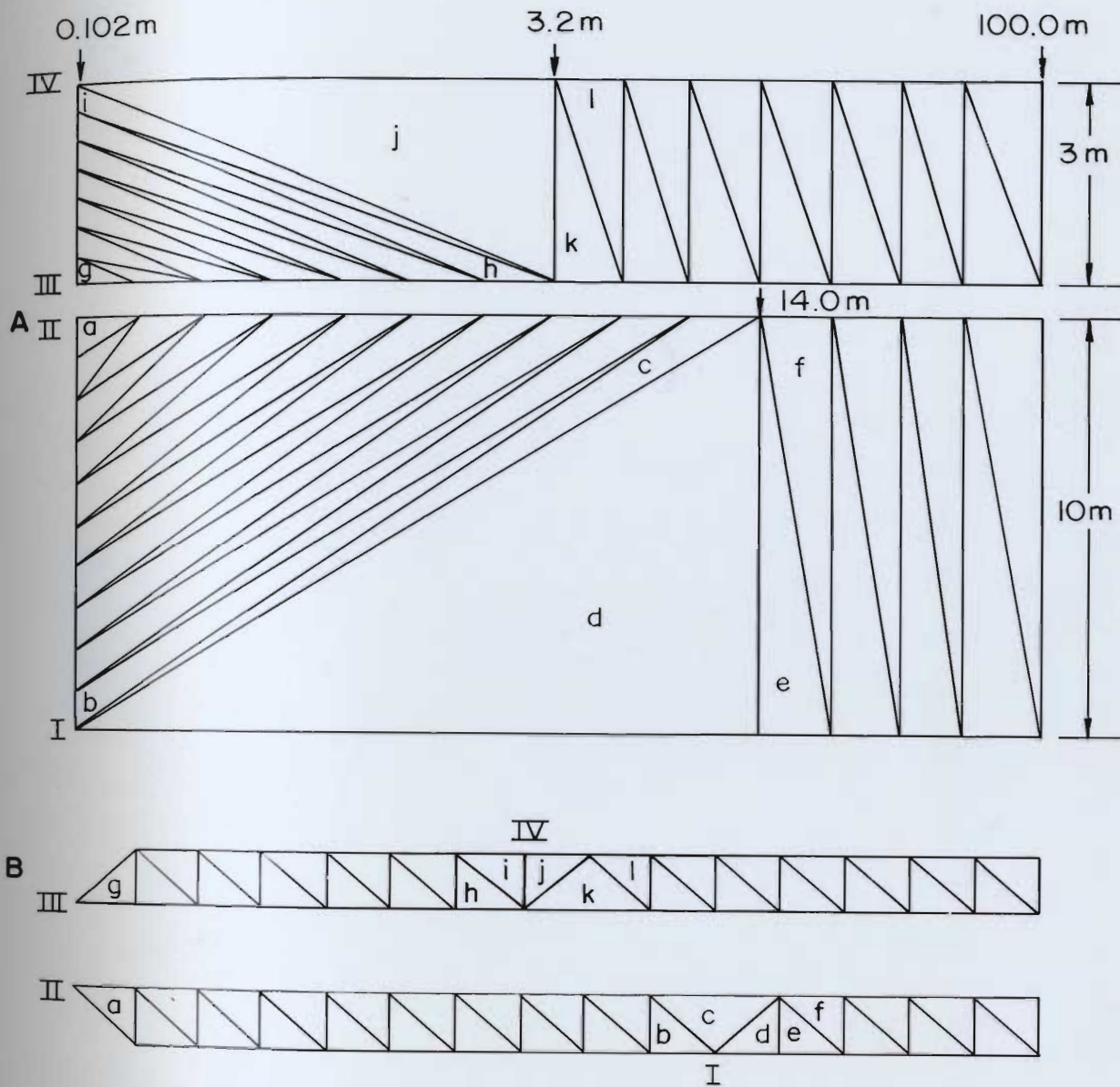


Figure C3 Finite element discretization generated by GRID-GEN for simulating hypothetical field problem with 1 fracture. A) "Log-log" diagram (one half only) showing boundaries of triangular axisymmetric elements. Note change in pattern beyond radial distance greater than thickness of rock layer. B) Schematic diagram or "map" of grid (see Figure C2 for comparison). Reference nodes (lower case letters) and elements (Roman numerals) are shown.

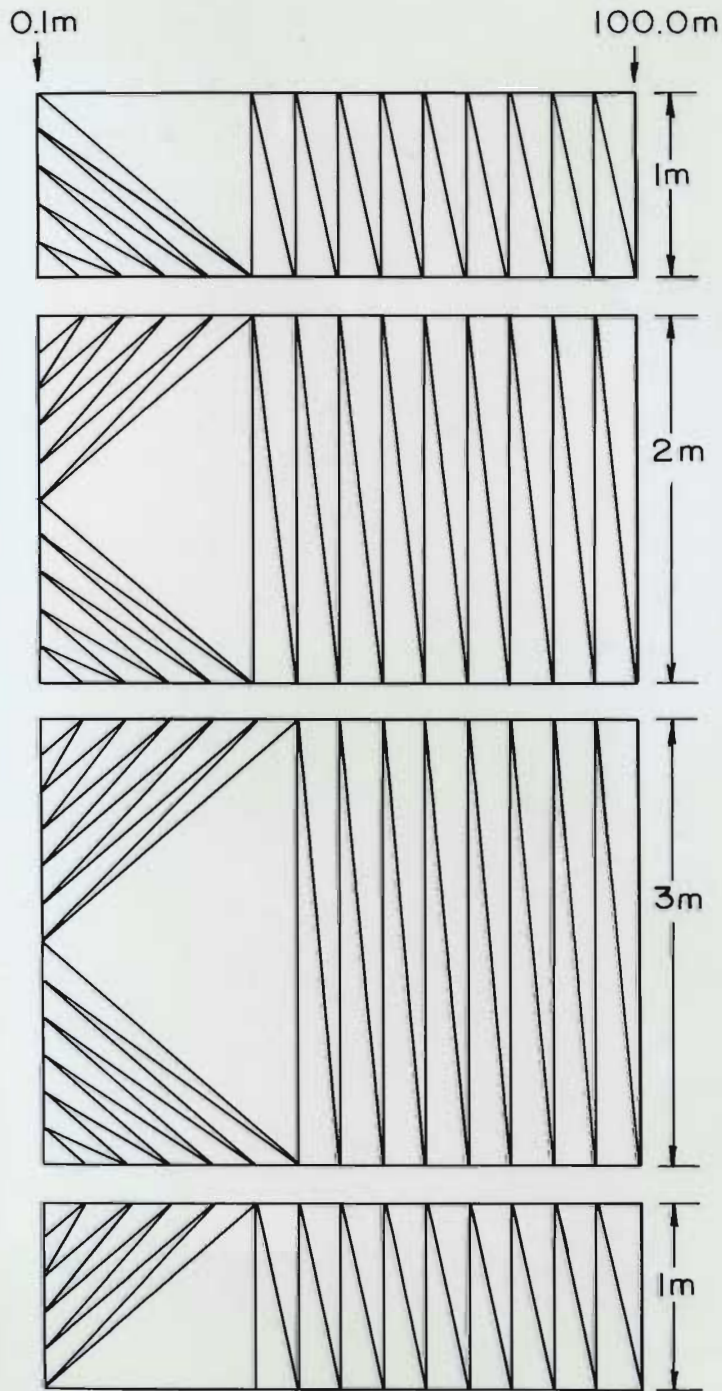


Figure C4 Finite element discretization (manually generated) for simulating hypothetical field problem with 3 fractures. "Log-log" diagram (one half only) shows dimensions of the 4 rock units.

C.2 Description of flow code

The flow code, comprising the routines DEFLOW, VISCRHO, FLO2REG, FLOLAW, and BANSOL, simulates steady-state, two-regime (i.e., both linear and non-linear), radial flow to a well through a rough, rigid, horizontal fracture of non-uniform aperture (uniformity simply being a special case). In this code, the rock matrix is assumed to be impermeable, so that all flow and, consequently, all aquifer head loss, is through the fracture(s) alone. Using the flow field boundaries shown in Table 2.1 (page 54) and Figure 1.6 (page 32), subroutine FLOLAW assigns to each node an appropriate value of hydraulic conductivity derived from the fracture flow laws of Louis (1969). The manner in which the Reynolds numbers are estimated is described in a later part of this section.

The Galerkin formulation of the two-regime, radial flow equation was described briefly in Section 2.2.3 (page 61). The two linear basis functions used for each 2-node flow element, are

$$\omega_1 = 1 - r'/L \quad (C1)$$

and

$$\omega_2 = r'/L \quad (C2)$$

where

$\omega_1, \omega_2 =$ basis functions,

$$r' = \ln (r/r_1),$$

$$L = \ln (r_2/r_1),$$

$r =$ radial coordinate of point along element, and

$r_1, r_2 =$ coordinates of nodes.

It should be noted that since the nodes are spaced at logarithmically increasing radial distances, L will be the same for all elements. Differentiating Equations C1 and C2 with respect to r' ,

$$\frac{d\omega_1}{dr'} = -\frac{1}{L} \quad (C3)$$

and

$$\frac{d\omega_2}{dr'} = \frac{1}{L} \quad (C4)$$

are obtained. Since there are two nodes in each element, there are four combinations or permutations of the differential terms inside the integrals shown in Equation 2.39 (page 63). For the first element (nodes 1 and 2) and with $i = 1$ and $j = 1$,

$$\int_{r_1}^{r_2} \bar{T}_{1,2} \frac{d\omega_1}{dr'} \frac{d\omega_1}{dr'} dr' = \int_{r_1}^{r_2} \bar{T}_{1,2} \left(-\frac{1}{L}\right) \left(-\frac{1}{L}\right) dr' = \int_{r_1}^{r_2} \bar{T}_{1,2} \frac{1}{L^2} dr'$$

$$= \bar{T}_{1,2} \frac{1}{L^2} r' \Big|_{r'_1}^{r'_2} = \bar{T}_{1,2} \frac{1}{L^2} L = \frac{\bar{T}_{1,2}}{L} \quad (C5)$$

where

$$\bar{T}_{1,2} = 2\pi \left(\frac{T_1 + T_2}{2} \right).$$

A similar derivation for $i = 1$ and $j = 2$ yields

$$\bar{T}_{1,2} \frac{d\omega_1}{dr'} \frac{d\omega_2}{dr'} dr' = - \frac{\bar{T}_{1,2}}{L}. \quad (C6)$$

After obtaining the other two terms by symmetry, it can be shown that the total contribution from the first element to the integrals in Equation 2.39 (page 63) is

$$\frac{1}{L} \begin{bmatrix} \bar{T}_{1,2} & -\bar{T}_{1,2} \\ -\bar{T}_{1,2} & \bar{T}_{1,2} \end{bmatrix}. \quad (C7)$$

The global matrix for the entire region R is assembled element by element, partitioning off any contributions from a node with a fixed head value. For the case in which a first type boundary condition (i.e., head) is specified at the well, the global matrix for N nodes becomes

$$\begin{array}{c}
 \text{NODE} \rightarrow \\
 \begin{array}{cccccc}
 N & 1 & 2 & 3 & \dots & N-1 \\
 \downarrow & & & & & \\
 N & \bar{T}_{N-1,N} & 0 & 0 & \dots & -\bar{T}_{N-1,N} \\
 1 & 0 & \bar{T}_{1,2} & -\bar{T}_{1,2} & \dots & 0 \\
 2 & \left\{ \begin{array}{l} 1 \\ - \\ L \end{array} \right\} & 0 & -\bar{T}_{1,2} & \bar{T}_{1,2} + -\bar{T}_{2,3} & -\bar{T}_{2,3} & \dots & 0 \\
 3 & 0 & 0 & -\bar{T}_{2,3} & \bar{T}_{2,3} + \bar{T}_{3,4} & \dots & 0 \\
 \vdots & \vdots & \vdots & \vdots & \vdots & \vdots & \vdots & \vdots \\
 N-1 & -\bar{T}_{N-1,N} & 0 & 0 & 0 & \bar{T}_{N-2,N-1} & \dots & \bar{T}_{N-1,N}
 \end{array}
 \end{array} \quad (C8)$$

The partitioning also must be done to the other two terms of the flow equation (Equation 2.41, page 63), and the partitioned version of the flow equation can be written as

$$\begin{bmatrix} T_{cc} & T_{cf} \\ T_{fc} & T_{ff} \end{bmatrix} \begin{Bmatrix} H_c \\ H_f \end{Bmatrix} = \begin{Bmatrix} Q_c \\ Q_f \end{Bmatrix} \quad (C9)$$

where the subscripts f and c refer to free and constrained, respectively. Writing Equation C9 as two separate matrix equations

$$[T_{cc}] \{H_c\} + [T_{cf}] \{H_f\} = \{Q_c\} \quad (C10)$$

and

$$[T_{fc}] \{H_c\} + [T_{ff}] \{H_f\} = \{Q_f\} \quad (C11)$$

are obtained. In order to obtain the unknown head values, it is necessary only to solve the second equation, which can be re-written as

$$[T_{ff}] \{H_f\} = [Q_f] - [T_{fc}] H_c. \quad (C12)$$

In the Galerkin formulation of the flow equation used in Section 2.2.3 (page 61), the operation of integration by parts produces the natural boundary condition

$$T\omega_i \left. \frac{dH}{dr'} \right|_{r'_w}^{r'_o} \quad (C13)$$

Recognizing, by reference to Equation 2.25 (page 59), that

$$T \frac{dH}{dr'} = Q, \quad (C14)$$

Equation C13 can be re-written as

$$Q\omega_i \left. \right|_{r'_w}^{r'_o} \quad (C15)$$

Since the volumetric flux cancels out at all internal nodes (node numbers 2 through N-1), Equation C15 reduces to

$$Q(\omega_o - \omega_w) \quad (C16)$$

From Equations C1 and C2 (page 197), it is obvious that the basic functions are equal to 1 at the end points, so this

further simplifies to

$$Q_0 - Q_w \quad (C17)$$

or, by dropping the subscripts and writing as an array,

$$\begin{Bmatrix} -Q \\ 0 \\ \vdots \\ \vdots \\ 0 \\ Q \end{Bmatrix} \quad (C18)$$

For a first type boundary condition, the right hand side of Equation C12 becomes

$$\begin{Bmatrix} 0 \\ \vdots \\ \vdots \\ \vdots \\ 0 \end{Bmatrix} = \frac{1}{L} \begin{bmatrix} 0 & -\bar{T}_{1,2} \\ \vdots & 0 \\ 0 & \vdots \\ -\bar{T}_{N-1,N} & 0 \end{bmatrix} \begin{Bmatrix} H_N \\ H_1 \end{Bmatrix} \quad (C19)$$

which by substituting H_0 and H_w for H_N and H_1 , respectively, can be simplified further to

$$= \frac{1}{L} \begin{bmatrix} -\bar{T}_{1,2} H_w & \\ 0 & \\ \vdots & \\ 0 & \\ -\bar{T}_{N-1,N} H_0 & \end{bmatrix} \quad (C20)$$

or

$$\begin{matrix} 1 \\ \vdots \\ L \end{matrix} \left\{ \begin{matrix} \bar{T}_{1,2} H_w \\ 0 \\ \vdots \\ 0 \\ \bar{T}_{N-1,N} H_o \end{matrix} \right\} \quad (C21)$$

From Equation C8 (page 200), it is readily apparent that the transmissivity matrix is a symmetric, tridiagonal matrix. Routine FLO2REG minimizes computer storage by assigning the values to a rectangular matrix with 2 columns (the third column is reproduced from symmetry during solution). The resulting matrix equation, which is solved by BANSOL, is

$$[T_{ff}] \{H_f\} = \{T_{fc} \cdot H_c\} \quad (C22)$$

where the dimensions are

$$\begin{aligned} [T_{ff}] &= [(N-2) \times 2] \\ \{H_f\} &= [(N-2) \times 1] \\ \{T_{fc} \cdot H_c\} &= [(N-2) \times 1] \end{aligned}$$

If a second type boundary condition (i.e., discharge rate) is specified at the well, the number of rows in all of the matrices/arrays will be increased by 1 and the right hand side of Equation C12 (page 201) becomes

$$\begin{pmatrix} -Q \\ 0 \\ \vdots \\ 0 \end{pmatrix} - \frac{1}{L} \begin{pmatrix} 0 \\ \vdots \\ 0 \\ -T_{N-1,N} \end{pmatrix} H_N \quad (C23)$$

or

$$\begin{pmatrix} -Q \\ 0 \\ \vdots \\ 0 \\ T_{N-1,N} H_N/L \end{pmatrix} \quad (C24)$$

The first equation of the matrix equation, Equation C11, can be used to calculate the discharge of the well, when a first type boundary condition is specified at the well. Referring to Equation C8 (page 200), it can be written in the form

$$\frac{1}{L} \begin{pmatrix} \bar{T}_{N-1,N} & 0 \\ 0 & \bar{T}_{1,2} \end{pmatrix} \begin{pmatrix} H_N \\ H_1 \end{pmatrix} + \frac{1}{L} \begin{pmatrix} 0 & \dots & 0 & -T_{N-1,N} \\ -\bar{T}_{1,2} & 0 & \dots & 0 \end{pmatrix} \begin{pmatrix} H_2 \\ H_{N-1} \end{pmatrix} = \begin{pmatrix} Q_N \\ Q_1 \end{pmatrix} \quad (C25)$$

or

$$\frac{1}{L} \left(\begin{pmatrix} \bar{T}_{N-1,N} \cdot H_N \\ \bar{T}_{1,2} \cdot H_1 \end{pmatrix} + \begin{pmatrix} -\bar{T}_{N-1,N} \cdot H_{N-1} \\ -\bar{T}_{1,2} \cdot H_2 \end{pmatrix} \right) = \begin{pmatrix} Q_o \\ Q_w \end{pmatrix} = \begin{pmatrix} Q \\ -Q \end{pmatrix} \quad (C26)$$

Since the unknown to be calculated is Q_w , only the second equation is used, from which

$$\bar{T}_{1,2} \frac{H_2 - H_1}{L} = Q_w \quad (C27)$$

This result, which is simply another form of the Thiem equation, should not be unexpected.

Fluid velocities at each flow node need to be determined for two reasons: 1) to estimate velocity heads, and 2) in order to be able to calculate Reynolds numbers for selecting appropriate flow laws. For a problem with a second type boundary condition, the velocity at each node can be determined simply from the continuity equation

$$v_i = \frac{Q}{A_i} = \frac{Q}{2\pi r_i (2b_i)} \quad (C28)$$

When head is specified at the well and the discharge rate is unknown, a generalized form of Equation C27, together with the continuity equation, can be used. Although the net flux (inflow less outflow) is 0 at any internal node, the relationship still holds for defining the discharge within an internal element by

$$v_e = \frac{2T_{1,i+1}(H_i - H_{i+1})}{\pi(r_i + r_{i+1})(2b_i + 2b_{i+1})L} \quad (C29)$$

The fluid velocity at each node then can be estimated by averaging the velocity in the two adjacent elements.

In the process of "linearizing" the non-linear flow laws (Section 2.2.2, page 59), transmissivity terms containing the gradient of the unknown value of head were obtained.

Therefore, a solution to the flow equation can be achieved only through iteration in which an approximate solution, derived from transmissivity values incorporating head values from the previous iteration, is continually revised until convergence is obtained utilizing a user-specified relative error value.

A standard iteration scheme (Hornbeck, 1975) is used by FLO2REG in which the solution of the head array is accelerated by

$$\{H\}^{k+1} = \{H\}^k + \theta[\{H\}^{k+1} - \{H\}^k] \quad (C30)$$

where

k = iteration number, and

θ = relaxation factor.

By re-arranging Equation C30 so that

$$\{H\}^{k+1} = \theta\{H\}^{k+1} + (1 - \theta)\{H\}^k, \quad (C31)$$

the flow equation can be re-written as

$$[T](\theta\{H\}^{k+1} + (1 - \theta)\{H\}^k) = \{Q\} \quad (C32)$$

or

$$[T]\{H\}^{k+1} = \{Q\}/\theta + [T](1 - 1/\theta)\{H\}^k \quad (C33)$$

which is the actual form solved by BANSOL. After each iteration, a check for convergence is made. If the convergence criterion is not met, new velocities, gradients (used in the non-linear transmissivity terms), and Reynolds numbers are

calculated and revised values of transmissivity are assigned. The transmissivity matrix and revised flux array are re-assembled and the equation is solved again. For most problems run during this study, convergence to a relative error of 1% could be achieved within 3 to 7 iterations using a relaxation factor of 1. There was no evidence suggesting solutions could be achieved significantly more quickly by using a relaxation factor other than 1.

Additional details concerning the flow code can be found in the various comments included in the listing of routines DEFLOW, FLO2REG, and FLOLAW.

C.3. Description of deformation code

The deformation code, comprised of the routines DEFLOW, BLOADS, DEFORM, FRACSTF, ROCKSTF, BANSOL, and STIFFEN, simulates displacement within the discontinuous rock mass resulting from changes in effective stress in the fracture(s) and wellbore due to flow-induced decreases in fluid pressure. Although the axisymmetric rock elements are geometrically much more complex (Equations 2.42 to 2.46 on pages 67 and 68) than the flow elements and require considerable numerical development (routine ROCKSTF) and, despite the additional "bookkeeping" (routine DEFORM) demanded by

the two degrees of freedom (both with respect to displacements and boundary conditions) of the structural nodes, the actual operation of the deformation code is simpler than that of the flow code.

As described in Section 2.3 (page 64), the rock matrix is modeled assuming a constant Young's modulus and Poisson's ratio. Thus, for a given problem, the contributions to stiffness from the rock elements do not change and need to be calculated only once. The behavior of the fracture elements, however, is stress-dependent; and their stiffnesses must be determined iteratively, following a user-defined constitutive relationship (Equation 2.50, page 70). During each iteration, the stiffness contributions of the fracture node pairs are added to the rock stiffness sub-matrix to form the total stiffness matrix. Under the given boundary conditions, which include the fluid pressures calculated in the flow code, the stiffness equation (Equation 2.52, page 71) is solved for the radial and vertical displacements of each node.

The displacements of primary interest are the vertical displacements of the fracture nodes. Net normal displacement or closure of the fracture is calculated from the relative vertical displacement of the two nodes comprising each fracture node pair. If any value differs from that of the previous iteration by a user-defined relative amount,

normal stress according to the fracture's constitutive relationship is calculated from Equation 2.50 (page 70). Then a new value for normal stiffness is assigned from

$$S_n = \sigma_n / \delta_n \quad . \quad (C34)$$

Referring to Figure 2.2 (page 71) this is the slope of the secant to the curve between the origin and the given (δ_n, σ_n) point on the constitutive curve. It was found that the solution could be achieved in fewer iterations using a relaxation factor, such that

$$S_n^i = 0.5(S_n^i + S_n^{i-1}) \quad (C35)$$

where i is an iteration counter.

In this code, the shear stiffness, which is of secondary importance, is simply given a value equal to a user-defined percentage of the normal stiffness. The revised stiffness values are then added to the rock stiffness submatrix and the stiffness equation is solved once again.

As is done with the flow equation, the stiffness equation also is partitioned into

$$\left[\begin{array}{c|c} S_{cc} & S_{cf} \\ \hline S_{fc} & S_{ff} \end{array} \right] \begin{Bmatrix} D_c \\ D_f \end{Bmatrix} = \begin{Bmatrix} F_c \\ F_f \end{Bmatrix} \quad (C36)$$

and the second equation

$$[S_{ff}]\{D_f\} = \{F_f\} - [S_{fc}]\{D_c\} \quad (C37)$$

is used to solve for the unknown displacements. However, in this code all of the fixed structural nodes have 0 displacements, (i.e., $D_c = 0$), so Equation C37 reduces simply to

$$[S_{ff}]\{D_f\} = \{F_f\} \quad (C38)$$

As shown in Figure 2.3 (page 73), the bottom structural nodes have been assigned $D_z = 0$ boundary conditions. This does not depict a normal situation. During development of the deformation code, other boundary conditions had been tested. It is impossible, because of computer round-off, to derive more realistic, statically determinate resultant (to applied and gravity loads) forces for the bottom nodes. The slightest imbalances in the vertical forces causes the model to "accelerate" which results in complete numerical instability. A hybrid method that was suggested by Booton (1984) was tried in which the lower, outermost node (the lower, rightmost node in Figure 2.3, page 73) was fixed (i.e., $D_z = 0$) and the approximate resultant forces were assigned to the other bottom nodes. The response of the fractures to this scheme differed negligibly from that when zero displacement boundary conditions were used, so only the latter boundary conditions have been incorporated into the code.

The stiffness matrix is symmetric and banded with a half bandwidth equal to twice the maximum difference between the incidences of any two nodes comprising any element

(either rock or fracture). The numbering system used for the nodes and elements in the finite element grid (Section C.1) was selected in an attempt to keep the bandwidth to a minimum. Routine DEFORM assembles half the stiffness matrix as a rectangular matrix with the resulting dimensions of the matrix and arrays in Equation C38 being

$$[S_{ff}] = [(2 \times N - NF) \times BW]$$

$$\{D_f\} = [(2 \times N - NF) \times 1]$$

$$\{F_f\} = [(2 \times N - NF) \times 1]$$

where

N = number of structural nodes,

NF = number of fixed displacement nodes, and

BW = bandwidth.

The stiffness equation is solved by BANSOL which reproduces the other half of the stiffness matrix during the solution process.

Additional details concerning the deformation code are contained within comments in the various routines (see program listing).

C.4 Determination of normal stress versus displacement relationship for a fracture

From laboratory data of normal stress versus displacement, a quantitative description of the constitutive rela-

relationship for a fracture (Figure 2.2, page 71) can be determined by non-linear regression. In this study, a relationship in the general form given in Equation 2.50 (page 70) has been presupposed. One advantage of this form over the hyperbolic function of Bandis et al. (1983) is that it is able to "emphasize" the linear relationship frequently observed at relatively low stress.

Applying the concept of least squares to Equation 2.50, the error term to be minimized is

$$\epsilon^2 = [\sigma - (S_1\delta + S_2\delta^n)]^2 \quad (C39)$$

First, by taking the derivative of Equation C39 with respect to S_1

$$\frac{d\epsilon^2}{dS_1} = 2[\sigma - (S_1\delta + S_2\delta^n)](-\delta) = 0 \quad (C40)$$

or

$$\sigma\delta = S_1\delta^2 + S_2\delta^{n+1} \quad (C41)$$

is obtained. Summing all data points, Equation C41 can be written as

$$\Sigma\sigma\delta = S_1\Sigma\delta^2 + S_2\Sigma\delta^{n+1} \quad (C42)$$

Likewise, by differentiating Equation C39 with respect to S_2

$$\frac{d\epsilon^2}{dS_2} = 2[\sigma - (S_1\delta + S_2\delta^n)](-\delta^n) = 0 \quad (C43)$$

or

$$\sigma\delta^n = S_1\delta^{n+1} + S_2\delta^{2n} \quad (C44)$$

By again summing all points, Equation C44 can be re-written as

$$\Sigma\sigma\delta^n = S_1\Sigma\delta^{n+1} + S_2\Sigma\delta^{2n} \quad (C45)$$

Equations C42 and C45 then can be solved simultaneously to determine the values of S_1 , S_2 , and n . The equation to be solved, written in matrix form, is

$$\begin{bmatrix} \Sigma\delta^2 & \Sigma\delta^{n+1} \\ \Sigma\delta^{n+1} & \Sigma\delta^{2n} \end{bmatrix} \begin{bmatrix} S_1 \\ S_2 \end{bmatrix} = \begin{bmatrix} \Sigma\sigma\delta \\ \Sigma\sigma\delta^n \end{bmatrix} \quad (C46)$$

A computer program, FRACLAW (for which a listing also is included at the end of the appendix) has been written to solve Equation C46. The solution involves iteration with the value of n being varied until a best fit is achieved.

The reader might have noted the mathematical similarity between Equations 2.50 (page 70) and 1.13 (page 9). In fact, FRACLAW is a modification of the program FASTEP (Labadie and Helweg, 1975) for solving the latter equation. FRACLAW is very brief, self explanatory, and no user's guide is necessary for it.

C.5 User's guide for DEFLOW

The following provides additional information for using the program DEFLOW. The program itself is highly annotated with comments, which together with the flow chart (Figure 2.5, pages 78-79) and routine descriptions (Figure C1) should allow the interested user to follow its execution.

A complete list of the variables used in the program is included as a header to the program listing. A few of the variable names differ by necessity from those used in the text of the thesis, and the user is alerted to following the notation used in the header.

C.5.1 Operating environment

The version of DEFLOW listed in Section C.6 is written in VAX-11 FORTRAN (an extension of FORTRAN-77) capable of running on the VAX/VMS system at Memorial University as of March, 1984. It contains the INCLUDE statement which might not be acceptable to some other FORTRAN compilers. Should that problem be encountered, those statements simply can be replaced by the actual COMMON and PARAMETER statements (see Section C.5.2) which they represent. If this is necessary, the PARAM.COM must be the first statement; the order of the others does not matter.

This version also is set up specifically to run interactively from remote terminal on the VAX/VMS operating system. To convert to a batch entry version, it will be necessary to delete the OPEN statements which assign logical units for READ (2) and WRITE (3) statements and to replace them with external SYSS\$INPUT and SYSS\$OUTPUT assignments or their equivalents. Terminal READ (5) statements and WRITE (6) statements also will have to be de-activated.

DEFLOW also contains the run-time CPU timer facility of the VAX/VMS system which might not be operational on other systems. It can be deleted without any effect on the execution of the program.

All potentially problematic statements are flagged with a "\$" in Column 73 of the listing.

C.5.2 External files

The following PARAMETER statement and labelled COMMON blocks are files which must be maintained on the same disk as the program and be accessible to it by means of the INCLUDE statement. This arrangement avoids unnecessary repetition of the blocks at the beginning of each routine. The PARAMETER statement is particularly useful. In order to change the variable dimensions of the various arrays for the needs of a particular problem, it is only necessary to

re-dimension the PARAMETER statement file, PARAM.COM. However, the program must be re-compiled and re-linked whenever the dimensions in PARAM.COM are changed.

The following is a listing of PARAM.COM:

```

C VARIABLE DIMENSIONS OF ARRAYS IN COMMON BLOCKS;
C     IBWD = HALF-BANDWIDTH OF STIFFNESS MATRIX
C     MAXDFITD = MAXIMUM NUMBER OF DEFORMATION-FLOW
C             ITERATIONS ALLOWED
C     NFED = NUMBER OF FLOW ELEMENTS PER FRACTURE
C           (ALWAYS EQUAL TO NFND-1)
C     NFND = NUMBER OF FLOW NODE PAIRS PER FRACTURE
C     NFNTD = TOTAL NUMBER OF FLOW NODE PAIRS
C           (NFRACD x NFND)
C     NFRACD = NUMBER OF FRACTURES
C     NRXD = NUMBER OF ROCK LAYERS
C     NRX2D = 2 x NUMBER OF ROCK LAYERS
C     NSED = NUMBER OF STRUCTURAL ELEMENTS
C     NSND = NUMBER OF STRUCTURAL NODES
C     NSN2D = 2 x NUMBER OF STRUCTURAL NODES
C     NWBBND = NUMBER OF WELLBORE BOUNDARY NODES
C     PARAMETER (     IBWD = 10,
*                   MAXDFITD = 12,
*                   NFED = 4,
*                   NFND = 5,           Note: These numbers
*                   NFNTD = 5,         are an example
*                   NFRACD = 1,        only.
*                   NRXD = 2,
*                   NRX2D = 4,
*                   NSED = 16,
*                   NSND = 20,
*                   NSN2D = 40,
*                   NTBND = 2,
*                   NWBBND = 10)

```

It is recommended that any new problem first be run without activating the flow or deformation codes (instructions given below) in order to get the correct value for the half-bandwidth. Then the arrays can be properly dimensioned before actual program execution.

The labelled COMMON blocks which also must be accessible to the program include:

BOTH.COM

```
CHARACTER*20 FILEOUT
CHARACTER*60 TITLE
COMMON /BOTH/ EPSILON, FILEOUT, FPROP(NFRACD,9),
*             IFPAIR(NFRACD,NFND,2),NDFIT,NFRAC,
*             RPROP(NRXD,4),RR(NFND),TITLE(2)
```

CONSTS.COM

```
COMMON /CONSTS/ G,PI,RHO,RHOG,TEMP,VISC
```

DEFORM.COM

```
COMMON /DEFORM/ D(NRXD,4,4),DELTA,DISP(NSN2D),DISPI(NSN2D),
*             FE(6),IBWS,ICODE(NSND),IFE,INC(NSED,4),
*             IOBN(NRX2D),ITBN(NTBND),IWBBN(NWBBND),
*             KN(NFNTD),KS(NFNTD),LC(NSN2D),LMS,NE,NFNT,
*             NOBN,NP,NPERT(MAXDFITD),NRX,NSE,NSN,NSN2,
*             NTBN,NTWBBN,NWBBN(NRXD),OBLOAD(NRX2D),
*             SE(6,6),TBLOAD(NTBND),TOPRESS
REAL KN,KS
```

DIMENS.COM

```
COMMON /DIMENS/ R(NSND),RO,RW,Z(NSND)
```

FLAGS.COM

```
LOGICAL FLAG1,FLAG2,FLAG3,FLAG4,FLAG5,FLAG6,FLAG7,FLAG8,
*             FLAG9
COMMON /FLAGS/ FLAG1,FLAG2,FLAG3,FLAG4,FLAG5,FLAG6,FLAG7,
*             FLAG8,FLAG9
```

FLOW.COM

```
COMMON /FLOW/ CL(NFND,EL,IBCWELL,LAW(NFND),MAXFIT,N1,NF,
*             NFE,NFN,NFIT,Q,RE(NFND)RELAXF,ROUGH(NFND),
*             TRANS(NFND),TWOB(NFND),TWOB1(NFRACD,NFND),
*             VEL(NFND)
```

HEAD.COM

```

COMMON /HEAD/  HO,HW(NFRACD),PHEAD(NFRACD,NFND),
*              PHEAD1(NFRACD,NFND),SEL,SWB(NFRACD),
*              THEAD(NFND),VHEAD(NFND),VHEADWB(NFRACD),
*              ZHEAD(NFRACD)

```

MATEQN.COM

```

COMMON /MATEQN/ A(NSN2D,IBWD),B(NSN2D),IBW,LM

```

C.5.3 Input files

The input files are organized by CHARACTER control words which either 1) indicate the type of input data to follow or 2) are commands for directing program execution. The words and their uses are:

Data organizers:

```

GENERAL = title and general set-up parameters
ROCK    = rock properties
FRACS   = fracture properties
WATER   = temperature of water
NODES   = nodal coordinates and boundary condition
         codes
FLOPAIRS = nodes comprising fracture/flow pairs
BCS     = boundary conditions for flow and deformation
         codes
ELEMENTS = nodal incidences of elements and material
         types

```

Commands:

```

GENGRID = activate routine GRIDGEN
PRINT   = print input data and related calculated
         values
GOFLOW  = activate flow code only
GODRILL = activate deformation code only (i.e., deter-
         mine displacements due to drilling of
         wellbore)

```

GOBOTH = initiate coupled solution using both flow and deformation codes
END = terminate program (only necessary if none of the codes are activated as in the case of wanting only to determine the half-bandwidth).

Table C1 is an example of an input file for a problem in which there is only one fracture and the optional grid generator is going to be used. The reader is referred to the program listing for the exact parameters following each data organizer control word and the required formats. All input (READ) statements are flagged with an "I" in Column 73. In this particular example, it has been assumed that the initial fracture apertures are variable. Therefore the fracture aperture is set equal to zero in the first line of the block of data and the individual nodal apertures are input beginning with the third line.

If there is only one fracture, the boundary condition at the well, IBCWELL, can be either 1 (first type or Hw specified) or 2 (second type or Q specified). If there is more than one fracture, only a first type boundary condition can be assigned.

The routine GRIDGEN can be used only if there is one fracture. It assigns nodal coordinates, flow node pairs, element incidences and material types, and boundary condition codes. Note in Table C1 that it is not necessary

Table C1 Example of input file for DEFLOW with one fracture and GRIDGEN used

```

GENERAL
SIMULATION OF LABORATORY MODEL, TEST2
SEPTEMBER 7, 1984
  1  15
  2
    0.032    0.002    0.750
  10  10    10      1.00    0.01
ROCK
    1.48  2.20E+03    33.4    0.10
    1.54  2.20E+03    33.4    0.10
FRACS
    0.000    5.0    0.240    100.0
    6.33E-03  2.50E+00    3.82    0.50
    1.38    1.39    1.39    1.40    1.40
    1.41    1.42    1.44    1.45    1.46
    1.47    1.49    1.50    1.52    1.55
WATER
25.6
GENGRID
BCS
  2      1.528E-03    13.684
  0      .184
PRINT
GOBOTH

```

to input NSN and NSE and that only IBCOB and TOPRESS need to be read in as deformation boundary conditions if GRIDGEN is used. If there is more than one fracture or for some reason the user wishes to use another discretization scheme, all boundary conditions and coordinates must be entered individually. The nodal boundary condition codes are given under ICODE in the header to the program.

Table C2 is an example with three fractures for which GRIDGEN cannot be used and all of the nodal and element information must be input. As with most finite element codes, nodal incidences of structural elements must be input in a counter-clockwise direction starting with the lowest numbered node in each element. The material type must also be designated for each structural element.

C.5.4 Example of output

Table C3 is an example of output from DEFLOW for a coupled solution (run under the command GOBOTH) with 3 fractures. Printout of all of the input data and related calculated values can be suppressed simply by eliminating the control word PRINT in the input file. This may be desirable after the initial run of a multi-run problem.

C.5.5 Additional notes on execution

The flow and stiffness equations solved by DEFLOW have the general matrix form

$$[A]\{X\} = \{B\} \quad (C47)$$

In the flow code, the matrix and arrays and their dimensions are

A(LM,2) = transmissivity matrix containing hydraulic and geometric properties of the fracture(s),

B(LM) = volumetric flux array,

X(LM) = total head array,

and for the deformation code

A(LM,IBWS) = stiffness matrix containing mechanical and geometric properties of the rock layers and the fracture(s),

B(LM) = force array,

X(LM) = displacement array

where

IBWS = half-bandwidth of the stiffness matrix, and

LM = length of matrices and arrays.

In both cases, routine BANSOL puts the solution values represented by {X} into {B}, which is re-usable, and returns them in the latter array in routines FLO2REG and DEFORM. The values of {B} are then reassigned to {THEAD} and {DISP}, respectively.

DEFLOW uses the following sign convention:

+ r radially outward (for all),

+ z downward for forces and displacements, and

+ z upward for coordinates.

The coordinate system is established with the (0,0) datum being the centerline of the wellbore at the base of the lowermost rock layer. The datum for elevation heads (i.e., where ZHEAD = 0) is the lowermost fracture.

Table C2 Example of input file for DEFLOW with three fractures

```

GENERAL
TEST WITH 3 FRACTURES AND 4 ROCK LAYERS
AUGUST 17, 1984
  3  15
  4 140 132
    0.100 0.003 100.00
10  15  15  1.00  0.02
ROCK
  1.000 2.64E+03 25.0 0.25
  3.000 2.64E+03 25.0 0.25
  2.000 2.64E+03 25.0 0.25
  1.000 2.64E+03 25.0 0.25
FRACS
  0.700 30.0 0.150 100.00
  1.07E-02 2.94E+04 7.75 0.50
  0.500 30.0 0.150 100.00
  1.07E-02 2.94E+04 7.75 0.50
  0.300 30.0 0.150 100.00
  1.07E-02 2.94E+04 7.75 0.50
WATER
10.0
NODES
  1  0  0.100  1.000
  2  0  0.100  1.000
  3  0  0.100  4.000
  4  0  0.100  4.000
  5  0  0.100  6.000
  6  0  0.100  6.000
  7 -2  0.100  0.935
  8 -1  0.164  1.000
  9 -1  0.164  1.000
 10 -2  0.100  1.065
 11 -2  0.100  3.935
  .  .  .  .
  .  .  .  .
  .  .  .  .
135  0 100.000  1.000
136  0 100.000  4.000
137  0 100.000  4.000
138  0 100.000  6.000
139  0 100.000  6.000
140  0 100.000  7.000
FLOPAIRS
  1  1  2
  2  8  9
  3 20 21

```

Table C2 Example of input file for DEFLOW
with three fractures (Continued)

| | | | | | | | |
|-----|-----|-----|------|----|---|------|--|
| 4 | 32 | 33 | | | | | |
| 5 | 44 | 45 | | | | | |
| 6 | 56 | 57 | | | | | |
| 7 | 70 | 71 | | | | | |
| 8 | 78 | 79 | | | | | |
| 9 | 86 | 87 | | | | | |
| 10 | 94 | 95 | | | | | |
| 11 | 102 | 103 | | | | | |
| 12 | 110 | 111 | | | | | |
| 13 | 118 | 119 | | | | | |
| 14 | 126 | 127 | | | | | |
| 15 | 134 | 135 | | | | | |
| 1 | 3 | 4 | | | | | |
| 2 | 12 | 13 | | | | | |
| 3 | 24 | 25 | | | | | |
| 4 | 36 | 37 | | | | | |
| 5 | 48 | 49 | | | | | |
| 6 | 60 | 61 | | | | | |
| 7 | 72 | 73 | | | | | |
| 8 | 80 | 81 | | | | | |
| 9 | 88 | 89 | | | | | |
| 10 | 96 | 97 | | | | | |
| 11 | 104 | 105 | | | | | |
| 12 | 112 | 113 | | | | | |
| 13 | 120 | 121 | | | | | |
| 14 | 128 | 129 | | | | | |
| 15 | 136 | 137 | | | | | |
| 1 | 5 | 6 | | | | | |
| 2 | 16 | 17 | | | | | |
| 3 | 28 | 29 | | | | | |
| 4 | 40 | 41 | | | | | |
| 5 | 52 | 53 | | | | | |
| 6 | 63 | 64 | | | | | |
| 7 | 74 | 75 | | | | | |
| 8 | 82 | 83 | | | | | |
| 9 | 90 | 91 | | | | | |
| 10 | 98 | 99 | | | | | |
| 11 | 106 | 107 | | | | | |
| 12 | 114 | 115 | | | | | |
| 13 | 122 | 123 | | | | | |
| 14 | 130 | 131 | | | | | |
| 15 | 138 | 139 | | | | | |
| BCS | | | | | | | |
| 1 | | | 10.0 | | | 60.0 | |
| 6 | 55 | 43 | 31 | 19 | 7 | 1 | |
| 133 | 134 | | | | | | |

Table C2 Example of input file for DEFLOW
with three fractures (Continued)

| | | | | | | | | | | | | | |
|----------|-----|-----|-----|----|----|-----|-----|-----|-----|-----|-----|----|---|
| 13 | 2 | 10 | 22 | 34 | 46 | 58 | 67 | 59 | 47 | 35 | 23 | 11 | 3 |
| 135 | 136 | | | | | | | | | | | | |
| 11 | 4 | 14 | 26 | 38 | 50 | 62 | 51 | 39 | 27 | 15 | 5 | | |
| 137 | 138 | | | | | | | | | | | | |
| 6 | 6 | 18 | 30 | 42 | 54 | 65 | | | | | | | |
| 139 | 140 | | | | | | | | | | | | |
| 11 | 65 | 68 | 76 | 84 | 92 | 100 | 108 | 116 | 124 | 132 | 140 | | |
| 1 | | 0.8 | | | | | | | | | | | |
| ELEMENTS | | | | | | | | | | | | | |
| 1 | 1 | 7 | 8 | 1 | | | | | | | | | |
| 2 | 7 | 19 | 8 | 1 | | | | | | | | | |
| 3 | 8 | 19 | 20 | 1 | | | | | | | | | |
| 4 | 19 | 31 | 20 | 1 | | | | | | | | | |
| 5 | 20 | 31 | 32 | 1 | | | | | | | | | |
| 6 | 31 | 43 | 32 | 1 | | | | | | | | | |
| 7 | 32 | 43 | 44 | 1 | | | | | | | | | |
| 8 | 43 | 55 | 44 | 1 | | | | | | | | | |
| 9 | 44 | 55 | 56 | 1 | | | | | | | | | |
| 10 | 55 | 66 | 56 | 1 | | | | | | | | | |
| 11 | 66 | 69 | 56 | 1 | | | | | | | | | |
| . | . | . | . | . | | | | | | | | | |
| . | . | . | . | . | | | | | | | | | |
| . | . | . | . | . | | | | | | | | | |
| 125 | 107 | 115 | 108 | 4 | | | | | | | | | |
| 126 | 108 | 115 | 116 | 4 | | | | | | | | | |
| 127 | 115 | 123 | 116 | 4 | | | | | | | | | |
| 128 | 116 | 123 | 124 | 4 | | | | | | | | | |
| 129 | 123 | 131 | 124 | 4 | | | | | | | | | |
| 130 | 124 | 131 | 132 | 4 | | | | | | | | | |
| 131 | 131 | 139 | 132 | 4 | | | | | | | | | |
| 132 | 132 | 139 | 140 | 4 | | | | | | | | | |
| PRINT | | | | | | | | | | | | | |
| GOBOTH | | | | | | | | | | | | | |

Table C3 Example of output file from DEFLOW

ANALYSIS
OF THE
COUPLED AXISYMMETRIC DEFORMATION-DRAWDOWN RESPONSE
RESULTING FROM
STEADY-STATE, TWO-REGIME, RADIAL FLOW TO A WELL
THROUGH A SERIES OF ROUGH, DEFORMABLE, HORIZONTAL FRACTURES
USING

* -DEFLOW- *

PROBLEM: SIMULATION OF LABORATORY MODEL, TEST2
SEPTEMBER 7, 1984

GENERAL SET-UP PARAMETERS:

| | |
|--|----|
| NUMBER OF FRACTURES ----- | 1 |
| NUMBER OF FLOW NODE PAIRS PER FRACTURE ----- | 15 |
| NUMBER OF ROCK UNITS ----- | 2 |
| NUMBER OF STRUCTURAL NODES ----- | 60 |
| NUMBER OF STRUCTURAL ELEMENTS ----- | 56 |

DIMENSIONS:

| | |
|--|-------|
| RADIUS OF WELL (M) ----- | 0.032 |
| RADIUS OF CONSTANT HEAD OUTER BOUNDARY (M) ----- | 0.750 |
| WELLBORE FRICTION FACTOR ----- | 0.070 |

BOUNDARY CONDITIONS:

| | |
|--------------------------------------|-----------|
| BOUNDARY CONDITION AT WELL ----- | FLUX |
| WELL DISCHARGE (M**3/S) ----- | 1.528E-03 |
| HEAD AT OUTER BOUNDARY (M) ----- | 13.684 |
| PRESSURE ON JOP BOUNDARY (MPa) ----- | 0.184 |

ITERATION CONTROLS:

| | |
|--|------|
| RELAXATION FACTOR FOR FLOW ITERATION ----- | 1.00 |
| RELATIVE ERROR FOR TESTING OF CONVERGENCE ----- | 0.01 |
| MAXIMUM ITERATIONS ALLOWED IN FLOW ROUTINE ----- | 10 |
| MAXIMUM DEFORMATION-FLOW ITERATIONS ALLOWED ----- | 10 |
| MAXIMUM FRACTURE STIFFNESS PERTURBATIONS ALLOWED ----- | 10 |

Table C3 (Example of output file from DEFLOW (Continued))

PROBLEM: SIMULATION OF LABORATORY MODEL, TEST2
SEPTEMBER 7, 1984

MATERIAL PROPERTIES

ROCK:

| | ROCK LAYER | | | |
|---------------------------|------------|----------|---|---|
| | 1 | 2 | 3 | 4 |
| THICKNESS (M) ----- | 1.48 | 1.54 | | |
| MASS DENSITY (KG/M**3) -- | 2.20E+03 | 2.20E+03 | | |
| YOUNG'S MODULUS (GPa) --- | 33.4 | 33.4 | | |
| POISSON'S RATIO ----- | 0.10 | 0.10 | | |

FRACTURES:

| | FRACTURE NO. | | |
|-----------------------------------|--------------|---|---|
| | 1 | 2 | 3 |
| INITIAL APERTURE * (MM) ----- | 0.000 | | |
| MAXIMUM CLOSURE (%) ----- | 5.0 | | |
| ABSOLUTE ROUGHNESS (MM) ----- | 0.240 | | |
| POROSITY (%) ----- | 100.0 | | |
| NORMAL STIFFNESS: K1 (GPa/MM) --- | 6.33E-03 | | |
| K2 (**) | 2.50E+00 | | |
| N () | 3.82 | | |
| TANGENTIAL STIFFNESS FACTOR ----- | 0.50 | | |

* If 0.0, non-uniform (see output for individual nodal aperture values)

** Units dependent on value of n

WATER:

| | |
|-----------------------------------|----------|
| TEMPERATURE (DEGREES C) ----- | 25.6 |
| KINEMATIC VISCOSITY (M**2/S) ---- | 8.81E-07 |
| MASS DENSITY (KG/M**3) ----- | 9.97E+02 |

Table C3 Example of output file from DEFLOW (Continued)

PROBLEM: SIMULATION OF LABORATORY MODEL, TEST2
 SEPTEMBER 7, 1984

NODE INFORMATION

| NODE NUMBER | R COORD (M) | Z COORD (M) | BC CODE | INITIAL BOUNDARY CONDITIONS | | | |
|----------------|-------------------|-------------------|------------|-----------------------------|-------------------|------------------|-------------------|
| | | | | R LOAD (N) | R DISPL (M) | Z LOAD (N) | Z DISPL (M) |
| 1 | 0.032 | 1.480 | 0 | 2.59E+01 | | 1.88E+01 | |
| 2 | 0.032 | 1.480 | 0 | 2.65E+01 | | -1.88E+01 | |
| 3 | 0.032 | 1.413 | -2 | 5.39E+01 | | | 0.0 |
| 4 | 0.040 | 1.480 | -1 | | 0.0 | 4.97E+01 | |
| 5 | 0.040 | 1.480 | -1 | | 0.0 | -4.97E+01 | |
| 6 | 0.032 | 1.549 | -2 | 5.46E+01 | | | 0.0 |
| 7 | 0.032 | 1.341 | -2 | 5.79E+01 | | | 0.0 |
| 8 | 0.050 | 1.480 | -1 | | 0.0 | 7.80E+01 | |
| 9 | 0.050 | 1.480 | -1 | | 0.0 | -7.80E+01 | |
| 10 | 0.032 | 1.622 | -2 | 5.80E+01 | | | 0.0 |
| 11 | 0.032 | 1.265 | -2 | 6.22E+01 | | | 0.0 |
| 12 | 0.063 | 1.480 | -1 | | 0.0 | 1.22E+02 | |
| 13 | 0.063 | 1.480 | -1 | | 0.0 | -1.22E+02 | |
| 14 | 0.032 | 1.701 | -2 | 6.15E+01 | | | 0.0 |
| 15 | 0.032 | 1.184 | -2 | 6.69E+01 | | | 0.0 |
| 16 | 0.079 | 1.480 | -1 | | 0.0 | 1.92E+02 | |
| 17 | 0.079 | 1.480 | -1 | | 0.0 | -1.92E+02 | |
| 18 | 0.032 | 1.785 | -2 | 6.51E+01 | | | 0.0 |
| 19 | 0.032 | 1.097 | -2 | 7.20E+01 | | | 0.0 |
| 20 | 0.099 | 1.480 | -1 | | 0.0 | 3.01E+02 | |
| 21 | 0.099 | 1.480 | -1 | | 0.0 | -3.01E+02 | |
| 22 | 0.032 | 1.875 | -2 | 6.90E+01 | | | 0.0 |
| 23 | 0.032 | 1.004 | -2 | 7.75E+01 | | | 0.0 |
| 24 | 0.124 | 1.480 | -1 | | 0.0 | 4.73E+02 | |
| 25 | 0.124 | 1.480 | -1 | | 0.0 | -4.73E+02 | |
| 26 | 0.032 | 1.971 | -2 | 7.30E+01 | | | 0.0 |
| 27 | 0.032 | 0.905 | -2 | 8.35E+01 | | | 0.0 |
| 28 | 0.155 | 1.480 | -1 | | 0.0 | 7.42E+02 | |
| 29 | 0.155 | 1.480 | -1 | | 0.0 | -7.42E+02 | |
| 30 | 0.032 | 2.074 | -2 | 7.72E+01 | | | 0.0 |
| 31 | 0.032 | 0.800 | -2 | 9.00E+01 | | | 0.0 |
| 32 | 0.194 | 1.480 | -1 | | 0.0 | 1.16E+03 | |
| 33 | 0.194 | 1.480 | -1 | | 0.0 | -1.16E+03 | |
| 34 | 0.032 | 2.183 | -2 | 8.15E+01 | | | 0.0 |

Table C3 Example of output file from DEFLOW (Continued)

| | | | | | | | |
|----|-------|-------|----|----------|-----|-----------|------|
| 35 | 0.032 | 0.687 | -2 | 9.70E+01 | | | 0.0 |
| 36 | 0.243 | 1.480 | -1 | | 0.0 | 1.83E+03 | |
| 37 | 0.243 | 1.480 | -1 | | 0.0 | -1.83E+03 | |
| 38 | 0.032 | 2.301 | -2 | 8.60E+01 | | | 0.0 |
| 39 | 0.032 | 0.567 | -2 | 1.05E+02 | | | 0.0 |
| 40 | 0.305 | 1.480 | -1 | | 0.0 | 2.87E+03 | |
| 41 | 0.305 | 1.480 | -1 | | 0.0 | -2.87E+03 | |
| 42 | 0.032 | 2.426 | -2 | 9.07E+01 | | | 0.0 |
| 43 | 0.032 | 0.439 | -2 | 1.13E+02 | | | 0.0 |
| 44 | 0.382 | 1.480 | -1 | | 0.0 | 4.50E+03 | |
| 45 | 0.382 | 1.480 | -1 | | 0.0 | -4.50E+03 | |
| 46 | 0.032 | 2.560 | -2 | 9.55E+01 | | | 0.0 |
| 47 | 0.032 | 0.302 | -2 | 1.22E+02 | | | 0.0 |
| 48 | 0.478 | 1.480 | -1 | | 0.0 | 7.06E+03 | |
| 49 | 0.478 | 1.480 | -1 | | 0.0 | -7.06E+03 | |
| 50 | 0.032 | 2.703 | -2 | 1.00E+02 | | | 0.0 |
| 51 | 0.032 | 0.156 | -2 | 1.32E+02 | | | 0.0 |
| 52 | 0.599 | 1.480 | -1 | | 0.0 | 1.11E+04 | |
| 53 | 0.599 | 1.480 | -1 | | 0.0 | -1.11E+04 | |
| 54 | 0.032 | 2.856 | -2 | 1.06E+02 | | | 0.0 |
| 55 | 0.032 | 0.000 | 2 | 6.87E+01 | | | 0.0F |
| 56 | 0.750 | 1.480 | 0 | 0.00E+00 | | 7.08E+03 | |
| 57 | 0.750 | 1.480 | 0 | 0.00E+00 | | -7.08E+03 | |
| 58 | 0.032 | 3.020 | 0 | 5.39E+01 | | 1.79E+04 | |
| 59 | 0.750 | 0.000 | 2 | 0.00E+00 | | | 0.0F |
| 60 | 0.750 | 3.020 | 0 | 0.00E+00 | | 3.37E+04 | |

BOUNDARY CONDITION CODES:

SIGN CONVENTION:

| CODE | R | Z | |
|------|------|------|---------------------|
| ---- | ---- | ---- | |
| -3 | - | DISP | R+ RADIALLY OUTWARD |
| -2 | LOAD | - | Z+ DOWNWARD |
| -1 | - | LOAD | |
| 0 | LOAD | LOAD | |
| 1 | DISP | LOAD | |
| 2 | LOAD | DISP | |
| 3 | DISP | DISP | |

F INDICATES FIXED DISPLACEMENT

Table C3 Example of output file from DEFLOW (Continued)

PROBLEM: SIMULATION OF LABORATORY MODEL, TEST2
 SEPTEMBER 7, 1984

NODE INFORMATION (CONT.)

| FLOW PAIRS: | FRACTURE NUMBER | FLOW PAIR | NODES | |
|-------------|--------------------|--------------|-------|-------|
| | ----- | ---- | ----- | ----- |
| | 1 | 1 | 1 | 2 |
| | 1 | 2 | 4 | 5 |
| | 1 | 3 | 8 | 9 |
| | 1 | 4 | 12 | 13 |
| | 1 | 5 | 16 | 17 |
| | 1 | 6 | 20 | 21 |
| | 1 | 7 | 24 | 25 |
| | 1 | 8 | 28 | 29 |
| | 1 | 9 | 32 | 33 |
| | 1 | 10 | 36 | 37 |
| | 1 | 11 | 40 | 41 |
| | 1 | 12 | 44 | 45 |
| | 1 | 13 | 48 | 49 |
| | 1 | 14 | 52 | 53 |
| | 1 | 15 | 56 | 57 |

| TOP BOUNDARY NODES: | NO. | NODE |
|---------------------|------|-------|
| | ---- | ----- |
| | 1 | 58 |
| | 2 | 60 |

| WELLBORE BOUNDARY NODES: | ROCK LAYER | NUMBER | NODE |
|--------------------------|---------------|--------|-------|
| | ----- | ----- | ----- |
| | 1 | 1 | 55 |
| | 1 | 2 | 51 |
| | 1 | 3 | 47 |
| | 1 | 4 | 43 |
| | 1 | 5 | 39 |
| | 1 | 6 | 35 |
| | 1 | 7 | 31 |
| | 1 | 8 | 27 |

Table C3 Example of output file from DEFLOW (Continued).

| | | |
|---|----|----|
| 1 | 9 | 23 |
| 1 | 10 | 19 |
| 1 | 11 | 15 |
| 1 | 12 | 11 |
| 1 | 13 | 7 |
| 1 | 14 | 3 |
| 1 | 15 | 1 |
| 2 | 1 | 2 |
| 2 | 2 | 6 |
| 2 | 3 | 10 |
| 2 | 4 | 14 |
| 2 | 5 | 18 |
| 2 | 6 | 22 |
| 2 | 7 | 26 |
| 2 | 8 | 30 |
| 2 | 9 | 34 |
| 2 | 10 | 38 |
| 2 | 11 | 42 |
| 2 | 12 | 46 |
| 2 | 13 | 50 |
| 2 | 14 | 54 |
| 2 | 15 | 58 |

 OUTER BOUNDARY NODES:

| NO. | NODE |
|-----|------|
| --- | ---- |
| 1 | 59 |
| 2 | 56 |
| 3 | 57 |
| 4 | 60 |

Table C3 Example of output file from DEFLOW (Continued)

PROBLEM: SIMULATION OF LABORATORY MODEL, TEST2
 SEPTEMBER 7, 1984

ELEMENT INFORMATION

HALF-BANDWIDTH OF STIFFNESS MATRIX = 10

| ELEMENT | ROCK LAYER | INCIDENCES | | |
|---------|---------------|------------|----|----|
| | | 1 | 2 | 3 |
| 1 | 1 | 1 | 3 | 4 |
| 2 | 1 | 3 | 7 | 4 |
| 3 | 1 | 4 | 7 | 8 |
| 4 | 1 | 7 | 11 | 8 |
| 5 | 1 | 8 | 11 | 12 |
| 6 | 1 | 11 | 15 | 12 |
| 7 | 1 | 12 | 15 | 16 |
| 8 | 1 | 15 | 19 | 16 |
| 9 | 1 | 16 | 19 | 20 |
| 10 | 1 | 19 | 23 | 20 |
| 11 | 1 | 20 | 23 | 24 |
| 12 | 1 | 23 | 27 | 24 |
| 13 | 1 | 24 | 27 | 28 |
| 14 | 1 | 27 | 31 | 28 |
| 15 | 1 | 28 | 31 | 32 |
| 16 | 1 | 31 | 35 | 32 |
| 17 | 1 | 32 | 35 | 36 |
| 18 | 1 | 35 | 39 | 36 |
| 19 | 1 | 36 | 39 | 40 |
| 20 | 1 | 39 | 43 | 40 |
| 21 | 1 | 40 | 43 | 44 |
| 22 | 1 | 43 | 47 | 44 |
| 23 | 1 | 44 | 47 | 48 |
| 24 | 1 | 47 | 51 | 48 |
| 25 | 1 | 48 | 51 | 52 |
| 26 | 1 | 51 | 55 | 52 |
| 27 | 1 | 52 | 55 | 56 |
| 28 | 1 | 55 | 59 | 56 |
| 29 | 2 | 2 | 5 | 6 |
| 30 | 2 | 5 | 9 | 6 |
| 31 | 2 | 6 | 9 | 10 |
| 32 | 2 | 9 | 13 | 10 |
| 33 | 2 | 10 | 13 | 14 |

Table C3 Example of output file from DEFLOW (Continued)

| | | | | |
|----|---|----|----|----|
| 34 | 2 | 13 | 17 | 14 |
| 35 | 2 | 14 | 17 | 18 |
| 36 | 2 | 17 | 21 | 18 |
| 37 | 2 | 18 | 21 | 22 |
| 38 | 2 | 21 | 25 | 22 |
| 39 | 2 | 22 | 25 | 26 |
| 40 | 2 | 25 | 29 | 26 |
| 41 | 2 | 26 | 29 | 30 |
| 42 | 2 | 29 | 33 | 30 |
| 43 | 2 | 30 | 33 | 34 |
| 44 | 2 | 33 | 37 | 34 |
| 45 | 2 | 34 | 37 | 38 |
| 46 | 2 | 37 | 41 | 38 |
| 47 | 2 | 38 | 41 | 42 |
| 48 | 2 | 41 | 45 | 42 |
| 49 | 2 | 42 | 45 | 46 |
| 50 | 2 | 45 | 49 | 46 |
| 51 | 2 | 46 | 49 | 50 |
| 52 | 2 | 49 | 53 | 50 |
| 53 | 2 | 50 | 53 | 54 |
| 54 | 2 | 53 | 57 | 54 |
| 55 | 2 | 54 | 57 | 58 |
| 56 | 2 | 57 | 60 | 58 |

Table C3 Example of output file from DEFLOW (Continued)

 * OUTPUT FROM DEFLOW *

PROBLEM: SIMULATION OF LABORATORY MODEL, TEST2
 SEPTEMBER 7, 1984

ROUTINE(S) USED: FLOW ONLY

RESULTS OF FLOW ROUTINE

FRACTURE NO. 1

NUMBER OF FLOW ITERATIONS ----- 6
 DISCHARGE FROM FRACTURE (M**3/S) ----- 1.528E-03

| RADIUS (M) | TOTAL HEAD (M) | DRAW- DOWN (M) | VEL. HEAD (M) | PRESS. LOSS (M) | APER- TURE (MM) | ROUGH NESS () | REYNOLDS NUMBER () | FLOW LAW |
|---------------|----------------------|----------------------|---------------------|-----------------------|-----------------------|----------------------|---------------------------|-------------|
| IN WELL | 10.992 | 2.692 | 0.012 | 2.701 | - | - | - | - |
| 0.032 | 11.584 | 2.100 | 1.546 | 3.644 | 1.380 | 0.087 | 1.72E+04 | 5 |
| 0.040 | 12.018 | 1.666 | 0.971 | 2.634 | 1.390 | 0.086 | 1.38E+04 | 5 |
| 0.050 | 12.391 | 1.293 | 0.619 | 1.909 | 1.390 | 0.086 | 1.10E+04 | 5 |
| 0.063 | 12.689 | 0.995 | 0.389 | 1.381 | 1.400 | 0.086 | 8.77E+03 | 5 |
| 0.079 | 12.926 | 0.758 | 0.248 | 1.003 | 1.400 | 0.086 | 7.00E+03 | 5 |
| 0.099 | 13.112 | 0.572 | 0.156 | 0.725 | 1.410 | 0.085 | 5.59E+03 | 5 |
| 0.124 | 13.258 | 0.426 | 0.098 | 0.521 | 1.420 | 0.085 | 4.46E+03 | 5 |
| 0.155 | 13.370 | 0.314 | 0.061 | 0.372 | 1.440 | 0.083 | 3.56E+03 | 5 |
| 0.194 | 13.457 | 0.227 | 0.038 | 0.262 | 1.450 | 0.083 | 2.84E+03 | 5 |
| 0.243 | 13.525 | 0.159 | 0.024 | 0.180 | 1.460 | 0.082 | 2.27E+03 | 5 |
| 0.305 | 13.578 | 0.106 | 0.015 | 0.118 | 1.470 | 0.082 | 1.81E+03 | 5 |
| 0.382 | 13.618 | 0.066 | 0.009 | 0.073 | 1.490 | 0.081 | 1.45E+03 | 5 |
| 0.478 | 13.644 | 0.040 | 0.007 | 0.044 | 1.500 | 0.080 | 1.15E+03 | 4 |
| 0.599 | 13.665 | 0.019 | 0.004 | 0.021 | 1.520 | 0.079 | 9.22E+02 | 4 |
| 0.750 | 13.684 | 0.000 | 0.003 | 0.000 | 1.550 | 0.077 | 7.36E+02 | 4 |

Table C3 Example of output file from DEFLOW (Continued)

PROBLEM: SIMULATION OF LABORATORY MODEL, TEST2

SEPTEMBER 7, 1984

LOG OF RUN

DATE = 28-OCT-84
TIME = 23:05:55
CPU = 0: 1.12

C.6 Listing of program DEFLOW

 * -DEFLOW- *

FINITE ELEMENT SOLUTION
 TO THE
 COUPLED AXISYMMETRIC DEFORMATION-HEAD LOSS RESPONSE
 RESULTING FROM
 STEADY-STATE, TWO-REGIME, RADIAL FLOW TO OR FROM A WELL
 THROUGH A SERIES OF ROUGH, DEFORMABLE, HORIZONTAL FRACTURES

by

Lee C. Atkinson
 Department of Earth Sciences
 Memorial University of Newfoundland

March 1984

PROGRAM VARIABLES (WITH DIMENSIONS) AND SI UNITS:

| VARIABLE | DESCRIPTION | UNITS |
|-------------|--|--------|
| ----- | ----- | ----- |
| CE | EXIT LOSS COEFFICIENT | [] |
| CL(NFN) | LAMINAR, RADIAL FLOW CORRECTION FACTOR (AFTER MURPHY, 1979) | [] |
| COND | HYDRAULIC CONDUCTIVITY | [M/S] |
| D(NRX,4,4) | ELASTICITY MATRIX OF ROCK LAYER | [Pa] |
| DELTA | AREA OF ROCK ELEMENT | [M**2] |
| DISP(NSN2) | R (I+I-1) AND Z (I+I) COMPONENTS OF DIS- PLACEMENT OF STRUCTURAL NODE I | [M] |
| DISPI(NSN2) | 'BACKGROUND' DISPLACEMENT ATTRIBUTABLE TO TOP BOUNDARY FORCES, GRAVITY (BODY) FORCES, AND HYDROSTATIC PRESSURE | [M] |
| EL | NATURAL LOGARITHM OF LENGTH OF FLOW ELEMENT | [] |
| ELGRAD(NFE) | AVERAGE HYDRAULIC GRADIENT IN FLOW ELEMENT | [] |
| ELVEL(NFE) | AVERAGE FLUID VELOCITY IN FLOW ELEMENT | [M/S] |
| EPSILON | RELATIVE ERROR FOR TESTING CONVERGENCE OF PRESSURE HEADS IN FLOW ROUTINE ITERATION AND DISPLACEMENTS IN STIFFNESS-DEFORMATION ITERATION | - |
| FE(6) | FORCE ARRAY FOR ROCK ELEMENT | [N] |
| FLAGS | EXECUTION CONTROL SIGNALS | - |

C.6 Listing of program DEFLOW (Continued)

```

FLAG          IF .TRUE.
----          -
FLAG1  GRIDGEN USED
FLAG2  MAXFIT EXCEEDED IN FLOW ROUTINE
FLAG3  PRINT OUT ORDERED BECAUSE OF FLAG2
FLAG4  PRINT OUT ORDERED BECAUSE EITHER
        MAXDFIT OR MAXPERT EXCEEDED
FLAG5  AREA OF STRUCTURAL ELEMENT <= 0;
        PROBABLY ERROR IN INPUT; PROGRAM
        TERMINATED WITH ERROR MESSAGE BUT
        WITHOUT PRINT OUT
FLAG6  FRACTURE(S) ASSUMED TO BE RIGID
        AND DEFORMATION ROUTINES BYPASSED
FLAG7  STIFFNESS-DISPLACEMENT ROUTINE
        HAS CONVERGED
FLAG8  PROGRAM HAS RUN TO COMPLETION
FLAG9  HYDROSTATIC CONDITIONS ASSUMED AND
        FLOW ROUTINES BYPASSED
FLAG10 WITHDRAWAL (PUMPING) CONDITIONS:
        INJECTION IF .FALSE.

```

```

FR(LM) = FORCE ARRAY FOR ALL ROCK ELEMENTS          [N]
FPROP(NFRAC, J) = PHYSICAL PROPERTIES OF FRACTURES:
    J=1  INITIAL APERTURE (ASSUMED TO BE UNIFORM; OTHERWISE ASSIGNED
        VALUE OF 0.0 AND READ IN BY INDIVIDUAL NODE)          [MM]
    J=2  MAXIMUM CLOSURE OF FRACTURE (EXPRESSED AS PERCENT OF INITIAL
        APERTURE)                                              [%]
    J=3  ABSOLUTE ROUGHNESS OF SURFACES                      [MM]
    J=4  POROSITY                                             [%]

```

COEFFICIENTS AND EXPONENT WHICH
DEFINE CONSTITUTIVE RELATIONSHIP
FOR NORMAL STIFFNESS IN FORM:

$$\text{SIGMA} = K1 * \text{DZ} + K2 * \text{DZ}^{**N}$$

WHERE DZ = FRACTURE CLOSURE IN [MM]

```

J=5  K1          [GPa/MM]
J=6  K2          [Variable]
J=7  N           [ ]

J= 8  MAXIMUM NORMAL STIFFNESS (CALC-
        ULATED BY PROGRAM USING SECANT
        METHOD)          [GPa/M]
J= 9  TANGENTIAL STIFFNESS FACTOR          [ ]
        (KS = FACTOR x KN)

```

C.6 Listing of program DEFLOW (Continued)

```

C          FW = WELLBORE FRICTION FACTOR
C          G = GRAVITATIONAL CONSTANT (9.80665)
C          GRAD(NFN) = HYDRAULIC GRADIENT AT FLOW NODE
C          HO = HEAD AT OUTER BOUNDARY
C          HW(NFRAC) = HEAD AT WELLBORE RADIUS (1ST TYPE B.C.)
C          IBCOB = CODE FOR LATERAL PRESSURE ON OUTER BOUNDARY
C                  (1=GEOSTATIC , 0=NONE, AS IN CASE OF LABORATORY MODEL)
C          IBCWELL = BOUNDARY CONDITION AT WELL (1=HEAD, 2=FLOW)
C          ICODE(NSN) = CODE INDICATING BOUNDARY CONDITION (LOAD OR
C                  DISPLACEMENT) SPECIFIED AT STRUCTURAL NODE:
C
C          ICODE  R    Z          WHERE
C          -----
C          -3    -    DISP BOTTOM (OTHER THAN CORNERS)
C          -2    LOAD - WELLBORE (OTHER THAN CORNERS)
C          -1    -    LOAD TOP BOUNDARY AND FRACTURES
C                  (OTHER THAN CORNERS)
C          0    LOAD LOAD CORNERS (OTHER THAN AT BOTTOM)
C          1    DISP LOAD NOT PRESENTLY USED
C          2    LOAD DISP BOTTOM CORNERS
C          3    DISP DISP NOT PRESENTLY USED
C
C          IFPAIR(NFRAC, = THE 2 NODES COMPRISING A FRACTURE/FLOW NODE
C                  NFN,2) PAIR
C          INC(NSE,I) = FOR I=1-3, NODAL INCIDENCES OF STRUCTURAL
C                  I=1,4 ELEMENT IN CCW DIRECTION STARTING WITH
C                  LOWEST-NUMBERED NODE; I=4 IS ROCK LAYER
C          IOBN(NRX2) = INCIDENCE OF OUTER BOUNDARY NODE
C          ITBN(NTBN) = INCIDENCE OF TOP BOUNDARY NODE
C          IWBBN(NWWBN) = INCIDENCE OF WELLBORE BOUNDARY NODE
C          KN(NFNT) = NORMAL STIFFNESS AT FLOW/FRACTURE NODE
C          KS(NFNT) = TANGENTIAL STIFFNESS AT FLOW/FRACTURE NODE
C          LAW(NFN) = FLOW LAW (AFTER LOUIS, 1969) BASED ON
C                  FRACTURE ROUGHNESS AND REYNOLDS NUMBER
C                  WHICH GOVERNS FLOW RELATIONSHIP AT NODE
C          LC(NSN2) = CONDENSATION CODE FOR STIFFNESS EQUATION
C          LMS = LENGTH OF CONDENSED STIFFNESS MATRIX AND
C                  FORCE ARRAY
C          MAXDFIT = MAXIMUM NUMBER OF DEFORMATION-FLOW ITERATIONS
C                  ALLOWED
C          MAXFIT = MAXIMUM NUMBER OF ITERATIONS ALLOWED IN FLOW
C                  ROUTINE
C          MAXPERT = MAXIMUM NUMBER OF PERTURBATIONS (ITERATIONS)
C                  ALLOWED IN FRACTURE STIFFNESS/DISPLACEMENT
C                  ROUTINE
C          N1 = LENGTH OF FLOW EQUATION MATRIX AND ARRAY

```


C.6 Listing of program DEFLOW (Continued)

```

C      IF IBCWELL=1 (NFE-1)
C      NDFIT = DEFORMATION-FLOW ITERATION COUNTER -
C      NFE = NUMBER OF FRACTURE-FLOW ELEMENTS PER FRACTURE -
C      NFET = NUMBER OF TOTAL FLOW ELEMENTS (NFRAC x NFE) -
C      NFIT = FLOW ITERATION COUNTER -
C      NFN = NUMBER OF FRACTURE-FLOW NODE PAIRS PER -
C      FRACTURE -
C      NFNT = TOTAL FRACTURE-FLOW NODES (NFRAC x NFN) -
C      NFRAC = NUMBER OF FRACTURES -
C      NOBN = NUMBER OF OUTER BOUNDARY NODES (2 x NRX) -
C      NP = FRACTURE STIFFNESS/DISPLACEMENT ITERATION -
C      COUNTER -
C      NPERT(NDFIT) = NUMBER OF ITERATIONS (PERTURBATIONS) IN -
C      STIFFNESS/DISPLACEMENT ROUTINE IN EACH -
C      DEFORMATION-FLOW FLOW ITERATION -
C      NRX = NUMBER OF ROCK LAYERS -
C      NSE = NUMBER OF STRUCTURAL ELEMENTS -
C      NSN = NUMBER OF STRUCTURAL NODES -
C      NSN2 = 2 x NSN -
C      NTBN = NUMBER OF TOP BOUNDARY NODES -
C      NTWBBN = TOTAL NUMBER OF WELLBORE BOUNDARY NODES -
C      (SUM OF ALL NWBBN(NRX)'S) -
C      NWBBN(NRX) = NUMBER OF WELLBORE BOUNDARY NODES PER ROCK -
C      LAYER -
C      OBLOAD(NOBN) = EFFECTIVE LATERAL LOADS ON OUTER BOUNDARY -
C      NODES -
C      PHEAD(NFRAC, = PRESSURE HEAD (THEAD-VHEAD-ZHEAD) AT FLOW [M]
C      NFN) NODE
C      PHEADI(NFRAC, = PRESSURE HEAD FROM PREVIOUS FLOW LOOP IN [M]
C      NFN) DEFORMATION-FLOW ITERATION
C      PI = 3.1415927 -
C      Q = DISCHARGE OF FRACTURE [M**3/S]
C      R(NSN) = RADIAL COORDINATE OF STRUCTURAL NODE [M]
C      RD = DIMENSIONLESS RADIUS [ ]
C      RE(NFN) = REYNOLDS NUMBER AT FLOW NODE [ ]
C      RELAXF = RELAXATION FACTOR FOR FLOW ITERATION [ ]
C      REO = OVERALL REYNOLDS NUMBER [ ]
C      RHO = DENSITY OF WATER FOR GIVEN TEMPERATURE [KG/M**3]
C      RHODATA(36) = STORED VALUES OF DENSITY OF WATER FOR [KG/M**3]
C      TEMPERATURE RANGE 0-35 DEGREES C
C      RHOG = PRODUCT OF RHO x G [N/M**3]
C      RO = RADIUS OF CONSTANT HEAD OUTER BOUNDARY [M]
C      ROUGH(NFN) = FRACTURE ROUGHNESS (FPROP(I,3)/(2*TWOB(I))) [ ]
C      RPROP(NRX, J) = ROCK PROPERTIES:
C
C      J=1 THICKNESS OF ROCK LAYER [M]
C      J=2 MASS DENSITY [KG/M**3]

```

C.6 Listing of program DEFLOW (Continued)

| | | |
|------------------|---|----------|
| | J=3 YOUNG'S MODULUS | [GPa] |
| | J=4 POISSON'S RATIO | [] |
| RR(NFN) | = GENERAL LOGARITHMIC RADIAL SPACING OF NODES | [M] |
| RW | = RADIUS OF WELL | [M] |
| SA(NFN) | = DRAWDOWN IN FRACTURE (HO-THEAD) AT FLOW NODE | [M] |
| SE(6,6) | = STIFFNESS MATRIX FOR ROCK ELEMENT | [N/M] |
| SEL | = "EXIT LOSS" (HEAD LOSS AS RESULT OF FLUID FLOWING FROM FRACTURE INTO WELLBORE) | [M] |
| SR(NSN2,IBWS) | = STIFFNESS SUB-MATRIX FOR ALL ROCK ELEMENTS | [N/M] |
| SWB(NFRAC) | = HEAD LOSS DUE TO FLOW IN WELLBORE | [M] |
| SWELL | = DRAWDOWN IN WELL [SA(1)+SEL] | [M] |
| TBLOAD(NTBN) | = EFFECTIVE VERTICAL POINT LOADS ON TOP BOUNDARY NODES | [N] |
| TEMP | = TEMPERATURE OF WATER | [DEG,C] |
| THEAD(NFN) | = TOTAL (BERNOULLI) HEAD AT FLOW NODE | [M] |
| THEADI(NFN) | = TOTAL HEAD FROM PREVIOUS ITERATION WITHIN FLOW ROUTINE | [M] |
| TITLE(2) | = IDENTIFIER OF PROBLEM TO BE SOLVED | - |
| TOPRESS | = APPLIED PRESSURE ON TOP BOUNDARY (ASSUMED TO BE UNIFORM AND CONSTANT) | [MPa] |
| TRANS(NFN) | = TRANSMISSIVITY OF FRACTURE AT FLOW NODE | [M**2/S] |
| TWOB(NFN) | = APERTURE OF FRACTURE AT FLOW NODE | [M] |
| | NOTE: INPUT AS FPROP(NFRAC,1) OR TWOBI(NFRAC,NFN) IN [MM] AND CONVERTED TO [M] WITHIN PROGRAM | |
| TWOBI(NFRAC,NFN) | = INITIAL FRACTURE APERTURE AT EACH NODE | [MM] |
| VEL(NFN) | = FLUID VELOCITY AT FLOW NODE | [M/S] |
| VHEAD(NFN) | = VELOCITY HEAD (VEL**2/2G) AT FLOW NODE | [M] |
| VFACTOR | = VELOCITY HEAD FACTOR (1.2 FOR LAMINAR FLOW; 1.0 FOR FULLY TURBULENT FLOW) | [] |
| VHEADWB(NFRAC) | = VELOCITY HEAD IN WELLBORE | [M] |
| VISC | = KINEMATIC VISCOSITY OF WATER FOR GIVEN TEMPERATURE | [M**2/S] |
| VISDATA(36) | = STORED VALUES OF KINEMATIC VISCOSITY OF WATER FOR TEMPERATURE RANGE 0-35 DEGREES C | [M**2/S] |
| WBL | = WELLBORE LENGTH | [M] |
| Z(NSN) | = VERTICAL COORDINATE OF STRUCTURAL NODE | [M] |
| ZHEAD(NFRAC) | = ELEVATION HEAD (DATUM: ZHEAD(1)=0.0) | [M] |

 BEGINNING OF PROGRAM

C.6 Listing of program DEFLOW (Continued)

```

C -----
C BLOCK DATA
C -----
INCLUDE 'PARAM.COM'
INCLUDE 'BOTH.COM'
INCLUDE 'CONSTS.COM'
DATA G/9.80665/,PI/3.1415927/
INCLUDE 'DEFORM.COM'
INCLUDE 'DIMENS.COM'
INCLUDE 'FLAGS.COM'
DATA FLAG1/.FALSE./,FLAG2/.FALSE./,FLAG3/.FALSE./,FLAG4/.FALSE./,
* FLAG5/.FALSE./,FLAG6/.FALSE./,FLAG7/.FALSE./,FLAG8/.FALSE./,
* FLAG9/.FALSE./,FLAG10/.FALSE./
INCLUDE 'FLOW.COM'
INCLUDE 'HEAD.COM'
INCLUDE 'MATEQN.COM'
END

C -----
C PROGRAM DEFLOW
C -----
INCLUDE 'PARAM.COM'
INCLUDE 'BOTH.COM'
INCLUDE 'CONSTS.COM'
INCLUDE 'DEFORM.COM'
INCLUDE 'DIMENS.COM'
INCLUDE 'FLAGS.COM'
INCLUDE 'FLOW.COM'
INCLUDE 'HEAD.COM'
INCLUDE 'MATEQN.COM'

C CHARACTER*8 BCS,ELEMENTS,END,FLOPAIRS,FRACS,GENERAL,GENGRID,
* GOBOTH,GODRILL,GOFLOW,NODES,PRINT,ROCK,WATER,WHAT
CHARACTER*12 DAY,HOUR
CHARACTER*20 FILEIN,ROUTINES
DIMENSION SA(NFND)
INTEGER*4 FINISH,MINS,START,STATUS
REAL NU
REAL*4 CPU,SECS
DATA BCS /'BCS',ELEMENTS/'ELEMENTS'/,
* END /'END',FLOPAIRS/'FLOPAIRS'/,
* FRACS /'FRACS',GENERAL/'GENERAL'/,
* GENGRID /'GENGRID',GOBOTH/'GOBOTH'/,
* GODRILL /'GODRILL',GOFLOW/'GOFLOW'/,
* NODES /'NODES',PRINT/'PRINT'/,
* ROCK /'ROCK',WATER/'WATER'/,
* WHAT /'WHAT'/

```

C.6 Listing of program DEFLOW (Continued)

```

C
C INITIALIZES VAX RUN-TIME LIBRARY TIMING FACILITY
  STATUS=LIB$INIT_TIMER.
  STATUS=LIB$STAT_TIMER(2,START)
C
C *****
C *           INPUT           *
C * (AND RELATED CALCULATED VALUES) *
C *****
C
  WRITE (6,*) 'Enter name of input file.'
  READ (5,1) FILEIN
  WRITE (6,*) 'What name do you want for output file?'
  READ (5,1) FILEOUT
1  FORMAT (A20)
  OPEN (UNIT=2,FILE=FILEIN,STATUS='OLD')
  OPEN (UNIT=3,FILE=FILEOUT,STATUS='NEW')
C
C INPUT FILES ARE ORGANIZED BY CONTROL WORDS
2  READ (2,3) WHAT
3  FORMAT (A8)
  IF (WHAT.EQ.GENERAL ) GO TO 4
  IF (WHAT.EQ.ROCK    ) GO TO 11
  IF (WHAT.EQ.FRACS   ) GO TO 15
  IF (WHAT.EQ.WATER   ) GO TO 19
  IF (WHAT.EQ.GENGRID ) GO TO 21
  IF (WHAT.EQ.NODES   ) GO TO 22
  IF (WHAT.EQ.FLOPAIRS) GO TO 44
  IF (WHAT.EQ.BCS     ) GO TO 47
  IF (WHAT.EQ.ELEMENTS) GO TO 63
  IF (WHAT.EQ.PRINT   ) GO TO 68
  IF (WHAT.EQ.GOFLOW  ) GO TO 124
  IF (WHAT.EQ.GODRILL ) GO TO 125
  IF (WHAT.EQ.GOBOTH  ) GO TO 126
  IF (WHAT.EQ.END     ) GO TO 198
C
C GENERAL SET-UP PARAMETERS AND ITERATION CONTROLS
4  READ (2,5) TITLE(1),TITLE(2)
5  FORMAT (A60,/,A60)
  READ (2,6) NFRAC,NFN
6  FORMAT (2I5)
C (NOTE: NOT NECESSARY TO INPUT NSN AND NSE IF GRIDGEN USED)
  READ (2,7) NRX,NSN,NSE
7  FORMAT (3I5)
  READ (2,8) RW,FW,RO
8  FORMAT (3F10,5)
  READ (2,9) MAXDFIT,MAXFIT,MAXPERT,RELAXF,EPSILON

```

C.6 Listing of program DEFLOW (Continued)

```

9 FORMAT (3I5,5X,2F10.5)
  NFNT=NFRAC*NFN
  NFE=NFN-1
  N1=NFN-2
  NOBN=2*NRX
C
C DIVIDES RADIAL DISTANCE INTO LOGARITHMICALLY-SPACED INTERVALS
  RLOG=ALOG10(RO/RW)/FLOAT(NFN-1)
  RWLOG=ALOG10(RW)
  DO 10 I=1,NFN
    TLOG=RWLOG+FLOAT(I-1)*RLOG
    RR(I)=10.**TLOG
  10 CONTINUE
C
C CALCULATES LENGTH OF FLOW ELEMENTS. IN FORMULATION OF RADIAL FLOW
C USED IN PROGRAM, ELEMENT LENGTH IS ACTUALLY DIFFERENCE IN LN'S OF
C THE RADIAL DISTANCES OF THE TWO NODES COMPRISING ELEMENT. SINCE
C THESE DISTANCES ARE GENERATED ON A LOGARITHMIC SPACING, ALL
C ELEMENT LENGTHS ARE THE SAME.
  EL=ALOG(RR(2)/RR(1))
  GO TO 2
C
C ROCK PROPERTIES
  11 DO 14 I=1,NRX
    READ (2,12) (RPROP(I,J),J=1,4)
    12 FORMAT (F10.5,E10.3,2F10.5)
C FORMS ELASTICITY MATRIX FOR AXISYMMETRIC STRAIN (SEE ZIENKIEWICZ,
C 1971) IN EACH ROCK LAYER
    DO 13 J=1,4
      DO 13 K=1,4
        D(I,J,K)=0.0
    13 CONTINUE
    E=RPROP(I,3)*1.0E+09
    NU=RPROP(I,4)
    D(I,4,4)=E/(1.0+NU)
    COMM=D(I,4,4)/(1.0-2.0*NU)
    D(I,1,1)=(1.0-NU)*COMM
    D(I,2,2)=D(I,1,1)
    D(I,3,3)=D(I,1,1)
    D(I,1,2)=NU*COMM
    D(I,1,3)=D(I,1,2)
    D(I,2,1)=D(I,1,2)
    D(I,2,3)=D(I,1,2)
    D(I,3,1)=D(I,1,2)
    D(I,3,2)=D(I,1,2)
    D(I,4,4)=D(I,4,4)*0.5
  14 CONTINUE

```

c.6 Listing of program DEFLOW (Continued)

```

      GO TO 2
C
C FRACTURE PROPERTIES
15 DO 18 NF=1,NFRAC
    READ (2,16) (FPROP(NF,J),J=1,4)
16 FORMAT (4F10.5)
    READ (2,17) (FPROP(NF,J),J=5,7),FPROP(NF,9)
17 FORMAT (2E10.2,2F10.5)
C IF INITIAL FRACTURE APERTURES NOT UNIFORM, READS IN VALUES FOR EACH
C NODE
    IF (FPROP(NF,1).EQ.0.0) GO TO 1701
    GO TO 1703
1701 READ (2,1702) (TWOB I(NF,I),I=1,NFN)
1702 FORMAT (5F10.3)
    CLOSMAX=TWOB I(NF,NFN)*FPROP(NF,2)*1.0E-02
    GO TO 1704
C CALCULATES MAXIMUM NORMAL STIFFNESS
1703 CLOSMAX=FPROP(NF,1)*FPROP(NF,2)*1.0E-02
1704 SIGMA=FPROP(NF,5)*CLOSMAX+FPROP(NF,6)*CLOSMAX**FPROP(NF,7)
    FPROP(NF,8)=SIGMA/CLOSMAX*1.0E+03
18 CONTINUE
    GO TO 2
C
C WATER PROPERTIES
19 READ (2,20) TEMP
20 FORMAT (F10.5)
C DETERMINES KINEMATIC VISCOSITY AND DENSITY OF WATER FOR GIVEN
C TEMPERATURE
C -----
    CALL VISCRHO
C -----
    GO TO 2
C
C OPTIONAL GRID GENERATOR (ONLY CAN BE USED IF NFRAC=1); ASSIGNS NODAL
C COORDINATES, FLOW NODE PAIRS, ELEMENT INCIDENCES AND MATERIAL TYPES,
C AND BOUNDARY CONDITION CODES
C -----
21 CALL GRIDGEN
C -----
    FLAG1=.TRUE.
    GO TO 25
C
C NODAL BOUNDARY CONDITIONS AND COORDINATES (IF GRIDGEN NOT USED)
22 DO 24 I=1,NSN
    READ (2,23) J,ICODE(J),R(J),Z(J)
23 FORMAT (2I5,2F10.5)
24 CONTINUE

```

C.6 Listing of program DEFLOW (Continued)

```

C INITIALIZES ALL DISPLACEMENTS AND LOADS TO 0
 25 NSN2=2*NSN
    DO 26 I=1,NSN2
      DISP(I)=0.0
      DISPI(I)=0.0
      B(I)=0.0
 26 CONTINUE
C CONDENSATION CODE USED IN SUBROUTINE 'DEFORM' TO ASSEMBLE CONDENSED
C STIFFNESS MATRIX EQUATION
  IF (ICOD(1).EQ.1.OR.ICOD(1).EQ.3) GO TO 27
  LC(1)=0
  GO TO 28
 27 LC(1)=1
 28 IF (ICOD(1).EQ.-3.OR.ICOD(1).GE.2) GO TO 29
  LC(2)=LC(1)
  GO TO 30
 29 LC(2)=LC(1)+1
 30 DO 43 I=2,NSN
    I2=I+I
    I1=I2-1
    IF (ICOD(I).EQ.0) GO TO 31
    GO TO 37
 31 ASSIGN 40 TO NEXT
    GO TO 33
 32 ASSIGN 41 TO NEXT
 33 LC(I1)=LC(I1-1)
    GO TO NEXT, (40,41)
 34 ASSIGN 40 TO NEXT
    GO TO 36
 35 ASSIGN 41 TO NEXT
 36 LC(I1)=LC(I1-1)+1
    GO TO NEXT, (40,41)
 37 IF (IABS(ICOD(I))-2) 38,39,42
 38 IF (ICOD(I).GT.0) GO TO 34
    GO TO 31
 39 IF (ICOD(I).GT.0) GO TO 32
    GO TO 31
 40 LC(I2)=LC(I1)
    GO TO 43
 41 LC(I2)=LC(I1)+1
    GO TO 43
 42 IF (ICOD(I).GT.0) GO TO 35
    GO TO 32
 43 CONTINUE
C CALCULATES LENGTH OF STIFFNESS MATRIX AND FORCE ARRAY
  LMS=NSN2-LC(NSN2)
  IF (FLAG1) GO TO 66

```

C.6 Listing of program DEFLOW (Continued)

```

      GO TO 2
C
C READS IN FRACTURE-FLOW NODE PAIRS
  44 DO 46 I=1,NFRAC
      DO 46 J=1,NFN
          READ (2,45) K,IFPAIR(I,K,1),IFPAIR(I,K,2)
  45 FORMAT (3I5)
  46 CONTINUE
      GO TO 2
C
C BOUNDARY CONDITIONS
C
C BOUNDARY CONDITIONS FOR FLOW
C IF NFRAC=1, IBCWELL CAN BE 1 OR 2
C IF NFRAC>1, IBCWELL CAN BE 1 ONLY
  47 READ (2,48) IBCWELL,HW(1),Q,HO
  48 FORMAT (I5,5X,3F10.5)
C DETERMINES IF WITHDRAWAL (PUMPING) OR INJECTION
  IF (IBCWELL-1.GT.0) GO TO 481
C 1ST TYPE BOUNDARY CONDITION AT WELL
  IF (HW(1).GT.HO) GO TO 483
  FLAG1=.TRUE.
  GO TO 483
C 2ND TYPE BOUNDARY CONDITION AT WELL
  481 IF (Q.GT.0.0) GO TO 482
      Q=-Q
      GO TO 483
  482 FLAG1=.TRUE.
  483 HWSTOR=HW(1)
C CALCULATES ELEVATION HEADS
  ZHEAD(1)=0.0
  IF (NFRAC.EQ.1) GO TO 50
  DO 49 NF=1,NFRAC-1
      ZHEAD(NF+1)=ZHEAD(NF)+RPROP(NF+1,1)
  49 CONTINUE
C ASSIGNS HYDROSTATIC HEADS AS INITIAL PRESSURE HEADS.
  50 DO 51 NF=1,NFRAC
      SWB(NF)=0.0
      HW(NF)=HO
C NOTE: THE VALUE OF HW(1) WILL HAVE TO BE RE-ASSIGNED TO THE
C INPUT BOUNDARY CONDITION VALUE USING HWSTOR BEFORE DOING
C ANY FLOW CALCULATIONS
  VHEADWB(NF)=0.0
  DO 51 L=1,NFN
      PHEADI(NF,L)=HO-ZHEAD(NF)
  51 CONTINUE
      IF (FLAG1) GO TO 56

```


C.6 Listing of program DEFLOW (Continued)

```

C
C BOUNDARY CONDITIONS FOR DEFORMATION
C IF GRIDGEN USED, NOT NECESSARY TO READ IN ANYTHING BUT 'TOPRESS'
  K=0
  DO 54 I=1,NRX
    I2=I+I
    I1=I2-1
C WELLBORE BOUNDARY NODES
  READ (2,52) NWBBN(I),(IWBBN(K+J),J=1,NWBBN(I))
  52 FORMAT (15I5)
  K=K+NWBBN(I)
C OUTER BOUNDARY NODES
  READ (2,53) IOBN(I1),IOBN(I2)
  53 FORMAT (2I5)
  54 CONTINUE
  NTWBBN=K
C TOP BOUNDARY NODES
  READ (2,55) NTBN,(ITBN(I),I=1,NTBN)
  55 FORMAT (15I5)
C OUTER BOUNDARY CODE AND APPLIED PRESSURE ON TOP BOUNDARY
  56 READ (2,57) IBCOB,TOPRESS
  57 FORMAT (I5,F10.5)
C
C CALCULATES EFFECTIVE VERTICAL POINT LOADS (IN N) ON TOP BOUNDARY NODES
C NOTE: THESE REMAIN CONSTANT
C THE 2*PI TERM HAS NOT BEEN INCLUDED SINCE IT APPEARS ON BOTH SIDES OF
C THE STIFFNESS EQUATION AND CAN BE CANCELLED OUT.
  DO 58 I=1,NTBN
    TBLOAD(I)=0.0
  58 CONTINUE
  DO 59 J=1,NTBN-1
    K=ITBN(J)
    L=ITBN(J+1)
    RES=0.5*TOPRESS*1.0E+06*(R(L)+R(K))*(R(L)-R(K))
    SUMOM=(TOPRESS*1.0E+06*(R(L)-R(K))*(R(L)**2+R(L)*R(K)+R(K)**2))/3.
  *0
    CENT=SUMOM/RES
    F2=RES*(CENT-R(K))/(R(L)-R(K))
    F1=RES-F2
    TBLOAD(J)=TBLOAD(J)+F1
    TBLOAD(J+1)=TBLOAD(J+1)+F2
  59 CONTINUE
  DO 60 I=1,NTBN
    J=2*ITBN(I)
    B(J)=TBLOAD(I)
  60 CONTINUE
C

```

C.6 Listing of program DEFLOW (Continued)

```

C CALCULATES EFFECTIVE GEOSTATIC LATERAL POINT LOADS (IN N) ON OUTER
C BOUNDARY NODES (NOTE: THESE ALSO REMAIN CONSTANT). THE 2*PI TERMS
C ALSO LEFT OUT HERE.
  M=NOBN
  P1=TOPRESS*1.0E+06*RPROP(NRX,4)/(1.0-RPROP(NRX,4))
  DO 61 I=1,NRX
    J=NRX-I+1
    DELTAP=RPROP(J,1)*RPROP(J,2)*G*RPROP(J,4)/(1.0-RPROP(J,4))
    OBLOAD(M)=-RPROP(J,1)*FLOAT(IBC0B)/6.0*(3.0*P1+DELTAP)*RO
    OBLOAD(M-1)=-RPROP(J,1)*FLOAT(IBC0B)/6.0*(3.0*P1+2.0*DELTAP)*RO
    P1=P1+DELTAP
    M=M-2
  61 CONTINUE
  DO 62 I=1,NOBN
    J=2*IOBN(I)-1
    B(J)=OBLOAD(I)
  62 CONTINUE
C
C CALCULATES INITIAL HYDROSTATIC LOADS ON FLOW NODES AND GEOSTATIC
C LOADS ON TO-BE WELLBORE NODES
  NDFIT=-1
C
  -----
  CALL BLOADS
  -----
C
  GO TO 2
C
C NODAL INCIDENCES OF STRUCTURAL ELEMENTS (MUST BE INPUT IN CCW
C DIRECTION STARTING WITH LOWEST NUMBERED NODE) AND MATERIAL TYPE
  63 DO 65 I=1,NSE
    READ (2,64) J,(INC(J,K),K=1,4)
  64 FORMAT (5I5)
  65 CONTINUE
C
C CALCULATES HALF-BANDWIDTH OF STIFFNESS MATRIX
  66 IBWS=0
  DO 67 N=1,NSE
    I2=2*INC(N,1)
    J2=2*INC(N,2)
    K2=2*INC(N,3)
    IBWTEMP=MAXO(IABS(I2-1-LC(I2-1)-J2+LC(J2)),IABS(I2-1-LC(I2-1)-K2+L
    *C(K2)),IABS(J2-1-LC(J2-1)-K2+LC(K2)))+1
    IF (IBWTEMP.GT.IBWS) IBWS=IBWTEMP
  67 CONTINUE
  GO TO 2
C
C
C
  *****

```

C.6 Listing of program DEFLOW (Continued)

```

C          * PRINT OUT OF INPUT *
C          *****
C
C HEADER
  68 WRITE (3,69) TITLE(1),TITLE(2)
  69 FORMAT (1H1,///,29X,'ANALYSIS',/,30X,'OF THE',/,8X,'COUPLED AXISYM
    *METRIC DEFORMATION-DRAWDOWN RESPONSE',/,26X,'RESULTING FROM',/,9X,
    *'STEADY-STATE, TWO-REGIME, RADIAL FLOW TO A WELL',/,3X,'THROUGH A
    *SERIES OF ROUGH, DEFORMABLE, HORIZONTAL FRACTURES',/,30X,'USING',/
    */,25X,16(1H*),/,25X,1H*,3X,'-DEFLOW-',3X,1H*,/,25X,16(1H*),/////;1
    *X,'PROBLEM:',1X,A60,/,10X,A60,/)
C
C GENERAL SET-UP PARAMETERS
  WRITE (3,70) NFRAC,NFN,NRX,NSN,NSE,RW,RO,FW
  70 FORMAT (1X,'GENERAL SET-UP PARAMETERS:',/,5X,'NUMBER OF FRACTURES
    * ',32(1H-),I4,/,5X,'NUMBER OF FLOW NODE PAIRS PER FRACTURE ',13(1H
    * -),I4,/,5X,'NUMBER OF ROCK UNITS ',31(1H-),I4,/,5X,'NUMBER OF STRU
    * CTURAL NODES ',25(1H-),I4,/,5X,'NUMBER OF STRUCTURAL ELEMENTS ',22
    * (1H-),I4,///,1X,'DIMENSIONS:',/,5X,'RADIUS OF WELL (M) ',33(1H-),
    * F8.3,/,5X,'RADIUS OF CONSTANT HEAD OUTER BOUNDARY (M) ',9(1H-),F8.
    * 3,/,5X,'WELLBORE FRICTION FACTOR',27(1H-),F8.3)
C
C BOUNDARY CONDITIONS
  IF (IBCWELL.EQ.2) GO TO 72
  WRITE (3,71) HWSTOR,HO,TOPRESS
  71 FORMAT (//,1X,'BOUNDARY CONDITIONS:',/,5X,'BOUNDARY CONDITION AT
    *WELL ',25(1H-),3X,'HEAD',/,5X,'HEAD AT WELL RADIUS IN LOWEST FRACT
    *URE (M) ',9(1H-),F8.3,/,5X,'HEAD AT OUTER BOUNDARY (M) ',25(1H-),F
    *7.3,/,5X,'PRESSURE ON TOP BOUNDARY (MPa) ',21(1H-),F8.3)
    GO TO 74
  72 WRITE (3,73) Q,HO,TOPRESS
  73 FORMAT (//,1X,'BOUNDARY CONDITIONS:',/,5X,'BOUNDARY CONDITION AT
    *WELL ',25(1H-),' FLUX',/,5X,'WELL DISCHARGE (M**3/S) ',28(1H-),3
    *X,1PE9.3,/,5X,'HEAD AT OUTER BOUNDARY (M) ',25(1H-),1X,OPF7.3,/,5X
    *,'PRESSURE ON TOP BOUNDARY (MPa) ',21(1H-),F8.3)
C
C ITERATION CONTROLS
  74 WRITE (3,75) RELAXF,EPSILON,MAXFIT,MAXDFIT,MAXPERT
  75 FORMAT (//,1X,'ITERATION CONTROLS:',/,5X,'RELAXATION FACTOR FOR F
    *LOW ITERATION ',15(1H-),F7.2,/,5X,'RELATIVE ERROR FOR TESTING OF C
    *ONVERGENCE ',10(1H-),F7.2,/,5X,'MAXIMUM ITERATIONS ALLOWED IN FLOW
    * ROUTINE ',9(1H-),I4,/,5X,'MAXIMUM DEFORMATION-FLOW ITERATIONS ALL
    *OWED ',8(1H-),I4,/,5X,'MAXIMUM FRACTURE STIFFNESS PERTURBATIONS AL
    *LOWED ',3(1H-),I4)

```

C.6 Listing of program DEFLOW (Continued)

C MATERIAL PROPERTIES

C ROCK

```

WRITE (3,76) TITLE(1),TITLE(2)
76 FORMAT (1H1,///,1X,'PROBLEM:',1X,A60,/,10X,A60,///,28X,'MATERIAL P
*ROPERTIES',/,28X,19(1H-),////,1X,'ROCK:',/,45X,'ROCK LAYER',/,35X,
*'1',9X,'2',9X,'3',9X,'4',/)
WRITE (3,77) (RPROP(J,1),J=1,NRX)
77 FORMAT (4X,'THICKNESS (M)',1X,11(1H-),3X,4(F4.2,6X))
WRITE (3,78) (RPROP(J,2),J=1,NRX)
78 FORMAT (4X,'MASS DENSITY (KG/M**3)',1X,2(1H-),3X,1PE8.2,2X,E8.2,2X
*,E8.2,2X,E8.2)
WRITE (3,79) (RPROP(J,3),J=1,NRX)
79 FORMAT (4X,7HYOUNG'S,' MODULUS (GPa)',1X,3(1H-),2X,4(F4.1,6X))
WRITE (3,80) (RPROP(J,4),J=1,NRX)
80 FORMAT (4X,9HPOISSON'S,' RATIO',1X,9(1H-),2X,4(1X,F4.2,5X))

```

C

C FRACTURES

```

WRITE (3,81)
81 FORMAT (///,1X,'FRACTURES:',/,48X,'FRACTURE NO.',/,43X,'1',9X,'2',
*9X,'3',/)
WRITE (3,82) (FPROP(J,1),J=1,NFRAC)
82 FORMAT (4X,'INITIAL APERTURE * (MM)',1X,9(1H-),3X,3(F5.3,5X))
WRITE (3,83) (FPROP(J,2),J=1,NFRAC)
83 FORMAT (4X,'MAXIMUM CLOSURE (%)',1X,13(1H-),2X,3(F4.1,6X))
WRITE (3,84) (FPROP(J,3),J=1,NFRAC)
84 FORMAT (4X,'ABSOLUTE ROUGHNESS (MM)',1X,9(1H-),3X,3(F5.3,5X))
WRITE (3,85) (FPROP(J,4),J=1,NFRAC)
85 FORMAT (4X,'POROSITY (%)',1X,20(1H-),1X,3(F5.1,6X))
WRITE (3,86) (FPROP(J,5),J=1,NFRAC)
86 FORMAT (4X,'NORMAL STIFFNESS: K1 (GPa/MM)',1X,3(1H-),2X,1PE9.2,1X,
*E9.2,1X,E9.2)
WRITE (3,87) (FPROP(J,6),J=1,NFRAC)
87 FORMAT (22X,'K2 (**)',1X,7(1H-),3X,1PE8.2,2X,E8.2,2X,E8.2)
WRITE (3,88) (FPROP(J,7),J=1,NFRAC)
88 FORMAT (22X,'N ( )',1X,9(1H-),3X,3(F4.2,6X))
WRITE (3,89) (FPROP(J,9),J=1,NFRAC)
89 FORMAT (4X,'TANGENTIAL STIFFNESS FACTOR',1X,5(1H-),3X,3(F4.2,6X))
WRITE (3,90)
90 FORMAT (/,5X,'* If 0.0, non-uniform (see output for individual',/,
*7X,'nodal aperture values)',/,4X,'** Units dependent on value of n
*')

```

C

C WATER

```

WRITE (3,91) TEMP,VISC,RHO
91 FORMAT (///,1X,'WATER:',/,4X,'TEMPERATURE (DEGREES C)',9(1H-),2X
*,F4.1,/,4X,'KINEMATIC VISCOSITY (M**2/S)',4(1H-),3X,1PE8.2,/,4X,'
*MASS DENSITY (KG/M**3)',10(1H-),3X,E8.2,/)

```

C.6 Listing of program DEFLOW (Continued)

```

C
C NODE INFORMATION
C COORDINATES, BC CODES, AND INITIAL BC'S
  WRITE (3,92) TITLE(1),TITLE(2)
92 FORMAT (1H1,///,1X,'PROBLEM:',1X,A60,/,10X,A60,///,29X,'NODE INFOR
*MATION',/,29X,16(1H-),////,36X,'INITIAL BOUNDARY CONDITIONS',/,12X
*, 'R',8X,'Z',18X,'R',19X,'Z',/,2X,'NODE',4X,'COORD',4X,'COORD',3X,'
*BC',5X,'LOAD',5X,'DISPL',6X,'LOAD',5X,'DISPL',/,1X,'NUMBER',4X,'(M
*)',6X,'(M)',3X,'CODE',4X,'(N)',7X,'(M)',7X,'(N)',7X,'(M)',/,1X,6(1
*H-),3X,5(1H-),4X,5(1H-),2X,4(1H-),4X,4(1H-),5X,5(1H-),6X,4(1H-),5X
*,5(1H-),/)
  DO 107 I=1,NSN
    I2=I+I
    I1=I2-1
    IF (ICODE(I).EQ.0) GO TO 93
    IF (IABS(ICODE(I))-2) 95,99,103
C FOR ICODE(I)=0
  93 WRITE (3,94) I,R(I),Z(I),ICODE(I),B(I1),B(I2)
  94 FORMAT (1X,I4,3X,F7.3,2X,F7.3,4X,I1,2X,1PE9.2,11X,E9.2)
    GO TO 107
  95 IF (ICODE(I).GT.0) GO TO 97
C FOR ICODE=-1
  WRITE (3,96) I,R(I),Z(I),ICODE(I),B(I2)
  96 FORMAT (1X,I4,3X,F7.3,2X,F7.3,3X,I2,15X,'0.0',4X,1PE9.2)
    GO TO 107
C FOR ICODE(I)=1
  97 WRITE (3,98) I,R(I),Z(I),ICODE(I),B(I2)
  98 FORMAT (1X,I4,3X,F7.3,2X,F7.3,3X,I1,15X,'0.0F',3X,1PE9.2)
    GO TO 107
  99 IF (ICODE(I).GT.0) GO TO 101
C FOR ICODE=-2
  WRITE (3,100) I,R(I),Z(I),ICODE(I),B(I1)
  100 FORMAT (1X,I4,3X,F7.3,2X,F7.3,3X,I2,2X,1PE9.2,24X,'0.0')
    GO TO 107
C FOR ICODE(I)=2
  101 WRITE (3,102) I,R(I),Z(I),ICODE(I),B(I1)
  102 FORMAT (1X,I4,3X,F7.3,2X,F7.3,4X,I1,2X,1PE9.2,24X,'0.0F')
    GO TO 107
  103 IF (ICODE(I).GT.0) GO TO 105
C FOR ICODE=-3
  WRITE (3,104) I,R(I),Z(I),ICODE(I)
  104 FORMAT (1X,I4,3X,F7.3,2X,F7.3,3X,I2,15X,'0.0',16X,'0.0F')
    GO TO 107
C FOR ICODE(I)=3
  105 WRITE (3,106) I,R(I),Z(I),ICODE(I)
  106 FORMAT (1X,I4,3X,F7.3,2X,F7.3,3X,I1,15X,'0.0F',16X,'0.0F')
  107 CONTINUE

```

C.6 Listing of program DEFLOW (Continued)

```

WRITE (3,108)
108 FORMAT (/,1X,20(1H-),//,1X,'BOUNDARY CONDITION CODES:',11X,'SIGN C
*ONVENTION:',//,6X,'CODE',6X,'R',10X,'Z',13X,'R+ RADIALLY OUTWARD',
*/,6X,4(1H-),5X,4(1H-),7X,4(1H-),11X,'Z+ DOWNWARD',//,7X,'-3',7X,'-
*',9X,'DISP',/,7X,'-2',6X,'LOAD',8X,'-',/,7X,'-1',7X,'-',9X,'LOAD',
*/,8X,'0',6X,'LOAD',7X,'LOAD',/,8X,'1',6X,'DISP',7X,'LOAD',/,8X,'2'
*,6X,'LOAD',7X,'DISP',/,8X,'3',6X,'DISP',7X,'DISP',//,3X,'F INDICAT
*ES FIXED DISPLACEMENT')
C
C FLOW NODE PAIRS
WRITE (3,109) TITLE(1),TITLE(2)
109 FORMAT (1H1,///,1X,'PROBLEM:',1X,A60,/,10X,A60,///,23X,'NODE INFOR
*MATION (CONT.)',/,23X,24(1H-),////,14X,'FLOW PAIRS:',4X,'FRACTURE',
*4X,'FLOW',/,30X,'NUMBER',5X,'PAIR',6X,'NODES',/,29X,8(1H-),4X,4(1H
*-),6X,5(1H-),/)
DO 113 I=1,NFRAC
DO 111 J=1,NFN
WRITE (3,110) I,J,IFPAIR(I,J,1),IFPAIR(I,J,2)
110 FORMAT (31X,I2,9X,I2,6X,I3,1X,I3)
111 CONTINUE
WRITE (3,112)
112 FORMAT (1H0)
113 CONTINUE
C
C TOP BOUNDARY NODES
WRITE (3,114) ((N,ITBN(N)),N=1,NTBN)
114 FORMAT (/,6X,'TOP BOUNDARY NODES:',8X,'NO.',5X,'NODE',/,33X,3(1H-)
*,5X,4(1H-),//,15(33X,I2,6X,I3,/)
C
C WELLBORE BOUNDARY NODES
WRITE (3,115)
115 FORMAT (//,1X,'WELLBORE BOUNDARY NODES:',4X,'ROCK',/,29X,'LAYER',4
*X,'NUMBER',4X,'NODE',/,29X,5(1H-),4X,6(1H-),4X,4(1H-),/)
K=0
DO 119 I=1,NRX
N=NWBBN(I)
DO 117 J=1,N
WRITE (3,116) I,J,IWBBN(K+J)
116 FORMAT (30X,I2,8X,I2,6X,I3)
117 CONTINUE
WRITE (3,118)
118 FORMAT (1H0)
K=K+NWBBN(I)
119 CONTINUE
C
C OUTER BOUNDARY NODES
WRITE (3,120) ((N,IOBN(N)),N=1,NOBN)

```

C.6 Listing of program DEFLOW (Continued)

```

120 FORMAT (/ ,4X, 'OUTER BOUNDARY NODES:', 6X, 'NO.', 5X, 'NODE', / , 31X, 3(1H
* -), 5X, 4(1H-), //, 8(31X, I2, 6X, I3, /))
C
C ELEMENT INFORMATION
WRITE (3,121) TITLE(1), TITLE(2), IBWS
121 FORMAT (1H1, ///, 1X, 'PROBLEM:', 1X, A60, /, 10X, A60, ///, 27X, 'ELEMENT IN
*FORMATION', /, 27X, 19(1H-), ///, 5X, 'HALF-BANDWIDTH OF STIFFNESS MATR
*IX = ', I2, ///, 17X, 'ROCK', 11X, 'INCIDENCES', /, 5X, 'ELEMENT', 5X, 'LAYER
*', 8X, '1', 5X, '2', 5X, '3', /, 5X, 7(1H-), 5X, 5(1H-), 7X, 3(3(1H-), 3X), /)
DO 123 I=1, NSE
WRITE (3,122) I, INC(I,4), (INC(I,J), J=1,3)
122 FORMAT (6X, I3, 9X, I2, 5X, 3(3X, I3))
123 CONTINUE
GO TO 2

C
C
C
C
C
C *****
C * START OF PROGRAM EXECUTION *
C *****
C
C
C FRACTURE(S) IS/ARE CONSIDERED TO BE RIGID AND DEFORMATION-RELATED
C ROUTINES WILL BE BYPASSED
124 FLAG6=.TRUE.
ROUTINES='FLOW ONLY'
GO TO 130

C
C HYDROSTATIC CONDITIONS ARE ASSUMED AND FLOW ROUTINES WILL BE
C BYPASSED. THIS OPTION ESSENTIALLY SIMULATES EFFECTS OF INSTANT-
C ANEOUS DRILLING OF WELLBORE
125 FLAG9=.TRUE.
ROUTINES='DEFORMATION ONLY'
GO TO 127

C
C FRACTURE(S) IS/ARE CONSIDERED TO BE DEFORMABLE, SO BOTH FLOW AND
C DEFORMATION ROUTINES WILL BE UTILIZED AND ARE COUPLED WITH 'PHEAD'
C AS THE LINKING PARAMETER. BEFORE GOING THROUGH FLOW ROUTINE, FIRST
C CALCULATES DISPLACEMENTS DUE TO DRILLING OF WELLBORE
126 ROUTINES='FLOW & DEFORMATION'
127 NDFIT=-1
NP=0
GO TO 141

C
C CALCULATES RADIAL DISTANCE-HEAD DISTRIBUTION IN FRACTURE(S) FOR
C GIVEN APERTURES
130 QSUM=0.0
HW(1)=HWSTOR
DO 135 NF=1, NFRAC
DO 131 L=1, NFN

```

C.6 Listing of program DEFLOW (Continued)

```

      K=2*IFPAIR(NF,L,1)
      J=2*IFPAIR(NF,L,2)
      IF (FPROP(NF,1).EQ.0.0) GO TO 1301
      TWOB(L)=FPROP(NF,1)/1000.+DISP(K)-DISP(J)
      GO TO 1302
1301 TWOB(L)=TWOB1(NF,L)/1000.+DISP(K)-DISP(J)
1302 ROUGH(L)=FPROP(NF,3)/(2000.*TWOB(L))
131 CONTINUE
C -----
      CALL FLO2REG
C -----
      IF (FLAG3.OR.FLAG4) GO TO 132
      IF (FLAG2) GO TO 186
132 DO 133 L=1,NFN
      SA(L)=ABS(HO-THEAD(L))
      VFACTOR=1.0
      IF (LAW(L).EQ.1.OR.LAW(L).EQ.4) VFACTOR=1.2
      VHEAD(L)=VFACTOR*VEL(L)**2/(2.0*G)
      PHEAD(NF,L)=THEAD(L)-VHEAD(L)-ZHEAD(NF)
133 CONTINUE
C IF 1ST TYPE BOUNDARY CONDITION AT WELL, CALCULATES VOLUMETRIC FLUX
C FROM 2ND EQUATION OF PARTITIONED MATRIX EQUATION. THIS IS NOTHING
C BUT THE THIEM EQUATION (A VERSION OF THE CONTINUITY EQUATION).
C NECESSARY TO DIVIDE BY POROSITY TO ACCOUNT FOR DIFFERENCE BETWEEN
C GEOMETRIC APERTURE AND EFFECTIVE APERTURE.
      IF (IBCWELL.EQ.1)
      *Q=2.0*PI*(TRANS(2)+TRANS(1))*ABS(THEAD(2)-THEAD(1))/(2.0*EL*FPROP(
      *NF,4)/100.0)
      QSUM=QSUM+Q
      IF (FLAG10) GO TO 1331
      GO TO 1332
C ESTIMATES EXIT LOSS USING RELATIONSHIP DERIVED FROM DATA GIVEN IN
C MURPHY AND PEARCE (1980)
1331 CE=0.23*(2.0*RW/TWOB(1))**1.41
      SEL=CE*Q**2/(2.0*G*PI**2*RW**4)
      SWELL=SA(1)+SEL
C CALCULATES WELLBORE FLOW LOSS USING DARCY-WEISBACH EQUATION
C FIRST SUBTRACTS LENGTH INCLUDED IN EXIT LOSS
      WBL=RPROP(NF+1,1)-10.0*RW
      IF (WBL.LT.0.0) WBL=0.0
      SWB(NF)=FW*WBL*QSUM**2/(4.0*G*PI**2*RW**5)
      THEADWB=THEAD(1)-SEL
      VHEADWB(NF)=1.0/(2.0*G)*(QSUM/(PI*RW**2))**2
      PHEADWB=THEADWB-VHEADWB(NF)
1332 IF (FLAG3.OR.FLAG4.OR.FLAG6.OR.FLAG8) GO TO 160
134 CONTINUE
135 CONTINUE

```


C.6 Listing of program DEFLOW (Continued)

```

IF (FLAG3.OR.FLAG4) GO TO 198
IF (FLAG6.OR.FLAG8) GO TO 184
IF (NDFIT.EQ.0) GO TO 138
C
C CHECKS FOR CONVERGENCE (USING RELATIVE CRITERION) OF PRESSURE
C HEAD VALUES
DO 136 NF=1,NFRAC
DO 136 L=1,NFN
RELCONV=ABS((PHEAD(NF,L)-PHEADI(NF,L))/PHEAD(NF,L))
IF (RELCONV.GT.EPSILON) GO TO 137
136 CONTINUE
FLAG8=.TRUE.
GO TO 130
137 IF (NDFIT.LT.MAXDFIT) GO TO 138
GO TO 189
C
C REASSIGNS 'PRESENT' VALUES OF PRESSURE HEAD TO 'PREVIOUS' VALUES
C BEFORE STARTING NEXT ITERATION
138 DO 139 NF=1,NFRAC
DO 139 L=1,NFN
PHEADI(NF,L)=PHEAD(NF,L)
139 CONTINUE
C
C DETERMINES DISPLACEMENTS IN FRACTURED ROCK MASS DUE TO DRILLING
C OF WELLBORE OR TO CHANGES IN EFFECTIVE STRESS RESULTING FROM FLOW.
C RESPONSE OF FRACTURE IS NON-LINEAR AND MUST BE SOLVED BY SUCCESSIVE
C APPROXIMATIONS.
140 NDFIT=NDFIT+1
NP=0
141 NP=NP+1
DO 142 N=1,NSN2
B(N)=0.0
142 CONTINUE
C
C ASSIGNS 2ND TYPE (FORCE) BOUNDARY CONDITIONS TO FORCE ARRAY
C CONSTANT VERTICAL LOADS (IN N) ON TOP BOUNDARY NODES CAUSED BY
C APPLIED PRESSURE
143 DO 144 I=1,NTBN
J=2*ITBN(I)
B(J)=TBLOAD(I)
144 CONTINUE
C CONSTANT GEOSTATIC LATERAL LOADS (IN N) ON OUTER BOUNDARY NODES
DO 145 I=1,NOBN
J=2*IOBN(I)-1
B(J)=OBLOAD(I)
145 CONTINUE
C CALCULATES VARIABLE VERTICAL LOADS ON FRACTURE-FLOW NODES AND

```

C.6 Listing of program DEFLOW (Continued)

```

C LATERAL LOADS ON WELLBORE NODES (IN N)
C -----
C   CALL BLOADS
C -----
C
C CONDENSES FORCE ARRAY
  K=0
  DO 153 I=1,NSN
    I2=I+I
    I1=I2-1
    IF (ICODE(I).EQ.0) GO TO 146
    GO TO 147
146 B(K+1)=B(I1)
    B(K+2)=B(I2)
    K=K+2
    GO TO 153
147 IF (IABS(ICODE(I))-2) 148,149,151
148 IF(ICODE(I).GT.0) GO TO 150
    GO TO 146
149 IF(ICODE(I).GT.0) GO TO 152
    GO TO 146
150 B(K+1)=B(I2)
    K=K+1
    GO TO 153
151 IF (ICODE(I).GT.0) GO TO 153
152 B(K+1)=B(I1)
    K=K+1
153 CONTINUE
C
C -----
C   CALL DEFORM
C -----
C
C   IF (FLAG5) GO TO 195
C
C MODIFIES FRACTURE STIFFNESS IF NECESSARY
C -----
C   CALL STIFFEN
C -----
C DETERMINES WHETHER TO CONTINUE ITERATING BETWEEN DEFORM-STIFFEN
C ROUTINES, PROCEED TO FLOW ROUTINE, OR QUIT
  IF (FLAG7.AND.NDFIT.LT.0) GO TO 158
  IF (FLAG7) GO TO 154
  IF (NP.LT.MAXPERT) GO TO 141
  NPERT(NDFIT+2)=NP
  GO TO 192
C
C DETERMINES NET DISPLACEMENT (I.E., TOTAL DISPLACEMENT CALCULATED LESS

```

C.6 Listing of program DEFLOW (Continued)

```

C 'BACKGROUND' DISPLACEMENT)
154 DO 155 I=1,NSN2
    DISP(I)=DISP(I)-DISPI(I)
155 CONTINUE
    IF (NDFIT.GT.0) GO TO 156
    NPERT(2)=NP
    GO TO 157
156 NPERT(NDFIT+2)=NP
157 IF (FLAG9) GO TO 161
    GO TO 130

```

```

C
C IF FIRST TIME THROUGH DEFORMATION ROUTINE, RE-ASSIGNS DISPLACEMENTS
C TO 'BACKGROUND' (I.E., THOSE WHICH CAN BE ATTRIBUTED TO EXISTING
C HYDROSTATIC CONDITIONS, TOP BOUNDARY FORCES, AND GRAVITY FORCES)
158 DO 159 I=1,NSN2
    DISPI(I)=DISP(I)
159 CONTINUE
    NDFIT=-1
    NPERT(1)=NP
    GO TO 140

```

```

C
C
C
C
C
C
C

```

```

*****
*.PRINT OUT OF RESULTS *
*****

```

```

160 IF (NF.GT.1) GO TO 177
161 WRITE (3,162) TITLE(1),TITLE(2),ROUTINES
162 FORMAT (1H1,///,25X,24(1H*),/,25X,* OUTPUT FROM DEFLOW *,/,25X
*,24(1H*),///,1X,'PROBLEM:',1X,A60,/,10X,A60,///,1X,'ROUTINE(S) USE
*D: ',A20,/)
    IF (FLAG6) GO TO 179

```

```

C
C FINAL LOADS AND DISPLACEMENTS (IF DEFORMATION ROUTINES USED)
    WRITE (3,163) NPERT(1)
163 FORMAT (19X,'RESULTS OF DEFORMATION ROUTINE',/,5X,'ITERATIONS TO
*CALCULATE BACKGROUND DISPLACEMENTS',1X,3(1H-),1X,I2)
    IF (NDFIT.LT.0) GO TO 168
    WRITE (3,164) NPERT(2)
164 FORMAT (5X,'ITERATIONS TO CALCULATE BOREHOLE EFFECTS',1X,10(1H-),1
*X,I2)
    IF (NDFIT.LE.0) GO TO 168
    WRITE (3,165) NDFIT
165 FORMAT (5X,'DEFORMATION-FLOW ITERATIONS',1X,23(1H-),1X,I2,/,20X,'
*DEF-FLOW',10X,'DISP-STIFF',/,20X,'ITERATION',9X,'ITERATIONS',/,20X
*,9(1H-),9X,10(1H-))

```

C.6 Listing of program DEFLOW (Continued)

```

DO 167 I=1,NDFIT
  J=I+2
  WRITE (3,166) I,NPERT(J)
166 FORMAT (23X,I2,16X,I2)
167 CONTINUE
168 WRITE (3,169)
169 FORMAT (//,1X,'DISPLACEMENTS:',/,1X,13(1H-),//,26X,'FINAL',16X,'BA
*CKGROUND',/,10X,'NODE',8X,'DR',9X,'DZ',11X,'DR',9X,'DZ',/)
DO 171 I=1,NSN
  I2=I+I
  I1=I2-1
  WRITE (3,170) I,DISP(I1),DISP(I2),DISPI(I1),DISPI(I2)
170 FORMAT (10X,I3,5X,1PE9.2,2X,E9.2,4X,E9.2,2X,E9.2)
171 CONTINUE
  WRITE (3,172)
172 FORMAT (/,10X,20(1H-),/,10X,'SIGN CONVENTION: R+ RADIALY OUTWARD'
*,/,27X,'Z+ DOWNWARD')
  WRITE (3,173)
173 FORMAT (1H1,//,4X,'FRACTURE DEFORMATION:',/,4X,20(1H-),//,13X,'FLO
*w',5X,'RADIAL',19X,'FINAL STIFFNESS',/,13X,'NODE',4X,'MOVEMENT',4X
*, 'CLOSURE',4X,'TANGENTIAL',4X,'NORMAL',/,2X,'FRACTURE',3X,'PAIR',6
*X,'(M)',9X,'(M)',7X,'[GPa/M]',5X,'[GPa/M]',/,2X,8(1H-),3X,4(1H-),4
*X,8(1H-),3X,9(1H-),3X,10(1H-),3X,8(1H-),/)
  N=0
  DO 175 I=1,NFRAC
    DO 175 J=1,NFN
      N=N+1
      I2=2*IFPAIR(I,J,1)
      I1=I2-1
      J2=2*IFPAIR(I,J,2)
      J1=J2-1
      DR=DISP(J1)-DISP(I1)
      DZ=DISP(I2)-DISP(J2)
      WRITE (3,174) I,J,DR,DZ,KS(N),KN(N)
174 FORMAT (4X,I2,8X,I2,4X,1PE9.2,3X,E9.2,3X,E9.2,3X,E9.2)
175 CONTINUE
      WRITE (3,176)
176 FORMAT (/,2X,20(1H-),/,5X,'SIGN CONVENTION: RADIAL MOVEMENT + TOP
* SURFACE OF FRACTURE',/,41X,'HAS MOVED OUTWARD RELATIVE',/,41X,'TO
* BOTTOM',/,30X,'CLOSURE - APERTURE HAS DECREASED')
      IF (FLAG9.AND.FLAG4) GO TO 198
      IF (FLAG9) GO TO 184
C
C APERTURES AND HEAD DISTRIBUTION
177 WRITE (3,178) TITLE(1),TITLE(2)
178 FORMAT (1H1,///,1X,'PROBLEM:',1X,A60,/,10X,A60,///)
179 IF (FLAG10) GO TO 1792

```

C.6 Listing of program DEFLOW (Continued)

```

WRITE (3,1791) NF,NFIT,Q
1791 FORMAT (24X,'RESULTS OF FLOW ROUTINE',///,1X,'FRACTURE NO. '),I2,/,1
*X,14(1H-),//,5X,'NUMBER OF FLOW ITERATIONS',1X,17(1H-),I3,/,5X,'IN
*JECTION RATE TO FRACTURE (M**3/S)',1X,7(1H-),2X,1PE9.3,///,11X,'TO
*TAL',2X,'EXCESS',3X,'VEL.',2X,'PRESS.',2X,'APER-',2X,'ROUGH',2X,'R
*EYNOLDS',20X,'HYD.',4X,'LAM.',/,2X,'RADIUS',3X,'HEAD',4X,'HEAD',4X
*,'HEAD',3X,'LOSS',3X,'TURE',3X,'NESS',4X,'NUMBER',3X,'FLOW',3X,'TR
*ANS.',4X,'COND.',4X,'FACT.',/,3X,'(M)',6X,'(M)',5X,'(M)',4X,'(M)',
*4X,'(M)',4X,'(MM)',4X,'( )',5X,'( )',5X,'LAW',3X,'(M**2/S)',3X,'(M
*/S)',5X,'( )',/,2X,6(1H-),3X,5(1H-),2X,6(1H-),3X,4(1H-),2X,6(1H-),
*2X,5(1H-),2X,5(1H-),2X,8(1H-),2X,4(1H-),2X,8(1H-),2X,8(1H-),2X,5(1
*H-))
GO TO 1811
1792 WRITE (3,180) NF,NFIT,Q
180 FORMAT (24X,'RESULTS OF FLOW ROUTINE',///,1X,'FRACTURE NO.',I2,/,1
*X,14(1H-),//,5X,'NUMBER OF FLOW ITERATIONS',1X,17(1H-),I3,/,5X,'DI
*SCHARGE FROM FRACTURE (M**3/S)',1X,10(1H-),2X,1PE9.3,///,11X,'TOTA
*L',3X,'DRAW-',3X,'VEL.',2X,'PRESS.',2X,'APER-',2X,'ROUGH',2X,'REYN
*OLDS',20X,'HYD.',4X,'LAM.',/,2X,'RADIUS',3X,'HEAD',4X,'DOWN',4X,'H
*EAD',3X,'LOSS',3X,'TURE',3X,'NESS',4X,'NUMBER',3X,'FLOW',3X,'TRANS
*.',4X,'COND.',4X,'FACT.',/,3X,'(M)',6X,'(M)',5X,'(M)',4X,'(M)',4X,
*'(M)',4X,'(MM)',4X,'( )',5X,'( )',5X,'LAW',3X,'(M**2/S)',3X,'(M/S)
*',5X,'( )',/,2X,6(1H-),3X,5(1H-),3X,5(1H-),3X,4(1H-),2X,6(1H-),2X,
*5(1H-),2X,5(1H-),2X,8(1H-),2X,4(1H-),2X,8(1H-),2X,8(1H-),2X,5(1H-
*)
PLOSSWB=ABS(PHEAD(NF,NFN)-PHEADWB)
WRITE (3,181) THEADWB,SWELL,VHEADWB(NF),PLOSSWB
181 FORMAT (/,1X,'IN WELL',1X,F7.3,1X,F7.3,1X,F6.3,1X,F7.3,4X,1H-,6X,1
*H-,7X,1H-,7X,1H-,7X,1H-,9X,1H-,8X,1H-)
1811 DO 183 L=1,NFN
PTWOB=1000.*TWOB(L)
PLOSS=ABS(PHEAD(NF,NFN)-PHEAD(NF,L))
IF (LAW(L).EQ.1.OR.LAW(L).EQ.4) GO TO 1813
WRITE (3,1812) RR(L),THEAD(L),SA(L),VHEAD(L),PLOSS,PTWOB,ROUGH(L),
*RE(L),LAW(L)
1812 FORMAT (3(1X,F7.3),1X,F6.3,1X,F7.3,2(2X,F5.3),2X,1PE8.2,3X,I1,7X,1
*H-,9X,1H-,8X,1H-)
GO TO 183
1813 COND=TRANS(L)/TWOB(L)
WRITE (3,182) RR(L),THEAD(L),SA(L),VHEAD(L),PLOSS,PTWOB,ROUGH(L),R
*E(L),LAW(L),TRANS(L),COND,CL(L)
182 FORMAT (3(1X,F7.3),1X,F6.3,1X,F7.3,2(2X,F5.3),2X,1PE8.2,3X,I1,4X,E
*8.2,2X,E8.2,2X,OPF5.3)
183 CONTINUE
GO TO 134

```

C
C COMPLETION MESSAGE

— C.6 Listing of program DEFLOW (Continued)

```

184 WRITE (6,185) FILEOUT
185 FORMAT (///,1X,'Program has run to completion.',/,1X,'Output has been
*een written to file : ',A20,///)
GO TO 198

C
C ITERATION TERMINATION MESSAGES
C MAXFIT EXCEEDED
186 WRITE (3,187) TITLE(1),TITLE(2),MAXFIT,NF
187 FORMAT (1H1,/,1X,'PROBLEM:',1X,A60,/,10X,A60,///,30X,'ATTENTION!!!
* ',/,6X,'THE FLOW ROUTINE HAS USED ',I2,' ITERATIONS (MAXIMUM ALLOWED
* BY INPUT',/,1X,'CONTROL) IN FRACTURE NO.',I2,' WITHOUT ACHIEVING
* CONVERGENCE WITH RESPECT',/,1X,' TO TOTAL HEAD.',/,6X,' THE PROGRAM
* HAS BEEN TERMINATED AND RESULTS AS OF THIS POINT HAVE',/,1X,' BEEN
* PRINTED OUT.')
```

```

WRITE (6,188) NFIT,NF,FILEOUT
188 FORMAT (1H1,///,30X,'ATTENTION!!!',/,6X,'The flow routine has used
*d ',I2,' iterations (maximum allowed by input',/,1X,'control) in fracture
* no.',I2,' without achieving convergence with respect',/,1X,' to total
* head.',/,6X,'The program has been terminated and results as of this
* point will',/,1X,'be printed out to file: ',A20,///)
GO TO 130

C
C MAXDFIT EXCEEDED
189 WRITE (3,190) TITLE(1),TITLE(2),MAXDFIT
190 FORMAT (1H1,/,1X,'PROBLEM:',1X,A60,/,10X,A60,///,30X,'ATTENTION!!!
* ',/,6X,'THE FLOW-DEFORMATION ITERATIVE SCHEME HAS USED ',I2,' ITERA
* TIONS',/,1X,'(MAXIMUM ALLOWED BY INPUT CONTROL) WITHOUT ACHIEVING
* COMPLETE',/,1X,'CONVERGENCE WITH RESPECT TO PRESSURE HEADS.',/,6
* X,'THE PROGRAM HAS BEEN TERMINATED AND RESULTS AS OF THIS',/,1X,'POI
* NT HAVE BEEN PRINTED OUT.')
```

```

WRITE (6,191) MAXDFIT,FILEOUT
191 FORMAT (1H1,///,30X,'ATTENTION!!!',/,6X,'The flow-deformation ite
*rative scheme has used ',I2,' iterations',/,1X,'(maximum allowed by
* input control) without achieving complete',/,1X,'convergence with
* respect to pressure heads.',/,6X,'The program has been terminated
* and results as of this',/,1X,'point will be printed out to file: '
*,A20,///)
FLAG4=.TRUE.
GO TO 130

C
C MAXPERT EXCEEDED
192 WRITE (3,193) TITLE(1),TITLE(2),MAXPERT,NDFIT
193 FORMAT (1H1,/,1X,'PROBLEM: ',A60,/,10X,A60,///,30X,'ATTENTION!!!',
* //,6X,'THE FRACTURE STIFFNESS/DISPLACEMENT ITERATIVE SCHEME HAS US
* ED ',I2,/,1X,'ITERATIONS (MAXIMUM ALLOWED BY INPUT CONTROL) DURING
* DEFORMATION-FLOW',/,1X,'ITERATION ',I2,' WITHOUT ACHIEVING CONVER
* GENCE.',/,6X,'THE PROGRAM WAS TERMINATED AND RESULTS AS OF THIS PO
```

C.6 Listing of program DEFLOW (Continued)

```

*INT HAVE BEEN',/,1X,'PRINTED OUT.')
WRITE (6,194) MAXPERT, NDFIT, FILEOUT
194 FORMAT (1H1,///,30X,'ATTENTION!!!',//,6X,'The fracture stiffness/d$
*isplacement iterative scheme has used ',I2,/,1X,'iterations (maxim$
*um allowed by input control) during deformation-flow',/,1X,'iterat$
*ion ',I2,' without achieving convergence.',/,6X,'The program has b$
*een terminated and results as of this point will be',/,1X,'printe$
* out to file: ',A20,///)
FLAG4=.TRUE.
IF.(FLAG9) GO TO 160
GO TO 130

C
C BAD ELEMENT ERROR MESSAGE
195 WRITE (3,196) TITLE(1),TITLE(2),NE
196 FORMAT (1H1,/,1X,'PROBLEM:',1X,A60,/,10X,A60,///,30X,'ATTENTION!!!
*',//,6X,'ELEMENT NO. ',I3,' HAS A ZERO OR NEGATIVE AREA.',/,6X,'TH
*E PROGRAM WAS TERMINATED AND ONLY INPUT HAS BEEN PRINTED OUT.')
WRITE (6,197) NE, FILEOUT
197 FORMAT (1H1,///,30X,'ATTENTION!!!',//,6X,'Element no. ',I3,' has a$
2 zero or negative area.',/,6X,'The program has been terminated and$
3 input will be printed out',/,1X,'to file:',A20,///)

C
C GENERATES LOG OF RUN
198 CALL DATE(DAY)
CALL TIME(HOUR)

C SHUTS OFF VAX TIMER AND DETERMINES CPU FOR RUN
STATUS=LIB$STAT TIMER(2,FINISH)
CPU=FLOATJ(FINISH-START)/10000.
MINS=JINT(CPU)
SECS=(CPU-FLOATJ(MINS))*100.
WRITE (3,199) TITLE(1),TITLE(2),DAY,HOUR,MINS,SECS
199 FORMAT (1H1,/,1X,'PROBLEM:',1X,A60,/,10X,A60,///,30X,'LOG OF RUN',
2//,10X,'DATE = ',A12,/,10X,'TIME = ',A12,/,11X,'CPU =',4X,I2,':',F
35.2)

C
STOP
END

C
C *****
C
C SUBROUTINES
C
C *****
C
C -----
C SUBROUTINE VISCRHO
C -----

```

C.6 Listing of program DEFLOW (Continued)

```

C CALCULATES KINEMATIC VISCOSITY AND DENSITY OF WATER FOR GIVEN
C TEMPERATURE IN RANGE OF 0-35 DEGREES C
C
  INCLUDE 'CONSTS.COM'
  DIMENSION RHODATA(36),VISDATA(36)
C
C VALUES OF DENSITY IN KG/M**3 (NOTE: 990.0 ADDED TO ALL VALUES IN
C CALCULATION BELOW) FROM WEAST AND ASTLE (1982)
  DATA RHODATA/9.842,9.902,9.943,9.967,9.975,9.967,9.943,9.904,
*           9.851,9.784,9.703,9.608,9.500,9.380,9.247,9.103,
*           8.946,8.778,8.599,8.408,8.207,7.996,7.774,7.542,
*           7.300,7.048,6.787,6.516,6.236,5.948,5.650,5.344,
*           5.029,4.706,4.374,4.035/
C VALUES OF KINEMATIC VISCOSITY IN M**2/S (NOTE: EXPONENTIAL OF
C 1.0E-06 IS ADDED BELOW) OBTAINED BY DIVIDING TABULATED VALUES OF
C ABSOLUTE VISCOSITY (WEAST AND ASTLE, 1982) BY DENSITY VALUES
  DATA VISDATA/1.787,1.728,1.671,1.618,1.567,1.519,1.472,1.428,
*           1.386,1.346,1.307,1.271,1.236,1.203,1.170,1.140,
*           1.110,1.082,1.054,1.029,1.004,.9799,.9569,.9348,
*           .9136,.8930,.8733,.8543,.8358,.8181,.8010,.7845,
*           .7685,.7531,.7382,.7237/
C
  ITEMP=INT(TEMP)+1
C USES LINEAR INTERPOLATION BETWEEN DEGREES
  VISC=1.0E-06*(VISDATA(ITEMP)-(TEMP-FLOAT(ITEMP-1))*(VISDATA(ITEMP)
*-VISDATA(ITEMP+1)))
  RHO=990.0+(RHODATA(ITEMP)-(TEMP-FLOAT(ITEMP-1))*(RHODATA(ITEMP)-RH
*ODATA(ITEMP+1)))
  RHOG=RHO*G
C
  RETURN
  END
C
C
C -----
  SUBROUTINE GRIDGEN
  -----
C
C OPTIONAL SUBROUTINE IF NFRAC=1 FOR ASSIGNING NODAL COORDINATES,
C FRACTURE-FLOW NODE PAIRS, BOUNDARY NODES, BOUNDARY CONDITION CODES,
C AND ELEMENT INCIDENCES AND MATERIAL TYPES
C
  INCLUDE 'PARAM.COM'
  INCLUDE 'BOTH.COM'
  INCLUDE 'DEFORM.COM'
  INCLUDE 'DIMENS.COM'
  INCLUDE 'FLOW.COM'

```


C.6 Listing of program DEFLOW (Continued)

```

      NSN=4*NFN
      NSE=NSN-4
C DETERMINES LIMITS AND SPACING FOR DISCRETIZING ROCK LAYERS SUCH
C THAT ELEMENTS WITH EXTREME ASPECT RATIOS ARE AVOIDED
      DO 201 LIM1=1,NFN
      IF (RR(LIM1).GE.RPROP(1,1)) GO TO 202
201 CONTINUE
      IF (LIM1.EQ.NFN+1) LIM1=NFN
202 DO 203 LIM2=1,NFN
      IF (RR(LIM2).GE.RPROP(2,1)) GO TO 204
203 CONTINUE
      IF (LIM2.EQ.NFN+1) LIM2=NFN
•204 NTBN=NSN/4-LIM2+2
      NWBBN(1)=LIM1
      NWBBN(2)=LIM2
      NTWBBN=LIM1+LIM2
      ZLOG1=ALOG10(RPROP(1,1)+1.0)/FLOAT(LIM1-1)
      ZLOG2=ALOG10(RPROP(2,1)+1.0)/FLOAT(LIM2-1)
C
C LEFTMOST, SINGULAR TRIANGULAR ELEMENTS
      R(1)=RW
      Z(1)=RPROP(1,1)
      ICODE(1)=0
      IWBBN(LIM1)=1
      R(2)=RW
      Z(2)=RPROP(1,1)
      ICODE(2)=0
      IWBBN(LIM1+1)=2
      IFPAIR(1,1,1)=1
      IFPAIR(1,1,2)=2
      INC(1,1)=1
      INC(1,2)=3
      INC(1,3)=4
      INC(1,4)=1
      L=2*NFN-1
      INC(L,1)=2
      INC(L,2)=5
      INC(L,3)=6
      INC(L,4)=2
C
C GENERATES GRID BASED ON RELATIVE THICKNESSES OF ROCK LAYERS
      IF (LIM1-LIM2) 205,205,211
205 IF (LIM1.EQ.NFN) GO TO 207
      JBOT=4*LIM1-5
      IF (LIM2.EQ.NFN) GO TO 206
      JTOP=JBOT+4*(LIM2-LIM1)+1
      LIM=JBOT-1

```

C.6 Listing of program DEFLOW (Continued)

```

GO TO 208
206 JTOP=JBOT+4*(LIM2-LIM1)+5
    LIM=JBOT-1
    GO TO 208
207 JBOT=4*LIM1-1
    JTOP=JBOT+1
    LIM=JBOT-1
    GO TO 220
208 IF (LIM1.EQ.LIM2) GO TO 217
C
C TRIANGULAR ELEMENTS TO RIGHT OF LOWER TRI-CLUSTER UP TO POINT OF
C SYMMETRY WITH UPPER ELEMENTS
    L=2*(LIM1-2)+3
    KL=0
    MN=0
    J=JBOT-1
    DO 209 ML=1,LIM2-LIM1
    J=J+4
    IF (ML.EQ.LIM2-LIM1) KL=-1
    IF (LIM2.EQ.NFN) KL=0
    IFPAIR(1,LIM1+MN,1)=J+1
    IFPAIR(1,LIM1+MN,2)=J-2
    INC(L,1)=J
    INC(L,2)=J+4+KL
    INC(L,3)=J+1
    INC(L,4)=1
    INC(L+1,1)=J+1
    INC(L+1,2)=J+4+KL
    INC(L+1,3)=J+5+KL
    INC(L+1,4)=1
    L=L+2
    MN=MN+1
209 CONTINUE
C
C TRIANGULAR ELEMENTS TO LEFT OF UPPER TRI-CLUSTER FROM POINT OF
C SYMMETRY WITH LOWER ELEMENTS
    L=2*(LIM1+NFN-3)
    J=JBOT-7
    KL=1
    MN=0
    IF (LIM2.EQ.NFN) MN=1
    DO 210 NL=1,LIM2-LIM1+MN
    J=J+4
    IF (NL.GT.1) KL=0
    INC(L,1)=J+KL
    INC(L,2)=J+4
    INC(L,3)=J+1+KL

```

C.6 Listing of program DEFLOW (Continued)

```

      INC(L,4)=2
      INC(L+1,1)=J+1+KL
      INC(L+1,2)=J+4
      INC(L+1,3)=J+5
      INC(L+1,4)=2
      L=L+2
210 CONTINUE
      GO TO 217
211 JTOP=4*LIM2-3
      IF (LIM1.EQ.NFN) GO TO 212
      JBOT=JTOP+4*(LIM1-LIM2-1)+1
      GO TO 213
212 JBOT=JTOP+4*(LIM1-LIM2)+1
213 LIM=JTOP-3
C TRIANGULAR ELEMENTS TO LEFT OF LOWER TRI-CLUSTER FROM POINT OF
C SYMMETRY WITH UPPER ELEMENTS
      L=2*LIM2-4
      J=JTOP-10
      MN=0
      IF (LIM1.EQ.NFN) MN=1
      DO 214 NL=1,LIM1-LIM2
      KL=0
      LL=0
      IF (NL.EQ.3) KL=-1
      IF (NL.EQ.2) LL=-1
      J=J+4+KL
      INC(L,1)=J
      INC(L,2)=J+4+LL
      INC(L,3)=J+1
      INC(L,4)=1
      INC(L+1,1)=J+1
      INC(L+1,2)=J+4+LL
      INC(L+1,3)=J+5+LL
      INC(L+1,4)=1
      L=L+2
214 CONTINUE
C
C TRIANGULAR ELEMENTS TO RIGHT OF UPPER TRI-CLUSTER UP TO POINT OF
C SYMMETRY WITH LOWER ELEMENTS OR TO END (IN CASE WHERE THICKNESS
C OF ROCK LAYER 1 IS GREATER THAN RO)
      L=NSE-2*(NFN-LIM2)+1
      MN=0
      IF (LIM1.EQ.NFN) MN=1
      KL=0
      J=JTOP-1
      DO 215 ML=1,LIM1-LIM2
      KL=0

```

C.6 Listing of program DEFLOW (Continued)

```

LL=0
IF (ML.EQ.(LIM1-LIM2+MN)) KL=-1
IF (ML.EQ.(LIM1-LIM2-1+MN)) LL=-1
J=J+4+KL
INC(L,1)=J
INC(L,2)=J+4+LL
INC(L,3)=J+1
INC(L,4)=2
INC(L+1,1)=J+1
INC(L+1,2)=J+4+LL
INC(L+1,3)=J+5+LL
INC(L+1,4)=2
L=L+2
215 CONTINUE
C LOWER, RIGHTMOST, SINGULAR, TRIANGULAR ELEMENT WHEN THICKNESS OF
C ROCK LAYER 1 IS GREATER THAN RO
IF (LIM1.EQ.NFN) GO TO 216
GO TO 219
216 R(JBOT)=RO
Z(JBOT)=0.0
ICODE(JBOT)=2
ICODE(JBOT-4)=2
IOBN(1)=JBOT
IOBN(2)=JBOT-3
IWBBN(1)=JBOT-4
L=2*NFN-2
INC(L,1)=JBOT-4
INC(L,2)=JBOT
INC(L,3)=JBOT-3
INC(L,4)=1
GO TO 219
C
C TRIANGULAR ELEMENTS IN LOWER TRI-CLUSTER
217 L=2*(LIM1-2)
LL=0
KL=0
IF (LIM1.EQ.LIM2) KL=-1
IF (LIM1-LIM2.EQ.1) LL=1
INC(L,1)=JBOT-4+LL
INC(L,2)=JBOT
INC(L,3)=JBOT-3+LL
INC(L,4)=1
INC(L+1,1)=JBOT-3+LL
INC(L+1,2)=JBOT
INC(L+1,3)=JBOT+4+KL
INC(L+1,4)=1
INC(L+2,1)=JBOT

```

C.6 Listing of program DEFLOW (Continued)

```

INC(L+2,2)=JBOT+3+KL
INC(L+2,3)=JBOT+4+KL
INC(L+2,4)=1
R(JBOT)=RW
Z(JBOT)=0.0
ICODE(JBOT)=2
ICODE(JBOT-3)=-1
ICODE(JBOT-4)=-2
IWBBN(1)=JBOT
IWBBN(2)=JBOT-4
IF (LIM2.EQ.NFN) GO TO 218
GO TO 219

```

C
C UPPER, RIGHTMOST, SINGULAR, TRIANGULAR ELEMENT WHEN THICKNESS OF
C ROCK LAYER 2 IS GREATER THAN RO

```

218 IFPAIR(1,NFN,1)=JTOP-1
IFPAIR(1,NFN,2)=JTOP-4
INC(NSE,1)=JTOP-4
INC(NSE,2)=JTOP
INC(NSE,3)=JTOP-3
INC(NSE,4)=2
R(JTOP)=RO
Z(JTOP)=RPROP(1,1)+RPROP(2,1)
ICODE(JTOP)=0
ICODE(JTOP-3)=0
IOBN(3)=JTOP-4
IOBN(4)=JTOP
ITBN(1)=JTOP-3
ITBN(2)=JTOP
IWBBN(LIM1+LIM2)=JTOP-3

```

C
C TRIANGULAR ELEMENTS IN UPPER TRI-CLUSTER

```

219 L=NSE-2*(NFN-LIM2+1)
KL=0
LL=0
MN=0
IF (LIM1.EQ.NFN) MN=1
IF (LIM1-LIM2.EQ.1) LL=-1
IF (LIM1.EQ.LIM2) KL=1
INC(L,1)=JTOP-4+KL
INC(L,2)=JTOP
INC(L,3)=JTOP-3+KL
INC(L,4)=2
INC(L+1,1)=JTOP-4+KL
INC(L+1,2)=JTOP+3+LL
INC(L+1,3)=JTOP
INC(L+1,4)=2

```

C.6 Listing of program DEFLOW (Continued).

```

INC(L+2,1)=JTOP
INC(L+2,2)=JTOP+3+LL
INC(L+2,3)=JTOP+4+LL
INC(L+2,4)=2
R(JTOP)=RW
Z(JTOP)=RPROP(1,1)+RPROP(2,1)
ICODE(JTOP)=0
ICODE(JTOP-3+KL)=-2
ICODE(JTOP-4+KL)=-1
IWBBN(LIM1+LIM2)=JTOP
IWBBN(LIM1+LIM2-1)=INC(L,3)
ITBN(1)=JTOP
GO TO 221

```

C
C RIGHTMOST, SINGULAR, TRIANGULAR ELEMENTS WHEN BOTH ROCK LAYERS 1
C AND 2 ARE THICKER THAN RO

```

220 R(JBOT)=RO
Z(JBOT)=0.0
ICODE(JBOT)=2
ICODE(JBOT-4)=2
IOBN(1)=JBOT
IOBN(2)=JBOT-3
IWBBN(1)=JBOT-4
R(JTOP)=RO
Z(JTOP)=RPROP(1,1)+RPROP(2,1)
ICODE(JTOP)=0
ICODE(JTOP-2)=0
IOBN(3)=JTOP-3
IOBN(4)=JTOP
ITBN(2)=JTOP
ITBN(1)=JTOP-2
IWBBN(LIM1+LIM2)=JTOP-2
L=2*NFN-2
INC(L,1)=JBOT-4
INC(L,2)=JBOT
INC(L,3)=JBOT-3
INC(L,4)=1
INC(NSE,1)=JTOP-3
INC(NSE,2)=JTOP
INC(NSE,3)=JTOP-2
INC(NSE,4)=2

```

C
C LEFT SYMMETRIC PORTION OF GRID

```

221 N=1
M=2*NFN-2
DO 223 I=3,LIM,4
IFPAIR(1,N+1,1)=I+1

```

C.6 Listing of program DEFLOW (Continued)

```

IFPAIR(1,N+1,2)=I+2
R(I)=RW
Z(I)=RPROP(1,1)+1.0-10.** (FLOAT(N)*ZLOG1)
R(I+1)=RR(N+1)
Z(I+1)=RPROP(1,1)
R(I+2)=R(I+1)
Z(I+2)=Z(I+1)
R(I+3)=RW
Z(I+3)=RPROP(1,1)-1.0+10.** (FLOAT(N)*ZLOG2)
IF (I.GE.LIM-3) GO TO 223
L=2*N
LL=0
ML=0
DO 222 J=1,2
  ICODE(I)=-2
  IWBBN(LIM1-N)=I
  ICODE(I+1)=-1
  ICODE(I+2)=-1
  ICODE(I+3)=-2
  IWBBN(LIM1+1+N)=I+3
  INC(L,1)=I+LL
  INC(L,2)=I+4+LL
  INC(L,3)=I+1+LL
  INC(L,4)=1+ML
  INC(L+1,1)=I+1+LL
  INC(L+1,2)=I+4+LL
  INC(L+1,3)=I+5+LL
  INC(L+1,4)=1+ML
  L=L+2*NFN-2
  LL=LL+2
  ML=1
222 CONTINUE
  N=N+1
223 CONTINUE
  IF (LIM1.EQ.NFN.AND.LIM1.LE.LIM2) GO TO 236
  IF (LIM1-LIM2)-228,227,224

```

C. NODES IMMEDIATELY BELOW UPPER TRI-CLUSTER

```

224 R(JTOP-2)=RW
  Z(JTOP-2)=RPROP(1,1)+1.0-10.** (FLOAT(N+1)*ZLOG1)
  ICODE(JTOP-2)=-2
  IWBBN(LIM1-N-1)=JTOP-2
  IWBBN(LIM1-N-2)=JTOP-6
  R(JTOP-1)=RR(N+2)
  Z(JTOP-1)=RPROP(1,1)
  ICODE(JTOP-1)=-1
  ICODE(JTOP-6)=-2

```

C.6 Listing of program DEFLOW (Continued)

```

      ICODE(JTOP-5)=-1
C
C  NODES BETWEEN TRI-CLUSTERS
      J=LIM2-1
      N=2
      DO 225 K=JTOP+1,JBOT-1,4
      IF (K.EQ.JBOT) GO TO 226
      KL=0
      IF (K.EQ.JTOP+1) KL=1
      J=J+1
      IFPAIR(1,J,1)=K-3+KL
      IFPAIR(1,J,2)=K+2
      R(K)=RW
      Z(K)=RPROP(1,1)+1.0-10.** (FLOAT(J)*ZLOG1)
      ICODE(K)=-2
      R(K+1)=RR(J+1)
      Z(K+1)=RPROP(1,1)
      ICODE(K+1)=-1
      R(K+2)=R(K-3+KL)
      Z(K+2)=RPROP(1,1)
      ICODE(K+2)=-1
      R(K+3)=R(K+2)
      Z(K+3)=RPROP(1,1)+RPROP(2,1)
      ICODE(K+3)=-1
      ITBN(N)=K+3
      N=N+1
225  CONTINUE
C
C  NODES ABOVE LOWER TRI-CLUSTER
226  IF (LIM1.EQ.NFN) MN=1
      J=LIM1-1
      R(JBOT+1)=RR(J)
      Z(JBOT+1)=RPROP(1,1)
      ICODE(JBOT+1)=-1
      R(JBOT+2)=RR(J)
      Z(JBOT+2)=RPROP(1,1)+RPROP(2,1)
      ICODE(JBOT+2)=-1
      ITBN(LIM1-LIM2+1)=JBOT+2
      IFPAIR(1,J,1)=JBOT-3
      IFPAIR(1,J,2)=JBOT+1
      IF (LIM1.EQ.NFN) GO TO 233
      NODE=JBOT+3
      LRAD=LIM1
      GO TO 230
227  NODE=JTOP+1
      LRAD=LIM2
      GO TO 230

```


C.6 Listing of program DEFLOW (Continued)

C
 C NODES ABOVE LOWER TRI-CLUSTER AND TO LEFT OF UPPER TRI-CLUSTER
 C AND TO RIGHT OF LOWER TRI-CLUSTER TO POINT OF SYMMETRY WITH
 C UPPER ELEMENTS

```

228 J=LIM1-1
    L=0
    DO 229 K=JBOT+1,JTOP-1,4
      J=J+1
      IFPAIR(1,J,1)=K+3
      IFPAIR(1,J,2)=K
      R(K)=RR(J)
      Z(K)=RPROP(1,1)
      ICODE(K)=-1
      R(K+1)=RW
      Z(K+1)=RPROP(1,1)-1.0+10.** (FLOAT(J-1)*ZLOG2)
      ICODE(K+1)=-2
      IWBBN(2*LIM1+L)=K+1
      R(K+2)=R(K)
      Z(K+2)=0.0
      ICODE(K+2)=-3
      R(K+3)=R(K)
      Z(K+3)=RPROP(1,1)
      ICODE(K+3)=-1
      L=L+1
229 CONTINUE
    IF (LIM2.EQ.NFN) GO TO 236
    NODE=JTOP+1
    LRAD=LIM2
  
```

C
 C RIGHT SYMMETRIC PORTION OF GRID

```

230 IF (LIM1-LIM2) 231,232,232
231 N=LIM1-LIM2+1
    GO TO 233
232 N=2
233 DO 235 K=NODE,NSN,4
      IFPAIR(1,LRAD,1)=K+1
      IFPAIR(1,LRAD,2)=K+2
      R(K)=RR(LRAD)
      Z(K)=0.0
      ICODE(K)=-3
      R(K+1)=R(K)
      Z(K+1)=RPROP(1,1)
      ICODE(K+1)=-1
      R(K+2)=R(K)
      Z(K+2)=RPROP(1,1)
      ICODE(K+2)=-1
      R(K+3)=R(K)
  
```

C.6 Listing of program DEFLOW (Continued)

```

Z(K+3)=RPROP(1,1)+RPROP(2,1)
ICODE(K+3)=-1
ITBN(N)=K+3
L=2*LRAD-1
LL=0
IF (K.GE.NSN-4) GO TO 235
ML=0
DO 234 J=1,2
INC(L,1)=K+LL
INC(L,2)=K+4+LL
INC(L,3)=K+1+LL
INC(L,4)=1+ML
INC(L+1,1)=K+1+LL
INC(L+1,2)=K+4+LL
INC(L+1,3)=K+5+LL
INC(L+1,4)=1+ML
L=L+NSN/2
LL=LL+2
ML=1
234 CONTINUE
LRAD=LRAD+1
N=N+1
235 CONTINUE
C
C DOES REQUIRED RE-CODING OF OUTER BOUNDARY NODES
IOBN(1)=NSN-3
IOBN(2)=NSN-2
IOBN(3)=NSN-1
IOBN(4)=NSN
ICODE(NSN-3)=2
ICODE(NSN-2)=0
ICODE(NSN-1)=0
ICODE(NSN)=0
C
236 RETURN
END
C
C
C
C -----
SUBROUTINE BLOADS
C -----
C CALCULATES EFFECTIVE POINT LOADS ON FLOW NODES FROM FLUID PRESSURE
C IN FRACTURE AND AT WELLBORE NODES FROM GEOSTATIC PRESSURE PRIOR TO
C DRILLING OF WELLBORE AND FROM FLUID PRESSURE AFTER WELL IS DRILLED
C
INCLUDE 'PARAM.COM'
INCLUDE 'BOTH.COM'

```

C.6 Listing of program DEFLOW (Continued)

```

INCLUDE 'CONSTS.COM'           $
INCLUDE 'DEFORM.COM'          $
INCLUDE 'DIMENS.COM'          $
INCLUDE 'FLOW.COM'            $
INCLUDE 'HEAD.COM'            $
INCLUDE 'MATEQN.COM'          $
C
C EFFECTIVE VERTICAL POINT LOADS (IN N) ON FRACTURE NODES
DO 301 N=1,NFRAC
DO 301 J=1,NFE
RES=(RR(J+1)-RR(J))/6.0*(PHEADI(N,J)*RHOG*(RR(J+1)+2.0*RR(J))+PHEA
*DI(N,J+1)*RHOG*(RR(J)+2.0*RR(J+1)))
SUMOM=(RR(J+1)**2+RR(J+1)*RR(J)+RR(J)**2)*RHOG*(PHEADI(N,J)*RR(J+1
*)-PHEADI(N,J+1)*RR(J))/3.0+0.25*RHOG*(PHEADI(N,J+1)-PHEADI(N,J))/(
*RR(J+1)-RR(J))*(RR(J+1)**4-RR(J)**4)
CENT=SUMOM/RES
F2=(CENT-RR(J))/(RR(J+1)-RR(J))*RES
F1=RES-F2
L1=2*IFPAIR(N,J,1)
L2=2*IFPAIR(N,J,2)
L3=2*IFPAIR(N,J+1,1)
L4=2*IFPAIR(N,J+1,2)
B(L1)=B(L1)+F1
B(L2)=-B(L1)
B(L3)=B(L3)+F2
B(L4)=-B(L3)
301 CONTINUE
C
IF (NDFIT.GE.0) GO TO 304
C EFFECTIVE LATERAL POINT LOADS (IN N) ON 'TO-BE' WELLBORE NODES
M=NTWBBN
P1=TOPRESS*1.0E+06*RPROP(NRX,4)/(1.0-RPROP(NRX,4))
DO 303 I=1,NRX
J=NRX-I+1
N=NWBBN(J)-1
DO 302 K=1,N
L1=IWBBN(M)
L2=IWBBN(M-1)
DELTAP=(Z(L1)-Z(L2))*RPROP(J,2)*G*RPROP(J,4)/(1.0-RPROP(J,4))
F1=(Z(L1)-Z(L2))/6.0*(3.0*P1+DELTAP)*RW
F2=(Z(L1)-Z(L2))/6.0*(3.0*P1+2.0*DELTAP)*RW
B(L1+L1-1)=B(L1+L1-1)+F1
B(L2+L2-1)=B(L2+L2-1)+F2
P1=P1+DELTAP
M=M-1
302 CONTINUE
M=M-1

```

C.6 Listing of program DEFLOW (Continued)

```

303 CONTINUE
GO TO 308

C
C EFFECTIVE LATERAL POINT LOADS (IN N) ON WELLBORE NODES
304 K=0
CUMTH=0.0
DO 307 I=1,NRX
N=NWBBN(I)-1
DO 306 J=1,N
L1=IWBBN(K+J)
L2=IWBBN(K+J+1)
IF (I.EQ.1) GO TO 305
C FOR POINTS ABOVE LOWERMOST FRACTURE
F1=(Z(L2)-Z(L1))/6.0*RW*RHOG*(3.0*(HW(I-1)-VHEADWB(I-1))-(2.0*Z(L1
*)+Z(L2)-3.0*CUMTH)*(1.0+SWB(I-1)/RPROP(I,1)))
F2=(Z(L2)-Z(L1))/6.0*RW*RHOG*(3.0*(HW(I-1)-VHEADWB(I-1))-(2.0*Z(L2
*)+Z(L1)-3.0*CUMTH)*(1.0+SWB(I-1)/RPROP(I,1)))
B(L1+L1-1)=B(L1+L1-1)+F1
B(L2+L2-1)=B(L2+L2-1)+F2
GO TO 306
C FOR POINTS BELOW LOWERMOST FRACTURE WHERE VEL=0 AND THERE ARE NO
C BOREHOLE FLOW LOSSES
305 F1=(Z(L2)-Z(L1))/6.0*RW*RHOG*(3.0*(HW(1)+RPROP(1,1))-2.0*Z(L1)-Z(L
*2))
F2=(Z(L2)-Z(L1))/6.0*RW*RHOG*(3.0*(HW(1)+RPROP(1,1))-2.0*Z(L2)-Z(L
*1))
B(L1+L1-1)=B(L1+L1-1)+F1
B(L2+L2-1)=B(L2+L2-1)+F2
306 CONTINUE
CUMTH=CUMTH+RPROP(I,1)
K=K+N+1
307 CONTINUE

C
308 RETURN
END

C
C
C -----
SUBROUTINE DEFORM
C -----
C
C
INCLUDE 'PARAM.COM'
INCLUDE 'BOTH.COM'
INCLUDE 'CONSTS.COM'
INCLUDE 'DEFORM.COM'
INCLUDE 'DIMENS.COM'
INCLUDE 'FLAGS.COM'

```

\$
 \$
 \$
 \$
 \$
 \$
 \$
 \$

C.6 Listing of program DEFLOW (Continued)

```

INCLUDE 'FLOW.COM'
INCLUDE 'HEAD.COM'
INCLUDE 'MATEQN.COM'
DIMENSION FR(NSN2D),SR(NSN2D,IBWD)
C
  DO 401 N=1,LMS
  DO 401 M=1,IBWS
  A(N,M)=0.0
401 CONTINUE
C
C CALCULATES STIFFNESS OF FRACTURE(S) AT FRACTURE-FLOW NODES
C -----
C CALL FRACSTF
C -----
C
C CALCULATES ROCK STIFFNESS CONTRIBUTIONS (ONLY NECESSARY TO DO ONCE
C SINCE THEY REMAIN SAME)
  IF (NDFIT.GE.0.OR.NP.GT.1) GO TO 420
  DO 402 I=1,LMS
  FR(I)=0.0
  DO 402 J=1,IBWS
  SR(I,J)=0.0
402 CONTINUE
C LOOP OVER ALL ROCK ELEMENTS
  DO 419 NE=1,NSE
C CALCULATES STIFFNESS OF ROCK ELEMENT
C -----
403 CALL ROCKSTF
C -----
  IF (DELTA.LE.0.0) FLAG5=.TRUE.
  IF (FLAG5) GO TO 430
C ASSEMBLES GLOBAL STIFFNESS MATRIX AND FORCE ARRAY FOR ROCK ELEMENTS
C NOTE: ONLY 'FREE' PART OF PARTITIONED MATRIX EQUATION IS ASSEMBLED.
C MATRIX IS ACTUALLY ASSEMBLED AS LMS x IBWS RECTANGULAR MATRIX
  DO 419 K=1,3
  K2=K+K
  K1=K2-1
  M=INC(NE,K)
C IGNORES ANY TERMS IN FIRST EQUATION OF PARTITIONED MATRIX EQUATION
  IF (ICODE(M).EQ.3) GO TO 419
C ASSIGNS ROW NUMBER IN CONDENSED MATRIX
  I2=M+M-LC(M+M)
  I1=I2-1
  DO 419 L=1,3
  L2=L+L
  L1=L2-1
  N=INC(NE,L)

```

C.6 Listing of program DEFLOW (Continued)

```

C ASSIGNS COLUMN NUMBER IN CONDENSED MATRIX
  J2=N+N-LC(N+N)-I2+1
  J1=J2-1
C DON'T NEED TO ADJUST B ARRAY FOR 'FC' TERM SINCE ALL FIXED
C DISPLACEMENTS = 0
  IF (ICODE(N).EQ.3) GO TO 419
  IF (ICODE(M).LE.0.AND.ICODE(M).GE.-2) GO TO 408
  IF (ICODE(M).EQ.2.OR.ICODE(M).EQ.-3) GO TO 414
C ICODE(M)=1
C ADDS ELEMENT GRAVITY LOADS TO FORCE ARRAY
  FR(I2)=FR(I2)+FE(K2)
  IF (J2.LT.1) GO TO 419
  ASSIGN 406 TO NEXT
  IF (ICODE(N).LE.0.AND.ICODE(N).GE.-2) GO TO 404
  IF (ICODE(N).EQ.2.OR.ICODE(N).EQ.-3) GO TO 407
  ASSIGN 419 TO NEXT
404 SR(I2,J2)=SR(I2,J2)+SE(K2,L2)
405 GO TO NEXT, (406,419)
406 IF (J1.LT.1) GO TO 419
  SR(I2,J1)=SR(I2,J1)+SE(K2,L1)
  GO TO 419
407 SR(I2,J2)=SR(I2,J2)+SE(K2,L1)
  GO TO 419
C ICODE(M)=-2,-1, OR 0
C ADDS ELEMENT GRAVITY LOADS TO FORCE ARRAY
408 FR(I2)=FR(I2)+FE(K2)
  ASSIGN 413 TO NEXT
  IF (ICODE(N).LE.0.AND.ICODE(N).GE.-2) GO TO 409
  IF (ICODE(N).EQ.2.OR.ICODE(N).EQ.-3) GO TO 411
  ASSIGN 419 TO NEXT
409 IF (J2.LT.1) GO TO 410
  SR(I2,J2)=SR(I2,J2)+SE(K2,L2)
410 IF (J2+1.LT.1) GO TO 419
  SR(I1,J2+1)=SR(I1,J2+1)+SE(K1,L2)
  GO TO NEXT, (413,419)
411 IF (J2.LT.1) GO TO 412
  SR(I2,J2)=SR(I2,J2)+SE(K2,L1)
412 IF (J2+1.LT.1) GO TO 419
  SR(I1,J2+1)=SR(I1,J2+1)+SE(K1,L1)
  GO TO 419
413 IF (J2.LT.1) GO TO 419
  SR(I1,J2)=SR(I1,J2)+SE(K1,L1)
  IF (J1.LT.1) GO TO 419
  SR(I2,J1)=SR(I2,J1)+SE(K2,L1)
  GO TO 419
C ICODE(M)=2 OR -3
414 IF (J2.LT.1) GO TO 419

```

C.6 Listing of program DEFLOW (Continued)

```

IF (ICODE(N).LE.0.AND.ICODE(N).GE.-2) GO TO 415
IF (ICODE(N).EQ.2.OR.ICODE(N).EQ.-3) GO TO 418
ASSIGN 419 TO NEXT
GO TO 416
415 ASSIGN 417 TO NEXT.
416 SR(I2,J2)=SR(I2,J2)+SE(K1,L2)
GO TO NEXT, (417,419)
417 IF (J1.LT.1) GO TO 419
SR(I2,J1)=SR(I2,J1)+SE(K1,L1)
GO TO 419
418 SR(I2,J2)=SR(I2,J2)+SE(K1,L1)
419 CONTINUE
C
C COMBINES ROCK AND FRACTURE CONTRIBUTIONS INTO SINGLE GLOBAL STIFF-
C NESS MATRIX
420 DO 421 I=1,LMS
B(I)=B(I)+FR(I)
DO 421 J=1,IBWS
A(I,J)=A(I,J)+SR(I,J)
421 CONTINUE
C
IBW=IBWS
LM=LMS
C SOLVES STIFFNESS EQUATION FOR VALUES OF DISPLACEMENT
C -----
CALL BANSOL
C -----
C
C EXPANDS CONDENSED DISPLACEMENT ARRAY TO INCLUDE ALL NODAL
C DISPLACEMENTS (INCLUDING FIXED DISPLACEMENTS)
K=LMS
DO 429 J=1,NSN
I=NSN-J+1
I2=I+I
I1=I2-1
IF (ICODE(I).EQ.0) GO TO 422
GO TO 423
422 DISP(I2)=B(K)
DISP(I1)=B(K-1)
K=K-2
GO TO 429
423 IF (IABS(ICODE(I))-2) 424,425,427
424 IF (ICODE(I).GT.0) GO TO 426
GO TO 422
425 IF (ICODE(I).GT.0) GO TO 428
GO TO 422
426 DISP(I2)=B(K)

```

C.6 Listing of program DEFLOW (Continued)

```

DISP(I1)=0.0
K=K-1
GO TO 429
427 IF(ICODE(1).LT.0) GO TO 428.
DISP(I2)=0.0
DISP(I1)=0.0
GO TO 429
428 DISP(I2)=0.0
DISP(I1)=B(K)
K=K-1
429 CONTINUE

430 RETURN
END

C
C
C -----
C SUBROUTINE FRACSTF
C -----
C
C INCLUDE 'PARAM.COM'
C INCLUDE 'BOTH.COM'
C INCLUDE 'DEFORM.COM'
C INCLUDE 'DIMENS.COM'
C INCLUDE 'FLOW.COM'
C INCLUDE 'MATEQN.COM'
C
C LOOP OVER ALL FRACTURE-FLOW NODE PAIRS
IFN=0
NF=1
DO 507 I=1,NFNT
IFN=IFN+1
IF (IFN.LE.NFN) GO TO 501
NF=NF+1
IFN=1
C INITIAL VALUE FOR KN ARBITRARILY TAKEN AS AVERAGE OF MINIMUM VALUE
C FPROP(NF,5), AND MAXIMUM VALUE, FPROP(NF,8), CALCULATED IN ROUTINE
C 'DEFLOW'. KS IS SET EQUAL TO FIXED AMOUNT OF KN. AFTER FIRST APPROX-
C IMATION OF FIRST ITERATION OF 'BACKGROUND' CALCULATION AND IN ALL
C-SUBSEQUENT ITERATIONS, REVISED VALUES OF STIFFNESS CALCULATED BY
C 'STIFFEN' ROUTINE ARE USED
C NOTE: NECESSARY TO CONVERT TO UNITS OF [Pa/M] FOR THIS ROUTINE
501 IF (NDFIT.GE.0.OR.NP.GT.1) GO TO 502
KN(I)=0.5*(FPROP(NF,5)*1.0E+03+FPROP(NF,8))*1.0E+09
KS(I)=KN(I)*FPROP(NF,9)
GO TO 503
502 KN(I)=KN(I)*1.0E+09

```


C.6 Listing of program DEFLOW (Continued)

```

      KS(I)=KS(I)*1.0E+09
503 M=IFPAIR(NF,IFN,1)
      I2=M+M-LC(M+M)
      I1=I2-1
C CALCULATES AREA OVER WHICH NODAL STIFFNESS APPLICABLE (DIVISION OF
C AREA BETWEEN NODES IS SIMPLY DONE AT MIDPOINT)
C NOTE: AS WITH ALL OTHER TERMS IN STIFFNESS EQUATION, AREA TERMS
C HAVE BEEN DIVIDED BY 2*PI
      IF (IFN.EQ.1) GO TO 504
      IF (IFN.EQ.NFN) GO TO 505
      AREA=0.125*(RR(IFN+1)-RR(IFN-1))*(RR(IFN+1)+RR(IFN-1)+2.0*RR(IFN))
      GO TO 506
504 AREA=0.125*(RR(2)*(2.0*RW+RR(2))-3.0*RW**2)
      GO TO 506
505 AREA=0.125*(3.0*RO**2-RR(NFN-1)*(2.0*RO+RR(NFN-1)))
506 A(I1,1)=A(I1,1)+KS(I)*AREA
      A(I2,1)=A(I2,1)+KN(I)*AREA
      A(I2+1,1)=A(I2+1,1)+KS(I)*AREA
      A(I2+2,1)=A(I2+2,1)+KN(I)*AREA
      A(I1,3)=A(I1,3)-KS(I)*AREA
      A(I2,3)=A(I2,3)-KN(I)*AREA
507 CONTINUE
C
      RETURN
      END
C
C
C
C -----
      SUBROUTINE ROCKSTF
C -----
C GENERATES STIFFNESS MATRIX AND LOAD ARRAY FOR AXISYMMETRIC, TRI-
C ANGULAR ROCK ELEMENTS REPRESENTING LINEAR, ELASTIC MATERIALS
C DETAILS OF AXISYMMETRIC ANALYSIS ARE DESCRIBED IN CHAPTER 4 OF
C ZIENKIEWICZ (1971)
C ROUTINE BASED ON CODE FROM GALE (1975)
C NOTE: THE 2*PI FACTOR HAS BEEN OMITTED FROM BOTH STIFFNESS AND
C LOAD TERMS
C
      INCLUDE 'PARAM.COM'
      INCLUDE 'BOTH.COM'
      INCLUDE 'CONSTS.COM'
      INCLUDE 'DEFORM.COM'
      INCLUDE 'DIMENS.COM'
      INCLUDE 'HEAD.COM'
      INCLUDE 'MATEQN.COM'
      DIMENSION DRZ(9),HH(3)

```

\$
 \$
 \$
 \$
 \$
 \$
 \$

C.6 Listing of program DEFLOW (Continued)

```

I=INC(NE,1)
J=INC(NE,2)
K=INC(NE,3)
NRL=INC(NE,4)
C
C CALCULATES AREA OF TRIANGULAR ELEMENT. IF AREA < OR = 0, ELEMENT
C INCIDENCES MUST BE WRONG AND PROGRAM IS TERMINATED (WITH ERROR
C MESSAGE)
  DELTA=(R(I)*(Z(J)-Z(K))+R(J)*(Z(K)-Z(I))+R(K)*(Z(I)-Z(J)))/2.0
  IF (DELTA.LE.0.0) RETURN
  DET=2.0*DELTA
C
C COMPUTES GEOMETRIC COEFFICIENTS DERIVED BY CYCLIC PERMUTATION OF
C TRANSCRIPTS
  DRZ(1)=R(J)*Z(K)-R(K)*Z(J)
  DRZ(2)=R(K)*Z(I)-R(I)*Z(K)
  DRZ(3)=R(I)*Z(J)-R(J)*Z(I)
  DRZ(4)=Z(J)-Z(K)
  DRZ(5)=Z(K)-Z(I)
  DRZ(6)=Z(I)-Z(J)
  DRZ(7)=R(K)-R(J)
  DRZ(8)=R(I)-R(K)
  DRZ(9)=R(J)-R(I)
C COMPUTES VALUES USED IN "CORRECTIVE TERM" OF AXISYMMETRIC ANALYSIS
  RMIJ=(R(I)+R(J))/2.0
  RMIK=(R(I)+R(K))/2.0
  RMJK=(R(J)+R(K))/2.0
  ZMIJ=(Z(I)+Z(J))/2.0
  ZMIK=(Z(I)+Z(K))/2.0
  ZMJK=(Z(J)+Z(K))/2.0
  B1=1.0/RMIJ
  B2=B1*ZMIJ
  B3=1.0/RMIK
  B4=B3*ZMIK
  B5=1.0/RMJK
  B6=B5*ZMJK
  H1=(B1+B3+B5)/3.0*DELTA
  H2=(RMIJ+RMIK+RMJK)/3.0*DELTA
  H3=(ZMIJ+ZMIK+ZMJK)/3.0*DELTA
  H4=(B2+B4+B6)/3.0*DELTA
  H5=(ZMIJ*B2+ZMIK*B4+ZMJK*B6)/3.0*DELTA
C ASSEMBLES (I.E., SUPERIMPOSES 2x2 SUBMATRICES) MATRIX RESULTING FROM
C PRODUCT OF [D]*[B]*[B]T PLUS CORRECTIVE TERM
  XL11=D(NRL,3,3)*H1
  XL12=(D(NRL,3,1)+D(NRL,3,3))*DELTA
  XL13=D(NRL,3,3)*H4+D(NRL,3,4)*DELTA
  XL15=D(NRL,3,4)*DELTA

```

C.6 Listing of program DEFLOW (Continued)

```

XL16=D(NRL,3,2)*DELTA
XL22=(D(NRL,1,1)+D(NRL,1,3)+D(NRL,3,1)+D(NRL,3,3))*H2
XL23=(D(NRL,1,3)+D(NRL,3,3))*H3+(D(NRL,1,4)+D(NRL,3,4))*H2
XL25=(D(NRL,1,4)+D(NRL,3,4))*H2
XL26=(D(NRL,1,2)+D(NRL,3,2))*H2
XL33=D(NRL,3,3)*H5+(D(NRL,3,4)+D(NRL,4,3))*H3+D(NRL,4,4)*H2
XL35=D(NRL,3,4)*H3+D(NRL,4,4)*H2
XL36=D(NRL,3,2)*H3+D(NRL,4,2)*H2
XL55=D(NRL,4,4)*H2
XL56=D(NRL,4,2)*H2
XL66=D(NRL,2,2)*H2
XI11=DRZ(1)/DET
XI12=DRZ(4)/DET
XI13=DRZ(7)/DET
XI21=DRZ(2)/DET
XI22=DRZ(5)/DET
XI23=DRZ(8)/DET
XI31=DRZ(3)/DET
XI32=DRZ(6)/DET
XI33=DRZ(9)/DET
R11=XI11*XL11+XI12*XL12+XI13*XL13
R12=XI11*XL12+XI12*XL22+XI13*XL23
R13=XI11*XL13+XI12*XL23+XI13*XL33
R15=XI11*XL15+XI12*XL25+XI13*XL35
R16=XI11*XL16+XI12*XL26+XI13*XL36
R21=XI12*XL15+XI13*XL16
R22=XI12*XL25+XI13*XL26
R23=XI12*XL35+XI13*XL36
R25=XI12*XL55+XI13*XL56
R26=XI12*XL56+XI13*XL66
R31=XI21*XL11+XI22*XL12+XI23*XL13
R32=XI21*XL12+XI22*XL22+XI23*XL23
R33=XI21*XL13+XI22*XL23+XI23*XL33
R35=XI21*XL15+XI22*XL25+XI23*XL35
R36=XI21*XL16+XI22*XL26+XI23*XL36
R41=XI22*XL15+XI23*XL16
R42=XI22*XL25+XI23*XL26
R43=XI22*XL35+XI23*XL36
R45=XI22*XL55+XI23*XL56
R46=XI22*XL56+XI23*XL66
R51=XI31*XL11+XI32*XL12+XI33*XL13
R52=XI31*XL12+XI32*XL22+XI33*XL23
R53=XI31*XL13+XI32*XL23+XI33*XL33
R55=XI31*XL15+XI32*XL25+XI33*XL35
R56=XI31*XL16+XI32*XL26+XI33*XL36
R65=XI32*XL55+XI33*XL56
R66=XI32*XL56+XI33*XL66

```

C.6 Listing of program DEFLOW (Continued)

C ARRANGES FINAL UPPER TRIANGULAR PORTION OF 6x6 ELEMENT STIFFNESS
C MATRIX

```

SE(1,1)=R11*XI11+R12*XI12+R13*XI13
SE(1,2)=R15*XI12+R16*XI13
SE(1,3)=R11*XI21+R12*XI22+R13*XI23
SE(1,4)=R15*XI22+R16*XI23
SE(1,5)=R11*XI31+R12*XI32+R13*XI33
SE(1,6)=R15*XI32+R16*XI33
SE(2,2)=R25*XI12+R26*XI13
SE(2,3)=R21*XI21+R22*XI22+R23*XI23
SE(2,4)=R25*XI22+R26*XI23
SE(2,5)=R21*XI31+R22*XI32+R23*XI33
SE(2,6)=R25*XI32+R26*XI33
SE(3,3)=R31*XI21+R32*XI22+R33*XI23
SE(3,4)=R35*XI22+R36*XI23
SE(3,5)=R31*XI31+R32*XI32+R33*XI33
SE(3,6)=R35*XI32+R36*XI33
SE(4,4)=R45*XI22+R46*XI23
SE(4,5)=R41*XI31+R42*XI32+R43*XI33
SE(4,6)=R45*XI32+R46*XI33
SE(5,5)=R51*XI31+R52*XI32+R53*XI33
SE(5,6)=R55*XI32+R56*XI33
SE(6,6)=R65*XI32+R66*XI33

```

C COMPLETES LOWER TRIANGULAR PORTION OF MATRIX BY SYMMETRY

```

DO 601 N=1,5
  K=N+1
  DO 601 M=K,6
    SE(M,N)=SE(N,M)

```

601 CONTINUE

C
C ADDITIONAL INTEGRALS FOR CALCULATING GRAVITY FORCES

```

HH(1)=H2/DET
HH(2)=(RMIJ*RMIJ+RMIK*RMJK+RMJK*RMJK)/6.0
HH(3)=(RMIJ*ZMIJ+RMIK*ZMIK+RMJK*ZMIK)/6.0

```

C CALCULATES GRAVITY (BODY) FORCES AND ASSIGNS TO ELEMENT LOAD

C ARRAY

```

DO 602 I=1,6
  FE(I)=0.0
602 CONTINUE
DO 604 M=1,3
  K=M
  DO 603 N=1,3
    FE(M+M)=FE(M+M)+HH(N)*DRZ(K)*RPROP(NRL,2)*G
  K=K+3

```

603 CONTINUE

604 CONTINUE

C

c.6 Listing of program DEFLOW (Continued)


```

RETURN
END

C
C
C -----
C SUBROUTINE BANSOL
C -----
C SOLVES MATRIX EQUATIONS WITH BANDED, SYMMETRIC COEFFICIENT MATRICES
C BY GAUSSIAN ELIMINATION AND BACKWARD SUBSTITUTION
C
C   INCLUDE 'PARAM.COM'
C   INCLUDE 'MATEQN.COM'
C
C DECOMPOSES COEFFICIENT MATRIX BY GAUSS ELIMINATION. SINCE MATRIX IS
C SYMMETRIC, ONLY UPPER TRIANGLE HAD TO BE STORED FOR THIS OPERATION
C   DO 704 I=1,LM
C   DO 704 J=2,IBW
C   C=A(I,J)/A(I,1)
C   K=I+J-1
C   IF (LM-K) 703,701,701
701 L=0
C   DO 702 M=J,IBW
C   L=L+1
C   A(K,L)=A(K,L)-C*A(I,M)
702 CONTINUE
703 A(I,J)=C
704 CONTINUE

C
C SOLVES FOR UNKNOWNNS BY BACK SUBSTITUTION. RE-USES [B] ARRAY TO STORE
C AND RETURN SOLUTION ARRAY
C   DO 708 I=1,LM
C   Y=B(I)
C   DO 706 J=2,IBW
C   K=I+J-1
C   IF (LM-K) 707,705,705
705 B(K)=B(K)-A(I,J)*Y
706 CONTINUE
707 B(I)=Y/A(I,1)
708 CONTINUE
C   I=LM
709 I=I-1
C   IF (I) 701,713,710
710 DO 712 J=2,IBW
C   K=I+J-1
C   IF (LM-K) 712,711,711
711 B(I)=B(I)-A(I,J)*B(K)
712 CONTINUE

```


 Listing of program DEFLOW. (Continued)

```

      GO TO 709
C
713 RETURN
  END
C
C
C -----
  SUBROUTINE STIFFEN
C -----
C ASSIGNS NEW STIFFNESSES TO FRACTURE(S) IF CLOSURE OCCURS
C
  INCLUDE 'PARAM.COM'
  INCLUDE 'BOTH.COM'
  INCLUDE 'DEFORM.COM'
  INCLUDE 'DIMENS.COM'
  INCLUDE 'FLAGS.COM'
  INCLUDE 'FLOW.COM'
  INCLUDE 'MATEQN.COM'
  DIMENSION DZO(NFNTD)
C
  FLAG7=.TRUE.
  L=0
C
C LOOP OVER ALL FRACTURE-FLOW NODE PAIRS
  DO 808 N=1,NFRAC
  DO 807 M=1,NFN
    IF (NDFIT.EQ.-1.AND.NP.EQ.1) DZO(L+M)=0.0
C NOTE: THIS ROUTINE REQUIRES STIFFNESS TO BE IN UNITS OF [GPa/M].
C THEREFORE NECESSARY TO RE-CONVERT FROM UNITS OF [Pa/M] LAST USED
C IN ROUTINE 'DEFORM'
    KN(L+M)=KN(L+M)*1.0E-09
    KS(L+M)=KS(L+M)*1.0E-09
C DETERMINES RELATIVE VERTICAL MOVEMENT AT FRACTURE NODE
C SIGN CONVENTION: IF DZ -'VE, FRACTURE IS CLOSING
    I2=2*IFPAIR(N,M,1)
    J2=2*IFPAIR(N,M,2)
    DZ=DISP(I2)-DISP(J2)
C DETERMINES IF NECESSARY TO ASSIGN NEW NORMAL STIFFNESS
    IF (DZ.NE.0.0) GO TO 801
    IF (ABS(DZO(L+M)).LT.1.0E-07) GO TO 806.
    GO TO 802
C CHECK FOR CONVERGENCE
  801 IF (ABS((DZ-DZO(L+M))/DZ).LE.EPSILON) GO TO 806
    IF (ABS(DZ).LE.1.0E-07) DZ=0.0
    IF (DZ.LT.0.0) GO TO 804
  802 IF (DZ.GT.0.0) GO TO 803
C IF FRACTURE HAS ZERO DISPLACEMENT, HALVES PREVIOUS STIFFNESS

```

C.6 Listing of program DEFLOW (Continued)

```

      KN(L+M)=0.5*KN(L+M)
      GO TO 805
C IF FRACTURE IS OPENING (WITH RESPECT TO ABSOLUTE ZERO DISPLACEMENT
C ON THE CONSTITUTIVE CURVE, NOT WITH RESPECT TO THE BACKGROUND
C DISPLACEMENT), ASSIGNS ZERO STIFFNESS
      803 IF (KN(L+M).EQ.0.0) GO TO 806
      KN(L+M)=0.0
      GO TO 805
C IF FRACTURE IS CLOSING, ASSIGNS NEW VALUE FOR NORMAL STIFFNESS
C BASED ON INPUT-DEFINED CONSTITUTIVE RELATIONSHIP FOR FRACTURE.
C MUST CONVERT DZ INTO UNITS OF [MM] TO PREVENT POSSIBLE UNDERFLOW
C (WHICH RESULTS IN VALUES BEING DISREGARDED BY VAX-11 FORTRAN SYSTEM
C USED AT MUN)
      804 DZMM=ABS(DZ)*1.0E+03
      SIGMA=FPROP(N,5)*DZMM+FPROP(N,6)*DZMM**FPROP(N,7)
      KN(L+M)=0.5*(KN(L+M)+SIGMA/ABS(DZ))
      805 FLAG7=.FALSE.
C ASSIGNS NEW TANGENTIAL STIFFNESS AS FUNCTION OF NORMAL STIFFNESS
      KS(L+M)=KN(L+M)*FPROP(N,9)
      806 DZO(L+M)=DZ
      807 CONTINUE
      L=L+NFN
      808 CONTINUE
C
      RETURN
      END
C
C
C -----
      SUBROUTINE FLO2REG
C -----
C CALCULATES RADIAL DISTANCE-TOTAL HEAD DISTRIBUTION IN RIGID FRACTURE
C UNDER LINEAR AND/OR NON-LINEAR FLOW CONDITIONS
C
      INCLUDE 'PARAM.COM'
      INCLUDE 'BOTH.COM'
      INCLUDE 'CONSTS.COM'
      INCLUDE 'FLAGS.COM'
      INCLUDE 'FLOW.COM'
      INCLUDE 'HEAD.COM'
      INCLUDE 'MATEQN.COM'
      DIMENSION THEADI(NFE)
C
      THEAD(NFN)=H0
      IF (NF.GT.1) HW(NF)=HW(NF-1)-SEL-SWB(NF-1)
      NFIT=0
      DO 901 I=1,NFE

```

C.6 Listing of program DEFLOW (Continued)

```

    THEADI(I)=HO
901 CONTINUE
C
    IF (FLAG2) FLAG3=.TRUE.
902 IF (NFIT.GE.MAXFIT) GO TO 903
    GO TO 904
903 FLAG2=.TRUE.
    RETURN
904 IF (NFIT.GT.0) GO TO 905
    ALPHA=1.0
    GO TO 906
905 ALPHA=RELAXF
906 DO 907 I=1,NFE
    B(I)=0.0
    DO 907 J=1,2
    A(I,J)=0.0
907 CONTINUE
C
C DETERMINES APPROPRIATE FLOW LAW FOR ASSIGNING TRANSMISSIVITY TO
C EACH FLOW NODE
C -----
C CALL FLOWLAW
C -----
C
C GENERATES TRANSMISSIVITY MATRIX AND FLUX ARRAY. TRANSMISSIVITY
C MATRIX IS DERIVED FROM SYMMETRIC, TRIDIAGONAL MATRIX AND IS
C ASSEMBLED INITIALLY AS N1 x 2 RECTANGULAR MATRIX
    DO 908 I=1,N1
C- MAIN DIAGONAL BECOMES LEFT COLUMN OF RECTANGULAR MATRIX
    A(I,1)=2.0*PI*(TRANS(I)+2.0*TRANS(I+1)+TRANS(I+2))/(2.0*EL)
C- UPPER RIGHT DIAGONAL BECOMES RIGHT COLUMN
    A(I,2)=-2.0*PI*(TRANS(I+1)+TRANS(I+2))/(2.0*EL)
908 CONTINUE
C
C IF 2ND TYPE BOUNDARY CONDITION AT WELL, ADDS ANOTHER ROW TO MATRICES.
C IN EITHER CASE, PARTITIONS MATRICES BECAUSE OF FIXED HEAD VALUE(S)
C AND CALCULATES FLUX VALUE AT FLOW NODES I AND NFN (WHICH BECOMES
C EITHER NFE OR N1 IN THE MODIFIED FLUX ARRAY)
    IF (IBCWELL.EQ.1) GO TO 910
    B(1)=-Q/ALPHA
    B(NFE)=2.0*PI*(TRANS(NFE)+TRANS(NFN))*HO/(2.0*ALPHA*EL)
    DO 909 I=1,N1
    K=N1-I+1
    DO 909 J=1,2
    A(K+1,J)=A(K,J)
909 CONTINUE
    A(1,1)=2.0*PI*(TRANS(1)+TRANS(2))/(2.0*EL)

```


C.6 Listing of program DEFLOW (Continued)

```

A(1,2)=-A(1,1)
LM=NFE
K=0
GO TO 911
910 B(1)=2.0*PI*(TRANS(1)+TRANS(2))*HW(NF)/(2.0*ALPHA*EL)
    B(N1)=2.0*PI*(TRANS(NFE)+TRANS(NFN))*HO/(2.0*ALPHA*EL)
    LM=N1
    K=1
C
C RELAXATION SCHEME TO ACCELERATE CONVERGENCE. MODIFIES 'KNOWN' VALUES
C DERIVED IN PREVIOUS ITERATION BY RELAXATION FACTOR AND ADDS TO FLUX
C TERMS
911 DO 912 I=2,LM-1
    DO 912 J=1,3
    B(I)=B(I)+A(I,J)*THEADI(I-2+J+K)*(1.0-(1.0/ALPHA))
912 CONTINUE
    B(1)=B(1)+A(1,2)*THEADI(K+1)*(1.0-(1.0/ALPHA))+A(1,3)*THEADI(K+2)*
    *(1.0-(1.0/ALPHA))
    B(LM)=B(LM)+A(LM,1)*THEADI(N1)*(1.0-(1.0/ALPHA))+A(LM,2)*THEADI(NF
    *E)*(1.0-(1.0/ALPHA))
C
    IBW=2
C SOLVES FLOW EQUATION
C -----
C CALL BANSOL
C -----
C
C EXPANDS HEAD ARRAY TO INCLUDE FIXED HEAD VALUE(S)
    DO 914 I=1,LM
    IF (IBCWELL.EQ.2) GO TO 913
    K=N1-I+1
    THEAD(K+1)=B(K)
    GO TO 914
913 THEAD(I)=B(I)
914 CONTINUE
    IF (IBCWELL.EQ.1) THEAD(1)=HW(NF)
    IF (NFIT.LE.0) GO TO 916
C
C CHECKS FOR CONVERGENCE (USING RELATIVE CRITERION) OF HEAD VALUES
    DO 915 I=1,NFE
    RELCONV=ABS((THEAD(I)-THEADI(I))/THEAD(I))
    IF (RELCONV.GT.EPSILON) GO TO 916
915 CONTINUE
    GO TO 918
C
C REASSIGNS "PRESENT" VALUES OF HEAD AS "PREVIOUS" VALUES PRIOR TO
C START OF NEXT ITERATION

```

C.6 Listing of program DEFLOW (Continued)

```

916 DO 917 I=1,NFE
      THEAD(I)=THEAD(I)
917 CONTINUE
      NFIT=NFIT+1
      GO TO 902
C
918 RETURN
      END
C
C
C -----
      SUBROUTINE FLOWLAW
C -----
C ASSIGNS APPROPRIATE FLOW LAW (AFTER LOUIS, 1969) BASED ON FRACTURE
C ROUGHNESS AND REYNOLDS NUMBER
C
      INCLUDE 'PARAM.COM'
      INCLUDE 'BOTH.COM'
      INCLUDE 'CONSTS.COM'
      INCLUDE 'FLOW.COM'
      INCLUDE 'HEAD.COM'
      DIMENSION ELGRAD(NFED),ELVEL(NFED),GRAD(NFND)
C
C FIRST TIME THROUGH ROUTINE, ASSUMES FLOW IS LINEAR AND ASSIGNS EITHER
C FLOW LAW 1 OR 4 BASED ON ROUGHNESS ONLY
      IF (NFIT) 1001,1001,1005
1001 DO 1004 I=1,NFN
      IF (ROUGH(I)-0.033) 1002,1002,1003
C FLOW LAW 1
1002 TRANS(I)=TWOB(I)**3*G/(12.0*VISC)
      GO TO 1004
C FLOW LAW 4
1003 TRANS(I)=TWOB(I)**3*G/(12.0*VISC*(1.0+8.8*ROUGH(I)**1.5))
1004 CONTINUE
      RETURN
C
C IN SUBSEQUENT RUNS THROUGH ROUTINE, ASSIGNS FLOW LAWS BASED ON
C BOTH ROUGHNESS AND REYNOLDS NUMBER (WHICH REQUIRES CALCULATION OF
C VELOCITY). FOR NON-LINEAR FLOW LAWS, ALSO NECESSARY TO INCORPORATE
C LINEAR GRADIENT (DETERMINED FROM HEAD DISTRIBUTION FROM PREVIOUS
C ITERATION) INTO TERM FOR TRANSMISSIVITY. DEPENDING ON BOUNDARY
C CONDITION AT WELL, VELOCITY IS CALCULATED EITHER FROM 1) CONTINUITY
C EQUATION AT EACH NODE OR 2) DARCY-TYPE EQUATION FOR EACH ELEMENT
C FROM WHICH AVERAGE VALUE OF TWO ADJACENT ELEMENTS IS ASSIGNED AT
C EACH NODE. DARCY VELOCITY IS DIVIDED BY POROSITY TO DETERMINE TRUE
C FLOW VELOCITY (AND TO ACCOUNT FOR DIFFERENCE BETWEEN GEOMETRIC
C AND EFFECTIVE APERTURE)

```

C.6 Listing of program DEFLOW (Continued)

```

1005 IF (IBCWELL.EQ.1) GO TO 1007
      DO 1006 J=1,NFN
        VEL(J)=Q/(2.0*PI*RR(J)*TWOB(J)*(FPROP(NF,4)/100.0))
1006 CONTINUE
      GO TO 1010
1007 DO 1008 J=1,NFE
        ELVEL(J)=2.0*PI*(TRANS(J)+TRANS(J+1))/((RR(J)+RR(J+1))*(TWOB(J)+TW
        *OB(J+1)))*ABS((THEAD(J+1)-THEAD(J)))/(PI*EL)
1008 CONTINUE
        VEL(1)=ELVEL(1)/(FPROP(NF,4)/100.0)
        VEL(NFN)=ELVEL(NFE)/(2.0*FPROP(NF,4)/100.0)
        DO 1009 J=1,N1
          VEL(J+1)=(ELVEL(J)+ELVEL(J+1))/(2.0*FPROP(NF,4)/100.0)
1009 CONTINUE
C
C CALCULATES GRADIENT (IN LINEAR COORDINATES) TO BE USED IN NON-LINEAR
C FLOW LAWS. AS WITH VELOCITIES FOR 1ST TYPE B.C.'S, GRADIENTS ARE
C FIRST CALCULATED FOR EACH ELEMENT AND THEN AVERAGED AT EACH NODE.
1010 DO 1011 J=1,NFE
        ELGRAD(J)=ABS((THEAD(J+1)-THEAD(J))/(RR(J+1)-RR(J)))
1011 CONTINUE
        GRAD(1)=ELGRAD(1)
        GRAD(NFN)=ELGRAD(NFE)/2.0
        DO 1012 J=1,N1
          GRAD(J+1)=(ELGRAD(J)+ELGRAD(J+1))/2.0
1012 CONTINUE
C
C DETERMINES REYNOLDS NUMBER AT EACH NODE USING CALCULATED VELOCITIES
      DO 1013 J=1,NFN
        RE(J)=2.0*TWOB(J)*VEL(J)/VISC
1013 CONTINUE
C
C ASSIGNS FLOW LAWS
      DO 1024 I=1,NFN
        CL(I)=1.0
C IF FRACTURE SMOOTH (THAT IS, K/DH=0, WHICH COULD RESULT IN DIVISION
C BY 0) OR BELOW LIMIT OF ABOUT 0.0004 (FOR WHICH EMPIRICAL FLOW LAWS
C HAVE BEEN ASSIGNED) NOMINAL ROUGHNESS IS ASSIGNED
        IF (ROUGH(I).LT.0.0004) ROUGH(I)=0.0004
        IF (ROUGH(I)-0.0168) 1014,1014,1019
C BOUNDARY BETWEEN LINEAR AND NON-LINEAR FLOW FOR K/DH < 0.0168
C IS RE=2300
1014 IF (RE(I)-2300.) 1015,1015,1016
C TRANSMISSIVITY BASED ON FLOW LAW 1 (POISEUILLE'S LAW)
1015 IF (IBCWELL.EQ.1) GO TO 10151
        REO=Q/(2.0*PI*VISC*TWOB(I))
        RD=(2.0*RR(I))/(TWOB(I)*SQRT(REO))

```

C.6 Listing of program DEFLOW (Continued)

```

      CL(I)=SQRT(1.0+(0.36/RD)**2.0)
10151 TRANS(I)=TWOB(I)**3*G/(CL(I)*12.0*VISC)
      LAW(I)=1
      GO TO 1024
C BOUNDARY BETWEEN FLOW LAWS 2 AND 3
1016 REK1=2.552*(ALOG10(3.7/ROUGH(I)))**8.
      IF (RE(I)-REK1) 1017,1017,1018.
C TRANSMISSIVITY BASED ON FLOW LAW 2 (LAW OF BLASIUS)
1017 TRANS(I)=4.71*TWOB(I)**1.714*G**0.571/VISC**0.143/GRAD(I)**0.429
      LAW(I)=2
      GO TO 1024
C TRANSMISSIVITY BASED ON FLOW LAW 3 (LAW OF NIKURADSE)
1018 TRANS(I)=4.0*SQRT(G)*TWOB(I)**1.5*ALOG10(3.7/ROUGH(I))/SQRT(GRAD(I
*))
      LAW(I)=3
      GO TO 1024
1019 IF (ROUGH(I)-0.033) 1020,1020,1021
C BOUNDARY BETWEEN FLOW LAWS 1 AND 3
C 0.0168 < K/DH < 0.033
1020 REK2=((142000.*(ALOG10(3.7/ROUGH(I)))**2))**0.568
      IF (RE(I)-REK2) 1015,1015,1018
C BOUNDARY BETWEEN FLOW LAWS 4 AND 5
1021 REK3=((142000.*(ALOG10(1.9/ROUGH(I)))**2))**0.568
      IF (RE(I)-REK3) 1022,1022,1023
C TRANSMISSIVITY BASED ON FLOW LAW 4
1022 IF (IBCWELL.EQ.1) GO TO 10221
      REO=Q/(2.0*PI*VISC*TWOB(I))
      RD=(2.0*RR(I))/(TWOB(I)*SQRT(REO))
      CL(I)=SQRT(1.0+(0.36/RD)**2.0)
10221 TRANS(I)=G*TWOB(I)**3/(CL(I)*12.0*VISC*(1.0+8.8*ROUGH(I)**1.5))
      LAW(I)=4
      GO TO 1024
C TRANSMISSIVITY BASED ON FLOW LAW 5
1023 TRANS(I)=4.0*SQRT(G)*TWOB(I)**1.5*ALOG10(1.9/ROUGH(I))/SQRT(GRAD(I
*))
      LAW(I)=5
1024 CONTINUE
C
      RETURN
      END

```

C.7 Listing of program FRACLAW

```
*****
* FRACLAW *
*****
```

```
PROGRAM TO DEFINE NORMAL STRESS VERSUS DISPLACEMENT
RELATIONSHIP FOR A FRACTURE
IN THE FORM
SIGMA = K1*DISP + K2*DISP**N
BY NON-LINEAR REGRESSION
```

```
BY
```

```
LEE C. ATKINSON
DEPARTMENT OF EARTH SCIENCES
MEMORIAL UNIVERSITY OF NEWFOUNDLAND
```

```
JANUARY, 1984
```

```
*****
```

```
INPUT FILE REQUIRED FOR FRACLAW:
```

| LINE | DATA | FORMAT |
|------|--|--------|
| ---- | ---- | ----- |
| 1 | NAME OR OTHER ID FOR DATA SET TO BE ANALYZED | A40 |
| 2+ | STRESS [GPa] AND DISPLACE- MENT [M] OF EACH DATA POINT (NOTE: PROGRAM CONVERTS ALL DISPLACEMENTS TO [MM] TO AVOID POTENTIAL UNDERFLOW) | 2E10.2 |

```
*****
```

```
DIMENSION DISP(50),SIGMA(50),SIGMA2(50)
CHARACTER*20 FILEIN,FILEOUT
CHARACTER*40 DATASET
REAL K1,K1STAR,K2,K2STAR,N,NSTAR
```

```
C DEFINES INPUT AND OUTPUT FILES
```

```
WRITE (6,*) 'Enter name of input file.'
READ (5,1) FILEIN
WRITE (6,*) 'Enter desired name for output file.'
READ(5,1) FILEOUT
```

C.7 Listing of program FRACLAW (Continued)

```

1 FORMAT(A20)
  OPEN (UNIT=2,FILE=FILEIN,STATUS='OLD')
  OPEN (UNIT=3,FILE=FILEOUT,STATUS='NEW')
C
C READS INPUT
  READ (2,2) DATASET
2 FORMAT (A40)
  NDAT=1
3 READ (2,4,END=5) SIGMA(NDAT),DISP(NDAT)
4 FORMAT (2E10.2)
C CONVERTS DISP'S TO [MM] TO PREVENT POSSIBLE OVERFLOW (WHICH WOULD
C RESULT IN VALUES BEING DISREGARDED)
  DISP(NDAT)=DISP(NDAT)*1.0E+03
  NDAT=NDAT+1
  GO TO 3
5 NDAT=NDAT-1
C
C INITIALIZES VALUES FOR ERROR, N, AND CHANGE IN N
  ERROLD=1.0E+08
  DELTN=1.0
  N=1.1
C
C CALCULATES TERMS IN NORMAL EQUATIONS INDEPENDENT OF N
  A11=0.0
  D1=0.0
  DO 6 I=1,NDAT
    A11=A11+(DISP(I)**2)
    D1=D1+SIGMA(I)*DISP(I)
6 CONTINUE
C
C DETERMINES BEST VALUES OF K1 AND K2 FOR GIVEN VALUE OF N
C CALCULATES REMAINING TERMS IN NORMAL EQUATIONS (THOSE WHICH ARE
C DEPENDENT ON N)
7 A12=0.0
  A22=0.0
  D2=0.0
  DO 8 I=1,NDAT
    A12=A12+(DISP(I)**(N+1.0))
    A22=A22+(DISP(I)**(2.0*N))
    D2=D2+SIGMA(I)*(DISP(I)**N)
8 CONTINUE
C SOLVES NORMAL EQUATIONS FOR COEFFICIENTS K1 AND K2 BY CRAMER'S
C RULE
  A21=A12
  DET=A11*A22-A12*A21
  K1=(D1*A22-A12*D2)/DET
  K2=(A11*D2-D1*A21)/DET

```

C.7 Listing of program FRACLAW (Continued)

```

C
C CALCULATES ERROR BY LEAST SQUARES CRITERION
  ERRNEW=0.0
  DO 9 I=1,NDAT
    ERRNEW=ERRNEW+(ABS(K1*DISP(I)+K2*DISP(I)**N-SIGMA(I)))**2
  9 CONTINUE
C
C IF ERROR IS DECREASING; CONTINUES INTERATING WITH CURRENT VALUE OF
C DELTN. IF ERROR IS INCREASING, CHANGES VALUE OF DELTN AND RESUMES
C ITERATION (UNLESS ACCURACY LIMIT HAS BEEN ACHIEVED)
  IF (ERRNEW-ERROLD) 10,10,11
10 ERROLD=ERRNEW
  K1STAR=K1
  K2STAR=K2
  NSTAR=N
  GO TO 13
11 IF (ABS(DELTN)-0.005) 14,14,12
12 DELTN=-DELTN*0.1
  ERROLD=ERRNEW
13 N=N+DELTN
  GO TO 7
C
C PRINTS RESULTS
14 WRITE (3,15) DATASET
15 FORMAT (//,19X,'RESULTS OF ANALYSIS USING',1X,9H'FRACLAW',///,1X,'
  2DATA SET:',1X,A40,///,18X,'INPUT',5X,'CALC',/,9X,'DISP',5X,'SIGMA',
  35X,'SIGMA',/,9X,'[M]',6X,'[GPa]',5X,'[GPa]',/,7X,8(1H-),2X,8(1H-),
  42X,8(1H-),/)
  DO 17 I=1,NDAT
    SIGMA2(I)=K1STAR*DISP(I)+K2STAR*DISP(I)**NSTAR
    DISP(I)=DISP(I)/1.0E+03
    WRITE (3,16) DISP(I),SIGMA(I),SIGMA2(I)
16 FORMAT (7X,1PE8.2,2X,E8.2,2X,E8.2)
17 CONTINUE
  WRITE (3,18) K1STAR,K2STAR
18 FORMAT (//,1X,'RESULTS:',//,20X,'SIGMA = K1*DISP + K2*DISP**n',//,
  211X,'K1 = ',1PE9.2,2X,'[GPa/MM]',/,11X,'K2 = ',E9.2,2X,'[units dep
  3endent on value of n]')
  WRITE (3,19) NSTAR
19 FORMAT (12X,'n = ',F5.2,///,11X,'Note: ',7HDISP's ',must be in unit
  2s of [MM] to apply',/,17X,'this relationship.',/,17X,'SIGMA is in
  3[GPa].')
  WRITE (6,20) FILEOUT
20 FORMAT (/,1X,'Successful execution.',/,1X,'Output has been written
  2 to file: ',A20,/)
C
  STOP
  END

```

APPENDIX D
SENSITIVITY ANALYSIS PLOTS

The following plots show the distribution of total head loss (or drawdown) versus the logarithm of radial distance that were calculated by DEFLOW as part of the analysis of sensitivity to changes in various fracture flow parameters. One of the primary reasons for using this distance-drawdown format is that it clearly shows the critical radius and emphasizes the short radial distance over which the greatest change occurs. The findings from the sensitivity analysis are discussed in Section 3.2 (page 82) of the text.

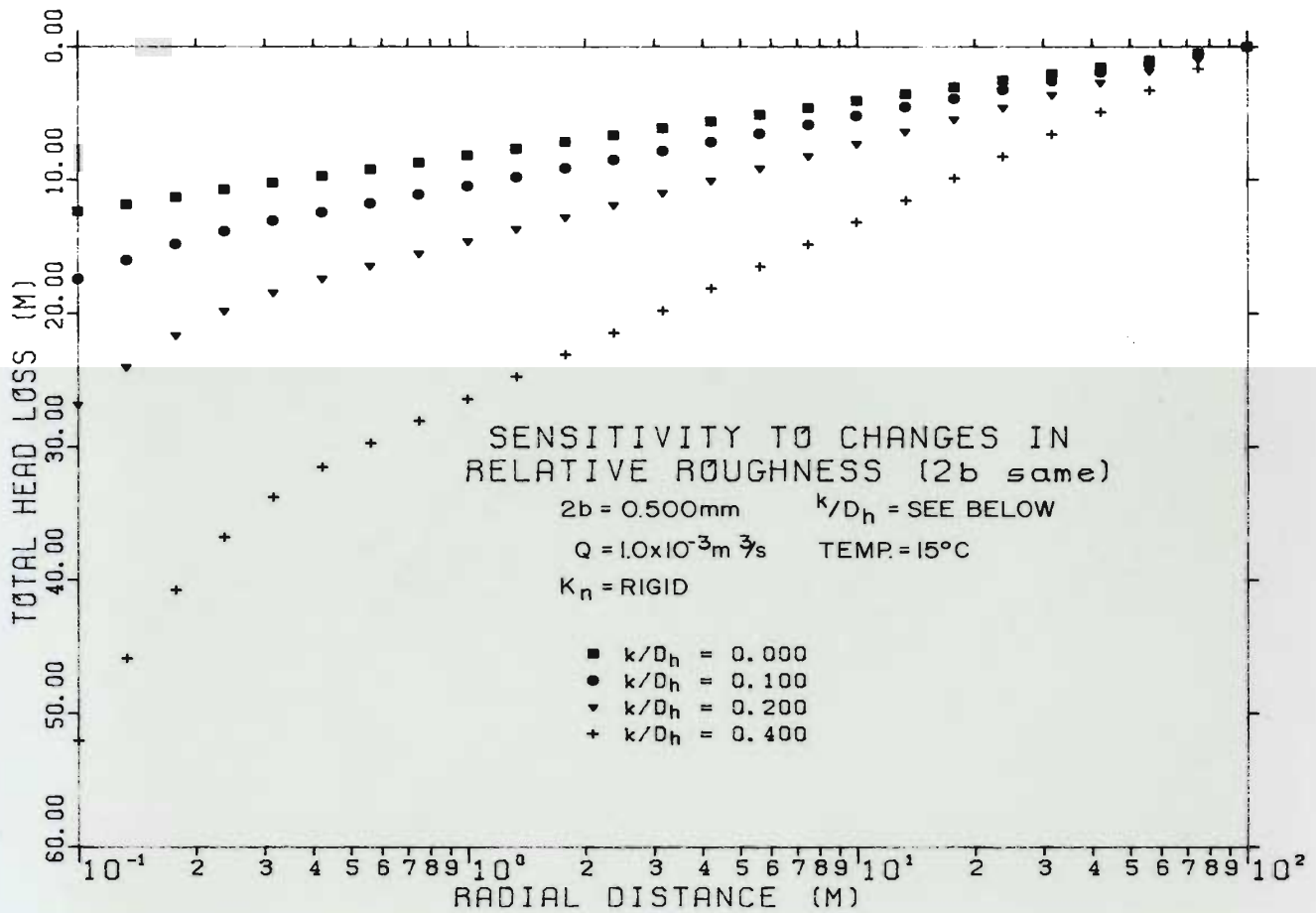


Figure D1 Sensitivity of head distribution to variation in relative roughness of fracture

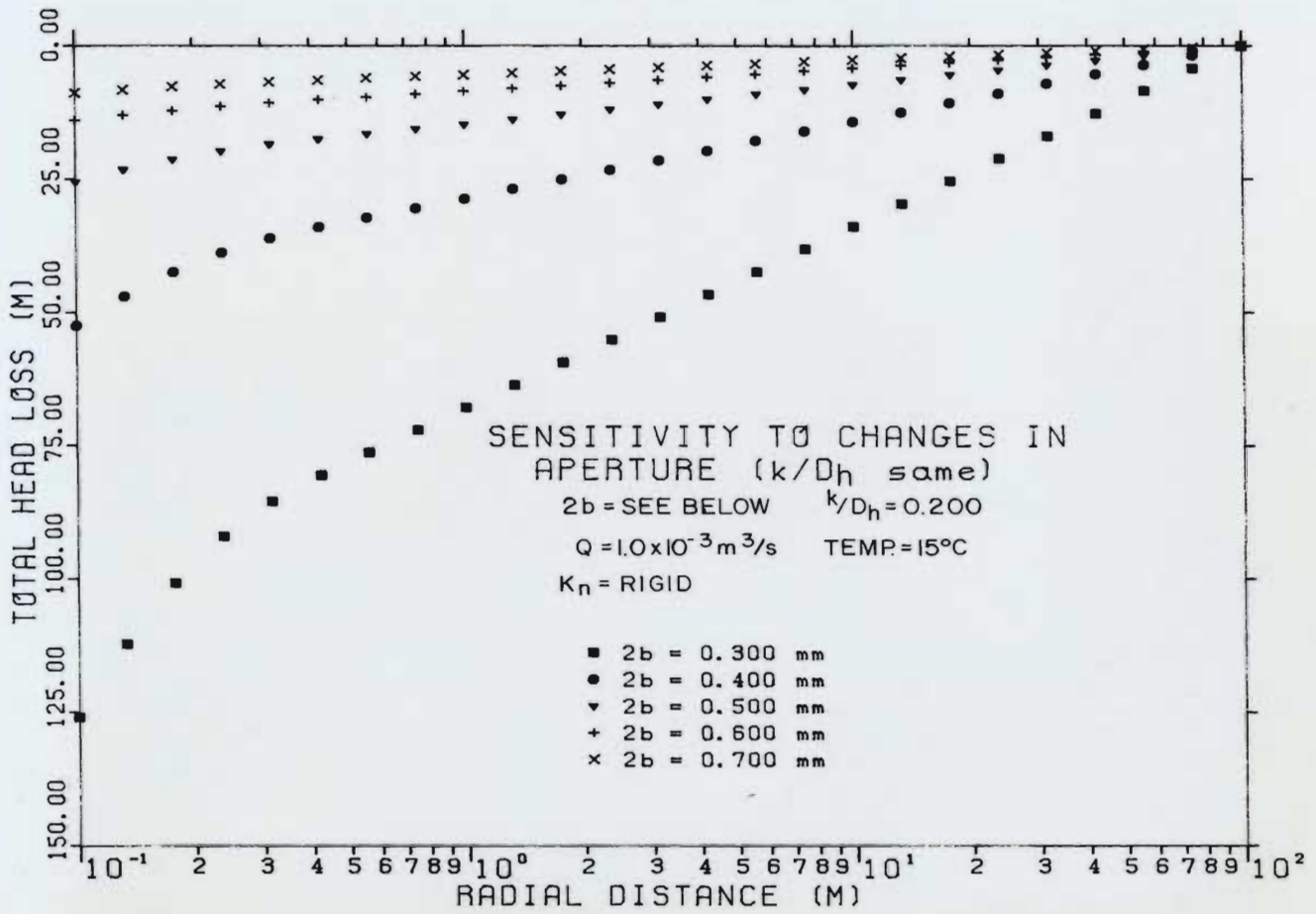


Figure D2 Sensitivity of head distribution to variation in fracture aperture (keeping relative roughness constant)

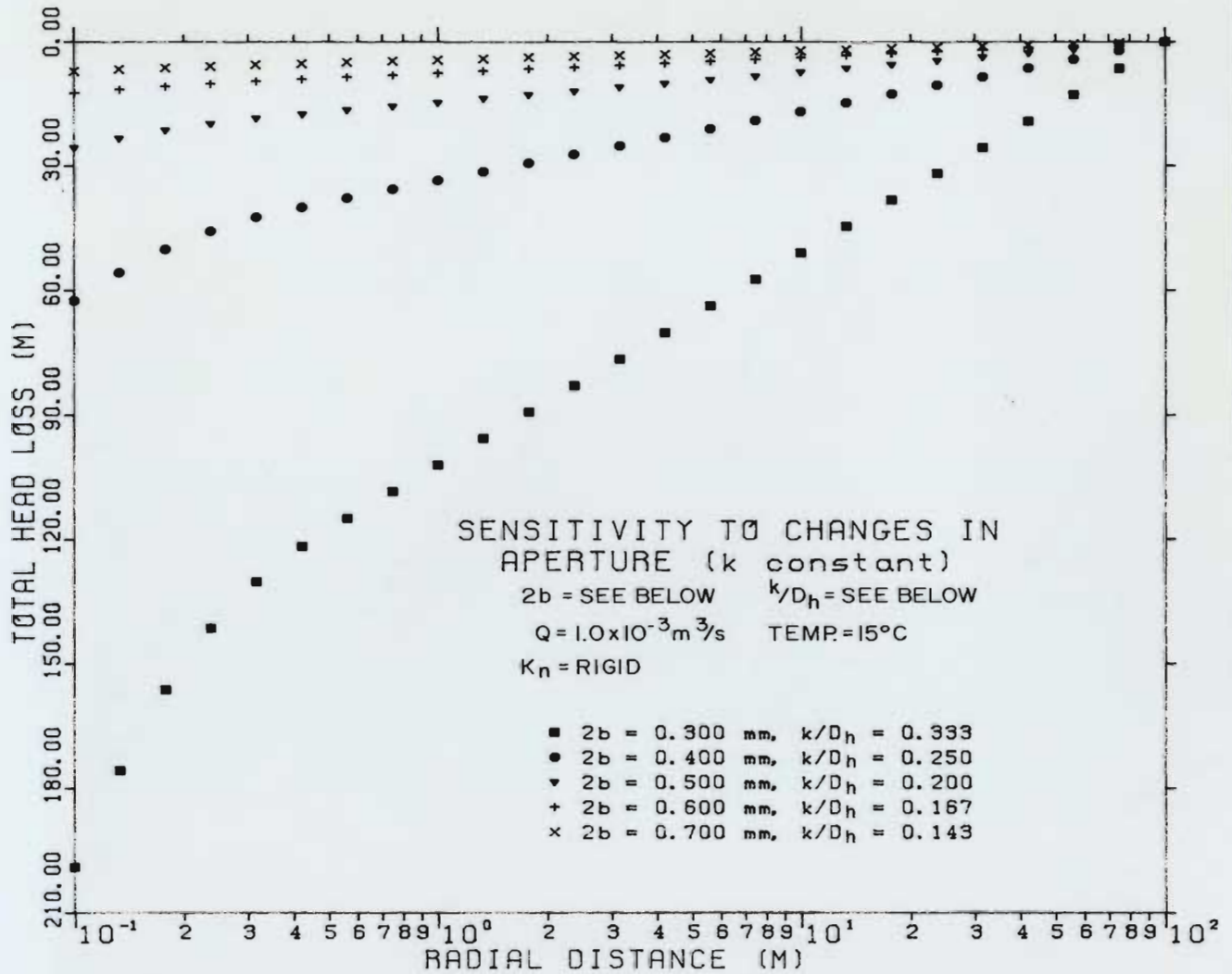


Figure D3 Sensitivity of head distribution to variation in fracture aperture (keeping absolute roughness constant)

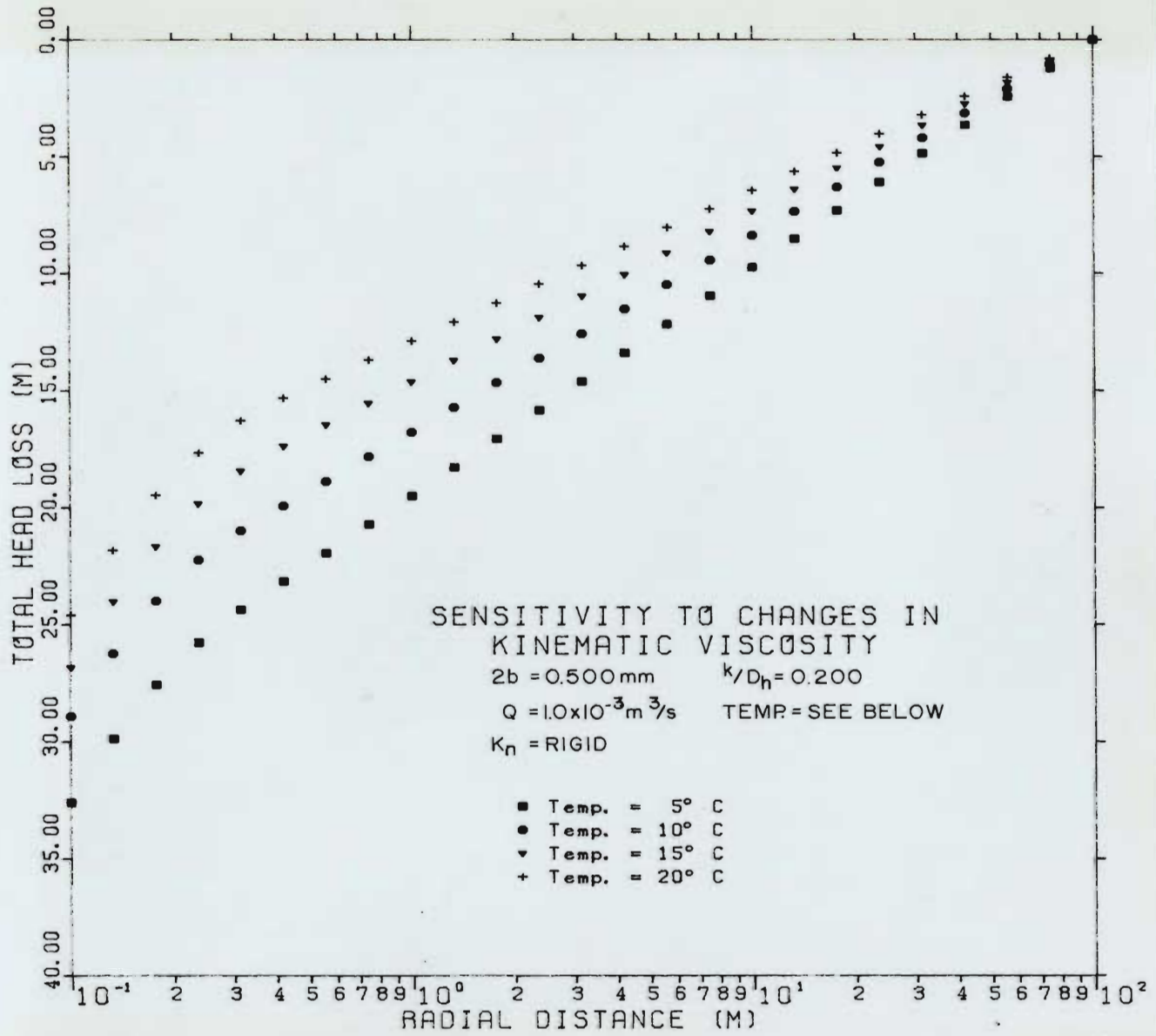


Figure D4 Sensitivity of head distribution to variation in kinematic viscosity of water

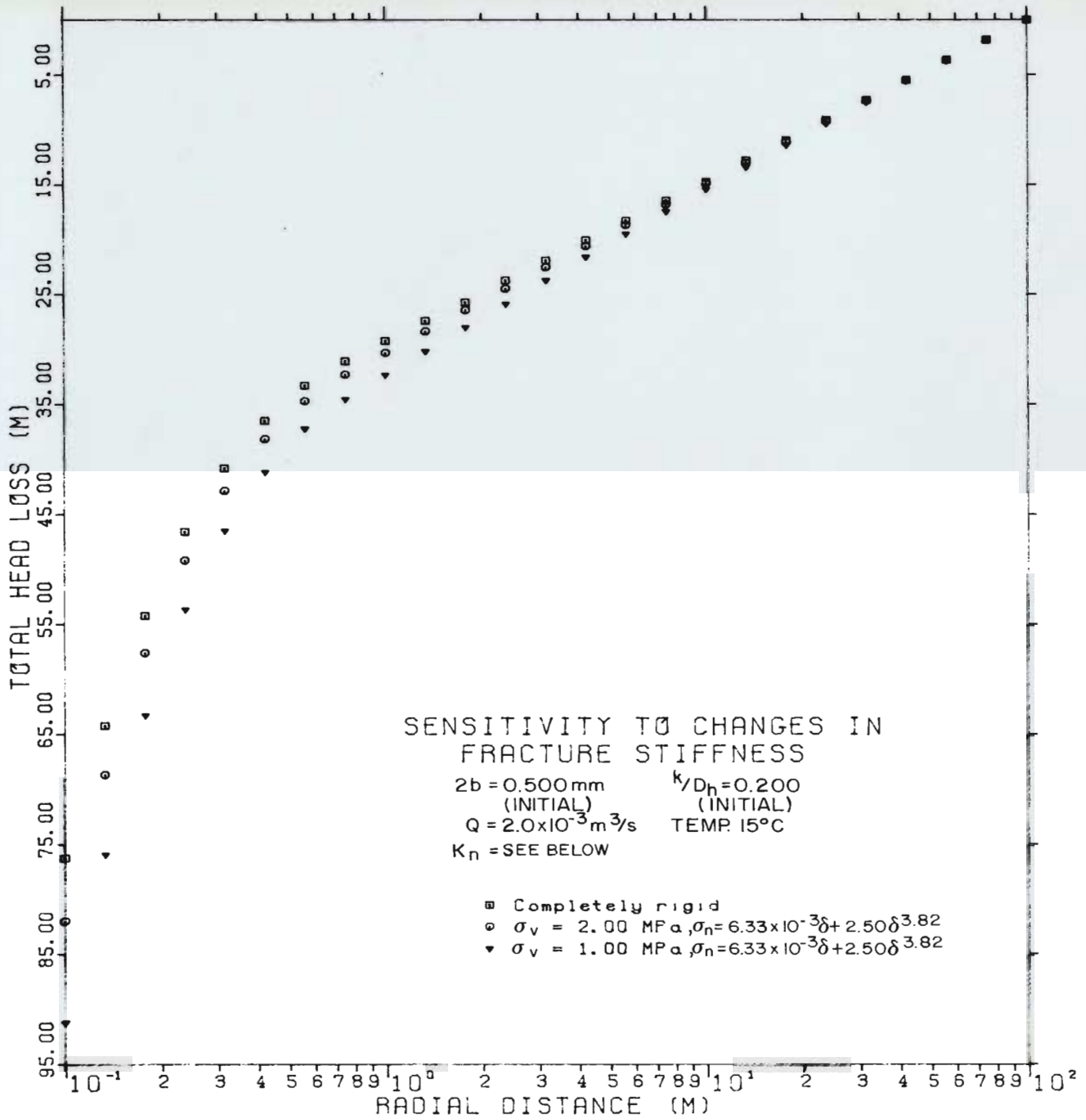


Figure D5 Sensitivity of head distribution to variation in normal stiffness of fracture

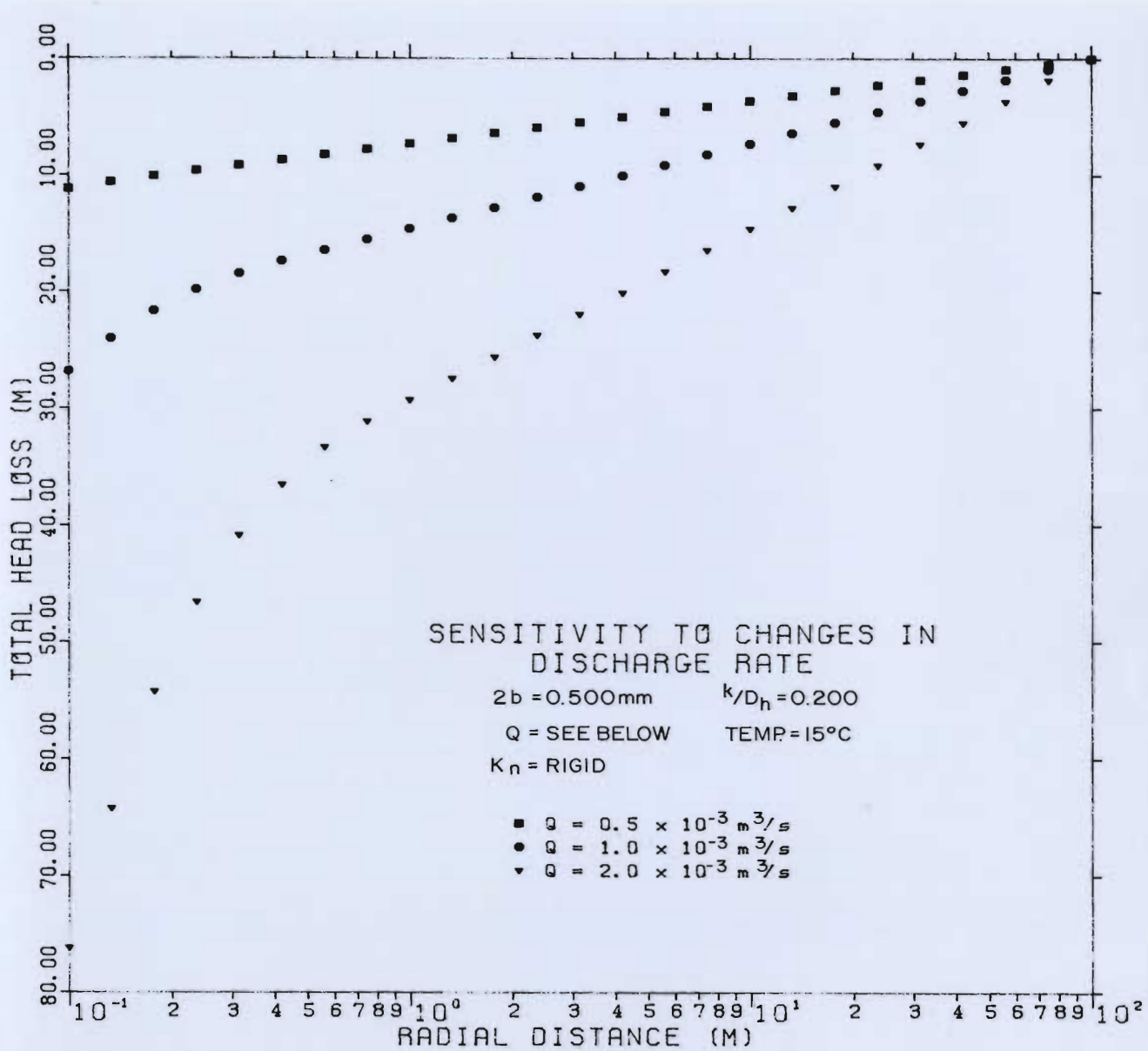


Figure D6 Sensitivity of head distribution to variation in discharge rate

APPENDIX E

DETAILS OF DESIGN AND CONSTRUCTION OF LABORATORY MODEL

The laboratory model built for this study was designed to simulate as realistically as possible the near-wellbore environment of a well obtaining water from a single, horizontal fracture. Factors considered in its design and descriptions and photographs of its construction and as-built components are presented in this appendix.

The purpose of the appendix is two-fold: 1) to give the critical reviewer sufficient insight to evaluate for himself the realism of the experimental data generated by the model and 2) to provide suggestions to the investigator who might be considering similar experimental work. To help serve the latter purpose, while avoiding excessive and disruptive footnotes, a list of sources for some of the more specialized materials used in constructing the model is included at the end (brand names are underlined when first introduced).

E.1 Design considerations

The geomechanical and hydraulic field conditions incorporated in the laboratory model are those which would most likely occur near a vertical well pumping a flow of

water on the order of 1 l/s from a single, horizontal, rough, deformable fracture at a depth of 100 m or less. This depth and production rate are within the ranges at which ground-water supply and dewatering wells are typically completed and pumped in non-karstic, fractured rock aquifers (Read, 1982; Whincup and Domahidy, 1982a,b; Woolley, 1982; Bair, 1980; Carpenter and Young, 1980; Williamson and Woolley, 1980; Stewart, 1978).

The model and experimental procedures were so designed that

- 1) axial loads, simulating overburden stress, could be applied as uniformly as possible,
- 2) steady-state flow could be maintained under conditions ranging from entirely linear to both linear and non-linear within the radial boundaries of the model,
- 3) pressure heads could be measured at several radial distances within the fracture and at several points along the borehole,
- 4) deformation of both the fracture and matrix resulting from changes in both total and effective stresses could be measured,
- 5) the boundary conditions H_0 , H_w , and σ_v could be changed easily, and
- 6) the wellbore could be enlarged.

The work of previous investigators summarized in Table 1.2 (page 37) was reviewed critically and taken into consideration during the design phase of the model.

E.1.1 Size of model

The first decision to be made was the relative scale of the model, that is, whether to use a full-scale or smaller model. The primary consideration is the effect of fracture roughness. Roughness is one of the most important parameters with regard to both the hydraulic and deformational response of the fracture (Tsang and Witherspoon, 1981). However, variation in its form, size and scale has put most work in fractured rock hydraulics into the semi-empirical realm (Pearce and Murphy, 1979). Gale (1982c) found that the apparent stress-flow relationship measured in the laboratory often depends on the size of the sample tested. Scale effects of roughness are probably the main cause. Therefore, it is very doubtful that fracture roughness is a parameter that can be scaled simply through geometric and hydraulic similitude as in pipe flow. Consequently, in attempting to reflect field conditions as closely as possible, it was decided to use a full-scale (with respect to fracture apertures and surface relief) model and to use water (instead of gas) for the fluid during the flow tests.

Before selecting actual model dimensions, two obvious questions had to be addressed:

- 1) How large are the apertures and how rough are the surfaces of fractures in relatively high permeability fractured rocks (i.e., those capable of yielding 1 l/s or more to a well)?
- 2) What would be the aperture and roughness of an artificial fracture that can be created in a large scale laboratory model?

There are few relevant data on apertures of natural fractures. Francis (1981) estimated effective apertures at depths of 60 m or less in a fractured sandstone to be in the range of 0.1 to 0.2 mm. Excluding a few relatively anomalous, large exfoliation partings, Gale (1977) concluded that effective apertures in the first 10 m in an outcrop of fractured quartz monzonite were about 0.2 mm. It should be noted, however, that the yield of the borehole he tested was only 0.04 l/s. Reddish and Smith (1982), using the analytical method of Barker (1981) to separate out the component of fracture permeability in a dual porosity rock, estimated the aperture of a single fracture in a coal seam at a depth of approximately 40 m to be 0.5 mm. The total discharge of the well they tested was 1.3 l/s.

None of these investigations considered the possible effects of roughness, and only Francis (1981) addressed the possibility of non-linear flow. By assuming the fractures to be hydraulically smooth (i.e., $k/D_h < 0.033$) and that only linear flow occurred during testing, the investigators probably underestimated aperture sizes (Appendix B).

Da Cruz and De Quadros (1984) conducted injection tests in a fractured basalt and compared the field results to those from laboratory tests, considering both roughness and non-linear flow. They estimated the aperture of a fracture which took 2 l/s during injection to be in the range of 0.6 to 1.0 mm.

Based on these very limited findings, it appears that the effective aperture of a "high yield" fracture is on the order of 0.5 mm, but roughness remains an unknown.

It was decided very early in the design phase to make the model out of concrete. Both to answer the second question and to gain some practical experience with concrete mixtures, a series of standard 15.25 cm diameter concrete test cylinders were prepared. The water-cement-aggregate ratio and size and uniformity of the aggregate were varied, and several different materials (e.g., rubber sheeting, triacetate fabric, and several different geotextiles) were used to form the joint that would constitute the "fracture" (additional considerations with regard to the surfaces of the fracture are described in Section E.1.3). Several of the joints were impregnated with resin and allowed to set under self weight (i.e., with no additional externally applied load). The artificial fractures created in this way had apertures in the range of 0.3 to 0.8 mm with relative roughnesses of approximately 0.1 to 0.2.

One of the primary goals of the testing program was to develop two-regime flow and to be able to identify the critical radius where the transition from linear to nonlinear flow occurs. Assuming that the artificial fracture will be rough, (i.e., $k/D_h > 0.033$) and using the value of critical Reynolds number for line D (Table 2.1, page 54 and Figure 1.6, page 32) in Equation 2.21, a plot of critical radius versus discharge rate with relative roughness as the parameter was generated (Figure E1).

Figure E1 suggested that a model with a radius of 0.75 m would allow an adequate range of testing. Using the standard 2:1 aspect ratio for testing under axial load, it was decided that the cylinder would, therefore, be 1.5 m in diameter by 3.0-m high.

E.1.2 Construction material for model

As mentioned in the preceding section, a decision to fabricate the model out of concrete was made early in the design phase. This obviously influenced much of the subsequent design. The relevant mechanical properties of rock and concrete, given in Table E1, are quite similar; and together with its general rock-like texture, this makes concrete a relatively ideal material for simulating natural field conditions in fractured rock.

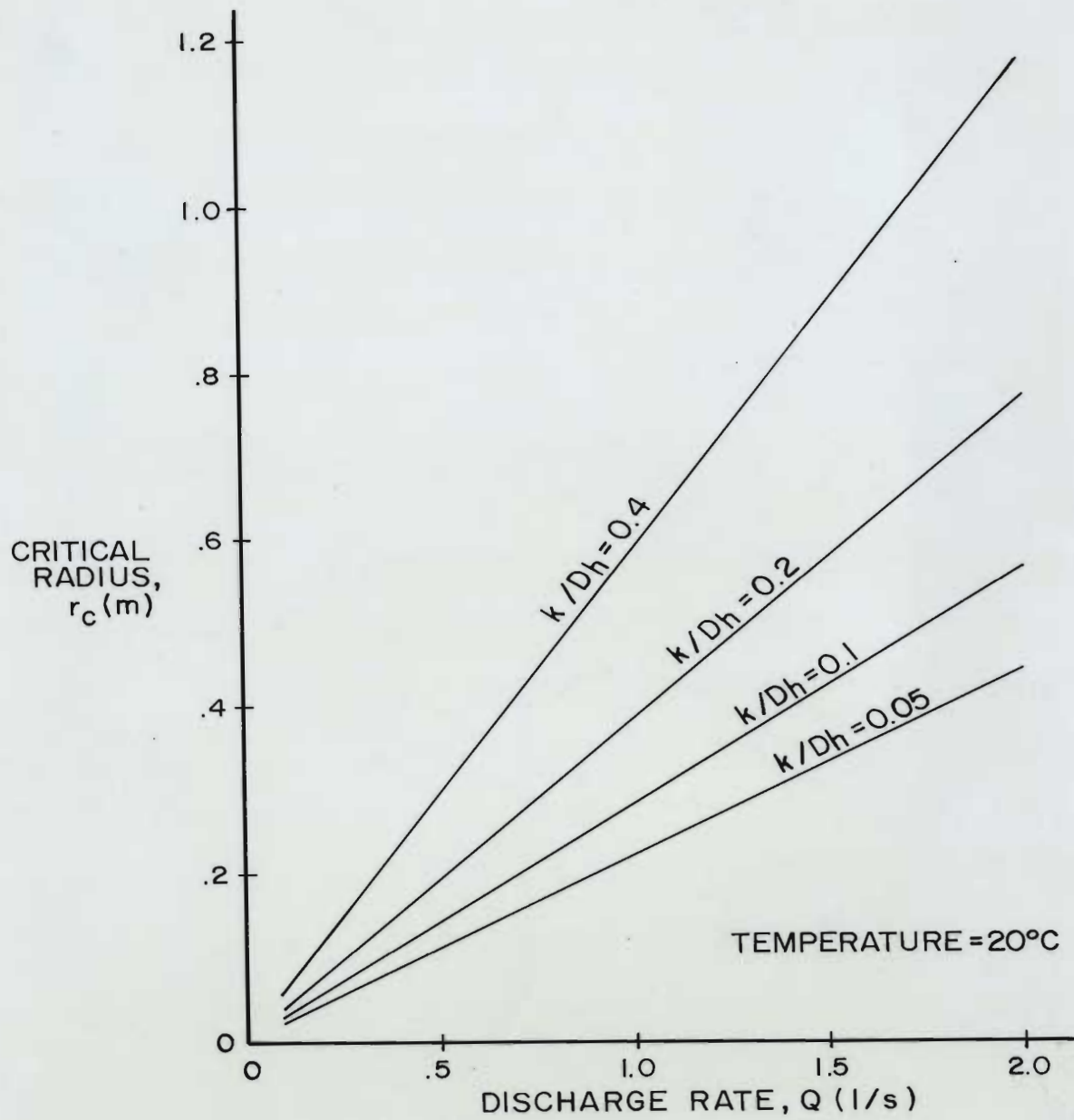


Figure E1 Critical radius as a function of discharge rate and fracture roughness

It should be mentioned that two other materials, rock and plastic, had been considered briefly. In keeping with the goal of making the laboratory model as realistic as possible, one option obviously was to construct it out of rock. There are numerous problems associated with acquiring, handling, and working with such large rock masses (Gale, 1977; Thorpe et al., 1980; and Watkins, 1981). In addition to the high cost of obtaining and transporting a sample from a suitable quarry site (most likely in the northeastern U.S.), there would be considerable difficulty in drilling the numerous small-diameter, closely spaced manometer holes required for this particular experiment.

Table E1 Comparison of mechanical properties of typical rock and concrete

| Property | Units | Typical Rock ¹ | Concrete ² |
|--|-------|---------------------------|-----------------------|
| Unconfined compressive strength, q_u | (Mpa) | 35 - 200 | 35 - 40 (note 3) |
| Poisson's ratio, μ | - | 0.1 - 0.4 | 0.15 - 0.25 |
| Young's modulus, E_r | (Mpa) | 3×10^4 | 3×10^4 * |

¹ From Goodman (1980) and Coates (1970)

² From Canadian Portland Cement Association (1981)

³ For water:cement ratio (by mass) of 0.40 to 0.45

* For concrete with dry unit weight of approximately 2,400 kg/m³

Although plastic has several desirable features such as workability and transparency which would permit visual detection of turbulence (by injecting dye into the flow field), its lack of rigidity requires a relatively complicated external support system (Rissler, 1978). More importantly, however, the roughness and deformational response of a plastic fracture surface would not be very realistic.

E.1.3 Surfaces of fracture

Although the fracture would be artificial, every effort was to be made to incorporate as many of the characteristics, both hydraulic and mechanical, of a natural fracture as possible. The two surfaces should be reasonable facsimiles of rock surfaces and should be matched imperfectly (i.e., supported by asperities) so that unrealistic, virtually complete closure could not occur at the relatively low levels of stress to be applied.

During the preliminary experimentation with the concrete test cylinders, it became obvious with consideration to large-scale construction that the fracture would have to be cast and that some type of membrane would have to be used as a bond breaker. This procedure also would impart more realistic characteristics to the fracture than those obtained from a tensile fracture or a "cold" joint (one

formed by pouring concrete on another completely or partially cured concrete surface). The aperture of a self-propped fracture is the result of mis-seating of asperities, shear dilatancy, or actual removal of material by weathering subsequent to formation of the fracture. Therefore, artificially induced tensile fractures and/or fresh, well-matched formed surfaces are probably poor simulators of real fractures. Laboratory data suggest that there are significant differences between the stress/deformation responses of natural and artificial, tensile fractures (Gale, 1982b).

It was found that a reasonably natural fracture could be obtained using MIRAFI 600X geotextile. The woven polypropylene fabric imparts a relatively uniform, grid-like texture to the concrete surface and is permeable. The latter property allows air to escape from the curing concrete, thereby preventing formation of pits due to entrapped air bubbles. This had been a serious problem with many of the other materials that were tested. The permeability of the geotextile also permitted the thin film of water rising to the top of the concrete during curing to bleed through so that it could be blotted up. This prevented formation of a weak mortar "skin" on the surface of the fracture.

E.1.4 Relative orientation of wellbore and fracture

The most simple of all geometric configurations, a horizontal fracture with a vertical wellbore, was selected. In addition to the obvious advantages in construction, a major reason for choosing this relative orientation is that a non-horizontal fracture could undergo significant shear displacement in response to increases in effective stress. This is a factor which must be addressed eventually (Gale, 1982d), but is beyond the scope of the present investigation.

E.1.5 Flow and deformation boundary conditions

The axial loads applied to the concrete cylinder were intended to simulate overburden pressure. Assuming a lithostatic pressure gradient for typical rock of 0.027 MPa/m (Goodman, 1980), the average vertical stress at a depth of 100 m (the originally specified depth limit) would be 2.7 MPa. The loads required to generate this stress, however, exceeded the design specifications of the existing loading frame that was available for the experiment. This being the limiting factor, it was necessary to keep the average vertical stresses applied during testing at 1.1 MPa or less (corresponding to a depth of approximately 41 m).

Ideally, the model would be tested under triaxial conditions, being subjected to a lateral confining pressure of $\sigma_v[\mu/(1-\mu)]$ where σ_v is the vertical or axial stress and μ is Poisson's ratio. The cost of the required pressure vessel, however, was far beyond the level of funding available for this study; so only uniaxial testing could be considered.

Fluid pressures in the fracture needed to be high enough to significantly decrease the effective stress on the fracture so that it could deform measurably in response to subsequent increases in effective stress. There also had to be adequate head for testing the model under two-regime flow conditions at flow rates on the order of 1 l/s. Pressure heads on the order of 40 to 50 m were required to meet these criteria.

E.2 Description of model as-built

A schematic diagram of the complete laboratory set-up (Figure 4.2, page 95) and a photograph of it as-built (Figure 4.1, page 94) are included in Section 4.0.

The 1.50-m diameter by 3.02 m high cylinder was cast of concrete having a water:cement:aggregate ratio (by mass) of 0.4:1:3 and aggregate consisting of 1:2 blend of fine sand and minus 6 mm crushed stone. Figure E2 shows the manometer networks, lifting hooks, rebar cages, and wire

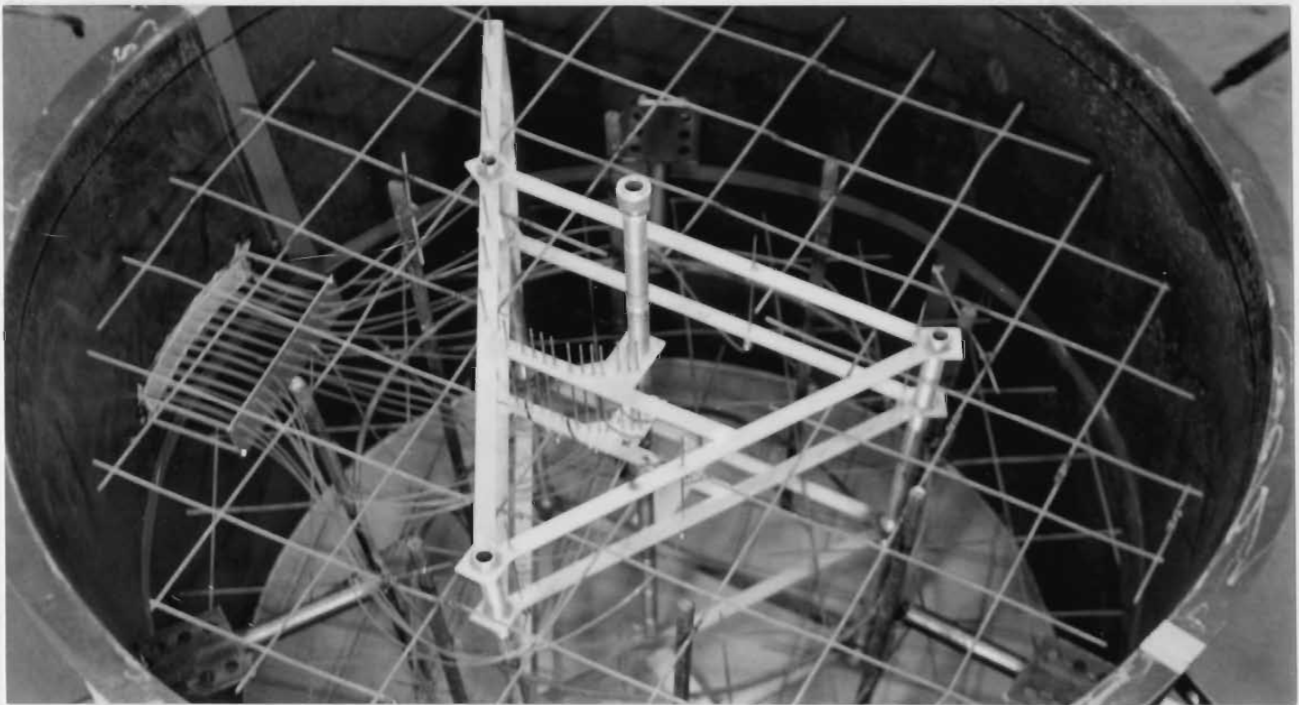
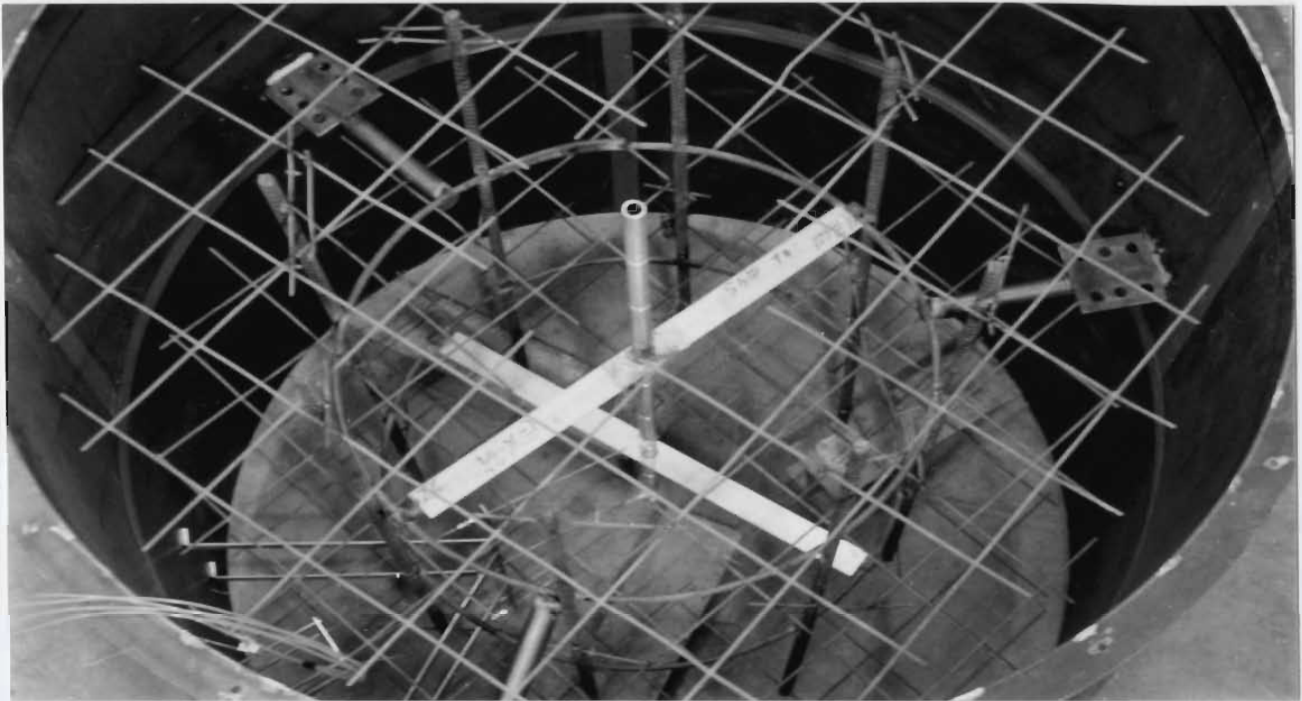


Figure E2 Cast-in-place components of concrete cylinder. Manometers for wellbore are in top half; manometers for fracture are in bottom half.

mesh reinforcement inside the forms for the top and bottom part of the cylinder prior to their being filled with concrete. Two percent (by mass) of a plasticizer, Melment, was used to increase the slump of the concrete (simply adding water would have decreased strength and increased shrinkage) in order to facilitate its flowing around the manometers tubes and other cast-in-place parts of the model. The cylinder was cast in two separate pours. After pouring the bottom half, a sheet of geotextile was pressed into its top surface (Figure E3). After allowing it to set for about 3 hours, the top part of the form was flanged on and the rest of the cylinder was poured (Figure E4).

During the 28-day curing period, the initial wellbore was drilled (Figure E5) using a 0.064-m diameter, diamond tipped core barrel modified to include a centralizing device. The centralizer followed a 19-mm diameter aluminum tube which had been cast in place (Figure E2) along the axis of the cylinder to assure that the wellbore would be centered, straight, and positioned correctly relative to the manometers. For subsequent tests, the wellbore was reamed to diameters of 0.108 m and 0.160 m using similar modifications to larger core barrels.

When the concrete had cured for approximately a month, the two halves were separated, the geotextile was removed, and the 3.2 mm diameter fracture manometer tubes (which had

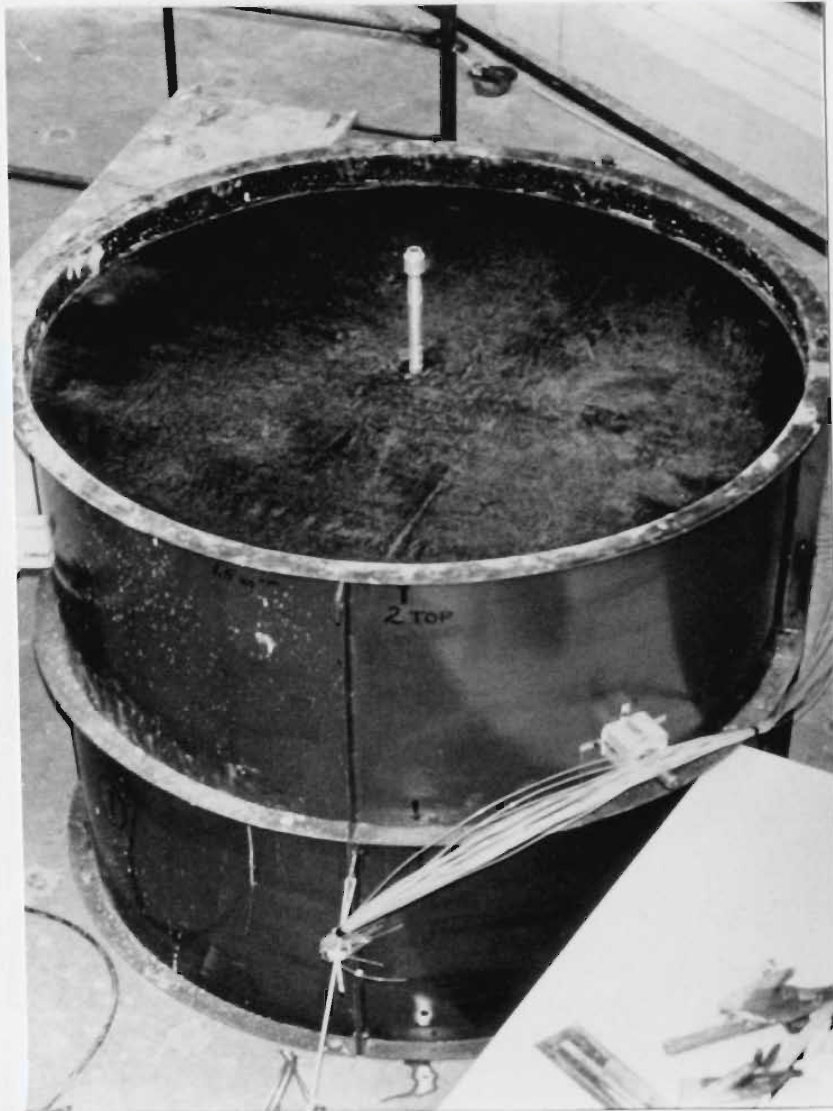


Figure E3 Bottom half of cylinder with geotextile in place

been sealed with plastic plugs to prevent the concrete from getting into them) were located using a template and drilled out with a small masonry bit.

After the forms were stripped away, a circumferential fluid reservoir (Figure E6) was mounted onto the cylinder

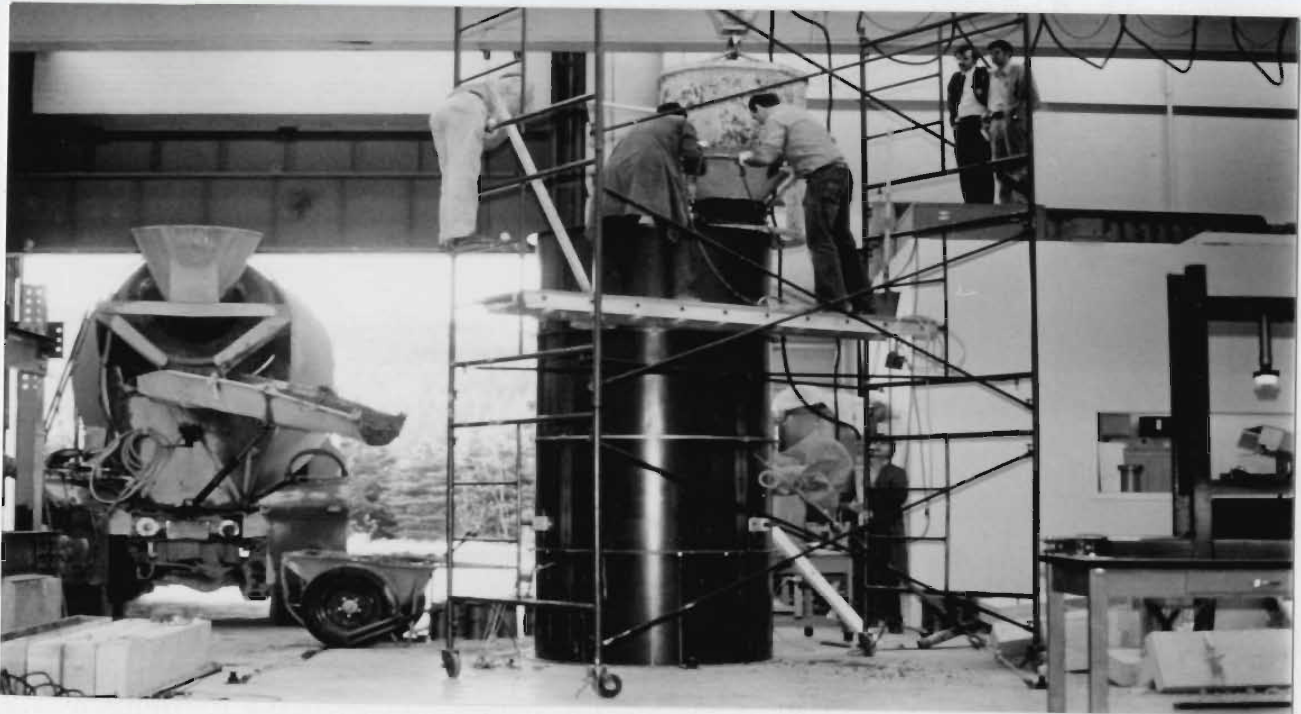


Figure E4 Pouring top half of concrete cylinder

straddling the fracture. A 6.5-mm thick, Flexane 80 gasket was poured into the annulus between each half of the reservoir and the concrete. The purpose of this thick gasket was to ensure that the reservoir would not impede deformation of the fracture during testing. Shear distortion within the Flexane should have effectively decoupled the two halves of the cylinder. The circumferential reservoir also contained three inflow/outflow ports, three manometers, and a thermocouple for measuring water temperature.



Figure E5 Drilling wellbore in concrete cylinder

For pumping tests, water was supplied to the circumferential reservoir by a submersible pump in a tank kept at constant temperature by a thermostat-controlled refrigeration unit. The desired outer boundary pressure was obtained

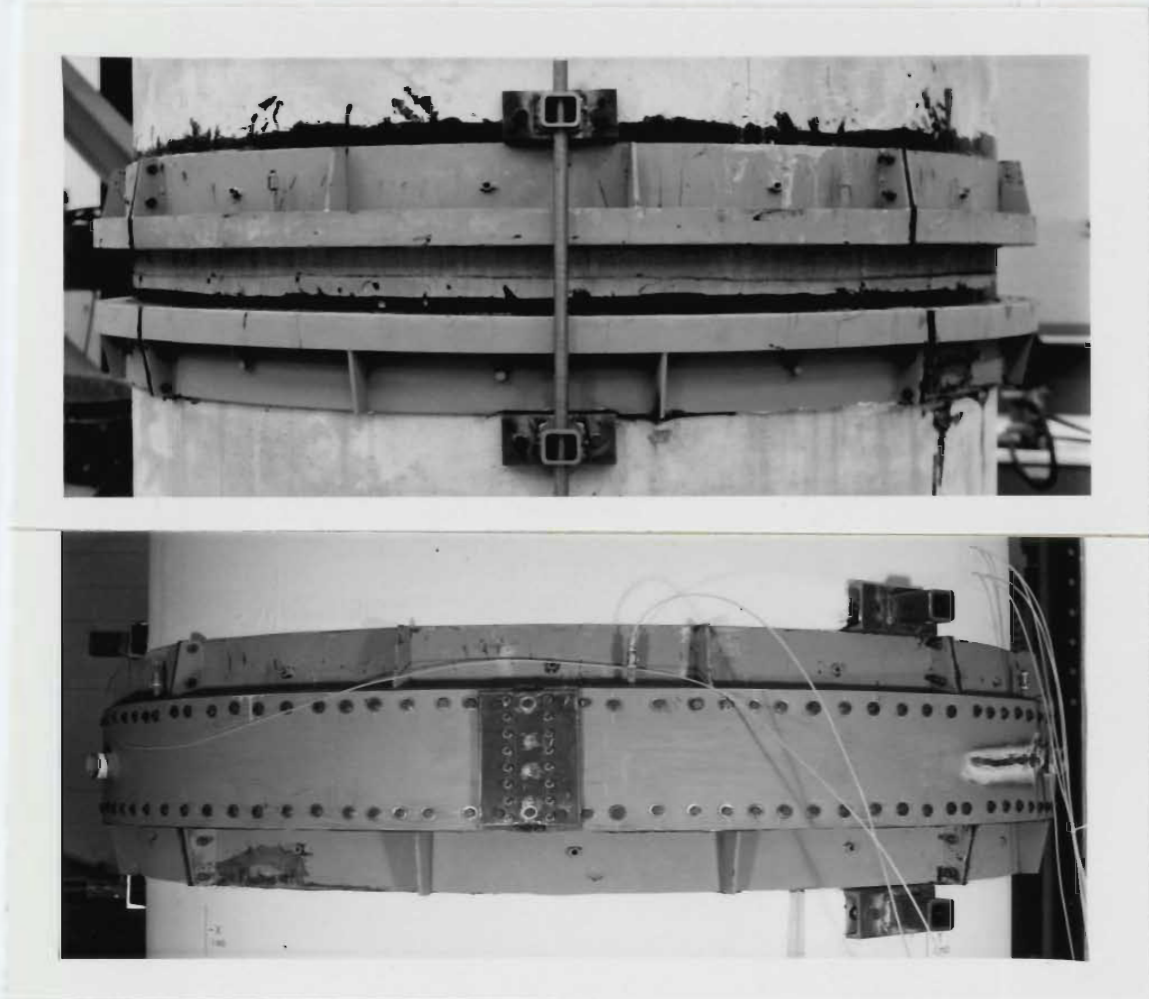


Figure E6 Circumferential reservoir before
and after outer band flanged on

by regulating the amount of flow that was allowed to bypass the model and go directly back to the tank (Figure 4.2, page 95). For injection tests, the inflow and outflow lines were simply reversed. In both cases, the flow rate was measured using a paddlewheel Flosensor.

Axial loads were applied using four symmetrically arranged (Figure 4.3, page 96) 90 metric ton hydraulic cylinders connected to a common pressure manifold. Load was transferred from the cylinder through gusseted load distributors to a steel plate imbedded in machine leveling grout on top of the cylinder. As shown in Figure 4.2 (page 95), it was necessary to "float" the columns of the loading frame to avoid the possibility of shear failure in the floor if the columns were bolted directly to the floor. Using this arrangement, the tension in the columns was transferred through the 0.76 m thick floor via 50-mm diameter bolts to another set of channel beams in the basement of the laboratory. The resultant loads were applied directly under the concrete cylinder, so that the net effect was to put the floor, the weakest member in the system, into compression.

A Hewlett-Packard (HP) 3497A data logger controlled by an HP 85 micro-computer was used to acquire, convert to engineering units, and store data from the various temperature, displacement, and pressure sensors.

Deformation of the fracture was monitored by a series of three equally spaced linear variable displacement transformers (LVDT's) on the perimeter of the cylinder (Figure E7). Because of the long span over the circumferential reservoir, thermally insensitive Invar rods were used as

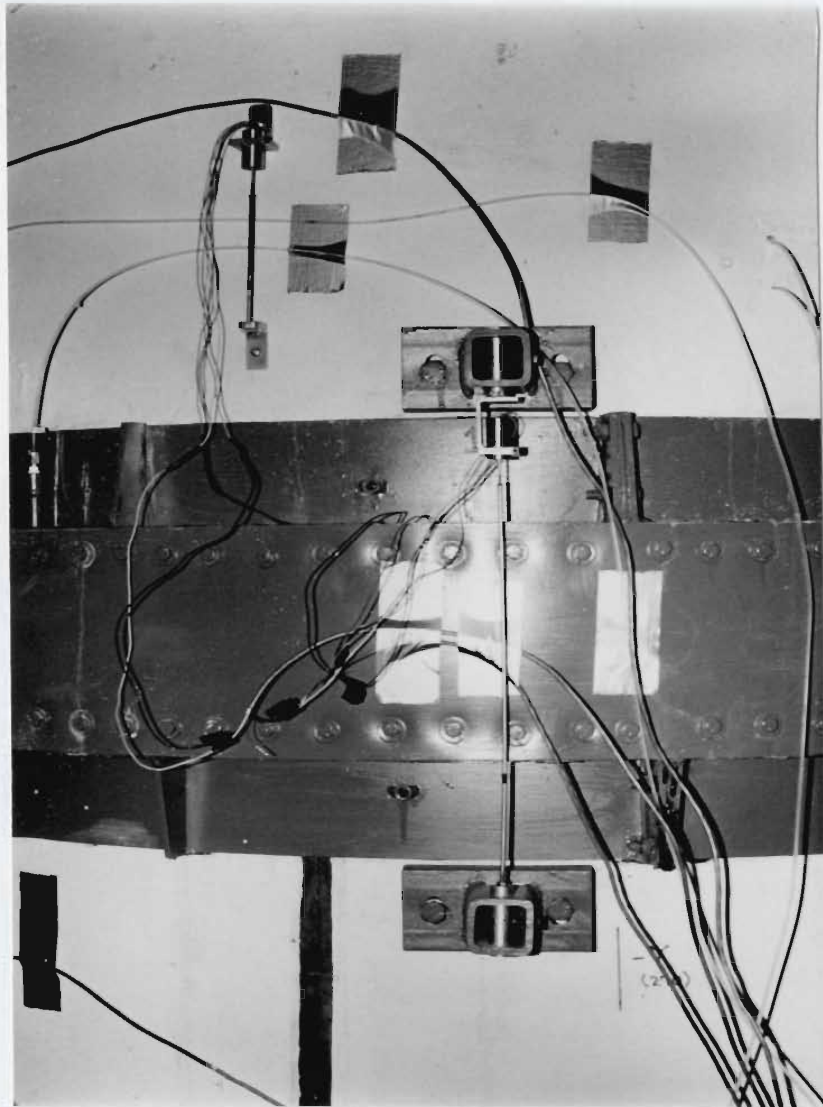


Figure E7 Linear variable displacement transformers (LVDT's) for measuring concrete and fracture deformation on perimeter of model

extensions of the LVDT cores. After the wellbore was reamed to a diameter of 0.160 m, another set of LVDT's was installed to allow displacement measurements to be made at the radius of the wellbore. Invar rods were anchored into circular, aluminum clamps (Figure E8) that were cemented onto the wall of the wellbore above and below the fracture using Matflint 2 epoxy. HDC hermetically sealed LVDT's were fastened to another clamp cemented near the top of the wellbore. The complete apparatus is shown assembled outside the wellbore. All electrical connections were waterproofed using Seal-Tite Fusion Tape.

Fluid pressures were measured using strain gauge type pressure transducers. A multiplexer panel consisting of a series of 5-way valves was used to channel the 31 manometers to two transducers.

E.3 Product information

Table E2 provides information on the manufacturers and/or suppliers of some of the more specialized products and materials used in the construction of the laboratory model.



Figure E8 LVDT system for measuring fracture deformation inside wellbore

Table E2 Special materials used to construct physical model

| Product | Description | Manufacturer |
|-----------------------|---|--|
| Flexane 80 | Rubber-like urethane | Devcon Canada Ltd. Scarborough, Ontario |
| HCD model LVDT's | Hermetically sealed LVDT's | Schaevitz Engineering P.O. Box 505 Camden, NJ 08101 |
| Invar | 3.81 mm diameter rods of alloy with very low coefficient of thermal expansion | Driver-Harris Canada Ltd. 56 Bramsteele Road Brampton, Ontario L6W 3M7 |
| Matflint 2 | Polyamide-cured epoxy 100% solids | Standard Mfg. Co. Ltd. P.O. Box 6090 St. John's, Newfoundland A1E 5X8 |
| Melment | Super plasticizer for concrete | Sternson Ltd. Brantford, Ontario |
| MIRAFI 600X | Woven polypropylene geotextile | Dominion Textile Inc. P.O. Box 186 415 Norwich Ave. Woodstock, Ontario N45 7W8 |
| FloSensor | Paddlewheel flowmeter and signal conditioner | Signet Scientific P.O. Box 5770 El Monte, CA 91734 |
| Seal-Tite Fusion Tape | Self-vulcanizing rubber tape | Rotanium Products Co. 4425 Euclid Ave. Cleveland, Ohio 44103 |



